~~Investigation of~~ Stimulated Brillouin Scattering in Single Mode Optical Fibre Ring Resonators

Polina L. Bayvel

Submitted to University of London for the degree of Ph.D.

Department of Electronic and Electrical Engineering
University College London
October 1989

Abstract

This thesis describes the theoretical and experimental investigation of stimulated Brillouin scattering (SBS) in single mode optical fibres and all-fibre ring resonators. SBS is a nonlinear threshold effect which occurs in single mode fibres at low optical pump powers, and can be a limitation in optical fibre coherent transmission systems. High finesse optical fibre ring resonators are attractive for the study of SBS as their geometry offers a very low round-trip loss coupled with a significant enhancement of the circulating power over the input power resulting in low SBS thresholds.

After a review of the SBS theory and an overview of the research work carried out in the field of SBS in single mode optical fibres, the system of coupled equations which described the generation of the SBS process is solved numerically. The numerical results are compared with existing analytical solutions and published experimental data, and the implications and applications of the results to optical fibre transmission systems and Brillouin amplifiers are discussed.

The evaluation of high finesse single-mode ring resonator operation carried out, including the fabrication, alignment, and characterisation of devices fabricated from ordinary and polarisation maintaining fibre, at 633 nm and 830 nm is described.

The theoretical and experimental investigation of SBS generation in all-fibre single mode ring resonators is presented. An analytical theory describing the operation and performance parameters of all-fibre Brillouin lasers is derived, and a numerical modelling of the transient operation of the Brillouin laser is carried out. The transient and steady-state characteristics of a Brillouin amplifier based on an all-fibre ring resonator are considered.

The experimental investigation of the operation of all-fibre Brillouin lasers is described. Particular attention focuses on the semiconductor laser pumped Brillouin laser and the first demonstration of this device operating at a submilliwatt threshold is presented. The processes of four wave mixing (FWM) and a related process of Brillouin enhanced four wave mixing (BEFWM) are observed for the first time in all-fibre ring resonators, and the physics of these processes is considered.

The applications of the work in this thesis including local oscillators, generation and distribution of high frequency microwave components, amplification, and phase conjugation are also discussed.

Acknowledgements

I would like to thank a number of people who have helped in the course of my PhD,

at UCL:

My supervisor, Dr Ian Giles for initiating the project and many interesting discussions in the course of this work. Dr Paul Radmore, for numerous discussions on the theoretical front and much patient help in conquering some of the difficult mathematics arising in this work. Dr John Halley is thanked for many helpful discussions on the theory of SBS. Particular thanks are due to my colleagues in the Fibre Optics Group: Mahmoud Farhadiroushan and Sotirias Markatos for many hours of discussions, practical advice and help. Dr Alwyn Seeds and Dr Hugh Griffiths are thanked for valuable and helpful comments. I am grateful to Tony Kerr for invaluable help with resonator fabrication; Tony Overbury and Henry Robinson for help in setting up some of the lasers, and Maurice Gillett together with the Engineering Workshop for their friendly and competent help.

I would also, especially, like to thank the people who have played a particularly important part in my days at UCL's Electronic Engineering Department:

Special thanks go to Professor Gareth Parry - for immeasurable support, advice, and encouragement, and seemingly limitless patience and kindness.
My three respective Heads of the Department: Prof Eric Ash, Prof 'D.E.N.' Davies, and Prof John Midwinter for taking interest in, and encouraging my work at UCL, both during my undergraduate and postgraduate days. I am, of course, indebted to Dr Roger Giblin, ex-Admissions Tutor, for introducing me to UCL.

I am exceptionally lucky in having accumulated many very good friends and colleagues at UCL, on whom I could always rely for general advice, sympathy, goodwill, and diversion - which were and are much appreciated. I would also like to thank my parents and close friends outside UCL for their much needed patience and tolerance in the course of doing and writing up of my PhD work.

At GEC Hirst Research Laboratories, I would like to thank:

My industrial supervisor, Dr Ayman El-Fatatry - for encouragement, invaluable suggestions, and constant interest and support in this work.
Adrian Greenham, Dr Mike Rowe, Dr Peter Ball, and Dr Cyril Hilsum for much advice and help in the course of this work and my association with GEC Hirst.
I would also like to acknowledge the good advice, optimism, and encouragement of Dr John McCormack (BICC) during our long term association within GEC Hirst Research Laboratories.

Finally, I am grateful to the Science and Engineering Research Council (SERC) for financial support in providing a CASE Award scheme together with GEC Hirst Research Laboratories, and for the financial support of the project.

Contents

Chapter 1

INTRODUCTION

Advances in quantum electronics in the 1950's and 60's, and the subsequent invention of the laser[1] created a revolution in the field of optics, as it made available for the first time a coherent monochromatic source of optical radiation. The invention of the laser also provided the impetus for the researchers to view the optical frequency spectrum for transmission as an extension to the radio and microwave spectrum, with optical communications systems offering a potentially tremendous capacity. The outcome of this new view was a dramatic increase in the study of all optical components; sources, modulators, detectors, waveguides, and complete systems. Since the initial proposals and demonstrations of the first optical fibres in the late 1960's[2], the last two decades have witnessed massive worldwide research efforts invested into the development of high speed, low loss fibre communications systems, both for long-haul and local area networks.

In addition to great advances in high speed communications, this work has led to development of a new research area of nonlinear fibre optics. In conventional nonlinear optics a focused geometry is used. The optical intensity is then $P/\pi a^2$ where P is the optical power, and the interaction length is limited to $L = 2\pi a^2/\lambda$ because of the beam waist 2a due to diffraction. In an optical fibre with the same field size as the diffraction limited beam waist, the intensity would be the same as for the focussed case, while the interaction length is limited by the absorption length of the fibre ($1/\alpha_o$). The enhancement in the (optical intensity x interaction length) product - a parameter which characterises the strength of optical probing, is $2\pi a^2/\lambda$, and can be as large as 10^8 - 10^9 in typical single mode optical fibres. Although usually considered as linear or passive media, it soon became apparent that optical fibres presented quite different operating conditions compared with bulk materials, even for familiar nonlinear processes, including stimulated Brillouin and Raman scattering, Kerr effect, second and third harmonic generation, and four wave mixing processes. The small cross-section areas and long interaction lengths possible in optical

fibres thus mean that many nonlinear effects can be observed in fibres at powers several orders of magnitude lower than in bulk materials[3-10]. There has also been growing appreciation that fibres have characteristics which have no parallel in conventional nonlinear optics, in particular the important role played by group-velocity dispersion. The combination of group velocity dispersion and nonlinearity has led to some interesting effects related to solitons and self-phase modulation[7,8]. Fibre nonlinearity has grown into a rich and diverse subject, while optical fibres have thus emerged as convenient media for the study of nonlinear effects, and their implications in fibre systems: viewed both as a source of deleterious effects, and for potentially promising applications such as all-optical frequency generation, switching, pulse compression, and amplification.

Most of the observable nonlinear effects, however, still require optical powers in the range of tens to hundreds of milliwatts (Kerr effect and four wave mixing) to several Watts (stimulated Raman scattering), with tens to hundreds of Watts for soliton effects, which are too high really for practical communication systems. In contrast, stimulated Brillouin scattering (SBS) is a particularly important nonlinear process since it is the first nonlinearity which is encountered in optical fibres as the transmitted power is increased, and can be observed at optical powers of as low as few milliwatts in single mode optical fibres with lengths of several kilometres. Briefly, in this process an incident optical wave, known as the pump wave with frequency f_p, gives rise to an acoustic wave, f_a, and a counter-propagating scattered optical wave having a lower frequency, f_S, known as the Stokes wave. The Stokes wave is shifted in frequency relative to the pump by the amount equal to the frequency of the acoustic phonon ($= 2nf_pv_a/c$, where v_a and c are the speeds of sound and light, respectively) so that the total energy in the process is conserved.

The pump wave strongly amplifies the Stokes wave, whose growth is proportional to the pump intensity and to the interaction length, as outlined above. There is a characteristic frequency bandwidth associated with the SBS amplification. This bandwidth is proportional to the attenuation of the acoustic phonons, and in optical glasses will be typically tens of megahertz in the far-red and near infra-red region of the spectrum. This means that the SBS is a highly coherent process and is most efficient when the pump spectral linewidth is comparable or lower than the intrinsic SBS linewidths. Discovered in optical fibres by Ippen and Stolen in 1972[11], it has since been shown to be a possible limitation in the practical performance of optical transmission systems that use narrow-linewidth, single frequency lasers[12]. Clearly in the SBS process the energy is transferred

from the pump to the Stokes wave which is backscattered relative to the pump. Thus a counter-propagating Stokes wave can lead to a severe additional attenuation of the forward propagating, information carrying pump, and in addition introduces a high intensity backward coupling into the transmission optics (leading to an increased relative intensity noise of the laser source). It may, therefore, be necessary to operate at power levels below the threshold at which SBS becomes a significant effect, so that it could place a severe limitation on the launch power and thus also the repeater spacing.

The nonlinear Brillouin gain in optical fibres can also be used to advantage in a number of important applications such as fibre amplifiers and Brillouin lasers. The principle of Brillouin amplification is to amplify an external signal by coupling into the fibre a certain amount of pump power, which provides a distributed gain at the signal wavelength. Although the inherently narrow intrinsic Brillouin gain can be broadened by varying the fibre composition, and frequency modulation of the pump laser, the narrowband Brillouin gain is of interest since it can be used to selectively amplify the residual carrier wave in homodyne detection system, and in densely packed wavelength division multiplexed systems.

The generation of SBS in a resonator with an SBS active medium can be considered as lasing where the pump provides the energy for the counter-propagating Stokes wave, giving a frequency shifted output. Work on fibre Brillouin lasers dates back to 1976[13]. The first fibre Brillouin lasers were hybrid devices composed of bulk optics (bulk reflectors and beamsplitters) coupled to long lengths of optical fibre. Consequently such a cavity had very high losses and a very low Q factor (approximately 4 in the first Brillouin laser). Devices made of such a long length of fibre had an inherently poor stability and a high round-trip loss (greater than 70%), and consequently high threshold levels.

The aims of achieving all-fibre systems, in order to eliminate the need for bulk optics components have led to considerable advances in the optical fibre fused and polished component fabrication technologies in the 1980's, resulting in high quality, low loss components. The foremost development was that of a directional coupler with the evanescent field (polished) devices having the advantages of their inherently low loss, tunability, and the ability to access the evanescent field of the fibre core by removing some of the cladding. This work opened the way for realisation of a number of new all-fibre devices, notably, the ring resonator. Essentially, the all-fibre ring resonator consists of

two halves of a polished directional coupler fabricated on the same length of optical fibre, and closed into a loop. Providing the coupler losses are small (losses of less than 0.03 dB were achieved in this work), very high finesse (> 300) resonators can be fabricated. Such a low-loss, high-finesse cavity leads to a significant enhancement of the optical intensity circulating in the loop over the input intensity. This, together with an increase in the effective path length, means that the power levels necessary for the observation of nonlinear effects are considerably reduced in these devices[14], thus making the resonator an attractive device for the study of stimulated Brillouin scattering.

The work in this thesis describes a wide ranging investigation of stimulated Brillouin scattering in single mode optical fibre ring resonators. The overall aim of the project was the study of SBS in optical fibres and fibre resonators, interesting both for Brillouin laser applications in local oscillators, linewidth narrowing, and frequency generation, amplifiers, and Brillouin gyroscopes, as well as a limitation in coherent fibre systems and resonator based devices.

A detailed review of the current state of research on SBS in optical fibres revealed that despite a considerable research effort invested into the experimental investigation of SBS, the mathematical treatment of SBS has been incomplete, with the adopted approximations often applied in an unjustified manner. Specifically, although experimental results have reported conversion efficiencies of the pump power into Stokes power in excess of 50%, the solutions of the equations describing the evolution of the pump and Stokes powers with fibre length and input power failed to take pump depletion into account, due to difficulties associated with finding solutions to the full SBS equations. Although intuitive statements about the form of the solutions can be made, it was felt that a quantitative approach to the problem would provide valuable insight into the physics of SBS, and the process of energy exchange between the pump and Stokes waves, both in the context of optical fibre systems and Brillouin lasing. A very flexible numerical method adopted in the work allowed the calculation of stable and accurate solutions which were shown to be in excellent agreement with published experimental results, and easily applicable to practical calculations.

Initially a detailed evaluation on a number of high finesse ring resonators was carried out. A number of high finesse resonators were successfully fabricated from standard and polarisation maintaining fibre and tested at wavelengths of 633 nm and 830 nm, with the

latter carried out using a single mode semiconductor laser. These experiments showed that the relatively broad linewidth of semiconductor lasers presented quite different and more complex experimental conditions than in the case of frequency stabilised gas lasers, but these experiments were judged as valuable as the use of semiconductor lasers offered an increased compatibility with current fibre systems for these devices.

The next step was to consider the operation of an all-fibre Brillouin laser. Although at the start of the work, the principle of all-fibre Brillouin laser operation with submilliwatt threshold had been established, the absence of any theory describing the performance parameters of this device as a function of resonator parameters was conspicuous. To enable the design and optimisation of resonator cavities for a given application, an analytical theory describing the steady state operation of the Brillouin laser was therefore derived[15]. Following this we proceeded to carry out a detailed experimental investigation of Brillouin laser operation, with particular emphasis on semiconductor laser pumping. The lowest reported Brillouin lasing threshold of 70 μW and the highest conversion efficiency of 23% were observed in a resonator fabricated from polarisation maintaining fibre at 633 nm[16]. We also reported the first demonstration of a semiconductor laser pumped Brillouin laser[17]. Very good agreement between the experiments and the developed theory was obtained in all cases. Because the generation of SBS in a ring resonator can be considered as lasing, the output linewidth of the Stokes wave is determined by the stability of the resonator cavity and its intrinsic finesse, and not by the pump linewidth, so that potentially considerable linewidth narrowing can be expected. The linewidth narrowing exhibited by the Stokes wave was demonstrated for the first time in this work in the case of the semiconductor laser pumped Brillouin laser, and this aspect of Brillouin lasing can be used as a means for narrowing the linewidths of semiconductor lasers for applications in coherent systems. We also evaluate the transient response of the Brillouin laser, and show that by operating it below threshold an external signal at the Stokes frequency can be amplified[18]. The advantage of such an amplifier is the very low pump power necessary to achieve a high gain for a range of very low pump powers, accompanied by a high signal-to-noise ratio.

Another interesting potential application of Brillouin lasing suggested by this work is that of optical generation and distribution of microwave signals by combining the pump and Stokes waves on a square law photodetector, to generate a high frequency. In the past, generation of several Stokes and anti-Stokes components by the four wave mixing (FWM)

process have been shown in hybrid bulk/fibre cavities at pump powers of hundreds of mW. Potentially, this could be another useful technique for optical generation of high frequencies, particularly if this could be shown at low pump powers. For example the Brillouin shift at the pump wavelength of 830 nm is 20 GHz, and the heterodyning of just the second-order Stokes and first order anti-Stokes components will result in the generation of spectrally narrow signal at 60 GHz, and higher at shorter pump wavelength, because of the λ^{-1} dependence of the Brillouin shift. In this work we have observed the process of nondegenerate four wave mixing for the first time in an all-fibre ring resonator at the lowest pump powers to date[19]. In addition we have also observed[20] a different four wave mixing process known as Brillouin enhanced four wave mixing (BEFWM), a technique which is of considerable interest for phase conjugation applications, and which has never previously been observed in optical fibres. This work opens a number of possibilities for investigation of phase conjugation through BEFWM in optical fibres, for example, in image transmission using an all-optical fibre phase conjugator at low pump powers.

The rest of this thesis is arranged as follows. The general background to molecular scattering processes , together with the physics and theory of stimulated Brillouin scattering are described in Chapter 2. Chapter 3 gives a comprehensive overview of the research on SBS in single mode optical fibres and ring resonators. The numerical method used to solve the SBS equations and the solutions are discussed in Chapter 4, which also describes the implications of these to optical fibre systems and Brillouin amplifiers. Theoretical and experimental behaviour of optical fibre ring resonator, together with the fabrication details are described in Chapter 5, and Chapter 6 is devoted to the all-fibre Brillouin ring laser. In the first part of the chapter the analytical steady-state theory describing the Brillouin laser is derived, while the second half of the chapter deals with the experimental investigation of the Brillouin laser operation, and discusses the possible application of this device in generation and distribution of microwave signals in phased arrays.

Chapter 7 deals with the derivation of the numerical model describing the transient generation of Brillouin scattering in the ring resonator. The characteristics of an amplifier based on this device are assessed, and are considered in the context of other optical amplifiers. FWM processes observed in Brillouin lasers are described in Chapter 8, and the summary and conclusions to this thesis are discussed in Chapter 9.

1.1. References for Chapter 1

1 T. H. Maiman, 'Stimulated optical radiation in ruby', Nature **187**, 493 (1960)

2 J. E. Midwinter, "Optical fibres for transmission", John Wiley & Sons, New York, 1978

3 E. P. Ippen, 'Nonlinear effects in optical fibres' in: "Laser applications to optics and spectroscopy", S. F. Jacobs and M. O. Scailly, eds., Reading, Mass., Addison-Wesley, 1975

4 R. H. Stolen, 'Nonlinear properties of optical fibres' in: "Optical fibre telecommunications", S. E. Miller and A. G. Chynoweth, eds, New York, Academic Press 1979

5 - 'Nonlinearity in fibre transmission', Proc. IEEE **68**, 1232 (1980)

6 L. B. Jeunhomme,"Single mode fibre optics", Marcel Dekker Inc, 1983, chapter 9

7 L. F. Mollenauer, R. H. Stolen, and J. P. Gordon, 'Experimental observation of picosecond pulse narrowing and solitons and optical fibres', Phys. Rev. Lett **45**, 1095 (1980)

8 R. H. Stolen, 'Active fibres' in: "New directions in guided waves and coherent optics", NATO advanced study institute, Cargese 1982, D. B. Ostrowskii ed., Martinus Nijhof publ, Amsterdam 1982

9 A. M. Prokhorov, 'Nonlinear phenomena in fibre light guides', Bulletin of USSR Academy of Sciences, Phys. ser. **47**, part 10, 1 (1983)

10 R. H. Stolen, 'Applications of nonlinear phenomena in optical fibres', Proc. SPIE **613**, 156 (1983)

11 E. P. Ippen and R. H. Stolen, 'SBS in optical fibres', Appl. Phys. Lett. **21**, 539 (1972)

12 D. Cotter, 'SBS in a monomode optical fibre', J. Opt. Commun. **4**, 10 (1983)

13 K. O. Hill, B. S. Kawasaki, and D. C. Johnson, 'cw Brillouin laser', Appl. Phys. Lett. **28**, 608 (1976); 'cw generation of multiple Stokes and anti-Stokes Brillouin shifted frequencies', ibid. **29**, 185 (1976)

14 L. F. Stokes, M. Chodorow, and H. J. Shaw, 'All-fibre stimulated Brillouin ring laser with submilliwatt pump threshold', Opt. Lett. **7**, 509 (1982)

15 P. Bayvel and I. P. Giles, 'Evaluation of performance parameters of single mode all-fibre Brillouin ring lasers', Opt. Lett. **14**, 581 (1989)

16 P. Bayvel, J. Halley, R. Kadiwar, and I. P. Giles, 'Theoretical and experimental investigation of all-fibre single mode Brillouin lasers', ECOC'88 Conference Proc. part 1,

IEE Conf. Publ. **292**, pp 123-126

17 P. Bayvel and I. P. Giles, 'Linewidth narrowing in the semiconductor laser pumped single mode all-fibre Brillouin ring laser', Electron. Lett. **25**, 260 (1989)

18 P. Bayvel, P. Radmore, and I. P. Giles, 'Transient and steady-state characteristics of a Brillouin amplifier based on the all-fibre single mode ring resonator' - to be published in the special issue of Optical and Quantum Electronics on 'Optical Amplifiers', November 1989

19 P. Bayvel and I. P. Giles, 'Frequency generation by four wave mixing in an all-fibre single mode ring resonator', Electron. Lett. **25**, 1179 (1989)

20 P. Bayvel and I. P. Giles, 'Observation of Brillouin enhanced four wave mixing (BEFWM) in an all-fibre single mode ring resonator', to be published in Optics Communications

Chapter 2

THEORY OF STIMULATED BRILLOUIN SCATTERING (SBS)

In this chapter we explain the concept and physics of stimulated Brillouin scattering (SBS). Initially in section 2.1 we review the various mechanisms responsible for the *spontaneous* scattering of light, and subsequently introduce the idea of a *stimulated* scattering process, together with the basic equations describing the process. The main steps used in the derivation of equations which describe the SBS process are outlined in section 2.2, and it is shown how the physical constraints and characteristics in this process are clearly described through the mathematical treatment. The reasons for the difficulties in finding analytical (and numerical) solutions to the coupled equations and the validity of various approximations generally used in solving these equations are discussed, while in Section 2.3 the transient behaviour in the Brillouin scattering of the three waves is described qualitatively.

Much of the mathematical treatment of the SBS process in the bulk optical material and optical fibres follows similar lines with both the equations and their approximate solutions being quite general, and applying equally in the case of bulk material and optical fibres. However, while the important differences between the process in the bulk materials and optical fibres are pointed out, the full overview of SBS in optical fibres which concentrates more on the description of SBS in the practical context and on the experimental work, is covered in the next chapter.

2.1. Spontaneous scattering processes

Although the interest in the scattering of light can be traced back through the centuries to Leonardo da Vinci and Newton, Tyndall (1868) was the first to demonstrate the scattering of light off particles small compared to the wavelength of light. This work was continued

by Lord Rayleigh (1899), whose calculation for the intensity of light scattered by spherical particles, small compared with wavelength of light, led to the celebrated formula: $I \propto \lambda^{-4}$. That is, the intensity of the scattered light is inversely proportional to the fourth power of wavelength.

It is important to differentiate between impurity scattering and molecular scattering. The former arises from inhomogeneities and nonuniformities of the medium through which light propagates. One example of this is termed *Rayleigh scattering* - which is just scattering of light from material nonuniformities in the limit $X << 1$, where $X = 2\pi a/\lambda$, and a is the size of the nonuniformity. In other words, Rayleigh scattering occurs in the limit of the nonuniformity being smaller than the wavelength of light[3]. This scattering process is known as *elastic* since the frequency of the scattered light is unchanged compared to the incident light. In optical glass fibres, Rayleigh scattering is inevitable as it arises from two separate effects - density and composition fluctuations (see, for example, Midwinter[4]). The density variations originate from thermally induced fluctuations in the density of the liquid glass before solidification. Constituent oxides and dopants in optical fibre glasses result in composition fluctuations. Rayleigh scattering determines the absolute minimum loss in optical fibres.

Molecular scattering arises from fluctuations of the electric permittivity or the refractive index which are caused by well defined elementary excitations of the medium and can occur in a homogeneous and impurity-free medium. The fluctuations are caused by local variations in the thermodynamic state of the medium: pressure, density, temperature, and entropy. Such variations in the dielectric constant of the medium will affect the amplitude and phase of the scattered light. A particular variation or modulation in the amplitude and phase of a light wave will lead to a change in the spectral content of the initially monochromatic incident light. The spectral characteristics will be dependent on the type of modulating function, or in other words - on the time dependence of the amplitude and phase of the scattered light. The molecular scattering of light caused by such fluctuations in density and anisotropy, resulting in the fluctuation of the dielectric permittivity, is known as *spontaneous* scattering. The scattering processes which fall into this category are Brillouin, Raman, Rayleigh-center and Rayleigh wing scattering. The frequency spectrum of these is schematically illustrated in figure 2.1, and each process is described below.

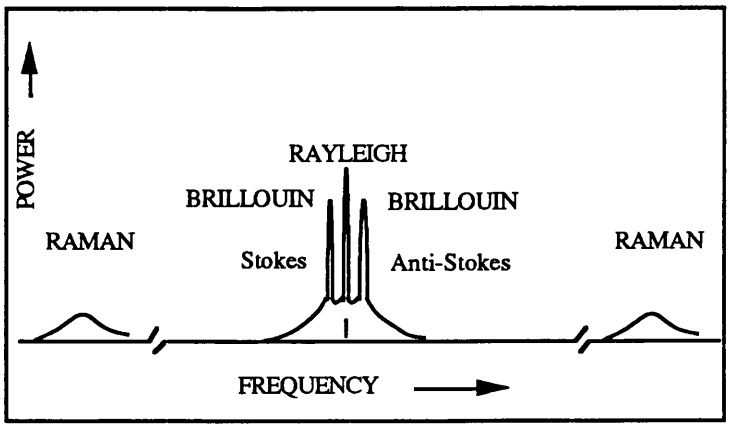

Figure 2.1. Schematic representation of the spontaneous scattering spectrum for Rayleigh, Brillouin and Raman scattering.

(a) *Brillouin scattering* is due to adiabatic fluctuations of density or fluctuations of pressure. These can be viewed classically to consist of propagating thermal *elastic* or sound waves. In other words, Brillouin scattered light arises from the variation in the electric permittivity caused by fluctuations in pressure (and density).

We can consider that each lattice vibration of frequency Ω, wave vector $\mathbf{q}$, will induce a perturbation in the dielectric constant, $\varepsilon_{q\,\Omega}$, so that the total perturbation to the dielectric constant ε is:

$$\varepsilon = \varepsilon_0 + \Sigma\varepsilon_{q\,\Omega}\exp j(\mathbf{q}.\mathbf{r} - \Omega t) = \varepsilon_0 + \delta\varepsilon \qquad (2.1)$$

When a plane monochromatic light wave $\mathbf{E_p}(\mathbf{r}, t) = E_p \exp j(\mathbf{k_p}.\mathbf{r} - \omega_p t)$ is incident on the medium, an excess polarisation $\delta\mathbf{P} = \delta\varepsilon\mathbf{E_p}$ is induced, which will give rise to a scattered field $\mathbf{E_S}(\mathbf{r}, t)$. The scattered field can be shown to be of the form[6]:

$$\mathbf{E_S}(\mathbf{r}, t) \propto \sum_{q,\,\Omega} \exp j\,[\mathbf{k_S}.\mathbf{r} - (\omega_p \pm \Omega)t] \int_{V'} \exp j[\mathbf{k_p} \pm \mathbf{q} - \mathbf{k_S}].\mathbf{r}'dV' \qquad (2.2)$$

The volume integral in eqn (2.2) gives a δ-function in $(\mathbf{k_p} \pm \mathbf{q} - \mathbf{k_S})$ which imposes wave vector conservation. Wave vector conservation from eqn (2.2), in fact, corresponds to the

Bragg matching condition which specifies the direction giving maximum diffraction:

$$\mathbf{k}_p - \mathbf{k}_S = \pm \mathbf{q} \tag{2.3}$$

The scattered light will, therefore, consist of two frequencies - $\omega_p \pm \Omega$ - which are symmetrical relative to the frequency of the incident light. The wave scattered with the negative shift is known as the *Stokes* wave, and the wave scattered with a positive shift is known as the *anti-Stokes* wave. The combination of the Stokes ($\omega_S = \omega_p - \Omega$) and anti-Stokes ($\omega_{AS} = \omega_p + \Omega$) frequencies is known as the Brillouin doublet, as shown in figure 2.1. From the quantum theory point of view, Brillouin scattering can also be viewed as due to propagating acoustic phonons (by analogy with the optical photons). Each lattice vibration can be described in terms of quanta (phonons) of energy $h\Omega$, and momentum $h\mathbf{q}$. Then scattering can be viewed as the creation and annihilation of a phonon, giving rise to the Stokes and anti-Stokes shifted lines, respectively.

Now, from equation (2.3) we obtain

$$|\mathbf{q}| = |\mathbf{k}_p - \mathbf{k}_S| \cong 2|\mathbf{k}_p| \sin(\theta/2) \tag{2.4}$$

where θ is the angle between the propagation vectors of the pump and the Stokes waves as shown in figure 2.2. It should be noted that the acoustic wave vector $\mathbf{q}$ is approximately a factor of 2 larger than the magnitude of the wave vectors corresponding to the pump and Stokes waves for backward scattering.

Analogously we can consider Bragg scattering of an incident pump wave from the thermally excited acoustic wave (with reference to fig. 2.2) where:

$$\lambda \text{ (in medium)} = \lambda_p/n = 2\lambda_a \sin(\theta/2) \tag{2.5a}$$

where λ_p, λ_a are the optical and acoustic wavelengths respectively, and n is the refractive index. Now, the Doppler shift associated with Bragg scattering from a moving grating is given by:

$$\omega_S = \omega_p \pm (v_a\, \omega_p c/n) \sin(\theta/2) = \omega_p \pm 2v_a n\, |k_p| \sin(\theta/2) \tag{2.5b}$$

where v_a is the sound velocity.

The Stokes light will be generated as a result of incident light scattered from the acoustic wave propagating away from it - or codirectionally with it for $\theta = 180^o$, and anti-Stokes light will be generated for the acoustic wave moving towards or contradirectionally with the incident light. Combining eqns (2.5a) and (2.5b) gives:

$$\omega_S = \omega_p \pm v_a |k_p| \lambda_p/\lambda_a = \omega_p \pm 2\pi v/\lambda_a = \omega_p \pm v_a|q| \qquad (2.6)$$

and since $v_a q = \Omega$,

$$\omega_S = \omega_p \pm \Omega \qquad (2.7)$$

as before. Rewriting (2.6) in standard form yields the expression for the *Brillouin frequency shift* or *Stokes shift*.

$$\Delta\omega_B = \Omega = \omega_p - \omega_S$$
$$= \pm 2v_a n|k_p| \sin(\theta/2) = \pm 4\pi n v_a \sin(\theta/2)/\lambda_p \qquad (2.8)$$

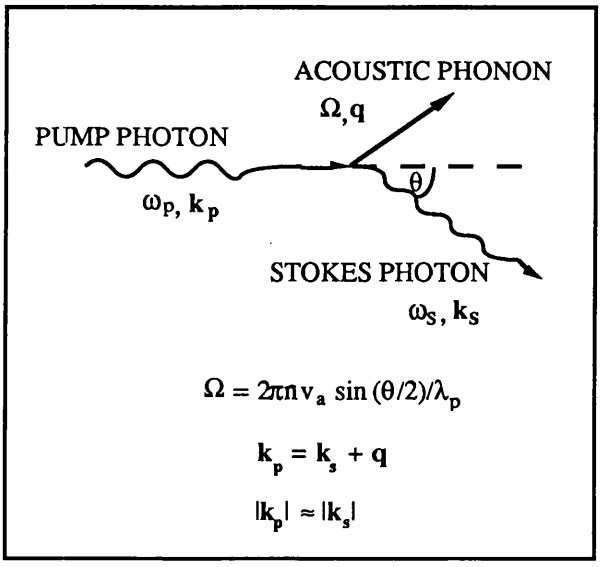

Figure. 2.2. Phasematching in the Brillouin scattering process for Stokes scattering [the direction of the acoustic phonon wave vector is reversed for anti-Stokes scattering].

Equation (2.8) was first derived by Brillouin (1922)[7] and independently by Mandelshtam (1926)[1, 8] - who share the name for this scattering process, which is referred to as Mandelshtam-Brillouin scattering in Soviet literature, and Brillouin (-Mandelshtam) in Western publications.

Equation (2.8) shows that the frequency shift in the Brillouin scattering process is a linear function of sin ($\theta/2$) so that the maximum shift is obtained for backscattering ($\theta = \pi$) and that the shift will tend to zero for $\theta \rightarrow 0$. This is particularly significant in the case of optical fibres, whose geometry will allow only forward or backward propagation - and therefore only backward Brillouin scattering will be observed. While Shelby et al.[9], and Rowell et al.[10] show that in the case of optical fibres, the acoustic wavelength will be comparable with the dimensions of single-mode fibre core, and so the acoustic wave may be guided, thus resulting in some forward scattering, this scattering will be many orders of magnitude smaller than the backscattering, and can be considered negligible in the applications dealt with later.

SBS was first demonstrated by Fabelinskii (1929), and comprehensive reviews of Brillouin scattering can be found in refs. [1], [6], [11]. Typical Brillouin shifts in optical glasses are 0.01 - 1 cm^{-1} corresponding to sound with frequencies equal to tens of gigahertz. Sound with such high frequencies is known as *hypersound*.

(b) Other scattering process depicted in figure 2.1. When the light is scattered by inter-molecular vibrations or optical phonons, the process is known as *Raman* scattering. Named after its discoverer, this effect was first reported in 1928[1,2], before the Brillouin-Mandelshtam theory was confirmed by experiment. The various frequency shifts (100 - 1000 cm^{-1}) generated in this process are determined by different vibrational frequencies of the molecules. For each molecular vibration, two lines will be generated: Stokes and anti-Stokes lines are connected with transitions from the ground to the excited state, and vice versa. An enormous bibliography exists for Raman scattering - a process, which has proved a very valuable molecular spectroscopic tool[4, 12,13]. Briefly, the other spontaneous scattering process mentioned are elastic: the unshifted narrow *Rayleigh-centre* line is caused by scattering due to non-propagating entropy fluctuations or isobaric density fluctuations, while the unshifted broad line *Rayleigh wing* scattering is due to orientation fluctuations of anisotropic molecules. Because of relatively small deviations of atoms from

their equilibrium positions compared with the inter-atomic spacing means that these molecular scattering processes will be negligible in solids, whether spontaneous or stimulated[1,2,12]. We, therefore, will not consider these processes any further, but detailed accounts of these can be found in numerous texts, including Fabelinskii[1], Kaiser and Maier[12], and Landsberg[5]. Depending on the experimental conditions Brillouin or Raman scattering will be the dominant inelastic scattering processes.

2.2. Stimulated Brillouin scattering (SBS)

So far we have discussed the cases of light scattering in which optical inhomogeneities affected the the characteristics of propagation of incident light, and the effect of the intensity of light on the optical properties of the medium was not considered. When the intensity of incident light is small, its effect on the optical properties is negligible, and can be ignored. However, at high intensities of incident light, the effect of the incident and the scattered light on the character of motion of the medium begins to play a significant role. The effect of a very high optical intensity on a medium leads to a series of nonlinear effects. One type of such effects is known as *stimulated scattering*. All the spontaneous scattering processes described above have their stimulated counterparts. However, stimulated Brillouin scattering is a nonlinear effect which occurs at lowest optical intensities, and it is therefore of most interest in optical fibres in relation to this work. Stimulated Raman scattering is also an important effect in fibres, and in the course of the discussion, similarities and distinctions between the two processes will be highlighted. All other molecular scattering processes, whether spontaneous or stimulated, are negligible in optical glasses in the range of the milliwatt optical powers of interest.

Stimulated Brillouin scattering can be explained as follows. When an intense optical signal, known as the *pump*, is incident on a material - an elastic wave of high intensity may be generated. This occurs if the electric field associated with an intense optical pump beam acts on a body to produce pressure in the medium leading to the effect of electrostriction which in turn produces an *elastic* or a *pressure* wave. The induced pressure wave can lead to scattering of the pump wave. The interaction of these can be explained by stimulated scattering, and can be considered entirely classically.

When an intense optical pump is incident on the material, the excess pressure produced by

the electric field associated with the optical wave (through electrostriction) can be shown to be

$$|\Delta p| = (\rho_0 \varepsilon_0 \partial\varepsilon/\partial\rho)E^2/2 \qquad (2.9)$$

where ρ_0 is the density. This is found by equating the work done in straining a unit volume $\Delta p \partial u/\partial x$, where $\partial u/\partial x$ is one-dimensional strain due to the change in energy density, $1/2\gamma_e(\partial u/\partial x)E^2$. γ_e is the electrostrictive coefficient, $\varepsilon_0\rho_0\partial\varepsilon/\partial\rho$ which is related to the Pockels elasto-optic or strain-optic coefficients. In fact, as the scattering arises from fluctuations in the dielectric constant - and these are caused by the strains produced by sound waves, the elasto-optic coefficients are defined by[14,15]:

$$\delta\left(\frac{1}{n^2}\right)_{ij} = \delta(\varepsilon_0\,\varepsilon^{-1})_{ij} = \sum_{kl} p_{ijkl} S_{kl} \qquad (2.10a)$$

where the strain tensor components, S_{kl} are related to the elastic deformation components, u_k along the coordinate axes x_k by $S_{kl} = 1/2[\partial u_k/\partial x_l + \partial u_l/\partial x_k]$. In the case of an isotropic solid, there are only two independent coefficients, p_{12} and p_{44}. So that eqn (2.10a) now reduces to:

$$\delta\varepsilon_{ij} = -\,\varepsilon_0\,\varepsilon^2\left[2p_{44}S_{ij} + p_{12}\{\sum_l S_{kk}\}S_{ij}\right] \qquad (2.10b)$$

The Pockels constants are related to the change in the dielectric constant caused in hydrostatic compression according to[14,15]:

$$\frac{\varepsilon_0\,\partial\varepsilon}{\partial\rho} = \frac{\varepsilon^4}{\rho_0}\{p_{12} + \frac{2}{3}p_{44}\} \qquad (2.10c)$$

Hence, the change in the dielectric permittivity can be easily related to material parameters (for further details see, for example references [12] -[15]), and the significance of this will be discussed in more details in the section dealing with material considerations.

The next step is to show the physical significance of eqn (2.9).by using the well-known approximation (for example refs. [1], [16]: the assumption is that the field in eqn (2.9)

consists of the sum of the incident pump wave $E_p\cos(\omega_p t - \mathbf{k_p}.\mathbf{r})$, the Stokes wave $E_S\cos[(\omega_p - \Omega)t - \mathbf{k_S}.\mathbf{r}]$, and the anti-Stokes wave $-E_{AS}\cos[(\omega_p - \Omega)t - \mathbf{k_{AS}}.\mathbf{r}]$ (these arose in the medium as a result of thermal (spontaneous) scattering). After squaring the three terms and using the identities $\cos A\cos B = 1/2\{\cos(A+B) + \cos(A-B)\}$, and $\cos^2 A = 1/2(1 + \cos 2A)$, equation (2.9) becomes:

$$
\begin{aligned}
|\Delta p| = (\rho_0\varepsilon_0\partial\varepsilon/\partial\rho)\{ & E_pE_S\{\cos[(2\omega_p - \Omega)t + (\mathbf{k_p} - \mathbf{k_S}).\mathbf{r}] + \cos[\Omega t - (\mathbf{k_p} - \mathbf{k_S}).\mathbf{r}]^*\} + \\
& E_pE_{AS}\{\cos[(2\omega_p + \Omega)t - (\mathbf{k_p} + \mathbf{k_{AS}}).\mathbf{r} - \cos[\Omega t - (\mathbf{k_p} - \mathbf{k_{AS}}).\mathbf{r}]^*\} + \\
& E_{AS}E_S\{\cos[2\omega_p t - (\mathbf{k_{AS}} + \mathbf{k_S}).\mathbf{r}] + \cos[2\Omega t - (\mathbf{k_{AS}} - \mathbf{k_S}).\mathbf{r}]^* + \\
& E_p^2\{1 + \cos 2[\omega_p t - \mathbf{k_p}.\mathbf{r}] + \\
& E_S^2\{1 + \cos 2[(\omega_p - \Omega)t - \mathbf{k_S}.\mathbf{r}] + \\
& E_{AS}^2\{1 + \cos 2[(\omega_p + \Omega)t - \mathbf{k_{AS}}.\mathbf{r}] \qquad (2.11)
\end{aligned}
$$

Now, this means that Δp consists of high frequency components at optical frequencies ω_p and $2\omega_p$, and hypersonic frequency components Ω and 2Ω. Clearly, the acoustic (pressure wave) cannot propagate at optical frequencies (the maximum acoustic vibration frequency is limited by the intermolecular spacing) and these components can be set to zero. Considering only the second terms of the cross-products*, it can be seen that if the pump propagates along the direction of its vector $\mathbf{k}$ (isotropic medium), and the Stokes wave in the opposite direction ($\theta = 180^o$), then the first component* gives the acoustic or pressure wave coinciding exactly with the original thermal acoustic wave, since $\mathbf{k_p} - \mathbf{k_S} = \mathbf{q}$, and the acoustic wave propagates in the same direction as $\mathbf{k_p}$ (since $|\mathbf{k_p}| > |\mathbf{k_S}|$). The second term gives a wave of this same frequency and phase, since $|\mathbf{k_{AS}}| > |\mathbf{k_p}|$, and consequently $\mathbf{k_{AS}} - \mathbf{k_p} = 2\mathbf{q}$. An acoustic wave of double frequency is similarly propagated in this direction. Thus, although the field of the scattered waves originally arose as a result of two thermal waves of single frequency Ω and opposite directions of propagation $\pm\mathbf{q}$, the wave of the same frequency and phase as the thermally excited acoustic wave which produces the Stokes component is amplified as a result of the electrostriction alone. The anti-Stokes component of stimulated scattering cannot appear in this approximation (this point is further clarified in Appendix A). As far as the Stokes component is concerned, it is clearly amplified, because the wave produced by electrostriction is added to the thermally excited wave, being identical with it in frequency and phase. Although E_S is initially small, because the pump intensity is very high, the product E_pE_S is sufficient such that the Stokes component increases the intensity, and this, in turn, leads to an increase in Δp and so on... In this process of parametric amplification,

the energy is transferred from the pump wave into Stokes wave and the acoustic wave. Thus backscattering as a result of parametric radiation for sufficient intensities of the pump wave can be used as a useful local oscillator source, emitting at a frequency of $\omega_p - \Omega$. Most of the work in this thesis is concerned with applications of this property.

2.2.1. Derivation of the steady-state SBS equations

Having described the background to the origin of the SBS process in the previous section, we can derive the equations governing the process in this section. [For most of the analysis we follow the work of authors of refs. 11, 12 and 18]. The starting point in the derivation of the SBS equations are Maxwell's equations with a nonlinear polarisation term. In linear situations, the polarisation is proportional to the electric field, where χ_{ij} - the linear susceptibility, is the proportionality constant. At high electric fields, χ_{ij} is no longer independent of field, and it is possible to write the polarisation induced in the medium as a power series:

$$P_i = \sum_j \chi_{ij}^{(1)} E_j + \sum_{j,\,k} \chi_{ijk}^{(2)} E_j E_k + \sum_{j,\,k,\,l} \chi_{ijkl}^{(3)} E_j E_k E_l + \ldots \qquad (2.12)$$

In isotropic materials, the induced polarisation is always parallel to the electric field, and is related to it by a scalar factor (the susceptibility) that is independent of the direction in which the field is applied. In anisotropic materials the latter is no longer true, and the linear susceptibility, χ_{ij} is responsible for natural birefringence, Faraday rotation and optical activity. The second term of eqn (2.11) is connected with mixing of two light fields, parametric amplification and oscillation, frequency doubling, and Pockels effect. The third term describes several processes, including third harmonic generation, self-focussing, Kerr effect, and stimulated light scattering. For a rigorous description of the third order susceptibility, see, for example, Shen[13] and Hellwarth[17].

As already mentioned, the density variation in the material perturbs the dielectric permittivity and produces a proportional variation in dielectric constant, $\delta\varepsilon$. This, in turn gives rise to nonlinear polarisation, $\mathbf{P}^{NL}$ which is $\delta\varepsilon\mathbf{E}$, so that,

$$\mathbf{P}^{NL} = \frac{\partial \varepsilon}{\partial \rho} \Delta\rho \mathbf{E} \tag{2.13}$$

where the nonlinear polarisation term does not include the variation of the dielectric constant with temperature, since the latter is small compared with the former[11, 12].

Maxwell's equations which incorporate the nonlinear polarisation term are:

$$\nabla \times \mathbf{H} = \alpha_o n \sqrt{\frac{\varepsilon_0}{\mu_0}}\, \mathbf{E} + \frac{\partial \mathbf{D}}{\partial t} \tag{2.14a}$$

and

$$\nabla \times \mathbf{E} = -\mu_0 \mu_r \frac{\partial \mathbf{H}}{\partial t} \tag{2.14b}$$

where the **D** is the electric displacement vector, and is given by:

$$\mathbf{D} = \varepsilon_0 \varepsilon \mathbf{E} + \mathbf{P}_{NL} \tag{2.14c}$$

where we have assumed an isotropic material with $\varepsilon = (1 + \chi_e)$, and the linear susceptibility χ_e is a tensor; $\mathbf{P}^{NL}$ is the nonlinear polarization vector, as before. In eqn (2.14a), the linear attenuation term is included. α_o represents optical losses, and the first term of (2.14a) having units of current density (Am^{-2}), and $[\alpha_o n(\varepsilon_0/\mu_0)^{1/2}]$ having units of conductivity ($\Omega^{-1}m^{-1}$). Moreover, we assume that in non-magnetic materials $\mu_r \approx 1$, so that $\mu_r\mu_0 \approx \mu_0$.

Now, taking curl of both sides of eqn (2.14b) and using the vector identity

$$\nabla \times \nabla \times \mathbf{e} = \nabla(\nabla \cdot \mathbf{e}) - \nabla^2 \mathbf{e}$$

together with the fact that when there are no free charges, from Gauss's theorem, $\nabla \cdot \mathbf{E} = 0$, we get:

$$\nabla^2 E = \mu_0 [\alpha_o n \sqrt{\frac{\varepsilon_0}{\mu_0}} \frac{\partial E}{\partial t} + \varepsilon\varepsilon_0 \frac{\partial^2 E}{\partial t^2} + \frac{\partial^2 P^{NL}}{\partial t^2}]$$

where **E** and **B** are the electric and magnetic vectors respectively, α_o is the power absorption coefficient n is the refractive index. Simplifying, using the fact that $1/(\mu_0\varepsilon_0)^{1/2} = c$, the speed of light in a vacuum, and $n = \varepsilon^{1/2}$ we obtain the wave equation with the nonlinear polarisation term as:

$$\nabla^2 E = \alpha_o \frac{n}{c} \frac{\partial E}{\partial t} + \frac{n^2}{c^2} \frac{\partial^2 E}{\partial t^2} + \mu_0 \frac{\partial^2 P^{NL}}{\partial t^2} \qquad (2.15a)$$

The equation for the density variation which describes the driven acoustic wave is derived from the linearised hydrodynamic equation for density (where $\rho = \rho_0 + \Delta\rho$). Together with the continuity equation and the Navier-Stokes equation for density variation which determines the damping of the sound wave, the density variation is described by[12, 13, 16]:

$$\frac{\partial^2 \rho}{\partial t^2} - \gamma_a \nabla^2 \frac{\partial \rho}{\partial t} - v_a^2 \nabla^2 \rho = -\nabla^2 (\Delta p) \qquad (2.15b)$$

where Δp is the electrostrictive pressure as given in eqn (2.9), γ_a is (for solids and liquids) equal to $(4/3)\eta$, where η is the shear viscosity and characterises the damping of acoustic waves. We also define the acoustic damping constant, Γ where $\Gamma = \gamma_a q^2$. An important relationship is also $\Gamma = \alpha_a v_a$, where α_a is the acoustic attenuation coefficient, with $2\pi\Gamma^{-1}$ is the characteristic acoustic damping time, and $2/\alpha_a$ is the acoustic attenuation length. [It should be noted that there is a factor of 2π difference between the acoustic damping time and the inverse of acoustic damping constant Γ, which will also be shown in eqn (2.23). In the literature, a discrepancy of a factor of 2π is often noted in the quoted values of the acoustic damping constants, often causes confusion and unexplained discrepancies].

For most experiments on isotropic media, specifically optical glasses, the acoustic waves

excited in the stimulated Brillouin process are in the microwave frequency range, and at room temperature are heavily damped. Typically, the attenuation length will be approximately 10^{-4} m and is proportional to the square of the acoustic wavelength[18]. With such a heavy acoustic loss, it can be assumed that photoelastically induced acoustic oscillation will not develop, and one can expect on the basis of the form of the damping terms in eqn (2.15b), the transient solutions to 'damp out' roughly in the time of the order of the acoustic damping time. Using data available on acoustic attenuation in optical glasses, [see for example, Heiman et al.[14]], this will be typically of the order of 10^{-7} - 10^{-8} seconds. It is therefore reasonable in most experimental situations, especially when using cw pumping to consider the steady-state solutions of the nonlinear equations (2.15a) and (2.15b). There are two important experimental situations in which the steady-state approximation is not valid. The first is the case of pulsed pumping, with pulse duration shorter than the acoustic damping time and transient effects associated with finite decay time of the acoustic wave (= $1/\Gamma$) become important. This must be differentiated from the second case which is concerned with relaxation oscillations; these are due to depletion of the gain, and may be much longer than the former. Although, the work in this thesis has not been concerned in detail with either of these effects, they may be important, and are explained qualitatively in Section 2.3.

2.2.2. Steady-state solutions of the SBS equations

We are now in the position to obtain the equations describing the relationship between the pump, Stokes, and acoustic fields. It is possible to write down the expression for the total electric field in the material as the sum of plane pump and Stokes waves, with slowly varying amplitudes. It is assumed (the significance of this will be discussed in the section on polarisation properties of SBS) that the pump, Stokes, and acoustic waves propagate in the z-direction, with the electric field polarized in the x-direction, so that:

$$\mathbf{E}(z, t) = E(z, t)\,\mathbf{x} \tag{2.16}$$

Then, for real field (using scalar quantities):

$$E(z, t) = \frac{1}{2}\{E_p(z)\exp j\,[k_p z - \omega_p t] + E_p^*(z)\exp - j[k_p z - \omega_p t] + E_s(z)\exp - j[k_s z + \omega_s t] + E_s^*(z)\exp j[k_s z + \omega_s t]\} \tag{2.17}$$

The acoustic wave is also monochromatic:

$$\Delta\rho(z, t) = \frac{1}{2}\{A(z) \exp j[q z - \Omega t] + c.c\} \qquad (2.18)$$

Equations (2.17) and (2.18) can now be substituted into eqns (2.15a) and (2.15b). Since we are considering steady state solutions all time derivatives can be set to zero.

The slowly varying approximation essentially means that the amplitude factors for the forward-travelling pump and acoustic waves and the backward travelling Stokes wave are always slowly varying functions of z when compared with the exponential propagation factors in equations (2.17) - (2.18), or: k_p, k_S, $q >> |1/E_p(z).\partial E_p(z)/\partial z|$, $|1/E_S(z)\partial E_S(z)/\partial z|$, $|1/A(z).\partial A(z)/\partial z|$. After some simplification, equations (2.15a) and (2.15b) reduce to, for pump and Stokes waves[11,12]:

$$\frac{\partial E_p(z)}{\partial z} + \frac{\alpha_o}{2}E_p(z) = \frac{j\omega_p}{cn}\frac{\partial \varepsilon}{\partial \rho}E_p(z)\, A(z) \exp [j\Delta kz] \qquad (2.19a)$$

$$\frac{\partial E_S(z)}{\partial z} - \frac{\alpha_o}{2}E_S(z) = -\frac{j\omega_S}{cn}\frac{\partial \varepsilon}{\partial \rho}E_S(z)\, A(z) \exp - [j\Delta kz] \qquad (2.19b)$$

and, for the acoustic wave,

$$\frac{\partial A(z)}{\partial z} + \frac{\alpha_a}{2}A(z) = jq\frac{\varepsilon_0\rho_0}{2}\frac{\partial \varepsilon}{\partial \rho}E_p(z)E_S^*(z) \exp [j\Delta k] \qquad (2.19c)$$

where Δk is the phase mismatch, and is equal to $(k_p + k_S - q)$.

[Although we do not go into considerable detail here, in order to have a clearer picture of the relationship between the pump, Stokes, and acoustic waves in the SBS process, we return to the physical consideration of the scattering by adopting a diffraction grating description of this process in Appendix A].

Clearly further approximations are needed to simplify the solution of this system of three coupled differential equations - where we can set the partial derivatives to straight derivatives in the steady-state case. Tang[18] in his paper on stimulated Stokes emission points out that as the rate of acoustic loss is very high compared to the rate of change of $E_S(z)$ and $E_p(z)$ due to both stimulated scattering or optical losses. In other words, $\alpha_a >>$

$|1/E_p(z).\partial E_p(z)/\partial z|$, $|1/E_S(z).\partial E_S(z)/\partial z|$. Equation (2.19c) is then just a first order differential equation dy/dx + ky = f(x), the solution to which can be expressed as:

$$y(x) = \int_0^x \exp\,[f(x') - k]\,x'dx' + y(0)$$

Similarly,

$$A(z) = \frac{j\gamma q}{4} E_p(z)E_S^*(z)\int_0^{z'} \exp\,[j\Delta k z' - \alpha_a/2](z - z')\,dz' + A(0)\exp - (\alpha_a/2)z \qquad (2.20)$$

Tang was the first to make the following, now generally accepted approximation. He pointed out, that due to the factor $\exp\,[-\alpha_a/2(z - z')]$, in the integrand, the major contribution to the integral must come from the range $(z - z') \leq 2/\alpha_p$. Following these conditions the *E*-field factors have been taken outside the integral and evaluated at z' = z, so it is possible to integrate directly:

$$A(z) = \frac{j\gamma q\, E_p(z)E_S^*(z)}{4\ (j\Delta k + \frac{\alpha_a}{2})}\,[\exp\, j\Delta k z - \exp - \frac{\alpha_a}{2}z] + A(0)\exp - \frac{\alpha_a}{2}z$$

$$\approx \frac{j\gamma q\, E_p(z)\, E_S^*(z)}{4\ (j\Delta k + \frac{\alpha_a}{2})}\exp\,[j\Delta k z] + A(0)\exp - \frac{\alpha_a}{2}z \qquad (2.21)$$

for $z >> (2/\alpha_a)$. The physical implication of eqn (2.21) is as follows. For negligible A(0), except for within the distance of $2/\alpha_a$ from the boundary z = 0, the acoustic intensity (proportional to $|A(z)|^2$, where A(z) is the amplitude of the acoustic wave or pressure, and was given in eqn (2.18) is approximately proportional to the product of the pump and Stokes intensities. Since these intensities decay in the forward, + z-direction, eqn (2.21) implies that the acoustic intensity actually builds up from its boundary value to a peak in a distance of $2/\alpha_a$, and then decays in the forward direction. If the acoustic loss was negligible, the acoustic wave would build up in the forward direction. Eqn (2.21) also shows that the acoustic intensity is inversely proportional to the denominator $[(\Delta k)^2 + (\alpha_a/2)^2]$. This characterises the interaction (or scattering) strength in terms of the frequency detuning from the optimum phase matching condition of $\Delta k = 0$, which is more frequently expressed as:

$$\Delta k = \frac{\omega_p}{c} - \frac{\omega_s}{c} - \frac{\Omega}{v_a}$$

and since $\omega_p - \omega_S = \Omega$

$$\Delta k = \frac{1}{v_a}[\frac{\Omega v_a}{c} - \Omega]$$

or if $\Omega v_a/c = \Omega'$, then

$$\Delta k = \frac{1}{v_a}[\Omega' - \Omega] \qquad (2.22)$$

In addition, there is clearly a bandwidth associated with the scattering process, even in the case when the phase matching condition is satisfied, which depends on the acoustic attenuation. That is,

$$\Gamma = \alpha_a v_a = 2\pi \ \Delta\upsilon_B \qquad (2.23)$$

where Γ is the acoustic damping constant (as defined before) and $\Delta\upsilon_B$ is the FWHM intrinsic Brillouin bandwidth, in Hz. This imposes a condition that the linewidth of the pump should be much less than $\Delta\upsilon_B$ for efficient scattering. Indeed, this is one of the principal differences between the experimental conditions necessary for observation of Raman and Brillouin processes. Efficient SBS requires a spectrally narrow pump, while stimulated Raman scattering is effectively a broadband process, which requires high pump intensities. Thus a spectrally narrow, single-frequency, low power pump will favour Brillouin scattering, while a high power broadband source will favour SRS.

Substituting eqn (2.22) into (2.19a) and (2.19b) and using $I = n\varepsilon_0 c|E|^2/2$, we obtain the following system of coupled equations:

$$\frac{dI_p(z)}{dz} = - g_B I_p(z) I_S(z) - \alpha_o I_p(z) \qquad (2.24a)$$

$$\frac{dI_S(z)}{dz} = - g_B I_p(z) I_S(z) + \alpha_o I_S(z) \qquad (2.24b)$$

where g_B is the Brillouin gain coefficient. Making use of the equation (2.24), it can be shown that[12, 16]:

$$g_B = \frac{\omega_p q}{2c^2 n^2 \rho_0 v_a^2 \alpha_a} \frac{\partial \varepsilon}{\partial \rho} \left[\frac{1}{1 + \{\frac{\Omega' - \Omega}{\alpha_a v_a}\}^2} \right] \qquad (2.25)$$

where g_B is proportional to the imaginary part of the third order susceptibility $\chi^{(3)}$ as given in equation (2.12). Since q is proportional to ω_p and α_a is proportional to ω^2, g_B is approximately independent of optical frequency (the speed of sound and other material parameters are not strongly frequency dependent). The variation of g_B with material parameters is discussed in the section on material considerations. The frequency dependence of the Brillouin gain is reflected in the denominator of (2.25), and in most of the work described it is assumed (unless stated otherwise) that the frequency mismatch $\omega_p - \omega_S - \Omega = 0$, and $\Delta k = 0$, and in all further discussion it is assumed that g_B is the peak Brillouin gain coefficient. One important case relevant to this work when the frequency mismatch should be considered is in Brillouin amplification, when an external signal at the Stokes frequency is input co-directionally with the Brillouin backscattered wave to be amplified. If the frequency of this external signal was to drift from the exact Stokes frequency, it would experience a diminished gain. This is of particular importance to Brillouin fibre amplifiers and will be discussed later. Another important factor which does not appear in the above equation is that of depolarisation, P; this factor characterises the degree of polarisation matching between the pump and the Stokes waves: 0 for completely mismatched polarisations to 1 (for pump and Stokes with identical polarisation). In the derivation of the Brillouin equations we have assumed that the polarisations of the interacting waves are linear and coinciding with each other. In this case, the above expression of the Brillouin gain coefficient applies. In Appendix B, the polarisation properties of SBS are considered, and the effects of polarisation mismatch between the pump and Stokes waves is shown. In particular, in optical fibres, because of long interaction lengths, polarisation scrambling may lead to polarisation mismatch between the pump and the Stokes wave, and hence to a reduction of the Brillouin gain coefficient g_B, which in this case should be multiplied by a factor P which varies between 0 and 1 (this is further discussed in the context of practical systems in the next two chapters), and is generally taken as 1/2 for ordinary fibre. [In order to minimize the polarisation mismatch, polarisation maintaining fibre can be used in which P equals 1].

It can also be noted that the gain coefficient is a function of the intrinsic Brillouin bandwidth, $\alpha_a v_a$. It is perhaps worth discussing the significance of this. As was mentioned previously, efficient Brillouin scattering demands that the pump linewidth, $\Delta\upsilon_p$ should be smaller than the Brillouin linewidth. If this condition is not fulfilled, and $\Delta\upsilon_p \approx \Delta\upsilon_B$, the gain coefficient becomes:

$$g_B' = g_B \frac{\Delta\upsilon_B}{\Delta\upsilon_p \otimes \Delta\upsilon_B} \qquad (2.26)$$

where $\otimes$ denotes convolution of the pump light linewidth and the Brillouin bandwidth; for Gaussian profiles $\Delta\upsilon_p \otimes \Delta\upsilon_B = (\Delta\upsilon_p + \Delta\upsilon_B)^{1/2}$ and for Lorentzian profiles $\Delta\upsilon_p \otimes \Delta\upsilon_B = (\Delta\upsilon_p + \Delta\upsilon_B)$. Equation (2.26) is plotted in fig. 2.3 for these two cases, and shows the gain reduction as a function of the pump linewidth. It should be noted that (2.26) reduces to (2.25) for $\Delta\upsilon_p << \Delta\upsilon_B$. This is of particular practical significance in the cases when semiconductor laser pumping is used. This is especially relevant in optical fibre systems where the broader spectral linewidths of semiconductor lasers are comparable to the Brillouin bandwidth, particularly at longer wavelengths in the near IR region of the spectrum, and accounts for the difficulty of observing highly efficient SBS with semiconductor laser pumping. This is one of the problems which has been approached and investigated in this work.

The effect of having a multimode pump on the Brillouin gain has been considered by a number of authors, notably by Dyakov[19], Valley et al.[20], Narum et al.[21] in liquids, and Lichtman et al.[22,23] in optical fibres. Two specific cases emerge from their work, which can be summarised as follows. Firstly, in the case of a pump consisting of N narrow linewidth modes, spaced by more than the Brillouin gain bandwidth, the gain coefficient will be reduced to g_B/N. The case when the pump modes lie within the Brillouin bandwidth is more complicated, since this situation allows interactions not only between corresponding pump and Stokes modes but also 'cross' interactions between other pump and Stokes modes within the bandwidth. Depending on the relative phase between the optical modes affecting their interference, such interactions may enhance or suppress the Brillouin gain. This was confirmed experimentally in ref. [22], and is again of importance in consideration of SBS in relation to optical fibre systems.

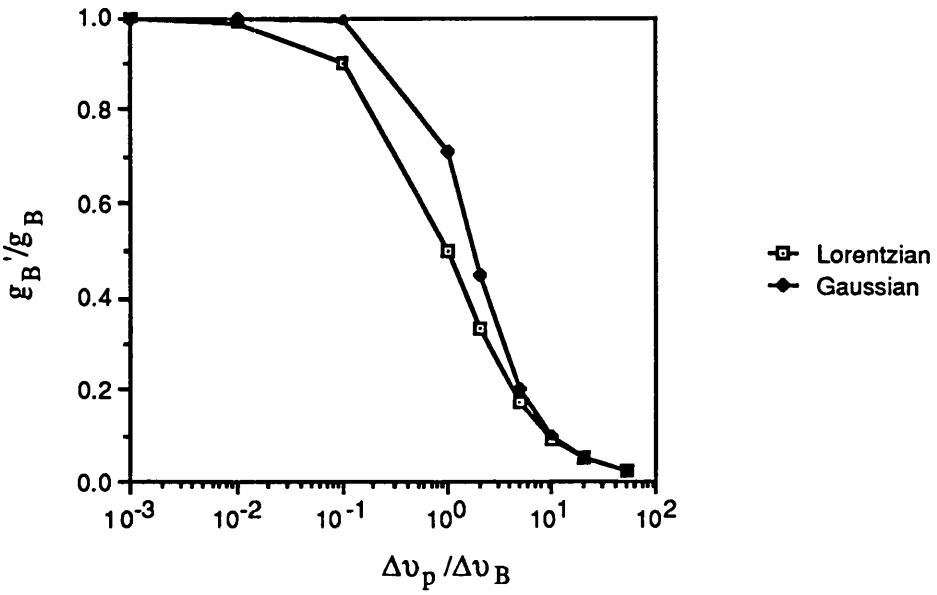

Figure 2.3. Showing the dependence of the Brillouin gain the pump linewidth for Lorentzian and Gaussian profiles [from eqn (2.26)].

Before reviewing possible solutions of equations (2.24), it is important to explain the form of these equations, and why they are interesting. It can be seen from the rate equations for the pump and the Stokes wave that both the pump and the Stokes wave *decrease* in the + z direction, whilst the attenuation term [$\alpha_o I_{p,S}$] is applied in different directions. This is so, because the Stokes wave propagates in the opposite direction to the pump wave, and in the case of zero losses ($\alpha_o = 0$), will be amplified in the - z direction, with the rate of amplification equaling the rate of loss of the pump intensity in the +z direction of propagation. In the case of finite attenuation, the - αI_S term is in the - z direction. As the equations describe the variation of the pump and the Stokes intensities in the +z direction, this explains the significance of the signs in the above equations. Thus, to solve these equations, the boundary condition on $I_p(z)$ should be applied at z = 0; but, since the Stokes wave propagates backwards, the boundary condition on $I_S(z)$ is applied at z = L where L is the length of the interaction region. This is illustrated in fig. 2.4.

In fact, this property makes the solution of these equations analytically - impossible. Whilst equations describing the pump and Stokes waves in stimulated Raman scattering

process (where the pump and Stokes propagate co-directionally) have been solved by various authors (see for example ref. [24]), analytical solutions for SBS are not available.

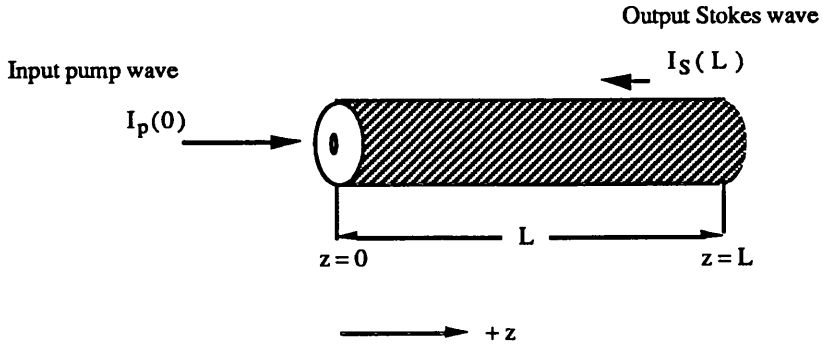

Fig. 2.4. Schematic diagram showing the incident pump beam of intensity, I_p and the backscattered Stokes wave, I_S in a length of optical material, L.

The difficulty is caused by having the attenuation terms of different signs, and the equations have been solved analytically with numerous approximations, which are discussed in the following section.

It can also be noted from these equations, that for the case of finite loss, at a certain pump intensity, the Stokes wave will be amplified when the Stokes gain $g_B I_p(z) \geq \alpha_o$ is equal or exceeds the absorption losses. Indeed, in the early work on SBS it was usual to define the condition for the amplification of the Stokes wave in the SBS process, as the threshold of the process, and the threshold pump intensity as the intensity required so that the Stokes gain is equal to or greater than the absorption losses, such that:

$$g_B I_p(0) \geq \alpha_o \quad \text{and:} \quad I_p(0) \geq \frac{\alpha_o}{g_B} \tag{2.27}$$

Indeed, in the first experimental observations of SBS in quartz and sapphire by Chiao et al. (1964)[25], and in the early studies of SBS this criteria was applied, although the experimentalists observed that pump intensity significantly higher than threshold was necessary to observe any significant increase in the Stokes intensity. Since the work in this

thesis has not been concerned with bulk solids or liquids, these studies are not discussed, and it suffices to mention that comprehensive reviews of the early work on SBS can be found in references [1], [12], [13]. It is perhaps worth mentioning the application of SBS in phase conjugation which has dominated the research in this area in recent years, as we will refer to it in later discussion. This application was originally suggested by Zeldovich et al.[26] who showed that the the Stokes wave generated through SBS is in fact phase conjugated with respect to the pump wave. This arises as a result of a very high effective gain in the SBS process, which can be shown to be maximum for the Stokes field whose local maxima coincide with the maxima of the pump field everywhere in space[16]. On propagation, both the pump and Stokes fields vary due to diffraction and interference, so that intensity inhomogeneities are maintained coordinated throughout the scattering volume only if the scattered Stokes field is phase conjugated with respect to the pump field, that is $\mathbf{E_S} \propto \mathbf{E_p}^*$. In this way, the physical mechanism for phase conjugation through SBS is based on preferential amplification of conjugated components of the Stokes wave in the field of an inhomogeneous pump wave.

Following the early studies of Zeldovich et al.[26] and Nosach et al.[27], numerous studies have been carried out in bulk solids and liquids[28-30], and multimode optical fibres[31,32] to investigate the feasibility of applications of this effect for phase correction of distortions both in high power lasers and in phase conjugate mirrors in laser resonators. The main disadvantages of this method of phase conjugation are the threshold nature of SBS which requires a high power for the wave to be conjugated, and a reflection coefficient (that is the ratio between the Stokes and pump intensities) which is always less than 1. For these reasons, an alternative method of phase conjugation utilising the Brillouin nonlinearity and known as the Brillouin enhanced four wave mixing (BEFWM) has been proposed, and which we shall discuss in more detail in Chapter 8.

2.2.3. Approximations used in solving equations (2.24)

As mentioned in the previous section, the form of the SBS equation, complicated by the presence of attenuation terms of different signs, precludes analytical solutions. The normal procedure for solving a system of coupled differential equations is to add (or subtract), and then to linearise the equations (the procedure which is followed in the solution of the

analogous equations describing the codirectional Raman process). However, in this case, addition yields

$$d(I_p(z) + I_S(z))/dz = - 2g_B I_p(z) I_S(z)$$

which leads to a complex integro-differential equation, which has to be solved numerically. Subtraction yields a fairly obvious result that

$$d(I_p(z) - I_S(z))/dz = - \alpha_o (I_p(z) + I_S(z))$$

Indeed, in the solutions of these equations, one of two following approximations is generally adopted.

a) zero optical loss approximation, $\alpha_o = 0$

If $\alpha_o = 0$, the solution of the above equations becomes much easier. These equations can now be linearized to yield transcendental solutions. Subtraction of one from the other in this case gives: $d(I_p(z) - I_S(z))/dz = 0$; Therefore $I_p(z) - I_S(z) = k$ (constant). This last expression is a re-statement of the conservation of energy condition.. The exact solutions for I_S and I_p can be shown to be (these are derived in Appendix C)[18]:

$$I_S(z) = \frac{I_p(0) - I_S(0)}{\frac{I_p(0)}{I_S(0)} \exp\left[g_B (I_p(0) - I_S(0)\right] - 1} \tag{2.28}$$

where,

$$I_p(z) = k + I_S(z)$$

$$I_p(0) - I_S(0) = I_p(L) - I_S(L) \tag{2.29}$$

Although, the input pump intensity is known, the output Stokes intensity $I_S(0)$ is not. It is therefore necessary to determine $I_S(0)$ from the given $I_S(L)$ (either Stokes noise or an actual input at the Stokes frequency, as for example, in an amplifier configuration). This approximation was first adopted by Tang and although the above equations can be solved exactly, has not been extensively used. In fact, we shall return to this case in the next chapter when considering the full numerical solutions of the SBS equations.

b) Undepleted pump approximation

This approximation has won by far the most widespread use due to its simplicity. In this

approximation, it is assumed that the pump depletion by the Stokes wave is small, that is $I_p(z) \approx$ constant, $(= I_p(0))$. In this case integration of eqn (2.24b) yields:

$$I_S(z) = I_S(L)\{ \exp [g_B I_p(0) - \alpha_o][L - z]\} \qquad (2.30)$$

Clearly, this approximation is valid only for very low values of the Stokes intensity.

Although both the equations, and their approximate solutions are quite general, and apply equally in the case of bulk optical materials (solids - both crystals and amorphous materials, liquids, and gases), as well as optical fibres, our discussion will focus on the case of single mode optical fibres. In fact, we shall return to the discussion of the solutions to the SBS equations in the the more practical context in the next chapter which presents a review of the previous work on stimulated Brillouin scattering in single mode optical fibres.

2.3. Transient characteristics of SBS

So far we have considered solely the steady-state intensity solutions of the SBS equations which form the main focus of the work in this thesis. However, as we later refer to the transient behaviour in the SBS, it would be useful to consider, at least qualitatively, the transient characteristics of SBS. The transient growth of light scattered inelastically from thermal or quantum fluctuations through the SBS process has been examined theoretically by several authors for a number of particular cases. A typical analysis begins with the set of coupled equations describing the motion of a limited number of modes of the optical field and of the medium. These are then simplified using various plausible assumptions about the mechanism responsible for a particular process analysed.

Kroll (1965)[33] has analysed the growth of SBS in the low conversion regime, where linearised equations are valid. Although Tang's analysis extended the theory of SBS to cover the high conversion regime in which strong depletion of the pump by the counter propagating Stokes signal can occur, his equations applied only to the steady-state situation, and Johnson and Marburger (1971)[34] were the first to develop the transient solutions for the stimulated Brillouin scattering case. They found that both the transmitted pump and the backscattered Stokes experience relaxation oscillations, which may be

sustained for a long period of time. The most relevant case is that of *finite-cell oscillations* which can occur when the forward travelling pump beam drives a stimulated scattering beam in the opposite direction, in a finite medium. The period of these oscillations is proportional to the cell length, L, and therefore no oscillations of this type can occur in an infinite medium. In fact the period of the oscillations is always 2Ln/c, where n is the refractive index. Initially, after the pump is switched on at t = 0, a portion of the backward Stokes signal which begins at the forward pump front grows exponentially throughout the pulse length, L_p during which it 'sees' the full incident intensity, $I_p(0)$. After time t = Ln/c, the maximum length of the undepleted pump seen by a portion of the backward signal diminishes from L_p to zero. Consequently, the backward travelling Stokes signal can not be amplified sufficiently from noise during the low-gain region. The result is a dramatic reduction in the Stokes level $I_S(0)$ after 2L/v. After the backward Stokes intensity has drops to a small value, the incident pump beam can pass beyond the input face before being depleted again. Thus this process repeats periodically with decreasing modulation depth until the steady state is reached. In this way the gain in the cell is modulated at the cell frequency.

It has to be pointed out that the oscillations described above will be observed for a pump which is cw (after being initially switched on) or pulsed with pulse length exceeding the round trip time. This particular behavior can be utilised to advantage in Brillouin lasers, as will be seen later. In this way, relaxation oscillations, which are due to depletion, must be differentiated from other transient effects, namely those associated with finite decay time of the acoustic wave (= $1/\Gamma$) and may be much longer than the latter. The transient effect associated with damping of the material excitation becomes important when the pump pulse duration is less than the decay time of the acoustic wave; the manifestation of this effect is in generation of very short pulses (pulse duration less than the acoustic decay time), and the influence of the finite acoustic decay (relaxation time) has been considered by a number of authors[35-37] who concluded that in situations where the transit time in the medium is less than acoustic decay time it is possible to obtain very short pulses, whose intensity exceeds pump intensity.

Clearly, these effects are very interesting and important for possible pulse compression. In the transient SBS regime, the tail of the Stokes pulse may experience a gain and loss modulation with the laser field resulting in a break up (and consequent compression) of the Stokes pulse; for example, Gorbunov[38] has theoretically predicted that quite considerable

pulse compression is possible (25 - 30 fold) providing certain experimental conditions are fulfilled, while previously Hon[39] showed more than ten-fold (20 ns to 2 ns) pulse compression in tapered waveguides using the SBS process. This technique uses convergently tapered waveguides with the pump pulse input from the wide end, and Stokes pulse spontaneously generated. As the pump pulse propagates along the waveguide into a decreasing area, its intensity increases. The gain is greatest near the exit of the waveguide, and by a suitable choice of input laser intensity and waveguide taper, a Stokes pulse of short duration propagates backwards, receiving amplification from the pump pulse. Amongst many advantages[40] of pulse compression by SBS as opposed to SRS is the fact that in that the compressed pulse is wave-front reversed (spatially phase conjugated) while the polarisation state behaves like a mirror reflection[40] - important for phase conjugation in laser cavities.

2.4. References for Chapter 2

1 I. L. Fabelinskii, 'Molecular scattering of light', transl. R. T. Beyer, Plenum Press, New York, 1968

2 J. D. Hey, 'Mandelshtam-Brillouin scattering by optically linear media' Part I, S. Afr. J. Phys. **5**, 65 (1982); Part II: ibid. **7**, 88 (1984)

3 L. P. Bayvel and A. R. Jones, "Electromagnetic scattering and its applications", Elsevier Applied Science Publ., London and New York, 1981

4 J. E. Midwinter, "Optical fibres for transmission", John Wiley &Sons Inc., New York, 1979, Chapter 8

5 G.S. Landsberg, "Optics", 5th edition, Nauka publ., Moscow 1976

6 H. Z. Cummins and P. E. Schoen, 'Linear scattering from thermal fluctuations' in Physical Applications, Laser Handbook, vol. 2, F. T.Arrechi and E. O. Schulz-Dubois eds, North-Holland Publ. Co., Amsterdam 1972

7 L.Brillouin, Ann. Physique (Paris), **17**, 88 (1922); 'Birth and growth of Brillouin scattering', Proc. Int. Conf. on "Light scattering spectra of solids", ed. G. B. Wright, Springer Verlag, Berlin, 1969

8 L. Mandelshtam, Zh. Russ. Khim. Obschestva **58**, 381 (1926)

9 N. L. Rowell, P. J. Thomas, H. M. van Driel, and G. I. Stegeman, 'Brillouin spectrum of single mode optical fibres', Appl. Phys. Lett. **34**, 139 (1979)

10 R. M. Shelby, M. D. Levenson, and P. W. Bayer, 'Guided acoustic-wave Brillouin

scattering', Phys. Rev. B **31**, 5244 (1985)

11 V. S. Starunov and I. L. Fabelinskii, 'Stimulated Mandelshtam - Brillouin scattering and stimulated entropy scattering of light', Sov. Phys. Uspekhi **12**, 463 (1970)

12 W. Kaiser and M. Maier, 'Stimulated Rayleigh, Brillouin and Raman spectroscopy' in Physical Applications, Laser Handbook, vol. 2, F. T.Arrechi and E. O. Schulz-Dubois eds., North-Holland Publ. Co., Amsterdam 1972

13 Y. R. Shen, "The principles of nonlinear optics", John Wiley & Sons, New York, 1984

14 D. Heiman, D. S. Hamilton and R. W. Hellwarth, 'Brillouin scattering measurements in optical glasses', Phys. Rev. B **19**, 6583 (1979)

15 J. F. Nye, "Physical properties of crystals", Oxford Univ. Press, 1957

16 B. Ya. Zeldovich, N. F. Pilipetskii, and V. V. Shkunov, "Principles of phase conjugation", Springer-Verlag, Berlin, 1985

17 R. W. Hellwarth, 'Third-order optical susceptibilities of liquids and solids', Prog. Quant. Electron. **5**, 1 (1977)

18 C. L. Tang, 'Saturation and spectral characteristics of the Stokes emission in the Stimulated Brillouin process', J. Appl. Phys. **37**, 2945 (1966)

19 Yu. E. Dyakov, 'Excitation of stimulated light scattering by broad-spectrum pumping', JETP. Lett. **11**, 362 (1970)

20 G. C. Valley, 'A review of SBS excited with a broad band pump laser', IEEE J. Quantum Electron. **QE-22**, 704 (1986); R. A. Mullen, R. C. Lind, and G. C. Valley, 'Observation of the SBS gain with a dual spectral line pump', Opt. Comms. **63**, 123 (1987)

21 P. Narum, M. D. Skeldon, and R. W. Boyd, 'Effect of laser mode structure on stimulated Brillouin scattering', ibid., 2161 (1986)

22 E. Lichtman, A. A. Friesem, R. G. Waarts, and H. H. Yaffe, 'Stimulated Brillouin scattering excited by two pump waves in single mode fibres', JOSA B **4**, 1397 (1987)

23 E. Lichtman and A. A. Friesem, 'SBS excited by a multimode laser in single mode optical fibres', Opt. Comms. **64**, 544 (1987)

24 J. Auyeung and A. Yariv, 'Spontaneous and Stimulated Brillouin scattering in long low loss fibres', IEEE J. Quantum Electron. **QE-14**, 347 (1978)

25 R. Y. Chiao, C. H. Townes, and B. P. Stoicheff, 'Stimulated Brillouin scattering and coherent generation of intense hypersonic wave', Phys. Rev. Lett. **21**, 592 (1964)

26 B. Ya. Zeldovich, V. I. Popovichev, V. V. Ragulskii, and F. S. Faizullov,

'Connection between the wave fronts of the reflected and excited light in stimulated Mandelshtam-Brillouin scattering', JETP Lett. **15**, 160 (1972)

27 O. Yu. Nosach, V. I. Popovichev, V. V. Ragulskii, and F. S. Faizullov, 'Cancellation of phase distortions in an amplifying medium with a "Brillouin mirror"', ibid. **16**, 435 (1972)

28 B. Ya. Zeldovich, N. F. Pilipetskii, and V. V. Shkunov, 'Phase conjugation in stimulated scattering', Sov. Phys. Usp. **25**, 713 (1982)

29 P. Suni and J. Falk, 'Theory of phase conjugation by SBS', JOSA B **3**, 1681 (1986)

30 M. M. Valley, 'Nonlinear phase conjugation for wavefront control', Proc. SPIE **622** "High power and solid state lasers", 168 (1986)

31 M. P. Petrov and E. A. Kuzin, Stimulated Brillouin scattering and phase conjugation in optical fibres', Sov. Tech. Phys. Lett. **8**, 316 (1983)

32 E. A. Kuzin, M. P. Petrov, and B. E. Davydenko, ' Phase conjugation by long optical fibres', ibid., 349 (1984)

33 N. M. Kroll, 'Excitation of hypersonic vibrations by means of photoelastic coupling of high intensity light waves to elastic waves', J. Appl. Phys. **36**, 34 (1965)

34 R. V. Johnson and J. H. Marburger, 'Relaxation oscillations in Stimulated Raman and Brillouin scattering', Phys. Rev. A **4**, 1175 (1971)

35 A. Ya. Karasik and A. V. Luchnikov, 'Generation of nanosecond radiation pulses as a result of SBS in a single mode fibreglass waveguide', Sov. J. Quantum Electron. **15**, 877 (1985)

36 E. M. Dianov, A. N. Pilipetskii, and V. N. Serkin, 'Influence of the finite relaxation time of a hypersonic wave on the kinetics of formation of pulses as a result of stimulated Brillouin scattering in single mode fibre waveguides', Sov. J. Quantum Electron. **16**, 259 (1986)

37 N. F. Andreev, V. I. Bespalov, A. M. Kiselev, A. M. Kubarev, and G. A. Pasmanik, 'Formation of pulses in stimulated scattering of light in extended media. Modulation of the intensities of transmitted and backscattered radiations', Sov. J. Quantum Electron. **6**, 1223 (1976)

38 V. A Gorbunov, 'Maximum time compression of light pulses in stimulated Brillouin scattering', Sov. Phys. Tech. Phys. **27**, 1418 (1982)

39 D. T. Hon, 'Pulse compression by stimulated Brillouin scattering', Opt. Lett. **5**, 516 (1980)

40 M. J. Damzen and M. H. R. Hutchinson, 'Laser pulse compression by stimulated Brillouin scattering in tapered waveguides', IEEE J. Quantum Electron. **QE-19**, 7 (1983)

Chapter 3

SBS IN SINGLE MODE OPTICAL FIBRES - AN OVERVIEW

The purpose of this chapter is to present a systematic overview of the considerable research work which has been done in the field of SBS in single mode optical fibres - transmission media which can offer unique experimental conditions as compared to bulk materials. The background and the reasons for the early interest in this field are outlined. The review covers the work on SBS in long optical fibres, considering on the one hand the limitations to single mode optical fibre communication systems and, on the other, applications in optical amplification, as well as Brillouin lasers. Finally a section on the material considerations is included. We shall discuss each of these areas in turn, outline the main results and achievements, and point out areas where further work is necessary. It is thought that a detailed review is necessary for full appreciation and understanding of the significance of the work in this thesis in relation to other work carried out in the field of the investigation of SBS in single mode optical fibres.

3.1. Early interest

As was briefly mentioned in Chapter 1, the late 1960s saw the start of the development of the first low loss optical fibres as transmission media for optical communications systems. This work was soon followed by the realisation that the advantages offered by optical fibres such as potential low losses, small interaction areas, and long interaction lengths would also lead to dramatically reduced power thresholds for the nonlinear stimulated Brillouin and Raman scattering processes.

Ippen and Stolen (1970, 1972)[1,2] were the first to show SRS and SBS experimentally in optical fibres. For SBS, they used a single mode xenon laser (with pulsewidth of ≈ 1 μs) with an intracavity etalon operating at 535.5 nm, with a linewidth of approximately 100

MHz. They observed thresholds of 2.3 Watts for a 5.8 m length of fibre, and a threshold of less than 1 Watt for a 20 m length of fibre. The loss of their fibre was 100 dB/km.

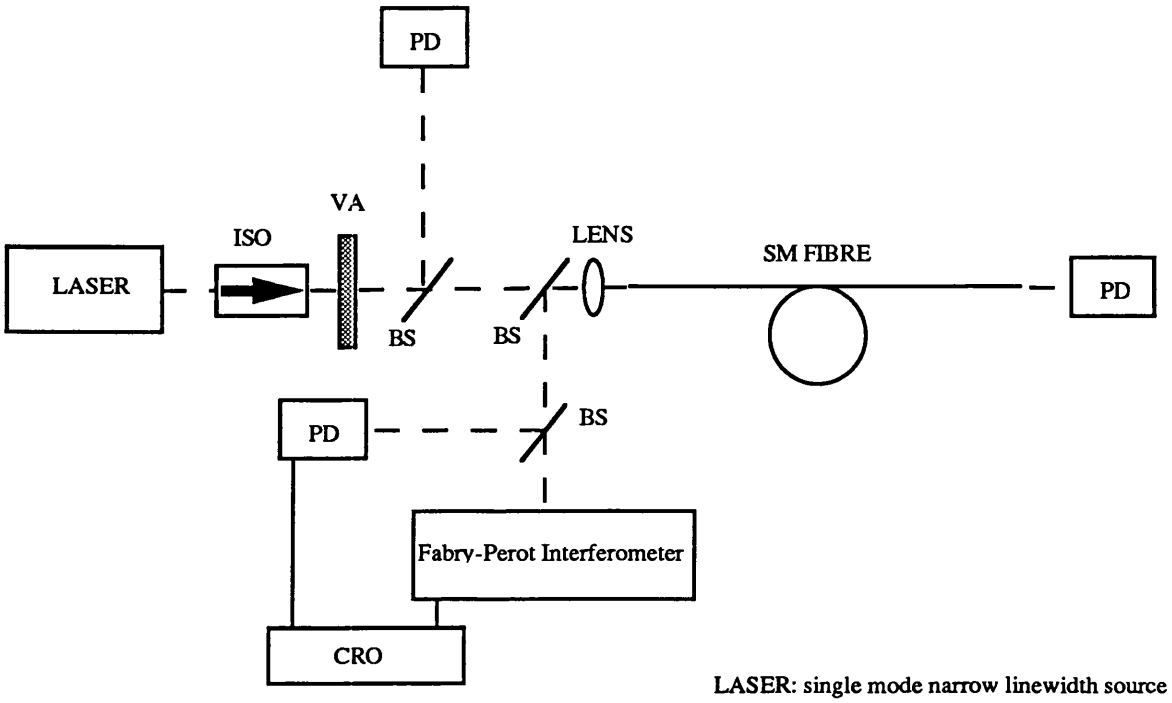

Figure 3.1. Typical experimental arrangement to observe SBS in a fibre.

They were also the first to observe the relaxation oscillations in the scattered signal at a frequency of 2nL/c, the round-trip transit time of the fibre. They explained this effect as due to periodic depletion of the pump wave near the input end of the fibre. This results in depletion of the gain in the fibre until the depletion region has passed out of the fibre, as described in the previous chapter. In later work, this effect has been identified as a mechanism for passive modelocking in Brillouin lasers, and will be discussed in the section dealing with Brillouin lasers. [A typical experimental set up for the investigation of SBS in optical fibres is shown in figure 3.1].

At about the same time, Smith (1972)[3] was the first to consider theoretically the optical power handling capacity of single mode low loss optical fibres (20 dB/km!) as determined by stimulated Brillouin and Raman scattering. Using the undepleted pump approximation he derived relationships for threshold (critical) powers at which the attenuation introduced

by the energy transfer from the pump to the stimulated backscattered wave becomes significant.

He arbitrarily defined the SBS threshold power as that input power necessary to bring the backscattered stimulated Brillouin power to the level of the input power, so that the pump depletion becomes significant. In other words, in optical fibre transmission systems, the threshold is that absolute limit to the input pump power at which point the nonlinear effect must be considered. In the case of SBS in single mode optical fibres, Smith derived this to be:

$$P_{th} \approx \frac{20A_{eff}}{g_B L_{eff}}, \quad \text{where: } L_{eff} = \frac{1 - \exp - \alpha_o L}{\alpha_o} \tag{3.1}$$

and the factor 20 is approximately the natural logarithm of the gain required to bring the spontaneous emission to the level of the input pump power. This figure was calculated for particular material parameters but, in fact, changes only by about 10% for a variation in $(A_{eff}/g_B L_{eff})$ of two orders of magnitude[2,3]. g_B is the Brillouin gain coefficient as defined in Chapter 2, and A_{eff} is the effective core area of the fibre. It must be pointed out that the plane wave analysis of SBS considered in the last chapter can be directly applied in the case of optical fibres. In the case of a single mode fibre we assume that both the pump and the Stokes wave propagate in the same mode (or more accurately, as they have slightly different frequencies, they propagate in the same type of mode with the same polarisation), so that the overlap integral can be taken as approximately equal to unity[4], and where the mode can be approximated by a Gaussian function $E(r) = E(0)\exp - (r^2/w^2)$ with w equal to 1/e field amplitude, then $A_{eff} = \pi w^2$. A more accurate approximation for the mode profile of a single mode fibre is the mode of an equivalent step index fibre[4-6]. Then a the ratio of A_{eff}/A_{core} can be calculated as a function of the characteristic number V (normalised frequency). Accurate measurements require a technique for determining the core size of the equivalent step index fibre. However, for simplicity, it is the former approach which is generally adopted in calculations[4]. [As an aside, we just mention that the picture is very much more complex for the case of a multimode fibre, where all pump and Stokes modes should be considered separately, and overlap integrals which describe the strengths of coupling between various waveguide modes have to be evaluated for all mode combinations[4]].

Smith also introduced the approximation that the initial or effective Stokes power at z = L (in the absence of an external Stokes signal) due to the spontaneous Stokes emission, for a single mode fibre, can be expressed as:

$$P_S(L)|_{eff} = \frac{hf_s B_{eff} kT}{hf_a \quad A_{eff}} \tag{3.2}$$

where h is Planck' constant, f_S is the frequency of the Stokes wave, A_{eff} is the effective core area, k is Boltzmann's constant, T is the absolute temperature, and f_a is the frequency of the acoustic phonon or the Brillouin shift. This expression is just the product of thermal noise kT per unit frequency, the ratio of the Stokes and acoustic energy and the effective Brillouin bandwidth B_{eff}, where the approximation of peak gain within the bandwidth $\Delta\upsilon_B$, and zero outside the band is made. Assuming a Lorentzian gain distribution with FWHM bandwidth $\Delta\upsilon_B$, and that the peak gain is high, the effective bandwidth is given by B_{eff}:

$$B_{eff} = \frac{\sqrt{\pi}\,\Delta\upsilon_B}{2\,[I_p(0)\,g_B\,(1 - \exp - \alpha_o L)/\alpha_o]^{1/2}} \tag{3.3}$$

In fact both of the above approximations were widely adopted in most of the work on SBS in optical fibre, particularly in the work concerning communication systems aspects.

3.2. SBS as a limitation to communication systems

In the 70s, intensive research and development of optical fibre systems led to lowering of the achievable fibre losses, and increases in potential transmission distances. This was accompanied by reported reductions in the observed Brillouin thresholds. The main results are summarised in Table 3.1.

Figure 3.2 (a) shows a plot of L_{eff} vs fibre length, L for different fibre losses. It is seen that an increased fibre loss limits the fibre length which can contribute to SBS. Clearly L_{eff} = L for zero fibre loss. Fig 3.2 (b) shows the plot of theoretical threshold power as derived by Smith against the fibre length for several fibre losses, with the 20 dB/km loss

Fibre length (km)	[L_{eff}] (km)	Fibre loss (dB/km)	Observed threshold (mW)	Max. conv efficiency (%)	Theoretical threshold* (mW)	λ, $\Delta\upsilon_{las}$	Reference
5.8×10^{-3} 20.0×10^{-3}	1.7	1300 (!) -	2300 < 1000	- -	2200 -	535.5 nm 74 MHz	Ippen et al (1972)[2]
4	1.1	4.0	30.1	56	15.6	710 nm 30 MHz	Uesugi et al ('81)[8]
13.6 31.6	7.7 10.1	0.41 "	5 "	65 -	2.8 2.0	1.3 2 µm <1.6 MHz	Cotter ('82)[9]
30	14.3	0.25	2	-	1.2	1.52 µm < 1 MHz	Cotter ('82)[11]
2	0.19	22	40 (PM)	-	50	514.5 nm -	Tsubokawa et al ('86)[14]
12.9	6.8	0.47	11.75	-	5.2	1.32 µm 3 MHz	Hadjifotiou et al ('86)[19]
30	8.7	0.46	9	80	4.0	1.3 µm 15 MHz (DFB-LD)	Aoki et al ('87)[20]

* Theoretical threshold as derived by Smith [3]

PM - polarisation maintaining fibre

'-' denotes parameter unspecified by author

All experimental parameters are stated with the accuracy specified by the author(s)

Table 3.1. Summary of the main experimental results of measurements of SBS in long single mode optical fibres.

considered by Smith plotted alongside the more practical losses for low-loss communication fibres. It is ideally assumed that P = 1 (no polarisation scrambling), and the peak value of the Brillouin gain coefficient g_B is used (for fused silica, $g_B = 4.6 \times 10^{-11}$ m^2), and the core area, A_{eff} is taken to be 5.0×10^{-11} m^2.

It can be seen that the SBS threshold decreases as the fibre length increases, and then asymptotically reaches a constant value which is governed by the fibre loss. This is

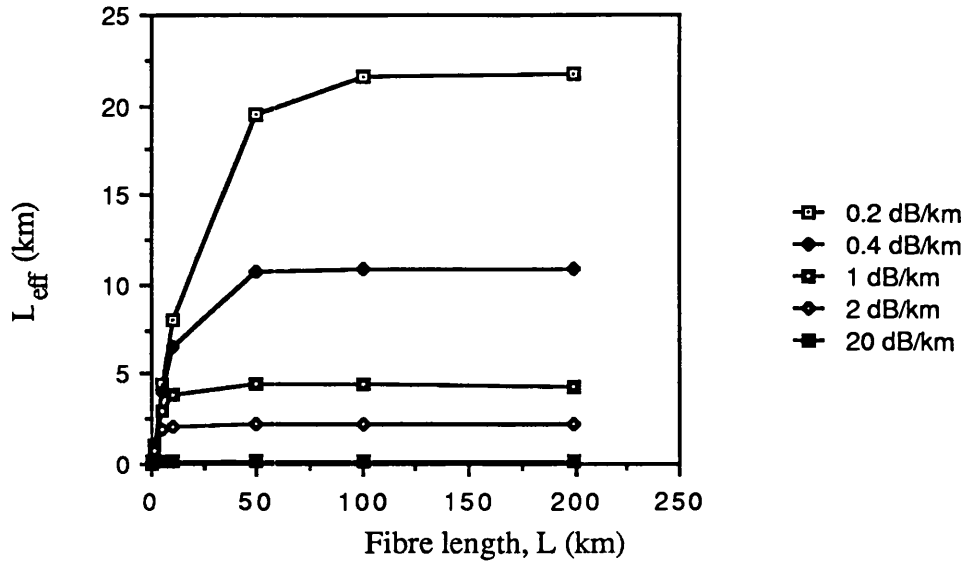

(a)

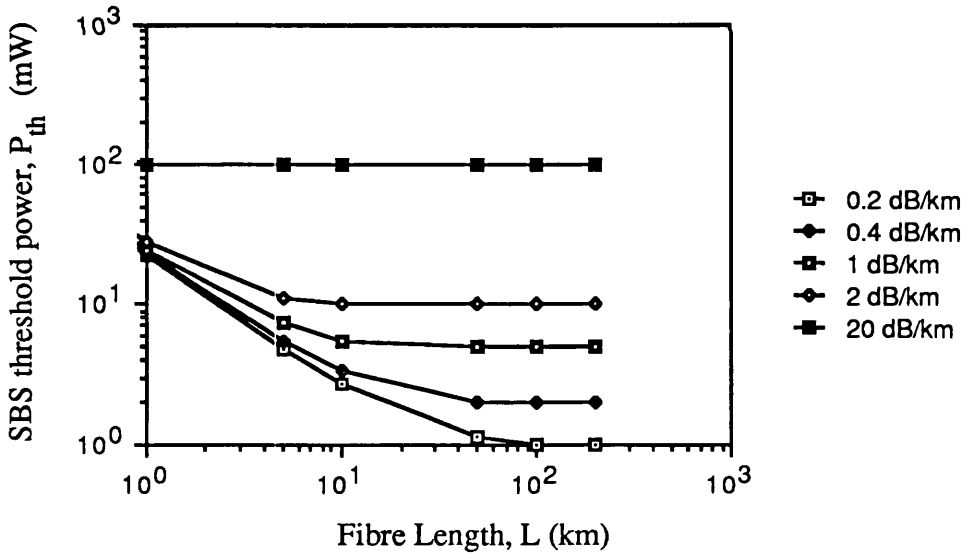

(b)

Figure 3.2. Variation of (a) L_{eff}, and (b) Brillouin threshold power vs fibre length for different fibre losses [plotted using eqn (3.1)].

because the effective interaction length, L_{eff} becomes $1/\alpha_0$ for long fibres.

In a series of careful experiments, Labudde et al.[7] demonstrated the importance of minimising the optical reflections at the fibre ends, which they observed led to the enhancement of the SBS. This enhancement, however, becomes significant only in shorter fibres where the 4% end reflection is greater than the round-trip fibre attenuation, and is virtually negligible in long distance links. In addition, through ineffective isolation between the laser and the fibre, a substantial proportion (approximately 30%) of the backwards Stokes light was re-injected into the fibre in the forward direction, and resulted in the generation of several orders of Stokes and anti-Stokes frequencies by four wave mixing (FWM) in the fibre. Although a clear limitation in the fibre transmission systems, it was suggested that this FWM process could be usefully applied in generation of narrow pulses in Brillouin lasers. Another application of this process proposed in this thesis (Chapters 6 and 8) is in generation of very high microwave frequencies.

As shown in Table 3.1, Uesugi and Ikeda (1981)[8] reported experimental results of SBS in a 4 km length of single mode fibre (fibre loss = 4 dB/km). They reported a maximum single frequency input power before the effect of SBS becomes significant, as 14.8 dBm (4.4 mW). Subsequently, Cotter[9] observed a Brillouin threshold of 5 mW in low loss single mode fibre of 13.6 and 32 km lengths at 1.3 μm together with the highest reported conversion efficiency at that time. From these results it was apparent that the observed thresholds were actually approximately double those predicted by Smith's formula. The reason for this was that in these longer lengths of fibre, the polarisation was not maintained, resulting in polarisation scrambling, and the reduction in the Brillouin gain coefficient, as outlined in the previous section. Despite this, it became clear that SBS could be the determining factor in the operating limit of advanced coherent communications systems. Subsequently a number of modulation schemes for increasing the SBS threshold have been proposed[10-12].

Most of the work has concentrated on the consideration of SBS with the three modulation schemes of binary ASK (amplitude shift keying), FSK (frequency shift keying) and PSK (phase shift keying) in the context of coherent communication systems[13]. In the ASK modulation, the pump light is completely amplitude modulated with a periodic square wave function representing the 1010.. sequence. In the FSK modulation, the optical frequency

is alternatively changed, where one frequency denotes a '1', and the other - '0' (with the difference in frequencies 1 and 2 is known as the frequency deviation). In the PSK case, the phase of the pump light is alternatively shifted from data '1' to '0'. The phase shift used in most PSK systems is π: '1' is transmitted by changing the optical phase by π, while '0' is transmitted with the optical phase unaltered.

For significant SBS to occur the optical field must be capable of building up a strong coherent acoustic wave within the decay time $2\pi/\Gamma$. Physically, in the case of ASK, optical pulses are additive to generate a coherent acoustic wave and the Brillouin threshold in an on-off keyed system can be increased only by a factor of 4 compared with the cw case. In frequency shift keying (FSK), providing the frequency shift is large, the continual phase change of optical field will result in a small acoustic excitation, thus enabling some suppression of SBS. In the case of phase shift keying (PSK) if an appropriate phase shift (180^o) is chosen, the net acoustic excitation can be minimised. Indeed, by using such a simplistic approach, PSK seems the most useful method of suppressing SBS. In addition, heterodyne PSK offers advantages in terms on the improved transmission S/N ratios.

Cotter[10-12] analysed the transient scattering theory for the various modulation schemes, although his time domain calculation of the SBS gain did not consider the frequency domain analysis of the gain as the convolution between the pump spectrum and the spontaneous Brillouin linewidth, $\Gamma/2\pi$. Several experimental results were published supporting the technique (proposed by Cotter) of imposing phase modulation on the optical field launched into the fibre to reduce the SBS gain. Instead of using a phase modulator the technique relied on the mode beating effect produced when the field comprises two frequencies spaced by greater than the Brillouin linewidth, thus reducing the Brillouin gain coefficient. This was achieved experimentally by operating a 1.32 μm Nd-YAG laser on two adjacent longitudinal modes simultaneously. An increase from the threshold of 6 mW (32 km fibre) to above 90 mW (maximum power available from the pump source used in the experiments), and an SBS threshold increase of more than 20 dB was predicted. Tsubokawa et al.[14] proposed an analogous method of suppressing SBS by using an acousto-optic modulator (AO). The principle of the method was to launch into the fibre a two-frequency beam (obtained from the AO) with the reported suppression ratio of 30 dB and frequency difference of 500 MHz between the beams. Although, initially it appeared that these results corroborated Cotter's predictions, it later transpired that such significant suppression of SBS was the result of the competition between SBS and FWM[15,16]. In this

way, such a technique would offer only limited SBS suppression. Moreover, to use this method for suppressing SBS in ASK, it would be necessary to modulate the total optical field (ie both frequencies), and to use a beat frequency which is larger than the detection bandwidth. Only one frequency would be detected, so only one half of transmitted power would be utilised for data transmission.

In a more detailed analysis, Lichtman et al.[17] developed the frequency domain solution of SBS which allowed direct calculation of the SBS suppression for the above modulation schemes. By representing the input pump and the backscattered Stokes wave as consisting of discrete equispaced frequencies, and considering a random modulation (ie a stochastic process which can take values 0 or 1 with equal probability), they showed that the Brillouin gain for each of the modulation schemes is determined by the parameter ΓT, which is the ratio of the modulation bandwidth $\Delta\omega_{mod}$ ($= T^{-1}$) and the spontaneous Brillouin linewidth, Γ. As expected, the gain decreases by increasing the modulation bandwidth, since then, the pump power spreads over a larger spectrum, and the net contribution to the SBS gain at the carrier frequency becomes smaller. They found that for the ASK case the gain is minimised by modulating with a 100% modulation depth. For PSK, minimum gain is achieved with a phase shift of $\pi(2n + 1)$, and in the FSK case the gain condition is practically independent of the frequency shift, providing the frequency shift, $f_k >> \Delta\upsilon_B$. Increasing the modulation frequency ($T \rightarrow 0$) results in the SBS gain converging to 1/4 of the gain in the CW case for ASK and FSK, while for PSK case, it converges to zero. (In fact the threshold increases by 10 dB for each factor of 10 increase in bit rate). This analysis is based on two major assumptions. The first is that the fibre length is larger than the pump coherence length, $c/\Delta\omega_{las}$ - valid in the case of most practical long-haul transmission systems. The second assumption is that the process is stochastic. The validity of this assumption depends on the input data and on the specific coding scheme. However, even in the cases where a stochastic process approximation does not hold, SBS gain can still be calculated using their method, providing that the spectrum of the modulated wave (or alternatively, its autocorrelation function) is known. The Brillouin threshold will then be between the threshold values for the cw and the randomly modulated wave.

Independently Aoki et al.[18] have investigated the effects of different modulation schemes on the SBS gain. Using a relatively simple method of considering the power contained in the largest frequency component in each modulation scheme, they analysed whether the reduction in the Brillouin gain as a result of modulating the data depends on whether the

particular modulation scheme has a fixed or random pattern. Their results indicate that for the ASK (for a mark-space ratio of 1) and FSK, the gain reduction is virtually independent of the modulation scheme and bit rate, confirming the work of Cotter (for ASK) and in agreement with Lichtman et al. However, for the PSK case, the reduction of a factor of 2.5 for fixed pattern modulation, increases to infinity with increasing bit rate.

Experimentally, the threshold increase with PSK modulation was first observed by Hadjifotiou and Hill[19] using an Nd-YAG laser at 1.3μm and an external $LiNbO_3$ phase modulator , but the experiment was limited to input powers of approximately 2.5 times the SBS cw threshold. Aoki et al.[18] have performed experiments confirming their theoretical predictions for PSK modulated light - using a cw DFB-LD and an external phase modulator. In fact, a notable feature of this work is that the systems measurements were performed using a practical DFB semiconductor laser as a pump (see also ref. [20]), rather than the specially stabilised, narrow single-frequency gas or solid-state lasers used by other authors. They also carried out some measurements for FSK modulation using a directly modulated DFB-LD[21]. However, their results for these latter measurements could not be unambiguously confirmed because of the nonlinear FM response of the laser diode (as indicated by a large spectral broadening: this is characteristic of many commercially available laser diodes). In the region where the FM response of their laser diode was linear, weak SBS was observed, with the suppression approximately in agreement with that predicted by theory. Bolle et al.[22-24] also investigated the Brillouin gain curve dependence on the frequency spectrum of PSK modulated signals and the type of modulation format, both experimentally and, and theoretically by Cosentino et al[25]. Using a colour-centre laser and a modulator, the experiments of Bolle et al. corroborate those of Hadjifotiou and Hill, Aoki et al. and Lichtman et al.

Recently, two further possible sources of distortion were suggested by Waarts et al.[26] and Horriguchi et al.[27] In ref. [26] it was reported that in the case of FM modulation, SBS gain, which is accompanied by a nonlinear phase shift arising from the interactions between the different spectral components of the pump and Stokes waves, can lead to the conversion of FM modulated to amplitude-modulated signal. This could cause distortion in coherent fibre systems. Horiguchi et al. published some surprising results on quite substantial (up to 30%) variation of Brillouin gain with polarisation state of pump and Stokes waves in fibres where the polarisation state is neither maintained nor completely

scrambled. Such a variation of gain could lead to cross talk fluctuations in frequency or wavelength division multiplexing systems, and degradation in Brillouin amplifier performance (discussed later). However, both of the above effects will have to be further investigated to establish how serious a limitation each would present in a practical system.

The work of Horriguchi et al. appears to contradict their later publication[28] in which he suggests an application of SBS for measurement of the optical fibre linear attenuation by measuring the Brillouin gain of the probe signal. This method, however, is only applicable in the low-gain (undepleted pump) regime, and assumes that g_B/A_{eff} does not fluctuate along the fibre length, both through material inhomogeneities and polarisation scrambling - conditions which clearly are not always fulfilled.

One of the reasons for discussing the current state of the research on SBS as a limitation in optical fibre systems in some details, is to indicate that in assessing the limitations presented by SBS, all the calculations were based on the input power threshold arrived at using the undepleted pump approximation. However, as can be seen, numerous papers have reported conversion efficiencies in excess of 50%. Indeed, in order to calculate the exact threshold for SBS, and the steady state pump and Stokes powers, pump depletion has to be taken into account. This means that the equations have to be solved numerically with the appropriate boundary conditions.

The boundary conditions - the initial values known in this case are: $P_p(0)$, the input pump power and $P_S(L)$ (in the case of no external Stokes input, it is just the spontaneous Stokes noise which can be calculated). The final steady-state values of the pump and the Stokes intensities: $P_p(L)$ and $P_S(0)$ are unknown and have to be calculated. This means that only *two* boundary conditions are known. However, if these equations can be solved, for the given practical parameters such as the input pump power and the fibre length, the solution will yield the amount of pump depletion for a given fibre link length, and the conversion efficiency, that is the amount of backreflected Stokes power. This information is practically very valuable, as it will specify the real limit on the optical power budget. In fact, this problem is tackled in the next chapter.

3.3. Brillouin amplification

Although the use of nonlinear SBS gain for amplification has been proposed by Tang as long ago as 1966[29], this was not explored in fibre systems until recently, with the important results summarised in Table 3.2.

The experimental configuration of a Brillouin amplifier is similar to that shown in figure 3.1, with the addition of another laser, serving as a signal and injected at the output end of the fibre, counterdirectionally to the pump laser. One or both lasers are tunable, so that the frequency difference between them is locked to the Brillouin shift. Waarts and Braun (1985)[30] investigated the interaction between two counterpropagating waves at different frequencies (separated by the amount approximately equal to the Brillouin shift) and observed signal gain of 10 % for one of the waves due to SBS. Thus, the conclusion of their work was that in coherent optical communications, systems which will use many narrowly spaced lasers (frequency multiplexing), the addition of one channel in the backward direction (subscriber channel) may lead to serious power limitations due to crosstalk. Although the aim of the work was to investigate yet another system limitation posed by the SBS process, and not Brillouin amplification, it must be emphasised that the authors were the first to measure the Brillouin gain using commercially available AlGaAs lasers.

Atkins et al. [31,32] suggested and demonstrated a very elegant application of the stimulated Brillouin gain, to selectively amplify the signal carrier in coherent homodyne detection, prior to photodetection. Since homodyne detection offers the optimum receiver sensitivity and is more efficient in the use of the available electrical receiver bandwidth than heterodyne detection, potentially such a technique can simplify the application of homodyne detection in long-haul transmission systems by eliminating the need for electronic phase-locking. In their experiment the pump was a colour centre laser at 1.5 μm, and a He-Ne laser at 1.52μm was used as the transmitter. Soon afterwards, Chraplyvy and Tkach[33] (again, using a tunable colour-centre laser as a pump, but external cavity semiconductor lasers for signals) showed that SBS amplification can be used for channel selection in densely packed WDM with direct detection at 1.5 μm. In their experiment they used a pump wave modulated at 45 Mbit/s to amplify (in a 10 km length of fibre) a counterpropagating signal from two multiplexed channels with low error (10^{-8}) transmission for channel separation of 140 MHz . However, to accommodate transmission

rates higher than the intrinsic Brillouin linewidth (approximately 20 MHz at 1.5 μm) it is necessary to broaden the amplification bandwidth by varying the material composition in the fibre or by modulating the laser frequency. Both of these methods were used by Olsson and Van der Ziel who demonstrated the operation of semiconductor pumped fibre amplifiers[34,35]. The pump and probe (signal) lasers were 1.5μm external cavity lasers. Fibre lengths of more than 30 km were used, and reported gains of 3.0 - 5.5 dB/mW achieved, depending on amplification bandwidth.

Fibre length (L_{eff})	Pump power (mW)	Fibre loss (dB/km)	Observed gain	Wavelength	Reference
3.5	0.3	2.1	0.4 dB (cw)	825 nm (AlGaAs LDs) 2.2 -	Waarts et al. ('85)[30]
30	5	0.25	48 dB (cw) 20 dB (80 Mbit/s)	1.52 μm	Atkins et al. ('86)[31]
37.5	2	0.27	4.3 dB/mW	1.52 μm (SC LD*)	Olsson et al. ('86)[34]
10	14	0.25	25 dB (45 Mbit/s)	1.52 μm (InGaAs LD*)	Chraplyvy et al. ('86)[33]
30	3.3	0.3	18 dB (cw) 10 dB (90Mbit/s)	1.52 μm (SC LD*)	Olsson et al. ('87)[35]
3.5	12	2.5	30 dB (600 MHz BW, 150 Mbits/s sig)	830 nm (AlGaAs LDs)	Tkach et al. ('88)[36], Tkach et al. ('89)[37]

Note: Where modulation rates are stated, ASK modulation with 50% duty cycle was used, except in refs. 36,37 where FSK was used.

Table 3.2. Summary of the published data and main results on Brillouin amplifiers.

Using the undepleted pump approximation they calculated the gain of the amplifier as a function of the fibre length, and signal-to-noise ratios (SNR) as a function of receiver sensitivities. From their calculations it can be concluded that Brillouin fibre amplifiers are excessively noisy (the noise in a Brillouin amplifier is mainly due to the amplified spontaneous scattering). This limits their usefulness as receiver preamplifiers, but they could be used successfully as in-line amplifiers. Recently, Tkach et al.[36,37] have published some impressive results which demonstrate successful optical demodulation and amplification of FSK signals using simple AlGaAs lasers for both pump and signals, and reporting 30 dB gain. In a further development of their original work on WDM systems, they demonstrated the feasibility using SBS to realise a tunable narrowband amplifier to demodulate, amplify, and select channels in a densely packed WDM network, for up to 1000 channels achieving small channel separation, and very low error rates. Indeed, it seems that because of the inherently narrowband nature of these amplifiers, and for reasons which shall be further discussed later (Chapter 7), this seem to be the best application of the Brillouin amplification. However, some systematic evaluation of potentially achievable Brillouin gain as a function of pump power and fibre length would be necessary to draw further conclusions.

When considering the high gain of amplifiers, it is necessary to take into account the depletion of the pump in order to evaluate the SNR and the gain of the device. In all the work described above pump depletion has not been considered due to considerable complexities involved in solving the coupled equations describing the propagation of the pump and Stokes waves (equations (2.24)). However, in order to assess accurately the performance parameters of fibre amplifiers, such as the achievable gain and saturation characteristics, as a function of pump power and fibre length, it will be necessary to solve these equations fully, taking into account pump depletion.

3.4. Brillouin lasers

Although the initial work on SBS lasers with single mode fibres as the gain medium was carried out by K. O. Hill, B. S. Kawasaki and D. C. Johnson as far back as 1976 - 1978[38-40], the state of research in this area at the start of this work had not significantly advanced beyond these initial experiments. In 1976 Hill et al.[38] demonstrated the operation

of the first Brillouin laser which was also the first observation of SBS with cw pumping. The ring resonator used in their experiments was a combination of fibre/bulk optics, with

Cavity length (m)	F	Brillouin laser linewidth	Lasing threshold (mW)	Conv. eff. (%)	Wavelength (nm) [pump linewidth]	Reference
9.5	2	20 MHz	250	4	514 .5 [25 MHz]	Hill et al. (1976)[38]
20	6	" "	100	–	" "	Hill et al. ('76)[39]
11	5	–	– [ML: 2 W]	–	" "	Kawasaki et al. ('78)[40]
83	4	100 kHz	77	4	514 .5 [3 KHz]	Ponikvar et al. ('81)[45]
10	93	–	0.43	3.3	633 [1 MHz]	Stokes et al. (1982)[49]
1.0	300	–	0.07	24	633 [1 MHz]	Chapter 6 (this work)
4.0	90	700 KHz	0.9	8	830* [10 MHz] * - SC LD	" "

ML - modelocking

'-' denotes results/parameters unspecified by author

Table 3.3. Main results on Brillouin lasers.

the beam path defined by partial (bulk optics) reflectors. The Brillouin threshold was measured as 250 mW (using an argon-ion single mode laser with 25 MHz linewidth as pump, wavelength 514.5 nm, fibre loss ≈100 dB/km. The conversion efficiency (that is the ratio of the output Stokes power to the input pump power) was approximately 1.6%, and 4% for finesse of ≈2. [In Table 3.3 we summarise the main results to date for Brillouin lasers].

Hill et al.[39] were the first to suggest that SBS lasers can be used as a source of high-repetition-rate short duration pulses (picoseconds) (providing modelocking suggested by atheoretical paper of Lugovoy and Streltsov[41] (1973) proved feasible). In that paper they

observed continuous wave generation of multiple Stokes and anti-Stokes Brillouin shifted frequencies in a Fabry-Perot configuration. 20 m of single mode optical fibre (loss ≈ 100 dB/km at 514.5 nm) was the gain medium with the high-reflectivity output mirror of the argon-ion laser as one of the mirrors (at the pump input end) and a 98% reflector at the output end). They observed 14 Brillouin shifted lines (over a bandwidth of 476 GHz) - hence the suggestion of picosecond pulse generation. However, this method for short pulse generation was never shown experimentally. Instead, in 1978, Kawasaki et al.[40], demonstrated mode-locking of the first Stokes component, with pulsewidths of approximately 7 - 8 ns at the repetition rate of 8 MHz (corresponding to 11 m fibre length: mode spacing = c/nL). The physical mechanism responsible for spontaneous modelocking is due to the periodic pump depletion in the gain medium as described earlier in Chapter 2. The pulsing was stabilised by using a Bragg cell in the cavity at the modulation frequency of cavity mode spacing, and the pulse width obtained represented nearly the full gain-bandwidth utilisation of the Brillouin line (≈ 150 MHz at 514.5 nm).

Although Stolen[42] suggested that the lasing thresholds in Brillouin and Raman lasers would be reduced if polarisation maintaining fibres were used, this was not demonstrated experimentally for the case of Brillouin lasers until the work carried out in this thesis (described in Chapter 5).

Thomas et al.(1980)[43] proposed that it might be possible to use an optical fibre Brillouin laser for inertial sensing, as an all-fibre alternative to the ring laser gyroscope - a proposal which has only very recently been confirmed experimentally. Smith et al.[44] were the first to report the measurement of rotation using a He-Ne laser and an all-fibre Brillouin laser. Their measurements, however, were only preliminary, and a number of issues which will influence the ultimate performance have to be studied and resolved.

Ponikvar and Ezekiel[45] reported the operation of a stabilised single frequency SBS laser (fibre length 83 m, cavity finesse of approximately 4, with a threshold of 77 mW and a maximum conversion efficiency of 4%), with the linewidth of the Brillouin laser output approximately limited by the finesse of the cavity. Bar-Joseph et al.[46] further discussed the operation of single and multi-mode pumped SBS lasers and reported that in both cases these are spontaneously mode-locked. They observed a stable train of modelocked SBS pulses 4 ns long (and thus utilizing nearly the full gain bandwidth of 150 MHz available at 514.5 nm). They also showed that at very high pump levels modelocking disappeared due

to severe gain depletion (in line with their theory, Bar-Joseph et al.[47]), and that spontaneous mode-locking is present in the case of a multi-moded pump. (In this case the threshold is proportional to the number of modes - which can possibly be exploited to generate pulses much shorter than have been obtained previously). Similar results have been demonstrated recently by Botineau et al.[48] who also analysed the amplification and compression of the backscattered Stokes pulses as limited by the nonlinear Kerr effect,by carrying out complex numerical calculations of the three coupled wave equations (for the pump, Stokes, and acoustic waves).

In 1982 Stokes et al.[49] showed the first operation of an all-fibre SBS laser at 633 nm using a polished directional coupler in a fibre resonator configuration as described in Chapter 5. The finesse of the resonator was 93, and the Brillouin threshold was observed at 0.43 mW of pump power in the fibre with the loop length L of 10 m. The advantage of using an all-fibre ring resonator as a laser cavity is that the round-trip loss of such a resonator is much lower than that of a hybrid bulk optics/fibre device, resulting in significant circulating power enhancement in the case of a high finesse cavity. Indeed, this property of the resonator makes it extremely attractive for the study of SBS, with a view to possible applications in frequency generation and amplification at low pump powers. This area forms the main focus of this thesis and the studies undertaken are described in Chapters 4 - 8. Running ahead, for comparison, we can say that using high finesse resonators fabricated from polarisation maintaining fibre, lasing thresholds as low as 70 μW were demonstrated at 633 nm and submilliwatt thresholds at 830 nm using a commercially available AlGaAs laser. Such low thresholds make these devices compatible with current fibre systems for a variety of applications, which will be further discussed later in this thesis.

3.5. Material considerations

As already mentioned earlier the gain in the Brillouin process is dependent on material constants. Therefore measurements of the Brillouin gain linewidth and the Stokes shift can reveal interesting information about the material and can also form a basis for material characterisation as well as sensing applications[50]. A more useful expression for the Brillouin gain coefficient, g_B in terms of material parameters is given by (from eqn (2.25)):

$$g_B = \frac{2\pi \upsilon_S \Omega\, n^6 (p_{12})^2}{\rho_0 v_a^3 c^2 \alpha_a} \qquad (3.4)$$

Remembering that $\alpha_a = 2\pi\Delta\upsilon_B/v_a$, and that $\Omega = 2\pi n v_a/\lambda_p$, and for small Brillouin shifts $\lambda_p\lambda_S \approx \lambda_p^2$, we obtain the more familiar and widely used expression for g_B:

$$g_B = \frac{2\pi n^7 (p_{12})^2}{c\lambda_p^2 \rho_0 v_a \Delta\upsilon_B} \qquad (3.5)$$

where $2/\alpha_a$ is the attenuation length for the acoustic pressure, $\alpha_a = 2\pi\Delta\upsilon_B/v_a$

p_{12} is the elasto-optic coefficient.

n is the refractive index

ρ_0 is the material density

v_a is the acoustic velocity

$\Delta\upsilon_B$ is the FWHM intrinsic Brillouin linewidth

For fused silica the currently accepted value for p_{12} is 0.286, n is 1.457, ρ_0 is 2.2×10^3 kg/m^3, v_a is 5990 m/s, and the most authoritative measurements of $\Delta\upsilon_B$ put it at approximately 100 MHz at 633 nm[51,52]. These values yield a figure of 4.6×10^{-11} m/W for g_B.

In coherent transmission systems, where SBS is a limitation to performance we clearly want to have fibres with material parameters which will lead to minimisation of g_B. However, for the investigation of SBS for applications in lasers and amplifiers, and for material characterisation, we want to maximize g_B, and minimise the threshold power (eqn (3.1)) for a given pump wavelength. The value of the Stokes shift or g_B can be varied either by changing the material composition or through the temperature dependence of the various material constants such as the refractive index and acoustic velocity[53].

There has been comparatively little work done in establishing the effects of dopant concentration and type on the above material parameters in low-loss single mode fibres. The variation in doping will mostly affect the material density, and the acoustic velocity, as well as n and α_a. The change in velocity will have a large effect on the Brillouin shift, Ω,

and this can be used as a method of material characterisation[53,54]. A change of 10% in n, however, results in a factor of 2 change in g_B, although the application of this technique for material characterisation has not been investigated.

It would be desirable, for example, to alter material composition of the fibres, so that the acoustic frequency is altered (through change in n and ρ_0, since the sound velocity v_a is proportional to $(\rho_0)^{-1/2}$). This would be useful, for example, in multi-channel networks. A single high power laser pump could be used to launch light into several fibres with different material characteristics, to generate Stokes waves at different frequencies. These could be used as local oscillator sources, or for amplification of light at a number of frequencies. Another possible application of the material dependence in SBS suggested recently is Brillouin spectroscopy for evaluation of tensile stress in fibres[55]. However, there are technical problems associated with varying the material composition in fibres[56,57]. Table 3.4. shows the comparison between the change in refractive index and the sound velocity of fused silica doped with several common types of dopants. Up and down arrows refer to higher and lower than those for pure fused silica, respectively.

	GeO_2	P_2O_5	TiO_2	B_2O_3	F_2	Al_2O_3
n	↑	↑	↑	↓	↓	↑
v_a	↓	↓	↓	↓	↓	↑

Table 3.4. Comparison of optical and acoustic properties of fused silica with different dopants.

Doping with germanium oxide (GeO_2) and P_2O_5 increases refractive index (by approximately 0.005 in n for 5 mol % of GeO_2), and density. But high doping levels of some dopants lead to devitrification and fracturing on pulling[56], and in order to increase the malleability of the material, it becomes necessary to add substances like fluorine and boron which reduce n with doping (approx 0.5 mol % for 0.002 in n for fluorine).

From the existing information on optical glasses[52, 58] it appears that there is no significant

variation in the elasto-optic coefficient(s) in silicate classes doped with B_2O_3, Al_2O_3, Na_2O, PbO, K_2O etc, but a large variation in p_{12} has been observed in halide and fluoride glasses[59-61]

Recently some results have been published[53,61] which reported the variation of the acoustic frequency with germanium and phosphorus (GeO_2, P_2O_5) citing values for the Brillouin shift coefficient defined by the frequency shift (= acoustic frequency) per unit mol % concentration, for GeO_2 and P_2O_5 as 125 and 162 MHz/mol % at 830 nm, and 154 MHz/mol % for GeO_2 at 1.5 μm[62]. More recently, Shibata et al.[63] quote the Brillouin shift coefficients as 107 MHz/mol % for GeO_2- doped core and 356 MHz/mol % for F_2-doped cladding. However, in all these results there has not been any quantitative or systematic evaluation of the effect of varying doping levels on density, and on other material parameters, and their effect on g_B. In comparison, the recently measured temperature variation of the Brillouin shift was reported to be approximately 2.7 - 6.4 MHz/°C, where the dominant effect producing this dependence is the change of refractive index with temperature, while the temperature dependence of the acoustic velocity is very small[54].

In addition, there is a large variation in the values quoted in the literature for the acoustic attenuation constant, and hence the intrinsic Brillouin linewidths, with such differences in FWHM linewidths of 53 MHz[12,63] and 215 MHz for silica fibre at 1.5 μm[62]. [The experimental set up to measure of the Brillouin linewidth is similar to that used in amplifier experiments, except in this case, the difference frequency between the pump and probe lasers is swept (over some frequency range of up to 3 GHz) to give the Brillouin gain profile.

Related to this, there is also some confusion as to the exact interpretation of the Brillouin gain spectra. In particular, there is some discussion as to whether the second resonance peak is due to scattering from acoustic phonons in the cladding[30,35] or in the core - for depressed-core index profile, where the field power of the HE_{11} mode is mostly concentrated[53, 62-65]. This led to quite a fierce debate, and slightly perturbed the serenity of the normally quiet scientific media. Some light was thrown on this matter by the work of N. Shibata et al.[65] and Jen et al.[66,67] who highlighted some significant and highly material dependent variations in the Brillouin spectra of different fibres. Particularly they evaluated the role of acoustic wave guidance on the strength of the SBS process. Since the

acoustic wavelength is comparable to the optical wavelength, both longitudinal and shear acoustic waves can be guided in an optical fibre when $v_{shear,\,clad} < v_{shear,\,core}$ for shear modes, and $v_{long,\,clad} < v_{long,\,core}$ for longitudinal modes. Since SBS is an acousto-optic process, it is enhanced if the optical fibre also guides acoustic waves. It has been found that the lowest order longitudinal modes have the highest backward collinear acousto-optic interaction coefficient. The interaction between the HE_{11} mode and these modes generates extra peaks in the Brillouin spectra, which can be traced as originating from the fibre core for fibres highly doped with GeO_2(9 mol-%). These extra peaks will serve to 'spread' the Brillouin intrinsic gain curve (more than by a factor of 2.5 compared to those predicted for bulk glass[63]), since the width of each acoustic resonance will be approximately equal to the intrinsic Brillouin bandwidth. Two points emerge as results of these studies. Firstly, that Brillouin gain bandwidth has to be evaluated with particular attention to the doping particulars; for example in commercially available fibres where the germanium doping is normally limited to approximately 3 mol-% doped core, the frequency interval between the peaks is so small as to be indistinguishable thus precluding the observation of these peaks or their existence in ordinary single mode fibre. Consequently, the evaluation of the variation Brillouin shift shift with doping must be carried out in fibres where $v_{long,\,clad} > v_{long,\,core}$ to give unambiguous, objective measurements.

Secondly, the acoustic properties of the core and cladding in single mode fibres can represent a criteria for the choice of fibre for particular application. For example, in communication systems where it is desirable to minimise the Brillouin gain, fibres with $v_{a,\,core} > v_{a,\,clad}$ should be chosen, since an increase in the velocity difference minimises the acoustic guidance, and serves to decrease the SBS gain. In addition, the discrete multiple gain peaks should be avoided in the design of coherent communication networks such as biderectional FDM/WDM transmission systems, since they can lead to increased crosstalk. Conversely, in amplification or lasing applications where a high Brillouin gain with a large bandwidth is desirable, good acoustic guidance is necessary. In conclusion to this section, it is possible to note that while Brillouin scattering undoubtedly appears to be a useful spectroscopic tool in characterising fibre properties for a particular application, further detailed and systematic studies should be undertaken to investigate the material dependence of the Brillouin gain in different fibres with varying compositions.

3.6. References for Chapter 3

1 E.P. Ippen, 'Low power quasi-cw Raman oscillator', Appl. Phys. Lett. **16**, 303 (1970)

2 E. P. Ippen and R. H. Stolen, 'SBS in optical fibres', ibid. **21**, 539 (1972)

3 R. G. Smith, 'Optical power handling capacity of low loss optical fibres as determined by Raman and Brillouin scattering', Appl. Opt. **11**, 2489 (1972)

4 R. H. Stolen, 'Active fibres' in: "New directions in guided waves and coherent optics', NATO Advanced Study Institute, Cargese 1982, D. B. Ostrowsky ed., Martinus Nijhof Publ., Amsterdam, 1982

5 C. A, Miller, 'Direct method of determining equivalent-step-index profiles for monomode fibres', Electron. Lett. **17**, 458 (1981)

6 M. Artiglia, G. Coppa, P. Di Vita, M. Potenza, and A. Sharma, 'Mode field diameter measurements in single mode optical fibres', J. Lightwave Tech. **LT-7**, 1139 (1989)

7 P. Labudde, P. Anliker, and H. P. Weber, 'Transmission of narrow band high power laser radiation through optical fibres', Opt. Commun. **32**, 385 (1980)

8 N. Uesugi, M. Ikeda, and Y. Sasaki, 'Maximum single frequency input power in a long optical fibre as determined by SBS', Electron. Lett. **17**, 380 (1981)

9 D. Cotter, 'Observation of SBS in low loss silica fibre at 1.3 μm', ibid. **18**, 638 (1982)

10 - 'Transient SBS in long single mode fibres', ibid., 504

11 - 'Suppression of stimulated Brillouin scattering during transmission of high power narrowband laser in monomode fibre', ibid., 638

12 - 'SBS in a monomode optical fibre', J. Opt. Commun. **4**, 10 (1983)

13 T. Okoshi and K. Kikuchi, "Coherent optical fibre communications", KTK Scientific Publishers, Tokyo, 1988

14 M. Tsubokawa, S. Seikai, T. Nakashima, and N. Shibata, 'Suppression of SBS in a single mode fibre by an acousto-optic modulator', Electron. Lett. **22**, 473 (1986)

15 E. Lichtman, A. A. Friesem, R. G. Waarts, and H. H. Yaffe, 'Stimulated Brillouin scattering excited by two pump waves in single mode fibres', JOSA B **4**, 1397 (1987)

16 Eyal Lichtman, Electronics Department, Weizmann Research Institute: personal communication

17 E. Lichtman, R. G. Waarts, and A. A. Friesem, 'Stimulated Brillouin scattering excited by a modulated pump wave in single mode fibres', J. Lightwave Tech. **LT-7**, 171 (1989)

18 Y. Aoki, K. Tajima, and I. Mito, "Input power limits of single mode optical fibres due to SBS in optical communication systems', J. Lightwave Tech. **6**, 710 (1988)

19 A. Hadjifotiou and G. A. Hill, 'Suppression of SBS by PSK modulation for high

power optical transmission', IEE Proceedings **133**, 256 (1986)

20 Y. Aoki, K. Tajima, and I. Mito, 'Observation of stimulated Brillouin scattering in single mode fibres with single frequency laser diode pumping', Opt. Quantum Electron. **19**, 141 (1987)

21 Y. Aoki, K. Tajima, and S. Murata, 'Input power limits of optical fibres due to SBS in FSK coherent optical transmission systems', in Technical Digest CLEO/IQEC'87 (Baltimore, MD), 1987, paper WH2

22 A. Bolle, G. Grosso, A. Consentino, A. Mortara, and B. Daino, 'Influence of phase modulation on the Brillouin gain curve', ECOC '88 conference proceedings, Pt. 1; IEE conf. publ. **292**, 123 (1988)

23 A. Bolle, G. Grosso, and B. Daino, 'Brillouin gain curve dependence on frequency spectrum of PSK-modulated signals', Electron. Lett. **25**, 2 (1989)

24 A. Bolle, G. Grosso, and B. Daino, 'Temporal characteristics of PM signals in the presence of SBS', to be presented at ECOC '89, Gotheburg, Sweeden, 10 - 14 September 1989

25 A. Cosentino, M. Martinelli, G. Grosso, and B. Daino, 'Pump spectrum dependence of SBS in single mode optical fibres', submitted to JOSA B, August 1989

26 R. G. Waarts, A. A. Friesem, and Y. Hefetz, 'Frequency-modulated to amplitude-modulated signal conversion by a Brillouin induced phase change in single mode fibres', Opt. Lett. **13**, 152 (1988)

27 T. Horriguchi, M. Tateda, N. Shibata, and Y. Azuma, 'Brillouin gain variation due to a polarisation change of the pump or Stokes fields in standard single mode fibres', ibid. **14**, 329 (1989)

28 - 'BODTA - nondestructive measurement of single mode optical fibre attenuation characteristics using Brillouin interaction', J. Lightwave Tech. **LT-7**, 1170 (1989)

29 C. L. Tang, 'Saturation and spectral characteristics of the Stokes emission in the Stimulated Brillouin process', J. Appl. Phys. **37**, 2945 (1966)

30 R. G. Waarts and R. P. Braun, 'Crosstalk due to SBS in monomode fibre', **21**, 1114 (1985)

31 C. G. Atkins, D. Cotter, D. W. Smith, and R. Wyatt, 'Application of Brillouin amplification in coherent optical transmission', Electron. Lett. **22**, 556 (1986);

32 D. Cotter, D. W. Smith, C. G. Atkins, and R. Wyatt, 'Influence of nonlinear dispersion in coherent narrowband amplification by SBS', ibid. 672

33 A. R. Chraplyvy and R. W. Tkach, 'Narrowband tunable optical filter for channel

selection in densely packed WDM systems', ibid. **22**, 1084 (1986)
34 N. A. Olsson and J. P. Van der Ziel, 'Cancellation of fibre loss by semiconductor laser pumped Brillouin amplification at 1.5 μm', Appl. Phys. Lett. **48**, 1329 (1986)
35 - 'Characteristics of a semiconductor laser pumped Brillouin amplifier with electronically controlled bandwidth', J. Lightwave Tech. **LT-5**, 147 (1987)
36 R. W. Tkach, A. R. Chraplyvy, R. M. Derosier, and T. Shang, 'Optical demodulation and amplification of FSK signals using AlGaAs lasers', Electron. Lett. **24**, 260 (1988)
37 R. W. Tkach, A. R. Chraplyvy and R. M. Derosier, 'Performance of a WDM network based on stimulated Brillouin scattering', Phot. Tech. Lett. **1**, 111 (1989)
38 K. O. Hill, B. S. Kawasaki, and D. C. Johnson, 'cw Brillouin laser', Appl. Phys. Lett. **28**, 608 (1976)
39 - 'cw generation of multiple Stokes and anti-Stokes Brillouin shifted frequencies', ibid. **29**, 185 (1976)
40 B. S. Kawasaki, D. C. Johnson, Y. Fuji, and K. O. Hill, 'Bandwidth limited operation of a modelocked Brillouin parametric oscillator', ibid. **32**, 429 (1978)
41 V. N. Lugovoy and V. N. Streltsov, Opt. Acta **20**, 165 (1973)
42 R. H. Stolen, 'Polarisation effects in fibre Raman and Brillouin lasers', IEEE J. Quantum Electron. **QE-15**, 1157 (1979)
43 P. J. Thomas, H. M. van Driel, and G. I. A. Stegeman, 'Possibility of using an optical fibre Brillouin ring laser for inertial sensing', Appl. Optics **19**, 1906 (1980)
44 S. P. Smith, F. Zarinetchi, and S. Ezekiel, 'Fibreoptic ring laser gyroscope', Proc. Conference on Optical Fibre Sensors (OFS'89), postdeadline paper Tu10-6, pp 48 - 53
45 D. R. Ponikvar and S. Ezekiel, 'Stabilized single frequency stimulated Brillouin fibre ring laser', Opt. Lett. **6**, 398 (1981)
46 I. Bar-Joseph, A. Dienes, A. A. Friesem, E. Lichtman, and R. G. Waarts, and H. H. Yaffe, 'Spontaneous mode-locking of single and multi-mode pumped SBS fibre lasers', Opt. Communs. **59**, 296 (1986)
47 I. Bar-Joseph, A. A. Friesem, E. Lichtman, and R. G. Waarts, 'Steady and relaxation oscillations of stimulated Brillouin scattering in single mode optical fibres', JOSA B **2**, 1606 (1985)
48 J. Botineau, C. Leycouras, C. Montes, and E. Picholle, 'Stabilisation of stimulated Brillouin fibre laser by strong pump modulation', ibid. **6**, 300 (1989)
49 L. F. Stokes , M. Chodorow, and H. J. Shaw, 'All-fibre stimulated Brillouin scattering ring laser with submilliwatt pump threshold', Opt. Lett. **7**, 509 (1982)
50 T. C. Rich and D. A. Pinnow, 'Evaluation of fibre optic waveguides using Brillouin

spectroscopy', Appl. Opt. **13**, 1376 (1974)

51 A. S. Pine, 'Brillouin scattering study of acoustic attenuation in fused quartz', Phys. Rev. **185**, 1187 (1969)

52 D. Heiman, D. S. Hamilton, and R. W. Hellwarth, 'Brillouin scattering measurements on optical glasses', Phys. Rev. B **19**, 6583 (1979)

53 R. W. Tkach , A. R. Chraplyvy, and R. M. Dorosier, 'Spontaneous Brillouin scattering for single mode optical fibre characterisation', Electron. Lett. **22**, 1011 (1986)

54 D. Culverhouse, F. Farahi, C. N. Pannel, , and D. Jackson, 'Potential of stimulated Brillouin scattering as a sensing mechanism for distributed temperature sensors', Electron. Lett. **25**, 913 (1989); 'Stimulated Brillouin scattering: a means to realise tunable microwave generator or distributed temperature sensor', ibid. 915

55 T. Horriguchi, T. Kurashima, and M. Tateda, 'Tensile strain dependence of Brillouin frequency shift in silica optical fibres', IEEE Phot. Tech. Lett. **1**, 107 (1989)

56 Adrian C. Grenham, Optical Fibre Systems Division, GEC Hirst Research Laboratories: personal communication

57 G. Ghigo, E. Modone, G. Parisi, and G. Roba, 'GeO_2-doped high NA multimode fibre made by pressurised MCVD', Proc. SPIE **584** 'Optical fibre characteristics - standard', 26 (1986)

58 J. Schroeder, 'Brillouin scattering and Pockels coefficients in silicate glasses', J. Non-crystalline Solids **40**, 549 (1980)

59 J. Schroeder, M. Fox-Bilmont, B. G. Pazol, V. Tsoukala, M. G. Drexhage, and O. H. El-Bayoumi, 'Rayleigh and Brillouin scattering in heavy metal fluoride glasses: intrinsic Rayleigh scattering', Opt. Eng. **24**, 697 (1985)

60 J. Schroeder, L. G. Hwa, M. C. Shyong, G. A. Floudas, D. A. Thompson, and M. G. Drexhage, 'Brillouin scattering and phonon attenuation in halide glasses: stimulated Brillouin emission', Electron. Lett. **23**, 1128 (1987)

61 L. Hwa, J. Schroeder, and X. Zhao, 'Intrinsic Brillouin linewidths and stimulated Brillouin gain coefficients in glasses studied by inelastic light scattering', JOSA B **6**, 833 (1989)

62 N. Shibata, R. G. Waarts, and R. P. Braun, 'Brillouin gain spectra for single mode fibres having pure silica, GeO_2-, and P_2O_5- doped cores', Opt. Lett. **12**, 269 (1987)

63 Y. Azuma, N. Shibata, T. Horiguchi, and M. Tateda, 'Wavelength dependence of Brillouin gain spectra for single mode optical fibres, Electron. Lett. **24**, 250 (1988)

64 N. Shibata, Y. Azuma, T. Horiguchi, and M. Tateda, 'Identification of longitudinal acoustic modes guided in the core region of single mode optical fibre by Brillouin gain

spectra measurements', Opt. Lett. **13**, 595 (1988)

65 N. Shibata, K. Okamoto, and Y. Azuma, 'Longitudinal acoustic modes and Brillouin gain spectra for GeO_2 - doped core single mode fibres, JOSA B **6**, 1167 (1989)

66 C. K. Jen, J. E. B. Oliveira, N. Goto, and K. Abe, 'Role of guided acoustic wave properties in single mode optical fibre design', Electron. Lett. **24**, 1419 (1988)

67 C. K. Jen, 'The role of acoustic properties in designs of acoustic and optical fibres', presented at European Materials Research Society Conference, 30 May - 2 June 1989, Strasbourg, France; to be published in the J. Materials Science B: Solid State Materials for Advance Technology

Chapter 4

SOLUTIONS OF THE SBS EQUATIONS IN SINGLE MODE OPTICAL FIBRES

As outlined in the previous chapter, a considerable amount of research effort has been invested into the experimental investigation of SBS in single mode optical fibres, viewed both as a limitation to the operation of coherent systems, as well as for amplification applications and lasing. In view of this, it is perhaps surprising that the equations describing the evolution of the pump and Stokes intensities with distance have not been solved. Although Smith's somewhat arbitrary threshold criterion is valid in the limit of the undepleted pump approximation, it would be very useful to obtain a continuous variation of the Stokes power as a function of input pump power and fibre length. Also, while intuitive statements can be made about the form of the solutions, such calculations would provide invaluable insight into the physics of SBS generation, particularly into the process of energy exchange between the pump and Stokes waves, of importance both in the context of optical fibre systems, and Brillouin lasing.

While, in the past, the absolute limit on the input power was considered to be governed by the SBS threshold, it is conceivable that operation at a transmitter power above Brillouin threshold might be acceptable even if it results in a certain amount of pump depletion. In addition, some recent results indicate that the relative intensity noise (RIN) of semiconductor lasers for use in communication systems sensitively depends on the amount of optical feedback into the cavity[1]; thus a measure for the Brillouin backscattered power for a given transmitter power would be invaluable in calculating noise margins in communication links. Moreover, the effects of modulation, pump linewidth, and depolarisation can all be contained in the expression for the Brillouin gain coefficient, g_B, leading to extremely versatile solutions covering a wide range of practical situations.

Bearing in mind the foregoing discussion, the aim of obtaining numerical solutions to the

SBS equations is the calculation of pump depletion, coupled with the more precise evaluation of the Brillouin threshold, and the amount of the Stokes power scattered backwards. On the other hand, although the Brillouin amplifier is normally pumped below threshold, the analysis could also be extended to cover Brillouin amplifier applications for estimation of the maximum achievable gain and saturation criteria in terms of practical parameters, such as fibre length and loss, Brillouin gain, and pump power. As will become clear in Chapters 6 and 7, these calculations can also form a tool for characterising Brillouin lasers.

The theory and the choice of the numerical method used, and its accuracy are explained in section 4.1, and the results are given in section 4.2. Of particular interest is the effect of the fibre loss, and the numerical results are compared with the exact analytical solutions available for the $\alpha_0 = 0$ case. In section 4.3, the validity of the solutions are further tested by comparing the theoretical results with published experimental data, both for SBS generation in long fibre links. The implications of the results are discussed with reference to long haul submarine type fibre links in 4.4, and applications to Brillouin amplifiers including a comparison with available amplification data in 4.5. Conclusions to this chapter are outlined in section 4.6.

4.1. Description of the numerical method

Although the pump and Stokes intensity equations as given by equations (2.25) have not been fully solved, analytically or numerically, there have been a number of attempts at these. As stated in the previous chapter, the equations can not be solved analytically. In fact, it would be more accurate to say that no analytical solutions are known that are valid over the range of interest. This point is illustrated in Appendix D in which the analytical solutions of the form: $I_{p,S}(z) = I_{p,S}(0)\exp - [K_{p,S}z]$, where $K_{p,S}$ is a constant or a slowly varying function of z. Although these are in fact solutions to the SBS equations, their range of validity is such that the inequality $g_B I_p(0)L < 1$ [or $I_p(0) < 2e^{0.5}(\alpha_0/g_B)$] is satisfied. Thus, although these are analytical solutions, they offer us no additional information compared to the undepleted pump approximation case. This illustrates the difficulty of attempting to find a suitable ansatz for solutions in this case.

It would also be unfair to imply that no solutions exist for the three coupled field PDEs

describing the interaction of the pump, Stokes, and acoustic waves in the SBS process. Notably, Enns and Batra[2] claimed to have analytically solved the intensity equations, while only obtaining the solutions in the situation analogous to the Raman process. Chu et al.[3] have obtained analytical solutions for the two coupled PDEs describing pump and Stokes fields for the case corresponding to the heavily damped acoustic wave. Recently, Coste and Montes[4] have numerically solved the three coupled nonlinear PDEs for the case of zero optical loss. Indeed, although the Coste and Montes solutions are interesting from the mathematical point of view, the results can not easily be related to practical values and real experimental parameters. It also turns out that the role of the optical loss is an important one, and can not be neglected. Indeed, in our case no additional advantage is gained from solving the three coupled equations since the strongly-damped acoustic wave approximation is completely justified. We also limit ourselves to the solution to two intensity equations for the time-independent, steady-state case.

The numerical method adopted in solving the SBS equations was the 4th order Runge-Kutta algorithm. As was outlined in the previous chapter, the form of the equations is such that the boundary conditions have to be applied at the opposite ends of the interaction region. We have adopted the 4th order Runge-Kutta algorithm[5] in solving the equations as the one which is easy to implement and self-starting, as well as resulting in stable solutions. Because the levels of the pump intensity and the Stokes noise differ by many orders of magnitude, the accuracy which is available in the Runge-Kutta algorithm was also a factor in the choice of this algorithm. In fact, the Runge-Kutta algorithm was used by Coste and Montes in solving the three coupled equations in both time and space, for the case of a pulsed pump wave. However, the numerical solutions in reference [4] are complicated by the fact that in the case of PDEs describing counterpropagating waves, a numerical instability occurs if the spatial step h is larger or equal to the temporal step, h'. This leads to a considerable complication of the numerical integration, both regarding the solutions and the CPU time[6].

The system being considered is diagrammatically shown in figure 4.1. It is a single mode fibre of length L, with a Brillouin gain coefficient g_B, as before. The equations describing the evolution of the pump and Stokes waves with z are:

$$\frac{dI}{dz} = - g_B BI - \alpha_o I \quad \text{and} \quad \frac{dB}{dz} = - g_B BI + \alpha_o B \tag{4.1}$$

where for simplicity $I_P(z) = I$ and $I_S(z) = B$, and $0 \leq z \leq L$.

Next, these equations can be normalised, by redefining the space variable, z, so that $\zeta = z/L$, and $0 \leq \zeta \leq 1$. It is further assumed that the input pump intensity, at $\zeta = 0$, is I_0. Then, we define normalised intensities, P and S, so that

$$P(\zeta) = \frac{I}{I_0} = P \quad \text{and} \quad S(\zeta) = \frac{B}{I_0} = S \tag{4.2}$$

where $P(0) = 1$, is the normalised input pump intensity.

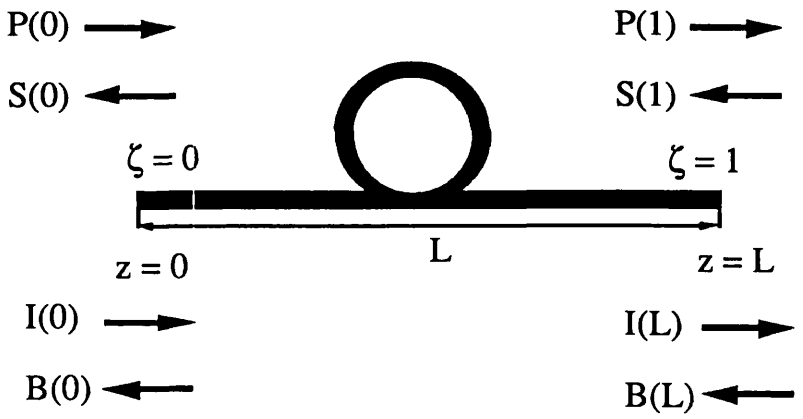

Figure 4.1 (a). Showing the propagation geometry of the pump and Stokes intensities in a length L of single mode fibre.

The pump and Stokes equations now become:

$$\frac{dP}{d\zeta} = - \sigma SP - \beta P \tag{4.3}$$

and,

$$\frac{dS}{d\zeta} = - \sigma SP + \beta S \tag{4.4}$$

where $\sigma = g_B L I_0$ is the gain factor, and $\beta = \alpha_0 L$ is the loss.

The boundary conditions are then, P(0) = 1, and $S(1) \approx 10^{-9}$. This latter is the value of the Stokes input noise or spontaneous scattering, and can be calculated from eqns (3.2) and (3.3) using Smith's approximation that the spontaneous Stokes noise within the Brillouin bandwidth is equal to the injection of one fictitious photon per mode. Alternatively, a similar value can be arrived at by calculating the scattered spontaneous Stokes power from scattering theory[7,8].

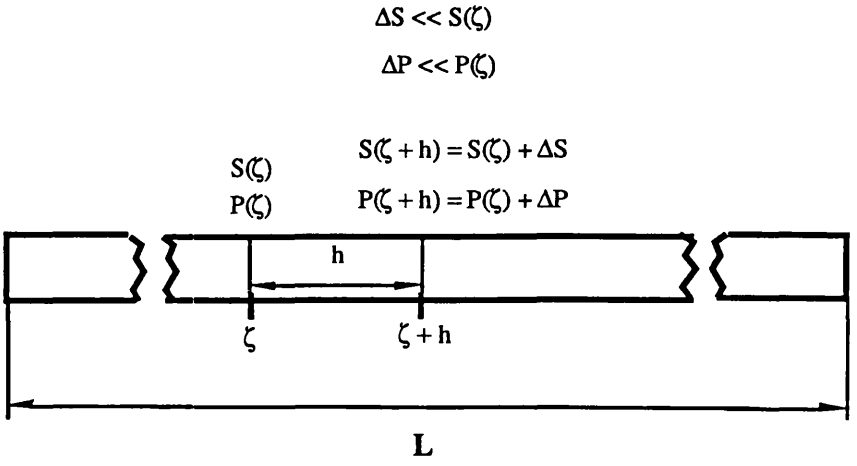

Figure 4.1 (b). Illustrating Runge-Kutta algorithm for the calculation of the pump and Stokes intensities in a length of optical fibre L: P(ζ) and S(ζ) are the pump and Stokes intensities; ΔP and ΔS are the incremental increases in the pump and Stokes intensities calculated over the length h, where h << L.

The details of the Runge-Kutta algorithm are given in Appendix E. Physically, the Runge-Kutta method can be explained as follows. The fibre of length L is split up into n sections

of length h, so that h << L, as depicted in figure 4.1 (b). If at the beginning of a section, say at ζ, the pump intensity is $P(\zeta)$ and the corresponding Stokes intensity is $S(\zeta)$, then at the end of the section, the pump and Stokes intensities can be taken as $P(\zeta + h)$ and $S(\zeta + h)$ respectively. The incremental changes in P and S over the length h are taken to be as ΔP and ΔS respectively. It is assumed that P and S do not change significantly over the length h, so that $\Delta P << P(\zeta)$ and $\Delta S << S(\zeta)$. However, we also assume that the length h is sufficiently long for the strongly damped acoustic wave approximation (as discussed in Chapter 2) to hold. [If we consider a length of fibre L =1 km and a step size h = L/1000 giving h = 1 m, which is three orders of magnitude greater than the acoustic damping length in fused silica in the visible and near infra-red region of the spectrum ($= v_a/\Delta\upsilon_B$, where $\Delta\upsilon_B \approx 100$ MHz and $v_a \approx 6000$ m/s)].

In addition, P and S are assumed to be sufficiently slowly varying with ζ that evolution over h does not vary P and S by more than terms of order h. Since the Runge-Kutta algorithm expresses the difference between $P(\zeta)$ and $P(\zeta + h)$, and $S(\zeta)$ and $S(\zeta + h)$ in terms of a series in h (as explained in Appendix E) and matches the terms in the equations relating P and S up to 4th order in h, the assumption that P and S are slowly varying functions also applies to their derivatives (neglecting terms involving higher orders of derivatives of P and S).

The step size h was chosen to be 0.002 (500 steps). Since the truncation error of the method is of the order of h^5 [5], the accuracy of this method should be sufficient, even bearing in mind the small values of the quantities being calculated. The accuracy of the method can also be verified by comparison with the exact analytical solutions to the equations, known for the case $\alpha_0 L = 0$ (Appendix C).

4.2. Discussion of the solutions

Initially, we plot the spatial dependence of the pump intensity, and the corresponding Stokes intensity as a function of the fibre loss for different values of gain, $g_B I_0 L$: 0 to 500, and loss $\alpha_0 L$: 0 to 8. These are shown in figures 4.2 and 4.3 which show the variation of the normalised pump and Stokes intensities vs the normalised fibre length $0 < \zeta < 1$. What immediately becomes apparent is that the linear attenuation plays a very important role in

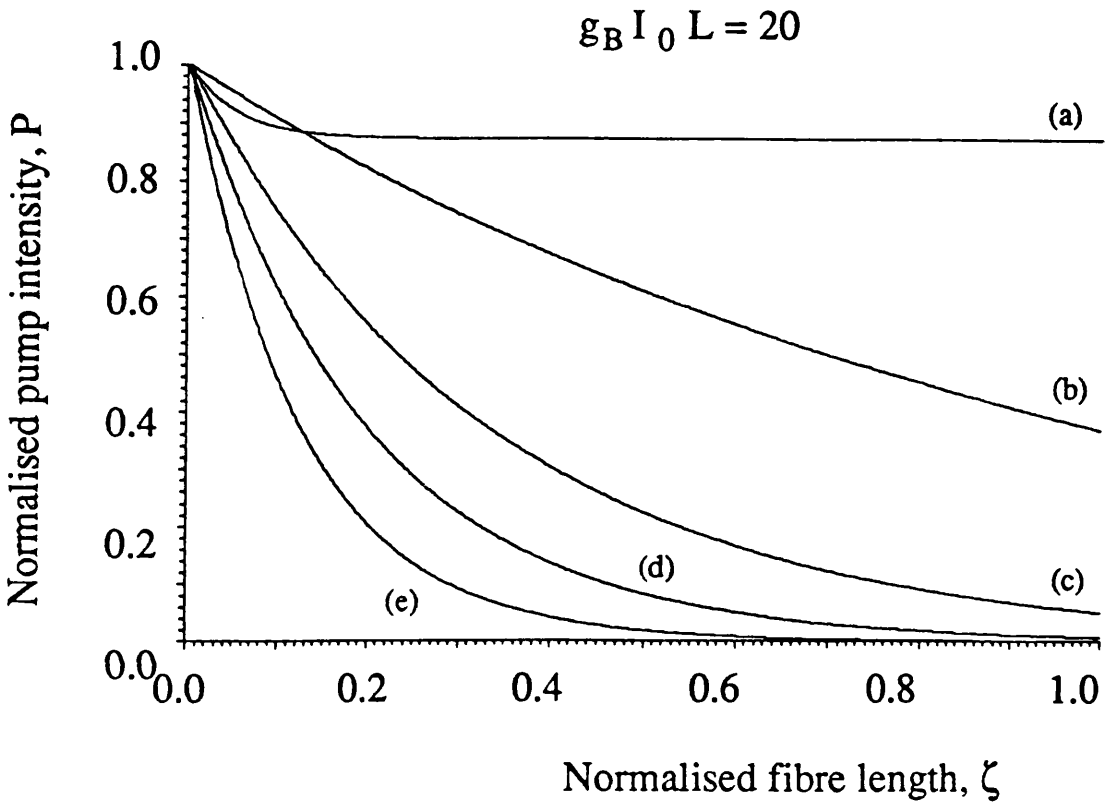

Figure 4.2 (i)

Figure 4.2 (i) - (v). Graphs showing normalised pump intensity P vs normalised fibre length, ζ plotted for different values of gain, $g_B I_0 L$ (= input pump intensity), and fibre loss, $\alpha_0 L$: (a) 0; (b) 1; (c) 3; (d) 5; and (e) 8.

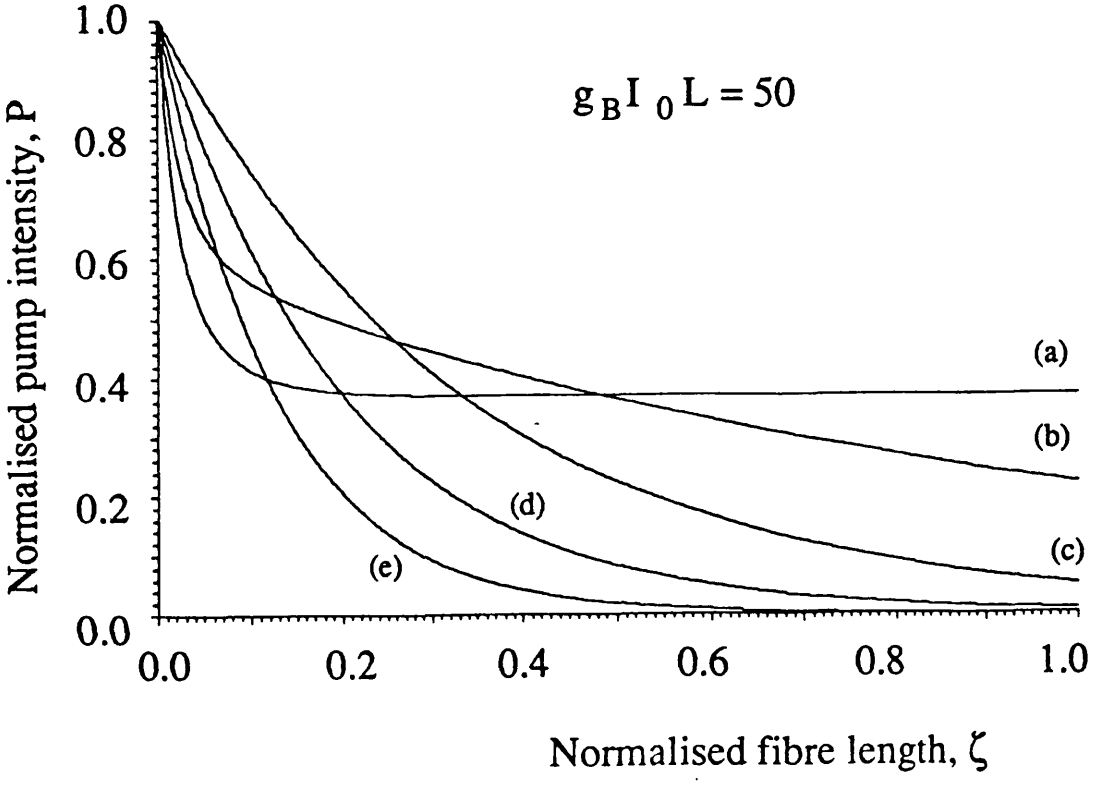

Figure 4.2 (ii)

Figure 4.2 (i) - (v). Graphs showing normalised pump intensity P vs normalised fibre length, ζ plotted for different values of gain, $g_B I_0 L$ (= input pump intensity), and fibre loss, $\alpha_0 L$: (a) 0; (b) 1; (c) 3; (d) 5; and (e) 8.

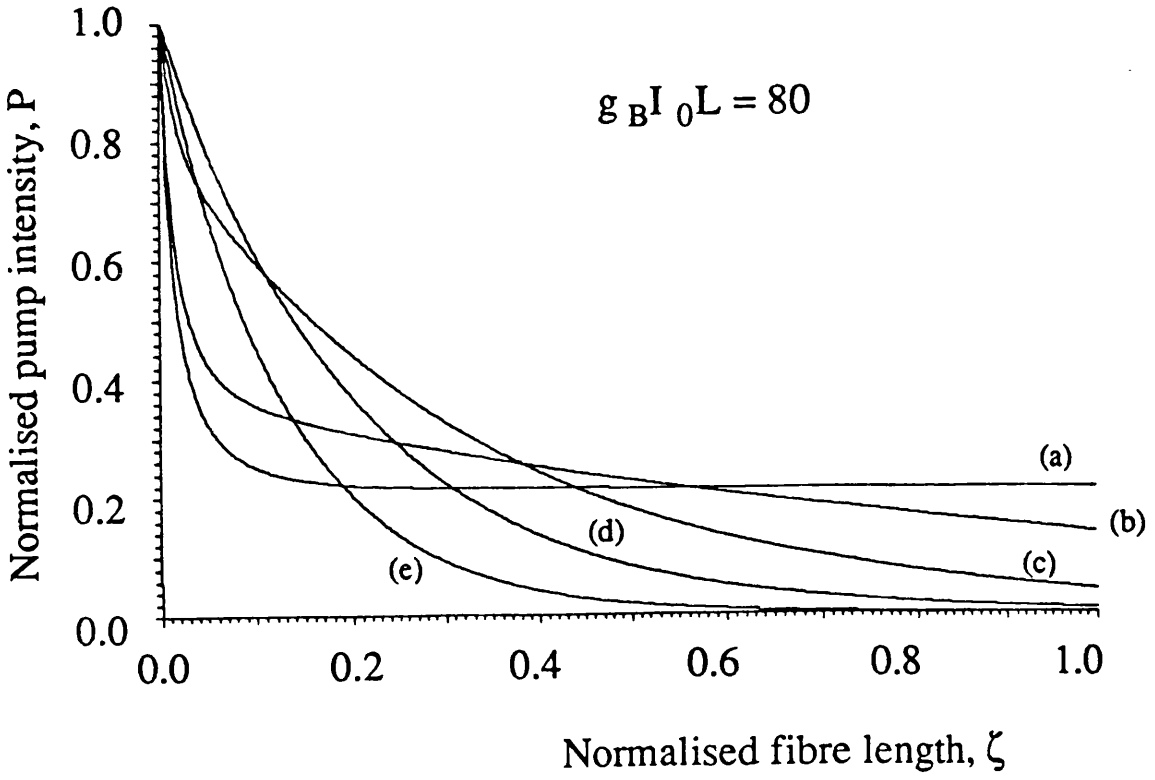

Figure 4.2 (iii)

Figure 4.2 (i) - (v). Graphs showing normalised pump intensity P vs normalised fibre length, ζ plotted for different values of gain, $g_B I_0 L$ (= input pump intensity), and fibre loss, $\alpha_0 L$: (a) 0; (b) 1; (c) 3; (d) 5; and (e) 8.

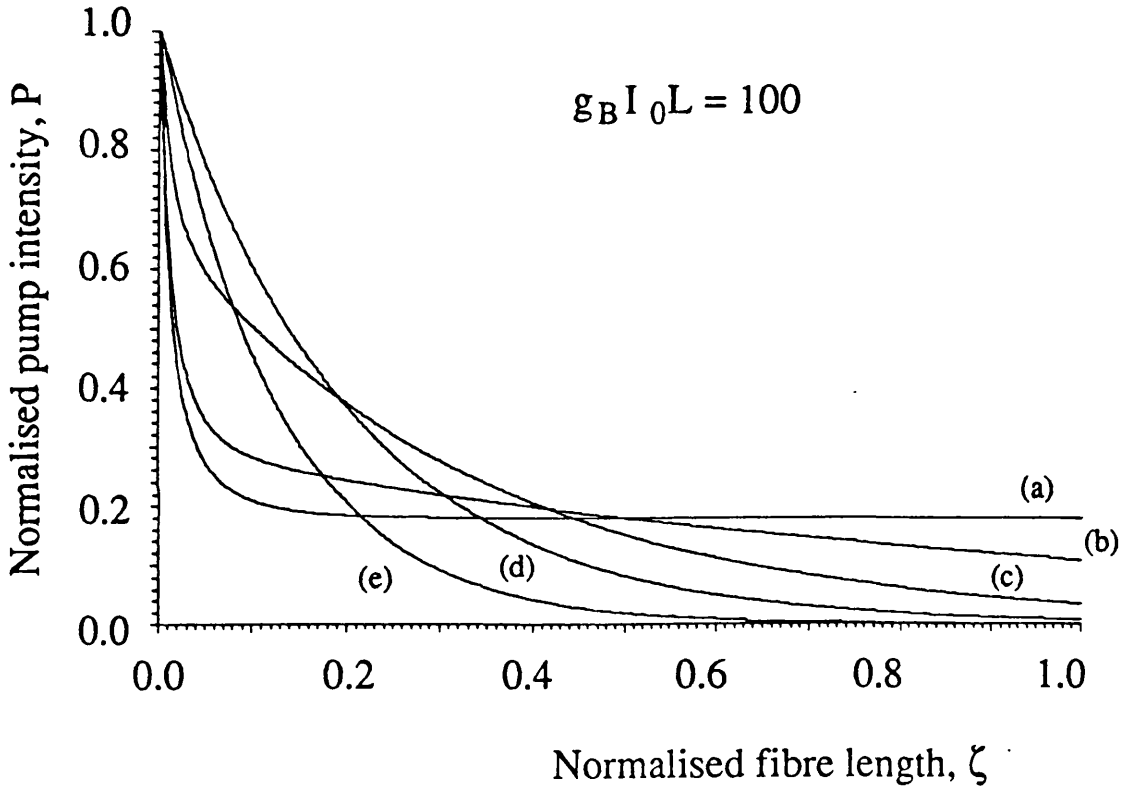

Figure 4.2 (iv)

Figure 4.2 (i) - (v). Graphs showing normalised pump intensity P vs normalised fibre length, ζ plotted for different values of gain, $g_B I_0 L$ (= input pump intensity), and fibre loss, $\alpha_0 L$: (a) 0; (b) 1; (c) 3; (d) 5; and (e) 8.

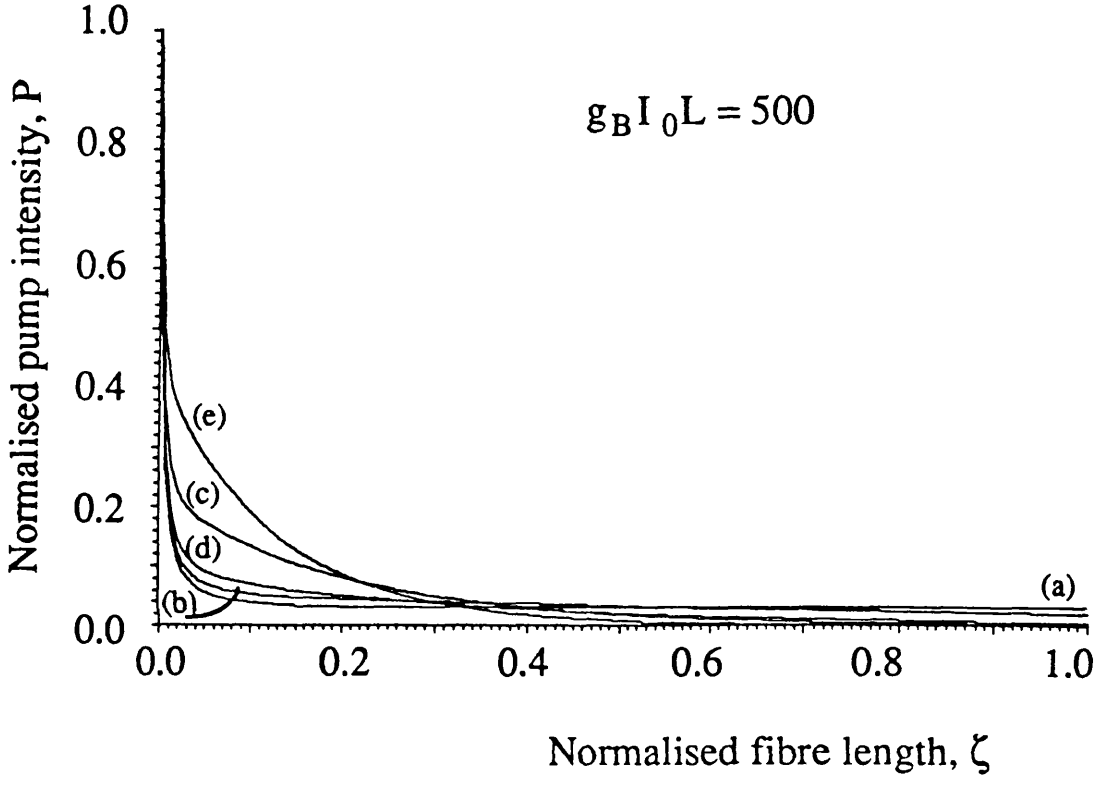

Figure 4.2 (v)

Figure 4.2 (i) - (v). Graphs showing normalised pump intensity P vs normalised fibre length, ζ plotted for different values of gain, $g_B I_0 L$ (= input pump intensity), and fibre loss, $\alpha_0 L$: (a) 0; (b) 1; (c) 3; (d) 5; and (e) 8.

the spatial evolution of the pump and Stokes intensities. Specifically, the graphs emphasise how sensitively the Brillouin threshold is dependent on the fibre loss. Specifically, the lower the fibre loss, the lower is the Brillouin power threshold. Fig 4.2 (i) shows the variation of the pump with low Brillouin gain ($g_B I_0 L = 20$), with the exponential decay $\exp[- \alpha_0 L]$ due only to the linear fibre loss, $\alpha_0 L$. In fig 4.3 (i), for the low value of the gain of $g_B I_0 L = 20$, only the Stokes intensity (in the case of $\alpha_0 L = 0$) is above threshold. As the gain (and hence the input pump intensity is increased, the figures 4.3 (ii) - (v) show the corresponding Stokes intensities as they exceed threshold in turn, and the pump deviates from the exponential decay (figs. 4.2 (ii) -(v)), as it becomes depleted by the counter-propagating Stokes intensity.

The Stokes intensity is plotted for $0 < \zeta < 0.2$, since the significant growth of the Stokes intensity only takes place close to the input end of the fibre (the Stokes wave is amplified from noise, starting at the $\zeta = 1$ (or $z = L$) end). For $g_B I_0 L = 50$ (figs. 4.2 (ii), 4.3 (ii)), only the Stokes intensity for $\alpha_0 L = 0$, 1 exceed threshold, and is just at threshold for $\alpha_0 L = 3$ at $g_B I_0 L = 80$ (fig. 4.2 (iii), 4.3 (iii)). As the gain is further increased, figs 4.2 (iv) and 4.3 (iv) show that for $g_B I_0 L = 100$ four Stokes intensities are above threshold, with conversion efficiencies ranging from 82% to 1% for $\alpha_0 L = 0$ to 5, with the pump intensity exhibiting severe depletion for the cases of high conversion efficiencies. Figures 4.2 (v) and 4.3 (v) show the pump and Stokes intensities for the case of very high gain $g_B I_0 L = 500$ and severe pump depletion in all cases with conversion efficiency ranging from 45% ($\alpha_0 L = 8$) to almost complete conversion of the pump intensity into the Stokes intensity of 97%. It follows that the pump depletion is thus most dramatic in the case of lowest fibre losses.

The reason for this is that extra gain has to be 'provided' (by increasing the input pump intensity) to overcome the higher losses, resulting in a higher threshold and a lower conversion efficiency.

Before going on to compare these results with some experimental data, it is necessary to discuss the accuracy and stability of the numerical method used. The first test of the numerical accuracy is to compare the results of the numerical calculations with the exact analytical solutions to the equations known for the case $\alpha_0 L = 0$. The solutions are derived in Appendix C and are plotted in figures 4.4 and 4.5 which show, respectively, the

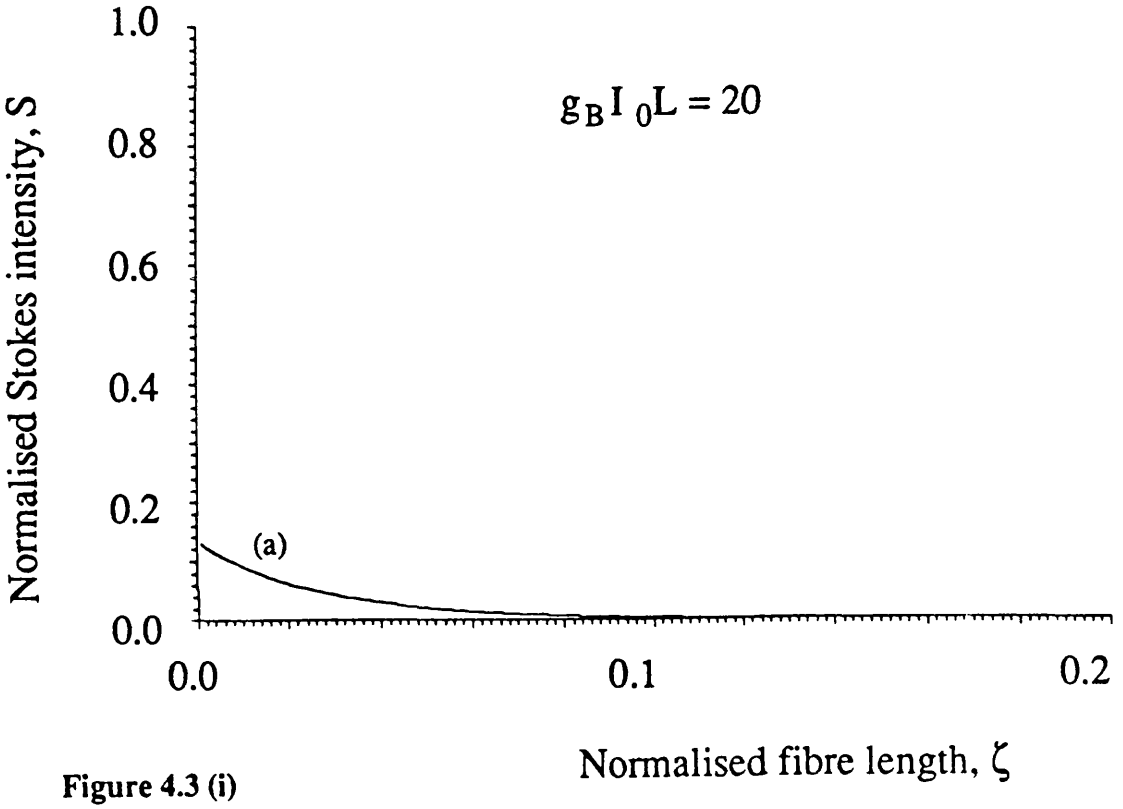

Figure 4.3 (i)

Figure 4.3 (i) - (v). Graphs showing normalised Stokes intensity S vs normalised fibre length, ζ, plotted for different values of gain, $g_B I_0 L$ (= input pump intensity), and fibre loss, $\alpha_0 L$: (a) 0; (b) 1; (c) 3; (d) 5; and (e) 8, corresponding to fig. 4.2.

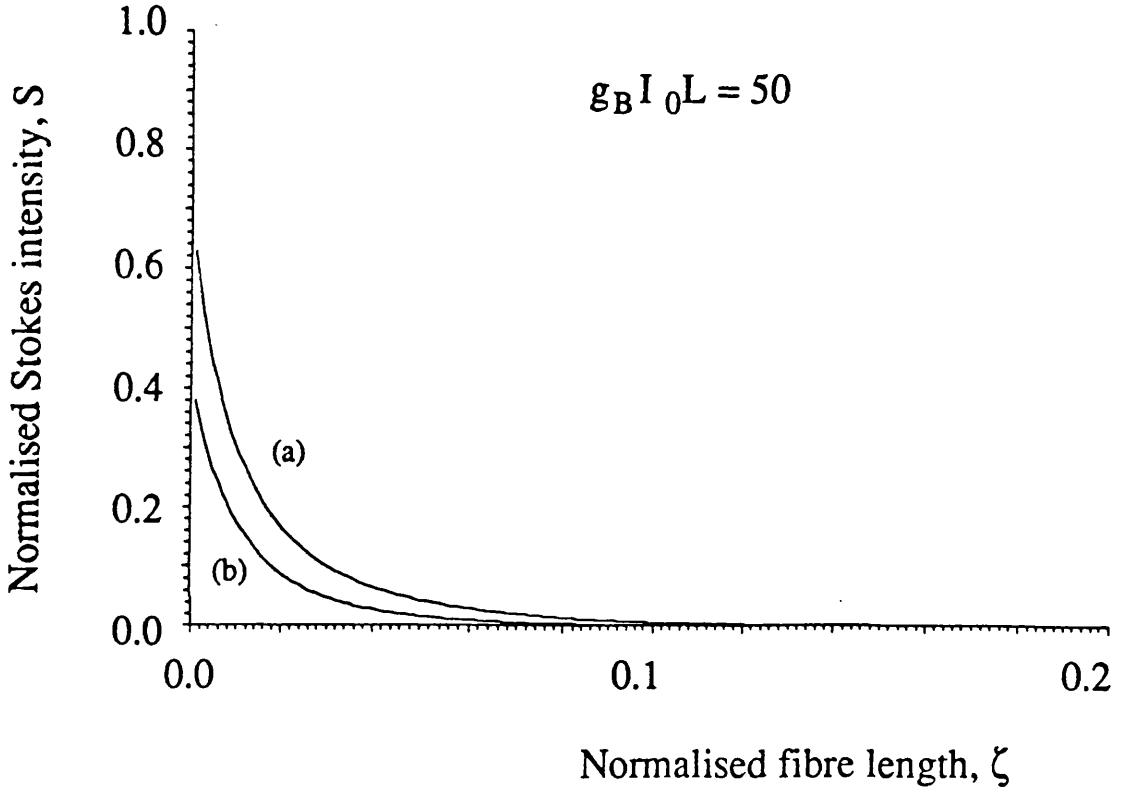

Figure 4.3 (ii)

Figure 4.3 (i) - (v). Graphs showing normalised Stokes intensity S vs normalised fibre length, ζ, plotted for different values of gain, $g_B I_0 L$ (= input pump intensity), and fibre loss, $\alpha_0 L$: (a) 0; (b) 1; (c) 3; (d) 5; and (e) 8, corresponding to fig. 4.2.

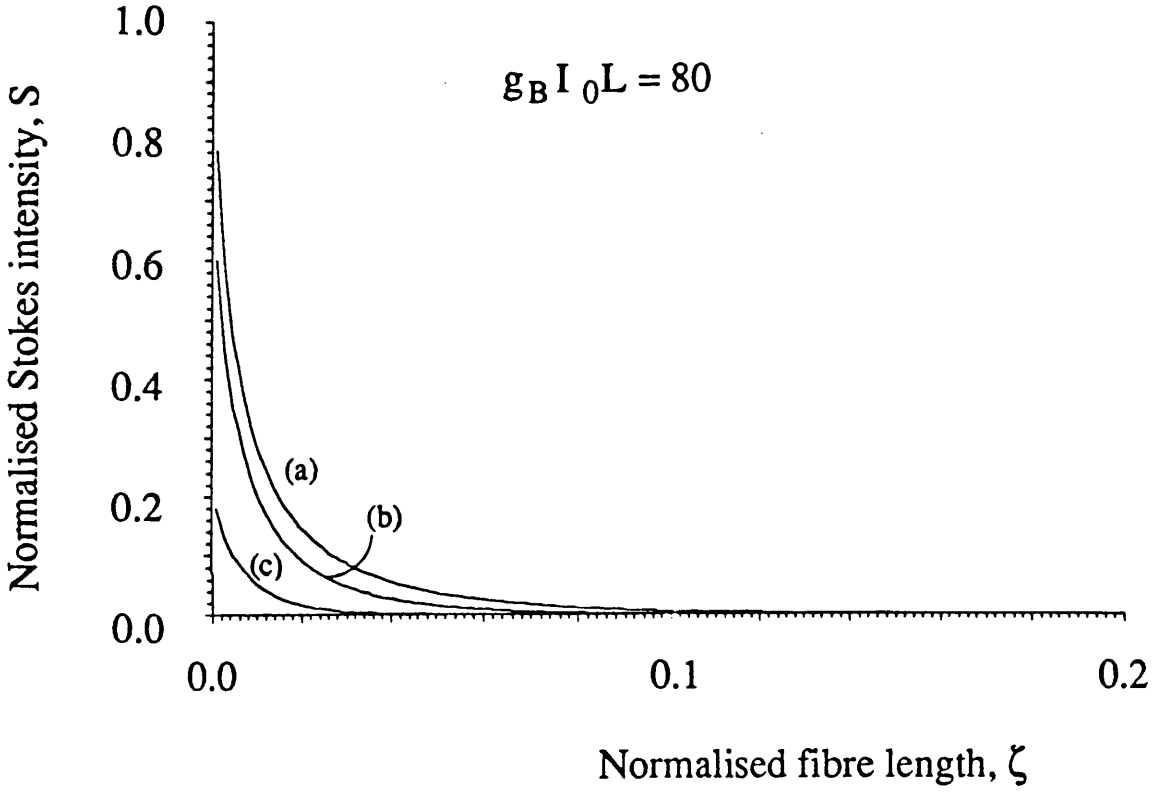

Figure 4.3 (iii)

Figure 4.3 (i) - (v). Graphs showing normalised Stokes intensity S vs normalised fibre length, ζ, plotted for different values of gain, $g_B I_0 L$ (= input pump intensity), and fibre loss, $\alpha_0 L$: (a) 0; (b) 1; (c) 3; (d) 5; and (e) 8, corresponding to fig. 4.2.

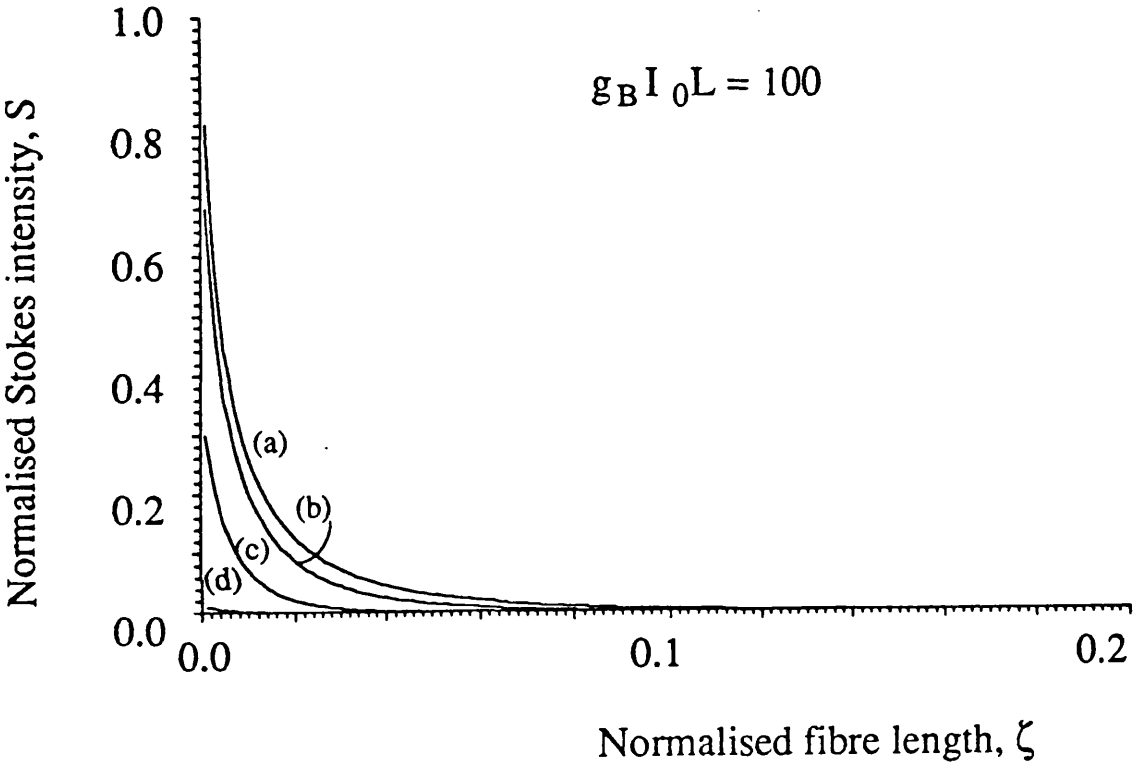

Figure 4.3 (iv)

Figure 4.3 (i) - (v). Graphs showing normalised Stokes intensity S vs normalised fibre length, ζ, plotted for different values of gain, $g_B I_0 L$ (= input pump intensity), and fibre loss, $\alpha_0 L$: (a) 0; (b) 1; (c) 3; (d) 5; and (e) 8, corresponding to fig. 4.2.

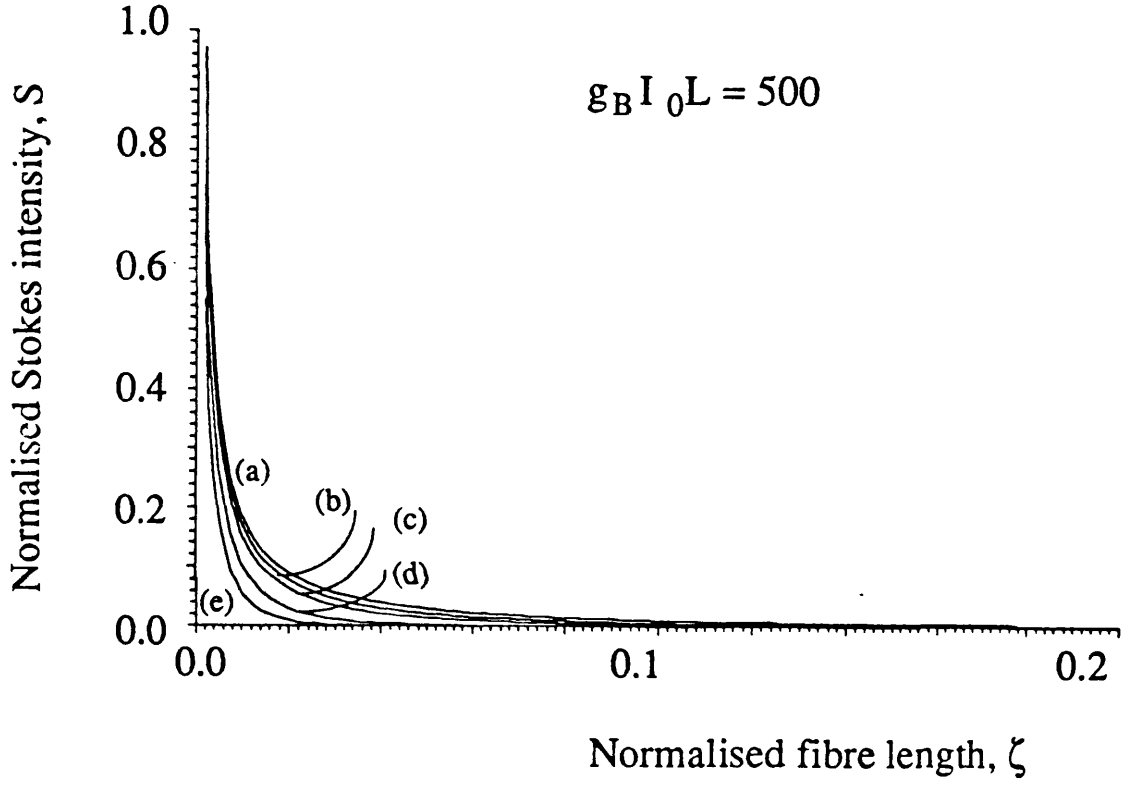

Figure 4.3 (v)

Figure 4.3 (i) - (v). Graphs showing normalised Stokes intensity S vs normalised fibre length, ζ, plotted for different values of gain, $g_B I_0 L$ (= input pump intensity), and fibre loss, $\alpha_0 L$: (a) 0; (b) 1; (c) 3; (d) 5; and (e) 8, corresponding to fig. 4.2.

variation of the normalised pump and Stokes intensities for different values of the Brillouin gain, $g_B I_0 L$ ranging from 20 to 100. The comparison of these graphs with their $\alpha_0 L = 0$ counterparts in figs 4.2 and 4.3, verifies the remarkable accuracy of this relatively simple numerical method. The main source of error is the value specified for the Stokes intensity boundary condition (the Stokes noise) at $\zeta = 1$.

The exact value of the Stokes noise is extremely difficult to obtain, and various estimates[7,8] have yielded its value to be approximately 10^{-9} times the input pump intensity (as it is a function of the pump intensity, as given, for example in eqns (3.2) and (3.3)); this is the value which has been adopted in this analysis. As it turns out, above threshold, the change in the boundary value of S(1) of up to an order of magnitude results in the change of less than 10% in the value of the output pump intensity P(1) or the output Stokes intensity S(0) (and hence the conversion efficiency). It also transpires that if in the numerical solutions, the value of the Stokes intensity S(1) is chosen so as to equal exactly the specified boundary condition on S(1) in the exact solutions, the error in the numerical solutions is less than 1part in 10^8. This implies a very encouraging stability of both the numerical method used and the solutions obtained.

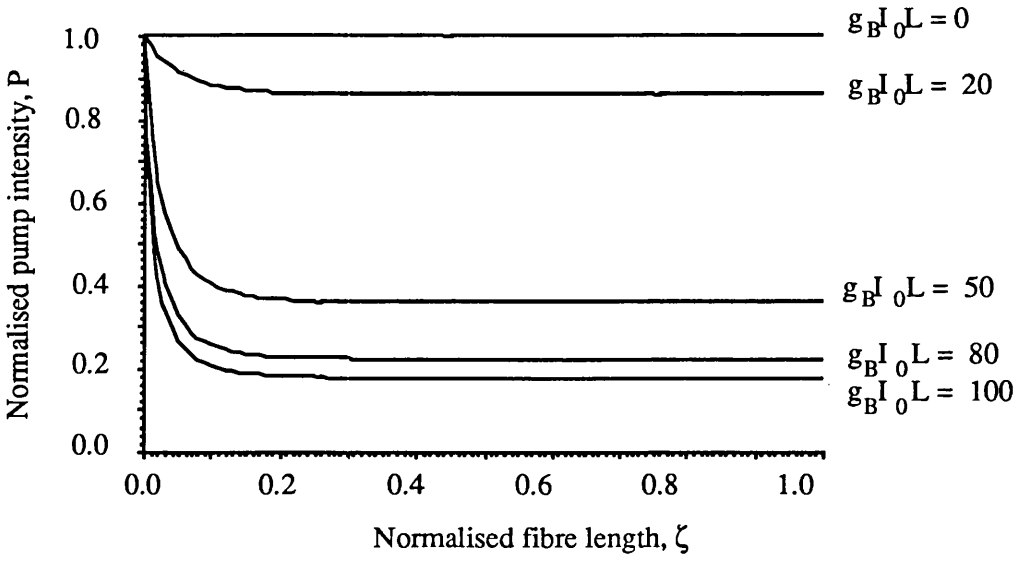

Figure 4.4. Showing plots of the the exact (analytic) solution for the normalised pump intensity vs normalised fibre length for different values of gain (or input pump intensity); $\alpha_0 L = 0$.

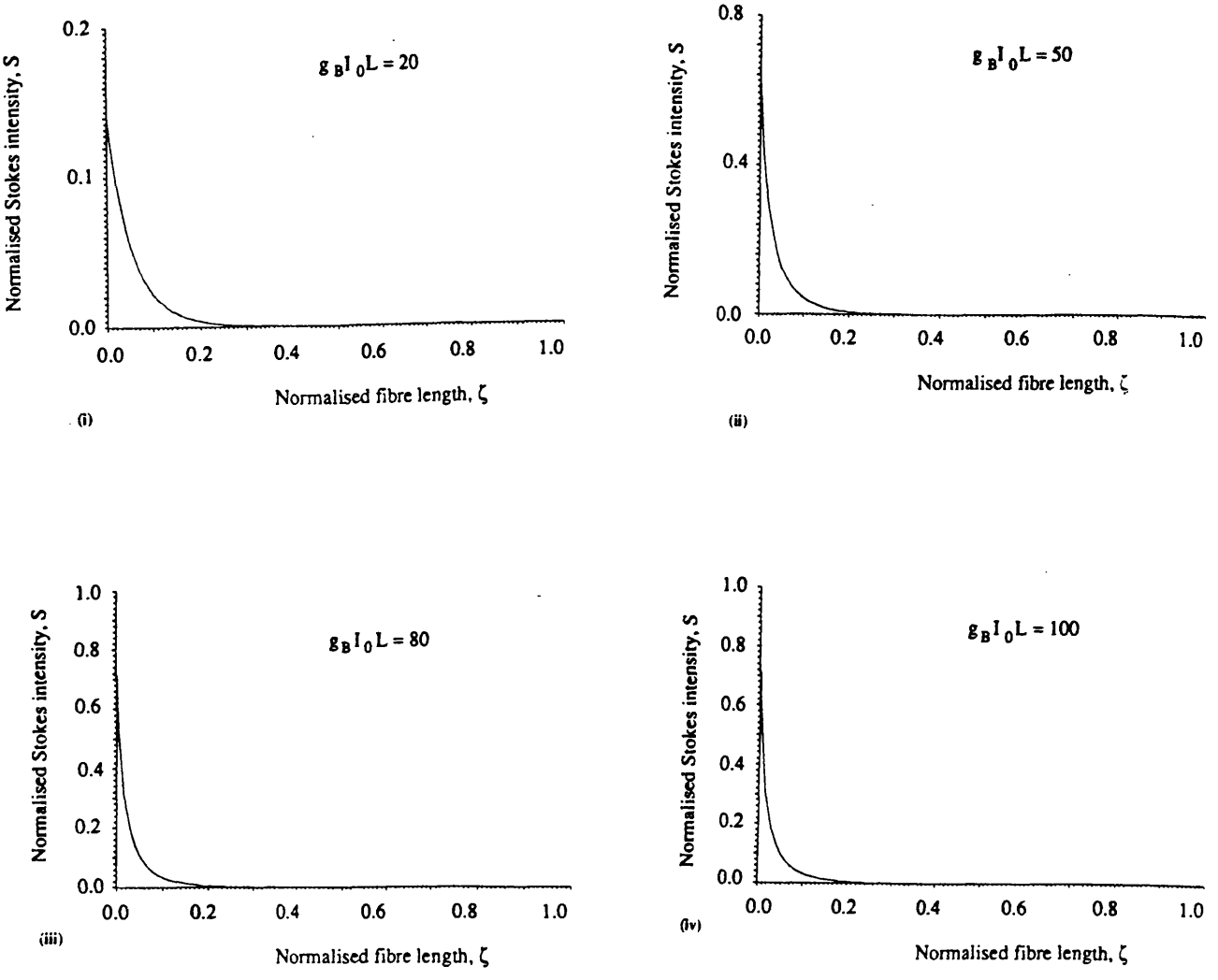

Figure 4.5 (i) - (iv) (corresponding to fig. 4.4). Exact solutions for the normalised Stokes intensity vs normalised fibre length for different values of gain; $\alpha_0 L = 0$.

To relate these results to some practical (experimental) values it is helpful to plot the variation of the *output* Stokes intensity S(0) and the pump intensity P(1) with Brillouin gain $g_B I_0 L$, which can correspond to the increased pump input intensity. In the next section these results will be compared to experimental results which are understandably measured in this way. The graphs of P(1) with gain for different values of $\alpha_0 L$ are given in figure 4.6.

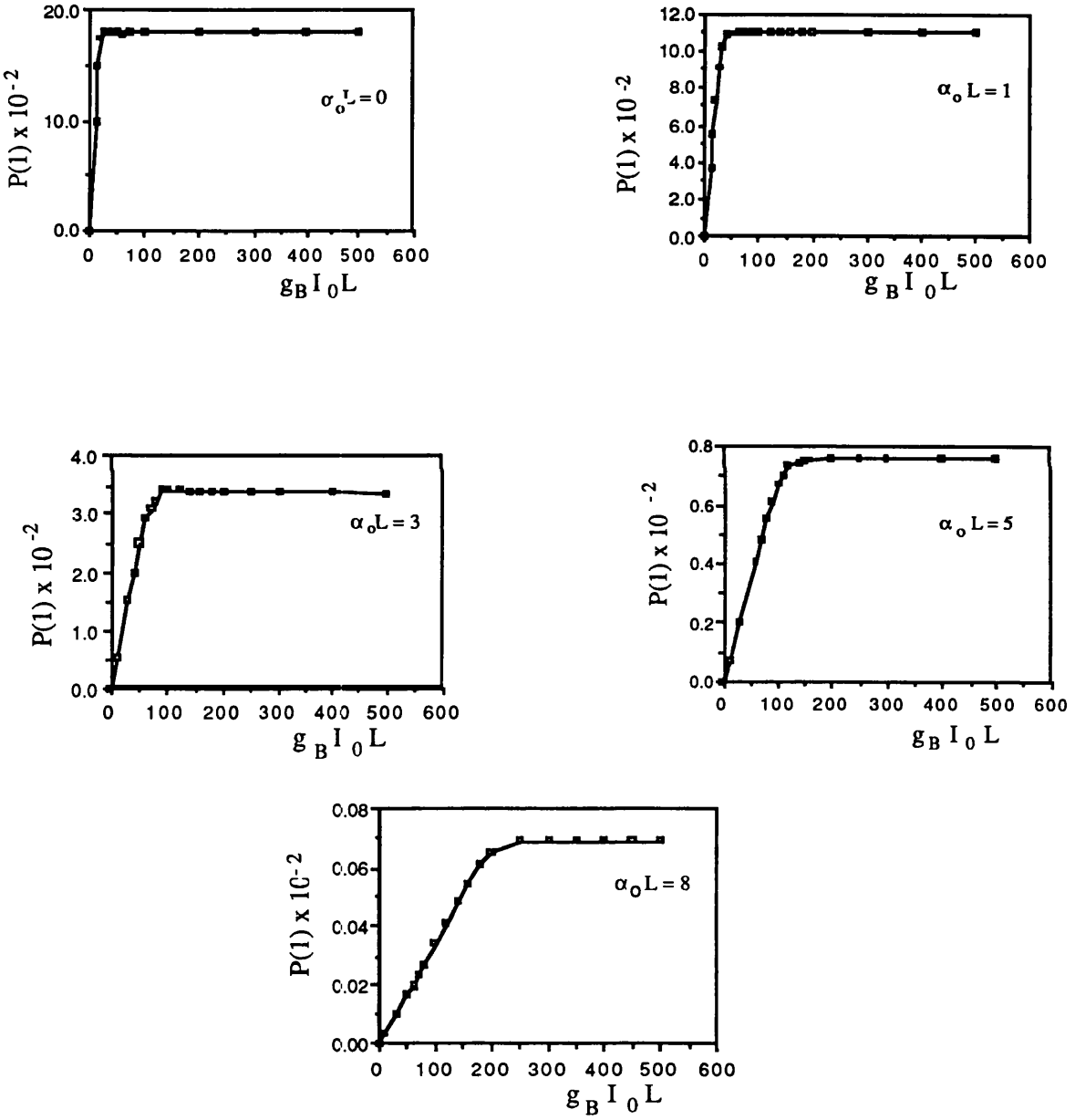

Figure 4.6. Theoretical plots showing variation of the output normalised pump power P(1) vs gain for different fibre losses.

The most apparent feature is that the pump intensity dramatically saturates (from the linear variation corresponding to linear fibre loss) to a constant value after the Brillouin threshold has been exceeded. In accordance with earlier figures, higher fibre loss means lower saturation level in the output intensity, as well as a threshold for a higher value of gain (and therefore input pump intensity). This again illustrates the sensitive dependence of the growth of SBS on the linear fibre loss, and is illustrated more clearly in figure 4.7 where the above curves are re-plotted on a $\log_{10}$ scale.

Next, it is important to see how the Stokes intensity varies with the gain. This variation is shown, as a function of fibre losses , in figure 4.8. As expected, the conversion efficiency or the normalised output Stokes intensity S(0) exhibits a clear threshold, and increases rapidly above this. Again, this figure illustrates that the increased fibre loss limits the conversion of the pump intensity into the Stokes intensity, as well as resulting in a higher threshold intensity.

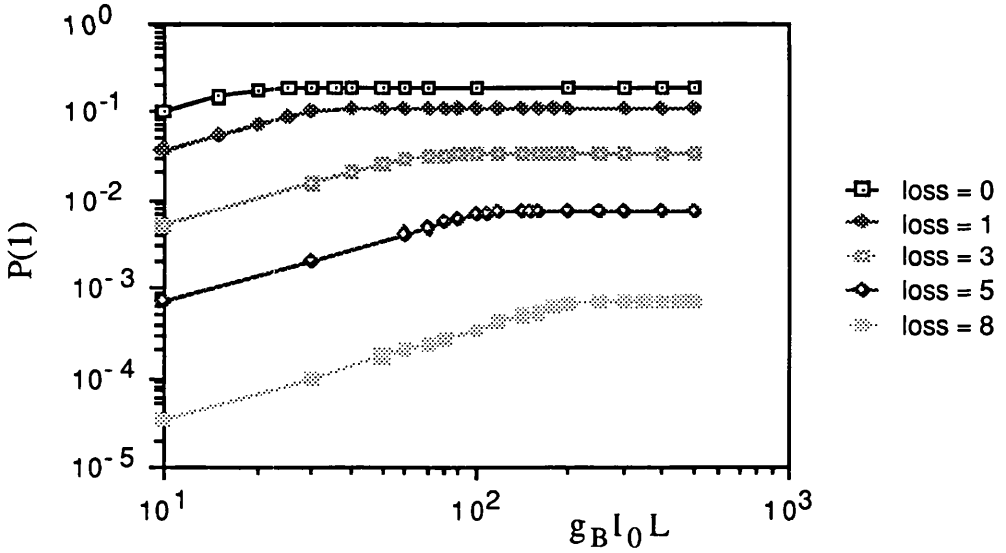

Figure 4.7. Variation of the normalised output pump power with Brillouin gain as a function of fibre loss replotted on a $\log_{10}$ scale. Note the increased threshold intensity and the decreased saturation power as the loss is increased.

It can be seen that the conversion efficiency rises sharply after the threshold has been reached, and as the gain increases, the growth slows down, asymptotically approaching 100% and signifying increasing pump depletion. It can be seen that for zero loss, almost all the pump intensity is converted into the Stokes intensity, while the conversion efficiency decreases for higher values of loss.

An important point which may not be readily apparent from the above graphs should be emphasised. This is concerned with the definition of Brillouin threshold threshold. According to Smith's somewhat arbitrary definition, it is that pump intensity (or power) which amplifies the Stokes noise to the level of the pump. Now, the above results indicate that the Stokes intensity begins to grow sharply accompanied by the depletion of the pump

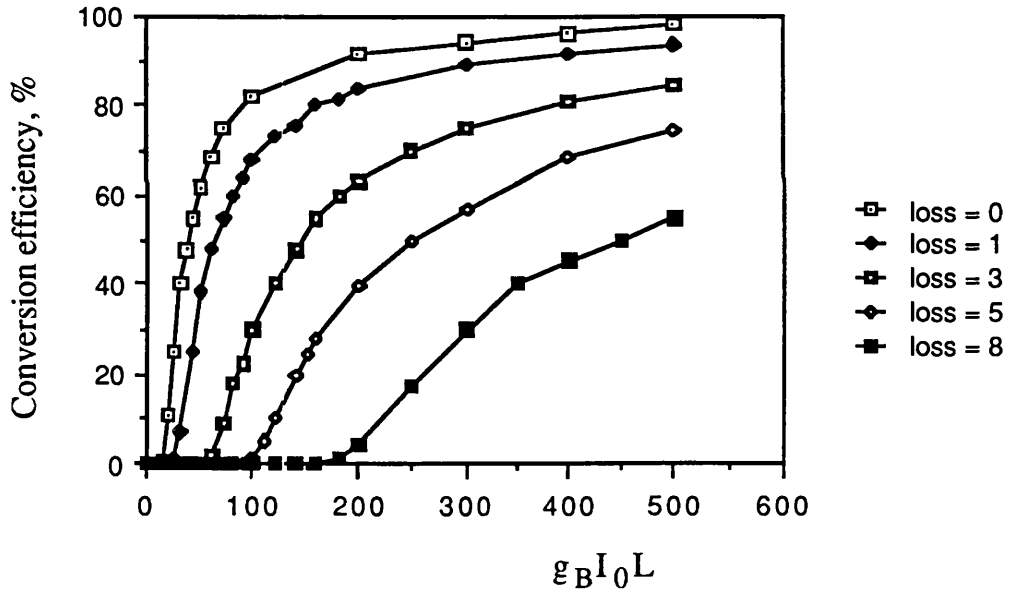

Figure 4.8. The variation of the conversion efficiency (or the normalised output Stokes intensity, S(0)/100) with gain, plotted for different values of the fibre loss.

approximately at the normalised Stokes intensity equal to 0.01 - or 1% conversion, the point which can be termed the Brillouin threshold. From the above normalised graphs, we can compare the 'threshold' values of gain for the case of zero loss. In this case, the onset of threshold as defined above is when $g_B I_0 L \approx 18$. We can directly compare this to

Smith's criteria of $g_B I_0 L \approx 20 - 21$, since at zero loss, L_{eff} is equal to L. This difference of a factor of approximately $e^2 - e^3$ implies that some care is needed in the definition of threshold. Further practical significance of this is discussed in the next section.

4.3. Comparison with published experimental results

Next, it is necessary to compare the results of the numerical calculations with experimental results. It is quite difficult to make such comparisons since the published data about SBS measurements are often not complete, omitting to state values of such important parameters as pump laser linewidth or the effective core area. In addition, easily interpretable data on the continuous variation of the output Stokes power with input pump power, and hence the conversion efficiency are generally not available (the output Stokes power is commonly plotted in arbitrary units), although the data on threshold powers can generally be extracted. Cotter's works[9,10] contain by far the most complete details on the measurements carried out, and thus can be related to the calculated parameters. Figure 4.9 gives the variations of the output pump power, output Stokes power, and the corresponding conversion efficiency vs input pump power and allows us to compare Cotter's results with theoretically calculated ones. It can be seen that the theoretical and experimental graphs clearly follow the same dependence, with the onset of saturation after the SBS threshold has been exceeded.

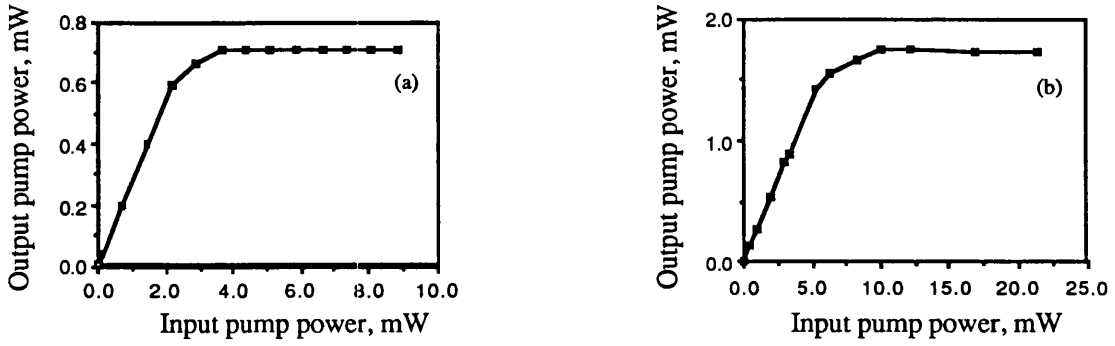

Figure 4.9. Showing the comparison between theoretical (a) and experimental (b) results for output pump power vs input pump power in a fibre link; experimental results after Cotter[9]: L = 13.6 km, loss = 0.41 dB/km.

A discrepancy of approximately factor of 2.3 can be noted in the two curves. The primary reason for this is that the theoretical curves have been plotted using the peak Brillouin coefficient, while in the experiments, depolarisation leads to the reduction of the Brillouin gain coefficient by approximately a factor of 2, leading to a corresponding increase in the threshold power, and output saturation power.

If the decrease in the gain due to the a finite spectral width of the laser pump (1.6 MHz) used in the experiments is calculated from the convolution of the pump and Brillouin spectrum (assuming Lorentzian lineshapes), the resultant agreement between the experimental and theoretical data is better than 5%. [It should be noted that in these comparison curves we deliberately plot the theoretical values without taking into account the effects of depolarisation and finite pump linewidth, alongside the experimental curves, to indicate how these effects can be easily incorporated into the calculations].

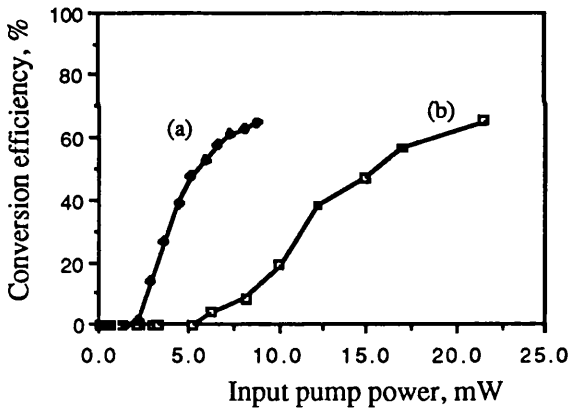

Figure 4.10. Theoretical and experimental conversion efficiency; corresponding to figure 4.9.

Indeed, having accounted for the factor of 2, the curves showing the corresponding theoretical and experimental conversion efficiency (figure 4.10) are in agreement to within a few %.

The comparison of the theoretical results with the experimental data for a fibre of length 32 km, loss = 0.47 dB/km (ref. [10]) shown in fig. 4.11 indicates an even closer agreement.

The difference in the threshold and the saturated output power level is again a factor of two and is due to the depolarisation amounting to the reduction of the gain by a factor of 2. The conversion efficiency in this case (figure 4.12) is also in close agreement between the theory and the experiment.

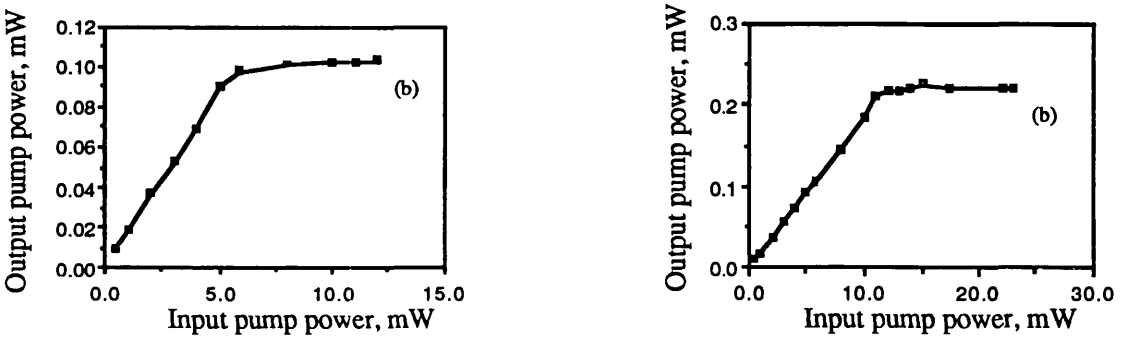

Figure 4.11. Showing the comparison between theoretical (a) and experimental (b) results for output pump power vs input pump power in a fibre link; experimental results after Cotter[10]: L = 32 km, loss = 0.47 dB/km.

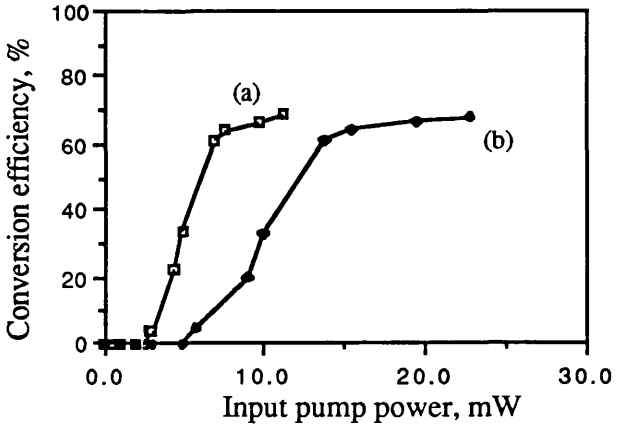

Figure 4.12 Theoretical and experimental conversion efficiency; corresponding to figure 4.11.

Experimental values		Theoretical values			Reference
Threshold (mW)	Max. conversion eficiency (%)	Threshold (mW) [this work]	Conv. eff. (%) [this work]	Undepleted pump approximation (mW) [Smith]	
30.1	56	30.0	58	32.5	Uesugi et al. ('81)
40 (PM)	-	45.0	-	50.0	Tsubokawa et al. ('86)
11.75	-	11.5	-	12.0	Hadjifotiou et al. ('86)
9	80	9.6	83	10.6	Aoki et al. ('87)
13	-	14.2	-	16.0	Aoki et al. ('88)

Table 4.1. Comparison of calculated and experimental results for Brillouin thresholds in long lengths of single mode fibres. Comparison in conversion efficiencies are given where experimental data are available. Complete sets of data are listed in Table 3.1.

Although the above comparisons are extremely encouraging, it would be desirable to obtainsuch good agreement with other published experimental results. However, as described above, published data in this field rarely contain enough information to enable complete comparisons. Consequently, we have carried out calculations to compare the Brillouin threshold powers (calculated theoretically) with those obtained in recent experiments, and the conversion efficiency, where given. Table 4.1 shows the results of these comparisons. The experimental data used are taken from Table 3.1, and Table 4.1 also includes a comparison with the threshold calculated using Smith's formula. In calculating Smith's threshold, compared with values listed in Table 2.1 the gain reduction due to depolarisation and finite pump linewidth (where given) was taken into account. The $g_B I_0 L$ values at threshold are also listed to enable comparisons between Smith's threshold

(given by $g_B I_0 L_{eff} \approx 20$) and the one defined in this chapter, since $g_B I_0 L_{eff} = g_B I_0 L[L_{eff}/L]$, and L_{eff} is easily calculable from eqn (3.1).

4.4. Implications for practical long-haul transmission systems

As we discussed in the previous chapter and in the introduction to this chapter, SBS can be a limitation to the operation of long distance transmission links. Having obtained the solutions to the SBS equations, in this section we shall assess the implications of above calculations in the context of practical long-haul transmission systems and indicate how the adopted numerical method leads to very flexible solutions in terms of practical system parameters. As an example we can consider an optical fibre transmission system where the transmitter is intensity modulated (mark-space ratio of 1) at 140 Mbit/s for a 10^{-9} BER (the transmission rate could be higher for a shorter link length[11]), and 7 dB is allowed for losses at the transmitter/receiver and connectors. Typically, the telecommunications single mode fibre has a core/cladding diameter of 8/125 μm, with fibre loss of 0.2 dB/km. A direct detection APD receiver sensitivity would typically be - 47 dBm. However, if coherent heterodyne detection is used, - 56 dBm receiver sensitivity could be ensured, allowing an extra 8 dB of losses allowing a further 40 km of fibre. In figure 4.13 we plot the transmitted power as a function of the input transmitter power, and the corresponding output Stokes power is plotted in fig. 4.14. The effective core area is taken as 5.0×10^{-11} m^2 and $g_B = 4.6 \times 10^{-11}$ m/W as before.

In these plots we have deliberately not taken into account the reduction in the Brillouin gain due to the pump linewidth, depolarisation, and modulation of the transmitter power, which we shall calculate in the following discussion. It can be seen that the threshold is observed at approximately 0.4 dBm of transmitter power. At threshold, the backscattered Stokes power is approximately - 20 dBm, corresponding to 1% of the pump power. The saturated level of the transmitted power is approximately - 40.4 dBm.

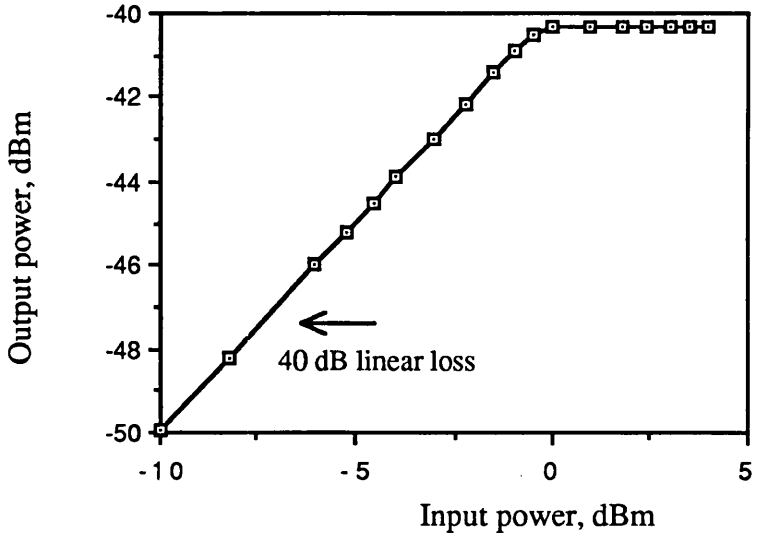

Figure 4.13. Theoretical transmitter output power against input power for a 200 km fibre communications link, fibre loss 0.2 dB/km.

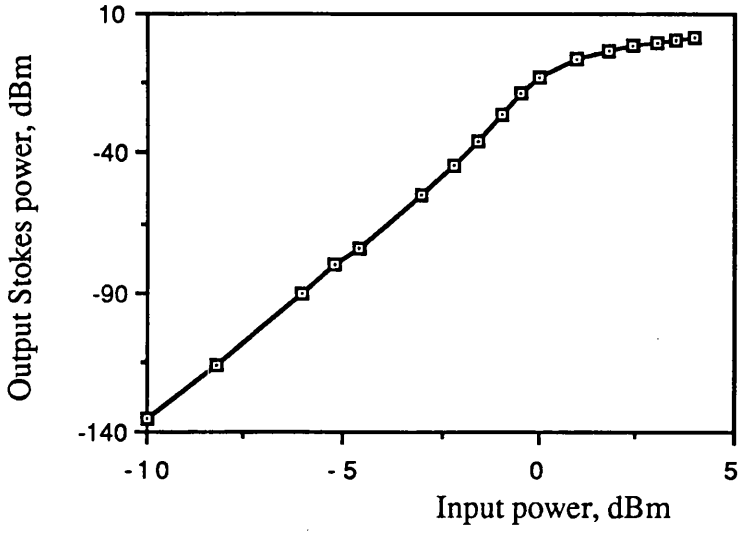

Figure 4.14. Output Stokes power vs input transmitter power, corresponding to figure 4.13.

In order to show how the variation of pump linewidth, depolarisation, and modulation can be taken into account in systems calculations, in fig 4.15 we also plot the conversion efficiency (equivalent to the normalised Stokes intensity, S (0)) vs gain, $g_B I_0 L$, for the fibre loss of $\alpha_0 L$ of 9.2 (= 40 dB) The graph of fig. 4.15 shows that the threshold occurs at the the value of $g_B I_0 L$ of 190. Thus, at the peak value of g_B, the threshold is then as given above equals 1.1 mW.

We can now very simply take into account the reduction of the gain due to finite pump linewidth, depolarisation, modulation, and the effective core area to calculate the realistic threshold, transmitted power, and the corresponding Stokes power with the help of figure 4.15.

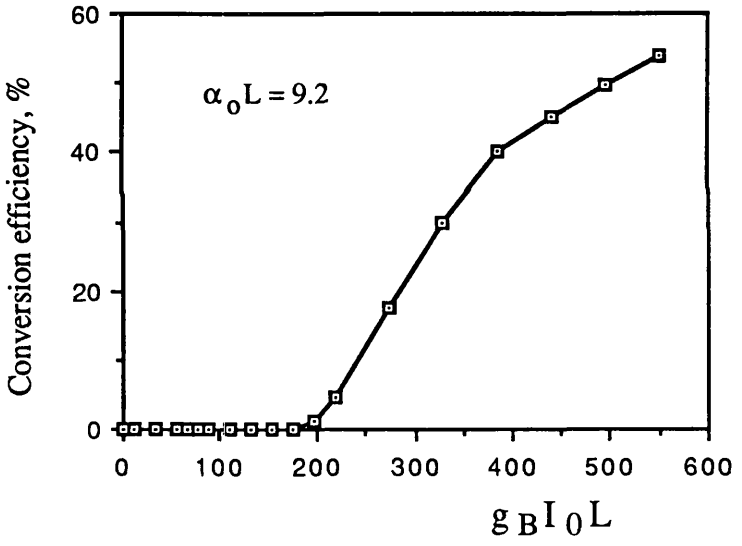

Figure 4.15. Conversion efficiency (= normalised Stokes intensity, S(0)/100) as a function of $g_B I_0 L$ (or the input intensity, I_0).

The intrinsic Brillouin linewidth (using values of bulk silica) at 1.55 μm is approximately 20 MHz, but may, in fact, be higher, say by a factor of 2, due to interactions with acoustic modes, as outlined in Chapter 3. Assuming Lorentzian profiles and an optimistic transmitter linewidth of 20 MHz, the reduction in gain from eqn (2.27) is between 0.5 and 0.7. The effective core area is approximately a factor of 1.5 larger than the actual core area. The gain reduction due to modulation, and depolarisation can be taken as 0.25 and 0.5,

respectively. As a result of these calculations, the Brillouin gain coefficient will be, in reality, reduced to approximately 0.05 - 0.07 g_B. This means that the predicted threshold is, in fact, approximately 20 times higher, and equals to 11 - 13 dBm (14 - 20 mW), with the corresponding Stokes power of - 8.5 to - 7.0 dBm. At a specified transmitter power of 0 dBm, the gain $g_B'I_0L$ where g_B' is the effective gain coefficient 0.05 - 0.07g_B the Stokes intensity is - 103 dBm. (If a 30 dB isolation between the fibre end and the transmitter is assumed[1], this implies backscattered power level at the transmitter of ≈- 130 dBm). According to recent calculations of the effect of backreflected power on RIN of DFB lasers[1], such levels of backscattered Stokes power will not introduce any system penalty. for a system penalty of < 0.5 dB, a RIN level of less than - 100 dB/Hz is required for the above bit rate. This can be achieved for reflection of less than roughly 30 - 10 dB (depending on the output power of the transmitter, as RIN varies as P^{-1} for high output powers, and P^{-3} for low output powers) at the transmitter power of up to 0 dBm.

It should be pointed out, however, that much research is currently being undertaken to develop single mode semiconductor laser sources with significantly narrower output linewidths (< 100 kHz) and able to operate at higher output powers (> 20 mW). When, incorporated into a long-haul link, the resultant Brillouin thresholds, increased levels of backscattered power and pump depletion may become far more important than currently.

4.5. Applications to Brillouin amplification

As described in the previous chapter, the utilisation of the Brillouin gain for amplification has been suggested and explored by a number of authors, and forms a subject of intense interest at present. [Despite this, systematic evaluation of the achievable gain, gain saturation, and/or noise characteristics have not been carried out, with the only available calculations being limited to the work of Olsson et al.[12] (undepleted pump approximation) and Siddiqui et al.[13] who unjustifiably used the Raman solutions[14] for calculating the Brillouin amplifier characteristics].

For amplification, the pump laser is operated at a power below threshold to ensure linear gain, as above threshold, the output power is no longer linearly dependent on the input power. This is clearly illustrated on the above figure 4.14. It can be seen that for input powers below threshold, the output Stokes power varies linearly with the input power. In

figure 4.16 we plot the amplification (that is the ratio of the output Stokes power and the input Stokes power) against the Brillouin gain $g_B I_0 L$ (or the input intensity). It can be clearly seen that the maximum linear gain is observed at threshold, since as the threshold is exceeded, the gain saturates as the stimulated scattering starts. In this case, the output signal power will not be proportional to the input signal power, and the device will no longer act as a linear amplifier. Although this particular graph is plotted for a value of linear loss of 40 dB, different values of linear loss will only vary the gradient of the graph, while the maximum achievable gain will clearly be the same for any value of loss. It can be seen that the maximum gain which can be obtained before the onset of saturation is approximately 90 dB. This figure is not dependent on the value of the fibre losses, and is actually related to the threshold power condition. Simple calculations show that it in facts corresponds to the value of exponential Brillouin gain given by Smith's threshold criterion of $g_B I_0 L_{eff} \approx 20$. In fact, the amplifier gain becomes slightly nonlinear after the point of threshold defined in this chapter, i.e.. at $g_B I_0 L_{eff} \approx 18$, saturating as the input power is increased.

A difference between Brillouin generation and amplification must be pointed out.

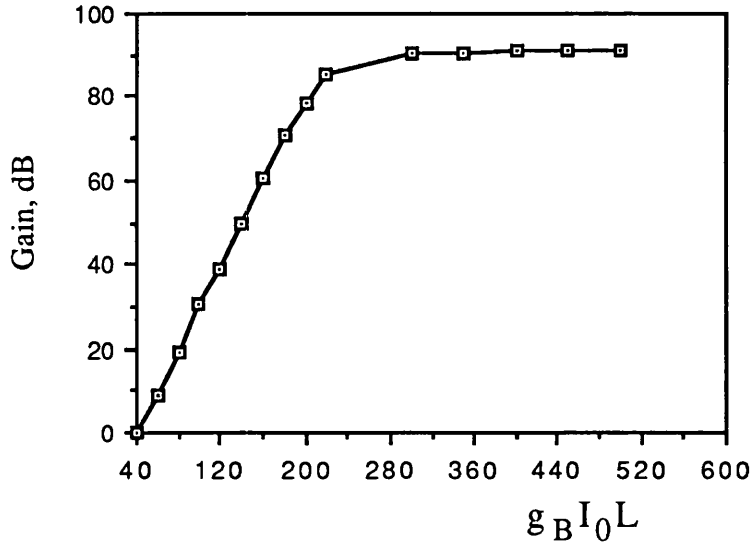

Figure 4.16. Showing the variation of Brillouin amplification as a function of the input intensity (or $g_B I_0 L$). Clear gain saturation above threshold is seen.

As described above, depolarisation causes the Brillouin gain coefficient to be reduced by a factor of 2. This is also true in the case of the amplifier, where some additional depolarisation or phase mismatch can be experienced between the signal and the Brillouin gain, causing additional gain reduction[15].

Measured gain dB	Calculated gain dB	Reference
0.4	0.8	Waarts et al.
48 20	46 16	Atkins et al.
9	19	Olsson et al. ('86)
25	28	Chraplyvy et al.
18 10	37 22	Olsson et al. ('87)
30	32	Tkach et al.

Table 4.2. Comparison of calculated and experimentally measured values of gain for Brillouin fibre amplifiers. Full sets of data are listed in Table 3.2.

Table 4.2 shows the comparison of the published amplifier data listed in Table 3.2, (given in previous chapter) with the values calculated using the Runge-Kutta method. It is extremely difficult to carry out calculations using the published amplifier data, since the experimental details are even more sketchy than in the case of systems experiments. It is thought that the reason for this is the fact that this work is still in the very early stages, and consequently other workers' priorities have focussed on attempting to show the feasibility of Brillouin amplification, rather than reporting detailed studies. In calculating the amplifier

gains using the published data we have taken into account possible depolarisation (resulting in the reduction of the gain by a factor of 2), but not any further reduction because of phase mismatch between the external signal and nonlinear gain. Moreover, the value of g_B is taken to be 4.6×10^{-11} m/W. The early result of Waarts et al., and the results of Olsson et al. exhibit the largest discrepancy with the calculated values.

This can be explained by the fact that in Olsson's experiments the fibre length consisted of several spools of different fibre spliced together, which means that the overall gain coefficient (not given in the paper) was markedly different from that of fused silica. Bearing these points in mind, the comparison between the calculated and measured values is very encouraging. Overall, good agreement is evident, and it is possible, at first sight, to conclude that in the amplifier experiments good correlation between the generated and the externally injected Stokes signals was obtained, without, it seems, any significant additional depolarisation. It should be pointed out that, although initial calculations are very encouraging, somewhat more detailed calculations are necessary for a systematic analysis and evaluation of performance characteristics of this type of Brillouin amplifier, including noise calculations. The numerical method described here could be easily extended to evaluate the amplifier noise parameters, by including an additional spontaneous noise contribution in the Brillouin equations, as for example in refs. [12], [14], where calculations were carried out for the undepleted pump case for SBS, and SRS, respectively.

4.6. Summary and conclusions

In conclusion, we have solved the SBS equations with loss using a relatively simple numerical method, the results of which can easily be related to practical values and experimental parameters. The method has been shown to yield stable and accurate solutions, and the results provide a very useful insight into the physics of SBS generation and the energy exchange process between the counterpropagating pump and Stokes intensities. The numerical solutions were compared with the exact (analytical) solutions for the pump and Stokes equations for the zero loss case, and were shown to be in excellent agreement. However, the importance of the fibre loss in the evolution of the pump and Stokes intensities was clearly demonstrated, with higher fibre loss leading to a higher Brillouin threshold and lower conversion efficiency at a given input pump intensity. We

have undertaken a comprehensive comparison of our results with published data on systems and amplifier experiments experiments, and have shown that good agreement was obtained for both. The implications of these results were discussed in relation to applications to practical long haul fibre links, where the flexibility and the ease of use of this particular method are particularly valuable, as the system information, such as the bitrate, transmitter linewidth, and depolarisation effects can *all* be included in the value for g_B, allowing easy estimation of the power budgets for a given link length and loss.

4.7. References for Chapter 4

1 T. C. Blackie, M. Fake, A. E. Green, M. P. Perry, and P. J. Sanders, 'The effect of reflected optical power on the relative intensity noise in DFB lasers', presented at the EFOC/LAN '89 Conference, June 1989, Amsterdam, Netherlands

2 R. H. Enns and I. P. Batra, 'Saturation and depletion in stimulated scattering', Phys. Lett. **28A**, 591 (1969)

3 F. Chu and C. F. F. Karney, 'Solution of the three wave resonant equations with one wave heavily damped', The Physics of Fluids, **20** (10/1), 1728 (1977)

4 J. Coste and C. Montes, 'Asymptotic evolution of Brillouin scattering: implications for optical fibres', Phys. Rev. A **34**, 3940 (1986)

5 E. Kreyszig, "Advanced Engineering Mathematics", J. Wiley & Sons Inc, New York, 1962

6 Claude Leycouras, Optics Group, University of Nice, personal communication; Paul Radmore, Dept. of Elec. Eng., UCL, personal communication

7 H. Z. Cummins and P. E. Schoen, 'Linear scattering from thermal fluctuations' in "Laser Handbook", ed. F. T. Arecchi and E. O. Schultz-Dubois, North Holland Publ. Co., Amsterdam, 1972; J. D. Hey, 'Mandelshtam-Brillouin scattering by optically linear media', S. Afr. J. Phys. **5**, 65 (1982)

8 E. M. Dianov, A. A. Manenkov, and A. I. Ritus, 'Brillouin and Rayleigh scattering in fibre waveguides: measurement of the angular distribution of the scattering intensities, scattering losses, and rotation of the plane of polarisation', Sov. J. Quantum Electron. **7**, 841 (1977);

9 D. Cotter, 'Observation of SBS in low loss silica fibre at 1.3 μm', Electron. Lett. **18**, 638 (1982)

10 D. Cotter, 'SBS in a monomode optical fibre', J. Opt. Commun. **4**, 10 (1983)

11 Peter Ball, Telecommunications Laboratory, GEC Hirst Research Centre, personal

communications

12 N. A. Olsson and J. P. Van der Ziel, 'Characteristics of a semiconductor laser pumped Brillouin amplifier with electronically controlled bandwidth', J. Lightwave Tech. **LT-5**, 147 (1987)

13 A. S. Siddiqui and S. Androniikidis, 'Transfer characteristics of Brillouin fibre amplifiers for use in self-homodyne coherent optical transmission systems', Electron. Lett. **25**, 265 (1989)

14 K. Mochizuki, 'Optical fibre transmission systems using stimulated Raman scattering: theory', J. Lightwave Tech. **LT-3**, 688 (1985)

15 E. Lichtman, A. A. Friesem, R. G. Waarts, and H. H. Yaffe, 'Stimulated Brillouin scattering excited by two pump waves in single mode fibres', JOSA B **4**, 1397 (1987)

Chapter 5

ALL-FIBRE SINGLE MODE RING RESONATORS

The aims of achieving single mode all-fibre systems in order to eliminate the need for bulk optics components, have resulted in considerable advances in the optical fibre component fabrication technology in the early 1980's. This work has led to the development of high quality fused[1,2] and polished optical components and directional couplers[3], and subsequently the all-fibre single mode ring resonator was reported in 1982[4]. The configuration of the optical fibre ring resonator (OFRR) is shown in fig 5.1 (a).

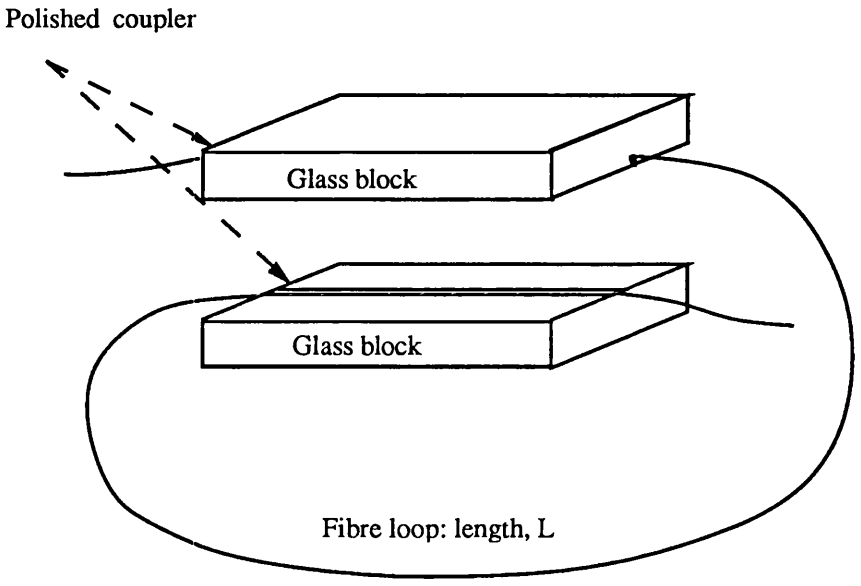

Fig. 5.1 (a). Showing the configuration of the single mode all-fibre ring resonator (OFRR).

The OFRR consists of two halves of a directional coupler fabricated on the same length of optical fibre, L. The half couplers are fabricated by the lap - polish technique, discussed in more detail in Section 5.2.1. Placing the two halves together to close the ring (as illustrated

in fig. 5.1 (a)), produces a fibre ring cavity of loop length L. As shown schematically on figure 5.1 (b), if the directional coupler has large coupling, the light in the fibre ring will couple from port 2 to port 3 and will continue to circulate. Similarly, light from port 1 will couple mostly to output port 4.

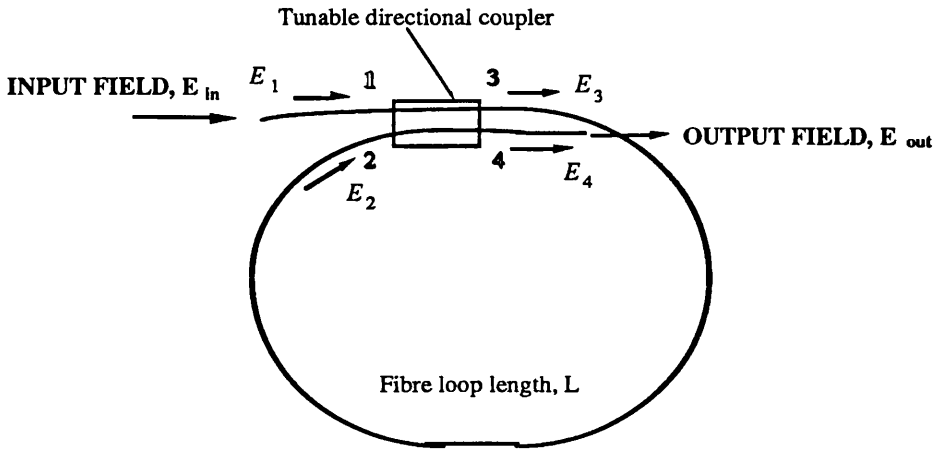

Figure 5.1 (b). Schematic diagram showing propagation of fields in an OFRR.

When the fibre loop length is tuned (by moving the coupler halves one relative to the other) for constructive interference at port 3 between fields from ports 1 and 2, the light from ports 1 and 2 will destructively interfere at port 4. When the coupling is optimum (this depends on losses), the two destructively interfering components are equal in amplitude, and cancel completely. From the conservation of energy point of view, the circulating power will grow until the power dissipated by losses in the loop equals the input power at port 1.

If the light frequency is continuously varied, the power which couples out at port 4 will undergo a series of sharp minima when the resonant condition is matched to the input optical frequency. This behaviour is analogous to the Fabry-Perot resonator, but in the case of the Fabry-Perot, the output power exhibits a series of sharp maxima at resonance.

The advantages of this device compared with other types of fibre resonators and cavities such as Fabry-Perot[5] and Fox-Smith resonators[6], and recently demonstrated fibre loop reflectors[7] are in tunability, relatively simple fabrication process, as well as experimentally

demonstrated highest finesses, particularly important for applications in fibre lasers[7]. Consequently, this device immediately received attention from researchers for these reasons. Primarily, the all-fibre ring resonator geometry offers a very low round-trip loss coupled with a significant enhancement of the circulating intensity over the input intensity. The resonant characteristics ensure that this device exhibits a very steep slope of its output transmission against phase. This means that any *small* additional phase changes (for example in the length of the resonator) result in *large* changes in transmission. Over the years very high cavity finesses, and consequently, high phase sensitivities have been reported[8,9]. This property makes the fibre resonator very useful for sensing applications, in particular rotation sensing using both the passive fibre ring resonator[10-14] and the all-fibre Brillouin laser[15] has been an area of much research.

The high finesse which can be obtained with these devices, coupled with small free spectral range (achieved simply by increasing the loop length) ensures a spectral resolution an order of magnitude better than is possible with commercially available confocal or parallel plate Fabry-Perot spectrum analysers. This means that the resonators can provide a tool for characterising laser sources[16,17].

Using a low coherence source the resonators have found application as recirculating delay lines and filters[18,19]. In the case of a narrow-linewidth, single mode source, because of the coherent addition of fields in a high finesse cavity a great enhancement of the intensity circulating inside the loop over the incident intensity, as well as an increase in the effective path length are possible. This means that the OFRR is a very convenient device for the investigation of many nonlinear effects, such as SBS (on which this work is focussed), SRS[20], the Kerr effect[21], and more recently - squeezed state generation and optical bistability[22]; these effects can then be observed in resonators at powers which are much lower than in the case of straight fibres or bulk materials, leading to many novel and potentially valuable applications. In general, all such research have been carried out using stabilised, narrow linewidth, single frequency gas lasers. However, as has already been mentioned in the previous chapter, most optical fibre system applications require a semiconductor laser as source. To assess the feasibility of achieving this, since these lasers have an inherently broader spectral linewidth, we first undertook the investigation of OFRR operation using commercially available single mode AlGaAs semiconductor lasers.

At the start of this work, the highest finesse reported for OFRR was 93[14]. However, in

the course of this work, the fabrication process was optimised and improved to result in resonators with extremely high finesses (up to 600), and very recently high finesse resonators have also been reported by others[8, 22]. We have also fabricated and investigated the operation of high-finesse OFRRs made of polarisation maintaining HI-BI fibre for the first time, both at stabilised, single frequency gas lasers (at 514.5 nm (described in Chapter 8) and 633 nm), and single frequency semiconductor lasers at 830 nm.

The general theory of the operation of the fibre resonator necessary to the understanding of the OFRR and subsequent analysis, is derived in Section 5.1. In this section the significance of the source coherence is also considered. The experimental investigation of OFRRs are described in 5.2 and this section also includes details of the fabrication process. Experimental observations at 633 nm and 830 nm are described, and the differences in resonator operation with the high and low coherence laser sources are explained. It should be clearly stated that the work on OFRRs undertaken in this project approached the investigation of OFRRs with a view of optimisation of SBS generation in these devices, and applications of Brillouin lasing, rather than a general study of OFRR behaviour.

5.1 Theory of the all-fibre single mode ring resonator

5.1.1 Steady state characteristics

In analysing the ring resonator it is assumed that the directional coupler is a lossless device with a lumped loss $2\gamma_0$ (in high finesse (>100) resonators $2\gamma_0$ will be less than 2%), and that the coupler loss is independent of the relative phases of light entering the coupler input ports, and of the coupling constant. It is also assumed that all the fields have the same state of polarisation. With reference to fig 5.1(b), the lumped coupler intensity loss $2\gamma_0$ is given by (this is proved in Appendix F):

$$|E_3|^2 + |E_4|^2 = (1 - 2\gamma_o)\{|E_1|^2 + |E_2|^2\} \tag{5.1}$$

where E_i is the complex electric field amplitude at the i-th port.

The fields in the fibres after the coupled-mode interaction therefore are related to the incident field amplitude by:

$$E_3 = (1 - 2\gamma_o)^{1/2}\left[(1 - k^2)^{1/2}E_1 + jkE_2\right] \tag{5.2}$$

and,

$$E_4 = (1-2\gamma_o)^{1/2}\left[jkE_1 + (1 - k^2)^{1/2}E_2\right] \tag{5.3}$$

where k^2 is the intensity coupling coefficient, and k is the amplitude coupling coefficient. When $k^2 = 0$, there is no coupling, and $k^2 = 1$ corresponds to complete cross-coupling. In addition the amplitude transmission coefficient in the loop, T_L is given by:

$$T_L = E_2/E_3 = \exp - (\alpha_o + j\beta)L \tag{5.4}$$

where α_o is the fibre (amplitude) attenuation coefficient (note that in the preceding chapters α_o referred to the intensity attenuation coefficient; the change in notation is to avoid factors of 1/2 in the expressions for field amplitudes), β is the phase of the field and is equal to $n\omega/c$, ω is the optical frequency of the light, n is the refractive index in the fibre, and c is the speed of light in the vacuum.

To obtain an expression for the field E_3 circulating in the loop eqn (5.2) is divided by E_3, and combined with eqn (5.4) to give:

$$\frac{E_3}{E_1} = \frac{[(1 - k^2)(1 - 2\gamma_o)]^{1/2}}{1 - jk(1 - 2\gamma_o)^{1/2}T_L} \tag{5.5}$$

Similarly, for the output field (dividing (5.3) by E_1, and using eqn (5.5)) we obtain:

$$\frac{E_4}{E_1} = (1 - 2\gamma_o)^{1/2}\left[jk + \frac{(1 - k^2)(1 - 2\gamma_o)^{1/2}T_L}{1 - jk(1 - 2\gamma_o)^{1/2}T_L}\right] \tag{5.6}$$

The first term in brackets - jk - is the 'straight - through' component of light from port 1 to port 4. The through component makes this situation different to that of the Fabry-Perot resonator, where all components emerging must pass through the cavity at least once. This special property allows the resonator operation where the output is zero, that is $E_4/E_1 = 0$.

That is:

$$jk\{1 - jk(1 - 2\gamma_o)^{1/2}T_L\} + (1 - k^2)(1 - 2\gamma_o)^{1/2}T_L = 0$$

where $T_L = \exp - (\alpha + j\beta)L$.

Using the fact that $e^{-jx} = \cos x - j\sin x$, and equating real and imaginary parts:

real:

$\cos \beta L = 0$, and since k, α_o, γ_o, and L are all positive, we must have

$$\sin \beta L = -1 \text{ and } \beta L = 2n\pi - \pi/2 \qquad (5.7)$$

and imaginary:

$$jk = (1 - 2\gamma_o)\, e^{-\alpha_o L} \text{ and } k^2 = (1 - 2\gamma_o)\, e^{-2\alpha_o L} = k^2_{res} \qquad (5.8)$$

The significance of equation (5.8) is in that for resonator operation, the resonator coupling coefficient must be tuned to be equal to the round-trip losses (that is, the coupler radiation loss and the fibre loss).

Both of these conditions must be fulfilled for resonator operation.

The circulating intensity is then given by:

$$\frac{|E_3|^2}{|E_1|^2} = \frac{(1 - 2\gamma_o)(1 - k^2)}{1 + k^2(1 - 2\gamma_o)e^{-2\alpha_o L} + 2k(1 - 2\gamma_o)^{1/2}e^{-\alpha_o L}\sin \beta L} \qquad (5.9)$$

We further use the fact that, $\sin(\beta L) = -(\cos \beta L + \pi/2) = 2\sin^2(\beta L/2 + \pi/4) - 1$, and substituting into (5.9), we obtain:

$$\frac{|E_3|^2}{|E_1|^2} = \frac{(1 - 2\gamma_o)(1 - k^2)}{[1 - k(1 - 2\gamma_o)^{1/2}e^{-\alpha_o L}]^2 + 4k(1 - 2\gamma_o)^{1/2}e^{-\alpha_o L}\sin^2\left(\frac{\beta L}{2} + \frac{\pi}{4}\right)} \qquad (5.10)$$

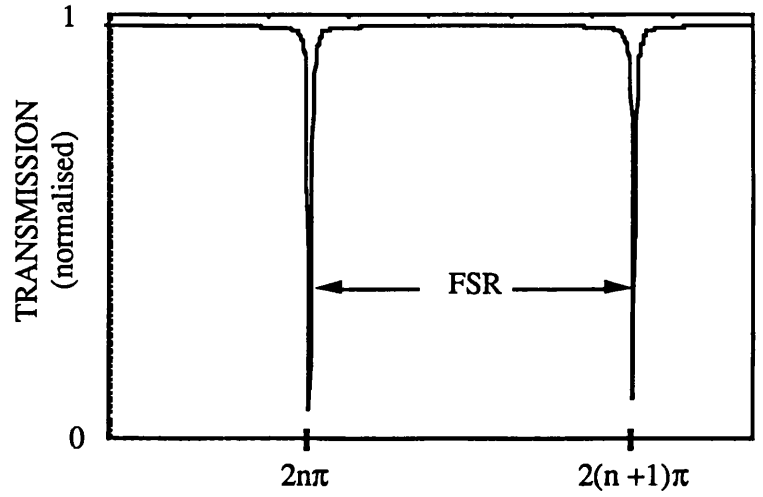

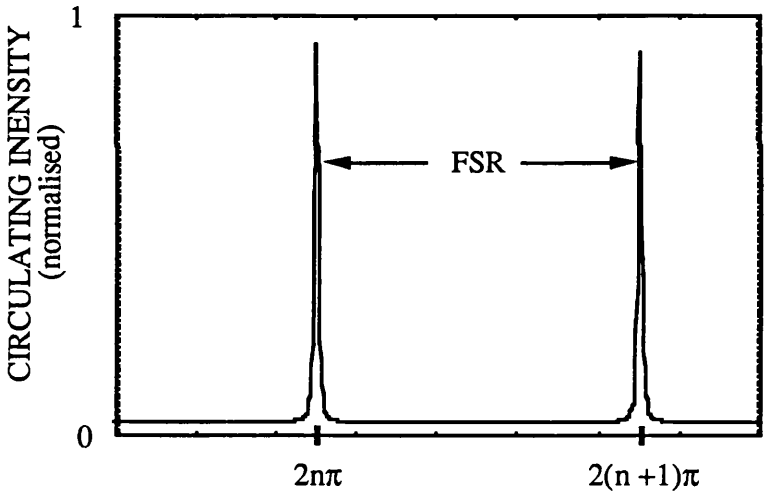

Figure 5.2. The resonator transmission characteristics for the transmitted (output) and the circulating intensities (powers) against phase in the loop. Minima in the transmitted intensity correspond to the maxima in the circulating intensity and represent the resonant condition for the round-trip phase delay. [Typical values: $2\gamma_0 = 0.02$, $\alpha_0 = 1.6 \times 10^{-3}$ /m (8.5 dB/km), L = 10 m]. FSR: free spectral range.

The resonator transmitted and circulating intensity as a function of the round-trip phase delay are plotted in figure 5.2, and the graphs clearly show the sharp minima at the resonant value of the roundtrip phase delay, $\sin(\beta L/2 + \pi/4) = 0$ as given by the resonance condition of eqn (5.7); at this value of the phase delay, the peak circulating intensity $I_3 = |E_3|^2$ in the loop is then given by (using eqn (5.10)):

$$\frac{I_3}{I_1} = \frac{(1 - 2\gamma_o)}{(1 - k^2)} \tag{5.11}$$

We plot the intensity enhancement I_3/I_1 as a function of the coupling coefficient in fig 5.3. For practical resonators, we expect k^2 to be as close to unity as possible. In this case, providing the coupler losses are low (ideally approaching zero), it can be seen from fig. 5.3 that the intensity circulating inside the ring will be *significantly* enhanced over the incident intensity. This property makes all-fibre ring resonators very convenient devices for investigation of nonlinear effects. For example, if $k^2 \approx 0.99$, and the coupler loss is, say 1%, then the circulating power will be enhanced 99 times over the incident power, allowing the observation of nonlinear effects such as SBS at powers much lower than in straight lengths of fibre, or in bulk materials. It will be shown quantitatively later by how much the Brillouin threshold can be lowered in a high finesse, all-fibre ring resonator.

The above analysis implies that the energy is conserved so that the condition, $P_{in} = P_{loss} + P_{out}$ is fulfilled. That is, the resonator power will grow until the power dissipated by the losses equals the input power. P_{loss} represents the power lost to the system as heat, and has two contributions: $P_{loss} = P_\alpha + P_\kappa$, where P_α represents the fibre loss, and P_κ is the coupler loss. However, the above condition has never been explicitly proved, and in the Appendix F, this proof is derived. This is particularly important for the case when there are additional losses in the system, for example due to nonlinear effects, where these will lead to a change in the output power, which may be undesirable in many sensor applications. This situation, its cause, and possible solutions will be further considered in the next chapter.

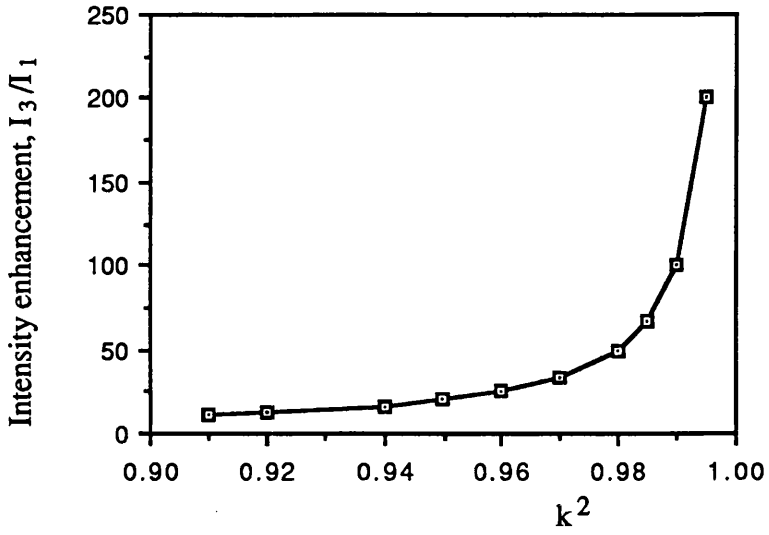

Figure 5.3. Enhancement of the circulating intensity over the input intensity as a function of the coupling coefficient; coupler loss = 0.

5.1.2. Resonator finesse and nonresonant coupling

The full width at half maximum (FWHM) linewidth of the resonator Δf can be found by equating eqn (5.11) with $1/2|E_3/E_1|^2$ as given by (5.9). Let ω_q' be the angular frequency at which the circulating power (or intensity) is half its maximum value ($\beta L = n\omega L/c$), as shown in figure 5.4, so that:

$$\frac{1}{2}\left[\frac{1 - 2\gamma_o}{1 - k_{res}^2}\right] = \frac{(1 - 2\gamma_o)(1 - k_{res}^2)}{(1 - k_{res}^2)^2 + 4k_{res}^2 \sin\left(\frac{n\omega_q' L}{2c} + \frac{\pi}{4}\right)} \tag{5.12}$$

and therefore:

$$\sin\left(\frac{n\omega_q' L}{2c} + \frac{\pi}{4}\right) = \pm \frac{1 - k_{res}^2}{2k_{res}} \tag{5.13}$$

at resonance, the angular frequency is given by $n\omega_q L/c = 2\pi q - \pi/2$, where the subscript q refers to q-th mode.

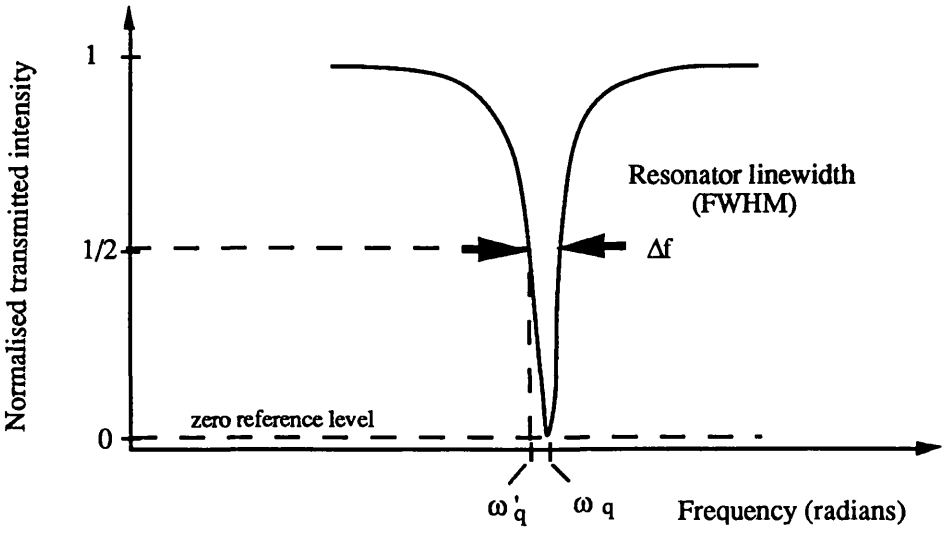

Figure 5.4. Showing the linewidth associated with OFRR response - one resonance dip is shown.

The solution to eqn (5.13) corresponding to this q-th resonance is denoted by ω_q' and the (FWHM) linewidth is therefore:

$$\Delta f = \frac{2}{\pi}|\omega_q - \omega_q'| = \frac{2c}{nL}\sin^{-1}\{\frac{1 - k_{res}^2}{2k_{res}}\} \qquad (5.14)$$

The free spectral range (FSR) of the resonator is conventionally defined as the frequency spacing between two adjacent resonant modes, that is:

$$FSR = c/nL \qquad (5.15)$$

Combining equations (5.14) and (5.15), together with the approximation that in order to achieve a high finesse, the coupling constant, k_{res} is close to one, so that that sin A ≈ A, we arrive at the following expression for the cavity finesse:

$$F = \frac{\pi k_{res}}{1 - k_{res}^2} \qquad (5.16)$$

where k^2_{res} was given by eqn (5.8).

Indeed, this equation for the finesse of the cavity is in general true for all values of the

coupling coefficient k^2, and although calculated for the circulating intensity peaks, this calculation applies to the output (inverted) peaks, as shown in figure 5.4. In figure 5.5 we plot the variation of the cavity finesse as a function of the coupling coefficient. From this graph, it is possible to appreciate further the importance of having a high-finesse (and thus a low-loss) cavity, as we can compare the direct relationship between the circulating power enhancement (as shown in figure 5.4) and the finesse as a function of the coupling coefficient. The variation of the coupling coefficient with fibre length for different values of fibre losses is shown in figure 5.6, from which it is clear that fibre losses can be a practical limitation in optimising the value of finesse. It therefore follows, that in designing and fabricating OFRRs, a judicious choice of the loop length must be made in order to maximise the finesse, or the interaction length (as for the case of observation of nonlinear effects in these devices, for example) appropriately.

It is interesting to note what happens when the coupling constant is not adjusted to its resonant value as given by eqn (5.8). For a general value of the coupling constant eqns (5.6) and (5.10) lead to the output and circulating powers, respectively:

$$\frac{|E_4|^2}{|E_1|^2} = \frac{(1 - 2\gamma_o)\left[\frac{(k^2 - \kappa^2)^2}{k^2} + 4\kappa^2 \sin^2\left(\frac{\beta L}{2} + \frac{\pi}{4}\right)\right]}{(1 - \kappa^2)^2 + 4\kappa^2 \sin^2\left(\frac{\beta L}{2} + \frac{\pi}{4}\right)} \qquad (5.17a)$$

and:

$$\frac{|E_3|^2}{|E_1|^2} = \frac{(1 - 2\gamma_o)(1 - \kappa^2)}{(1 - \kappa^2)^2 + 4\kappa^2 \sin^2\left(\frac{\beta L}{2} + \frac{\pi}{4}\right)} \qquad (5.17b)$$

and $\kappa^2 = k(1 - 2\gamma_0)^{1/2}\exp - \alpha_0 L$. Note that when $k^2 = (1 - 2\gamma_0)\exp - 2\alpha_0 L$, κ reduces to k_{res} (eqn (5.8)), and the above equations reduce to (5.6) and (5.10).

The result of equations (5.17a) and (5.17b) are as follows. When the coupling constant is less than the resonant value - this is known as undercoupling, the finesse decreases. However, for $k_{res} < k < 1$ (overcoupling), the finesse is higher or the same as in the resonant case, while the circulating power drops, and the output power becomes non-zero.

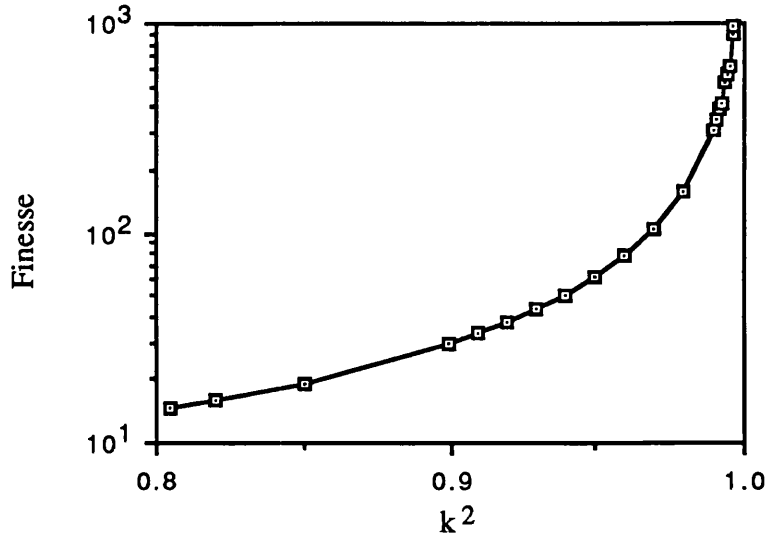

Figure 5.5. Variation of resonator finesse as a function of the coupling coefficient.

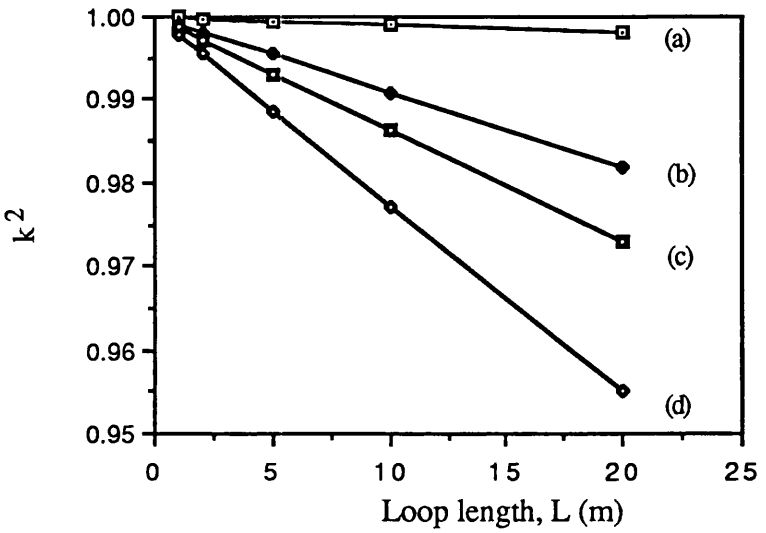

Figure 5.6. Plot of coupling coefficient vs loop length, L for different fibre losses: (a) 0.4 dB/km; (b) 4 dB/km; (c) 6 dB/km; (d) 10 dB/km.

5.1.3. The significance of pump linewidth in resonator transmission

In analysing the response of the OFRR we have assumed a single frequency light input. In this section we consider the effect on the resonator characteristics of having the input light of finite spectral width. Although all lasers have a finite spectral width, most stabilised single frequency gas or colour centre lasers have laser linewidths (< 1 MHz) which are comparable or less than the resolution of even a very high finesse OFRR. However, semiconductor lasers in general have broader linewidths which are sensitively dependent on variations in the optical feedback into the laser cavity. For this reason, the effects of the pump linewidth on the resonator transmission have to be carefully evaluated in the case of semiconductor lasers.

In the case of high finesse resonator, the resonant characteristic $\phi_{res}(f)$ of the output signal is approximated by the Lorentzian profile as follows[16]:

$$\phi_{res}(f) = \frac{\psi_{res}/\pi}{\psi_{res}^2 + (f - f_0)^2}$$

$$\text{and } \psi_{res} = \frac{\Delta f_{res}}{2} \qquad (5.18)$$

where f_0 is the resonant frequency. However, in the case of a low-coherence source, such as a semiconductor laser, the output linewidth of the resonator Δf_{res} is strongly dependent on the spectral linewidth of the pump laser (although the actual resonator linewidth which is governed by the resonator finesse, as given in eqn (5.15), is, of course, unchanged). Now, it is possible to derive the formula for the resonant characteristics $\phi(f)$ of the ring resonator with a with a broad linewidth laser source. The power spectral density of a single mode laser diode $\phi_{las}(f)$ is also assumed to have a Lorentzian profile[16] so that:

$$\phi_{las}(f) = \frac{\psi_{las}/\pi}{\psi_{las}^2 + f^2}$$

$$\text{and } \psi_{las} = \frac{\Delta f_{las}}{2} \qquad (5.19)$$

where Δf_{las} is the laser spectral linewidth. The resonant characteristic $\phi(f)$ is found by taking the correlation between $\phi_{res}(f)$ and $\phi_{las}(f)$:

$$\phi(f) = \int_{-\infty}^{\infty} \phi_{res}(f')\phi_{las}(f' - f)df'$$

$$= \frac{(\psi_{las} + \psi_{res})/\pi}{(\psi_{las} + \psi_{res})^2 + (f - f_0)^2} \qquad (5.20)$$

From eqn (5.14), (5.15), and (5.20) an effective transmission characteristic of the entire system can be worked out. This 'effective' finesse ('effective' because the actual Q-factor of the resonator, which depends on losses, is actually not altered in any way by employing a broad linewidth source), F' is given by:

$$F' = \frac{c/nL}{2(\psi_{las} + \psi_{res})} = \frac{cF}{nLF\,\Delta f_{las} + c} \qquad (5.21)$$

It can be seen that the effective transmission is strongly dependent on the laser spectral linewidth. This is illustrated in fig. 5.7 (a) - (c). Graphs on figure 5.7 show this variation of the 'effective' finesse, plotted against the actual cavity finesse, as a function of the laser linewidths, and plotted for different loop lengths. It can also be seen that for longer loop length, and hence - a smaller FSR, the effective finesse decreases most dramatically. This follows from eqn (5.15) which states that for a given finesse, an decrease in the FSR leads to a smaller resonator linewidth. In this case, the resonator transmission becomes completely determined by the spectral width of the source. The use of a low-coherence pump source leads to a reduction in the 'effective finesse' and as a result - to a lower circulating power in the ring. Conversely, when the ring resonator is used as a recirculating delay line, a low coherence source with coherence much less than the delay time is deliberately used so that the optical summations are linear in the intensities of the interacting waves, rather than in amplitudes[23].

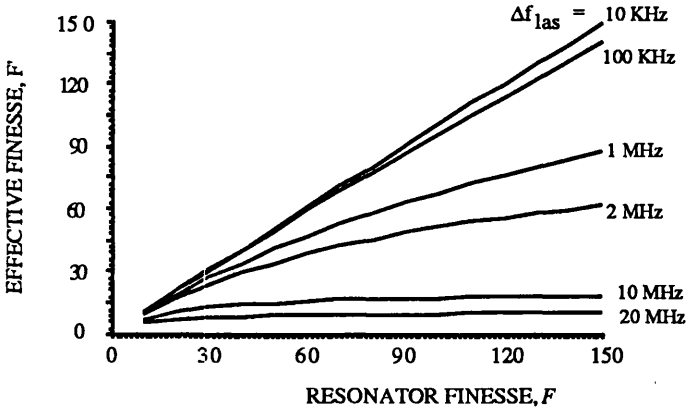

(a)

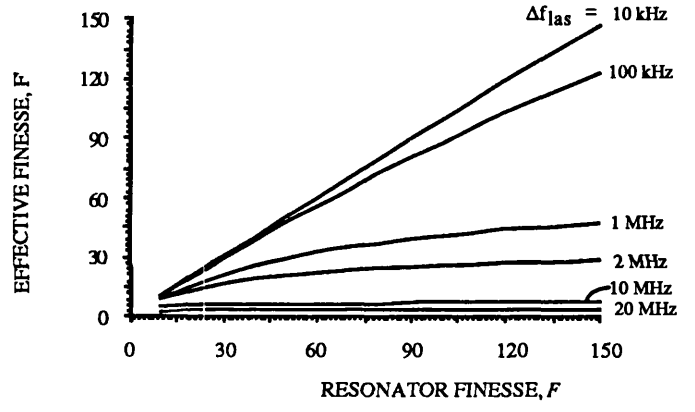

(b)

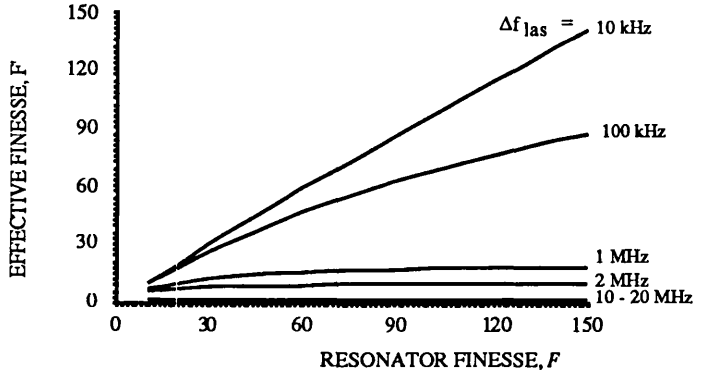

(c)

Figure 5.7. Showing the relationship between the 'effective' finesse and actual cavity finesse as a function of laser linewidth for different loop lengths: (a) 1 m; (b) 3 m; and (c) 10 m.

5.2. Experimental investigation of OFRRs

5.2.1. Resonator fabrication details

Since the resonator fabrication process has such a profound influence on the resulting device, and many aspects of the process have been developed and perfected at UCL, it seems worthwhile to describe some details of fabrication. The resonator high performance, characterised by its finesse, is dependent upon achieving very high quality, low loss polished directional couplers. The main steps in the polishing process are outlined below.

(a) Preparation: for ordinary (polarisation non-preserving) single mode fibre, the fibre is bonded into glass blocks (generally 1.5 cm x 3.0 cm) in which curved grooves have been cut (using a diamond impregnated circular saw blade of thickness 200 - 225 μm, to achieve a clean cut). The groove depth is approximately 150 μm and the radius of curvature is 25 cm which ensures a convenient effective interaction length of approximately 1 mm, as derived by Digonnet and Shaw (ref. 3). Approximately 1 - 1.5 cm of the bonded section of the fibre is stripped of its protective plastic jacket, and the fibre is held in the groove with quick curing epoxy at the edges, and then cured with UV curing epoxy. For resonator fabrication, two glass blocks - forming the two halves of the directional coupler are mounted on one strand of fibre, separated by the required resonator loop length. One half of a directional coupler is illustrated in figure 5.8 (a).

(b) Polishing: the lapping and polishing was carried out on a Logitech polishing machine with 1 μm resolution. Initially, each glass half is lapped on a coarse lapping plate, until approximately 25 μm of the glass block surface (for an ordinary 125 μm cladding diameter fibre) and 40 - 45 μm of the cladding have been removed. The fibre is then examined under a microscope, and the characteristic 'ellipse' showing the remaining fibre in the groove, is measured. When its length is equal to 9.0 - 9.5 mm, the lapping plate is changed for a polishing plate, to polish away the remaining cladding to within 1 - 2μm of the fibre core until the evanescent field is exposed. The fibre is polished for several minutes to remove the surface damage from lapping, and then inspected every few minutes (depending on the polishing speed). The proximity to the core is judged by performing the 'oil drop' test. This is done by launching some light into the fibre, and then , in turn

placing a drop of Corning index matching oil of refractive index slightly higher than that of the core, to test the degree of coupling. The oil of refractive index 1.464 has generally been used for fibres at 800 and 600 nm. The polishing is stopped when the ratio of the light coupling out after the insertion of the oil compared to no oil, is 1000 or 30 dB. All the values quoted in this sub-section on polishing have been arrived at through experimentation and continual development of the polishing process within the Optical Fibre Group at UCL, and by considering in detail the coupling vs the degree of polish. Indeed, these values have been established as optimum in achieving low-loss couplers. The polished directional coupler is shown on fig. 5.8 (b).

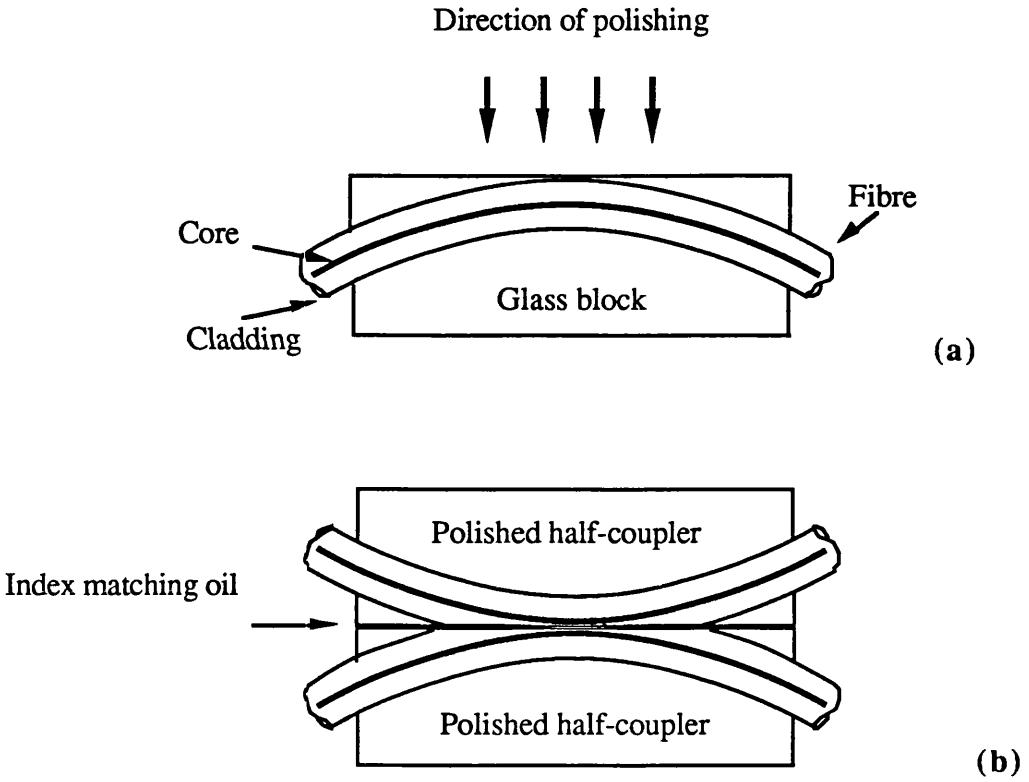

Figure 5.8. Schematic diagram showing: (a) half-coupler - single mode fibre is fixed in the groove of a glass block, ready for lapping and polishing; (b) polished coupler. [Not to scale].

5.2.2. Experimental investigations of OFRR operation

5.2.2.1. Experiments at 633 nm

A number of resonators have been fabricated and characterised as a result of this work. Initially the work was carried out at 633 nm using a Barr & Stroud polarised, single mode, frequency stabilized He-Ne laser with output power of 0.8 mW. The experimental set-up used in investigation of OFRRs is shown in fig. 5.9.

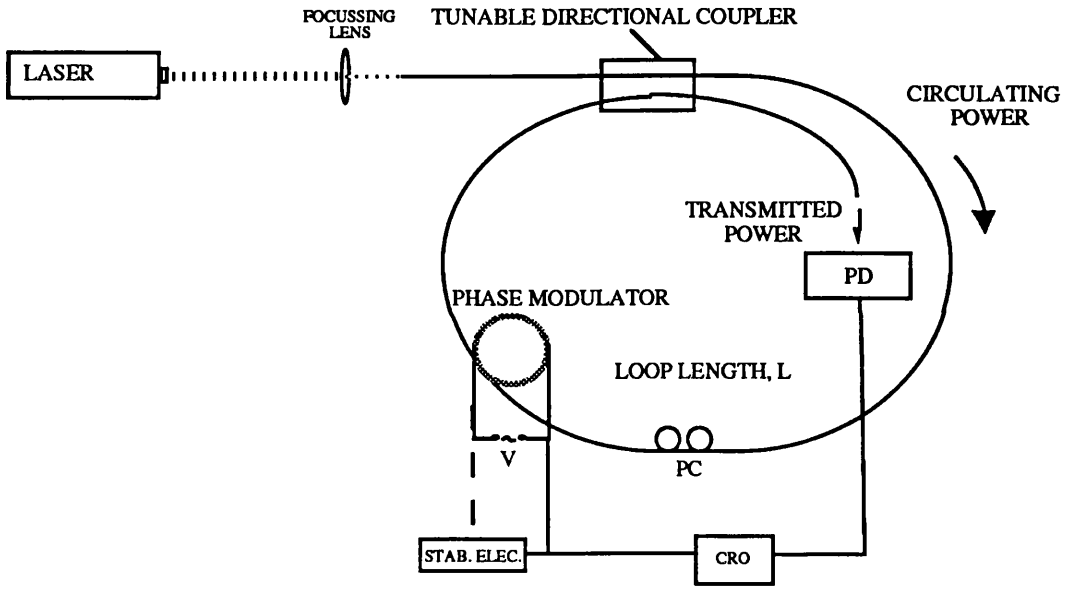

Figure 5.9. Experimental set-up used to investigate the operation of OFRR. PC is the polarisation controller.

Because the available laser power was limited, it was necessary to optimise the efficiency of focussing the light into the single mode OFRR. By considering the Gaussian beam propagation[24] of the laser beam at the launch end of the fibre, it was calculated that the focal length of the lens for which the numerical apertures (NA) of the fibre and lens are matched (providing all the lens aperture is effectively filled) is approximately 4 mm for the NA of 0.14 (York single mode fibre). Following this a 4.5 mm focal length Melles-Griot anti-reflection (AR) coated lens was used for focussing the light into the fibre, rather than the more conventional x10 or x20 microscope objectives. The achieved launch efficiency

into the fibre was approximately 70%. The phase modulator was a PZT tube around which the fibre was wound tightly, and to which a triangular ramp voltage was applied. In this configuration, the resonator acts as a scanning spectrum analyser. The directional coupler is held in a special jig with the lower half being clamped stationary, and the upper half which can adjusted by two micrometer screws. The resonator can then tuned by moving the top half of the directional coupler (by means of a micrometer screw) to give a zero output at resonance. The OFRRs investigated included a 10 m resonator made of York single mode 600 nm fibre, loss 8.5 dB/km and 1 m resonator made of polarisation maintaining bow-tie fibre, loss 10 dB/km.

When using resonators made of ordinary single mode fibre, it is necessary to include a polarisation controller in the loop in order to ensure a single resonance. In the absence of a polarisation controller, two resonant modes are observed, corresponding to two polarisation eigenmodes (shown in fig 5.10) which are defined by the net birefringence in the ring. These two modes resonate at two different scanned positions due to slightly different propagation velocities of the two nondegenerate polarisation modes.

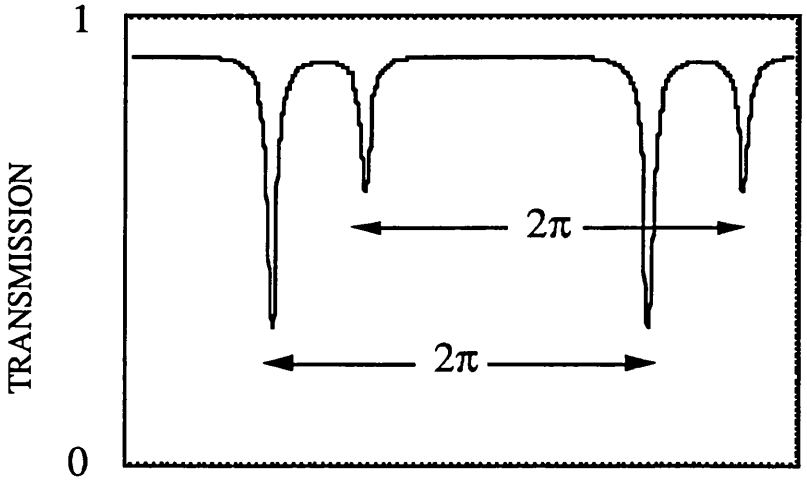

Figure 5.10. Showing the resonator transmission with both polarisation modes resonant.

A typical transmission response for the 10 m resonator is shown in fig. 5.11(a). A small notch corresponding to the second polarisation eigenmode can be discerned separated from the main dip by just over a third of the FSR. The stabilisition electronics used in some

experiments to lock the resonator length to its resonant value, and is described in Section 5.2.3. The finesse was approximately 100, giving k_{res}^2 of 0.969 (from eqn (5.16)), and 8.5 dB/km (1.96×10^{-3} Np/m) loss gives the coupler loss of 1.3% or 0.06 dB (eqn (5.8)). The circulating power is enhanced over the incident power by a factor of approximately 30 (using eqn (5.11)). In this case when the coupler losses are so low, the finesse is effectively limited by fibre loss, since for zero coupler loss, the maximum obtainable finesse for this length of fibre (as limited by fibre losses) can be calculated as approximately 150. As the main emphasis of this work was in optimisation of Brillouin generation in OFRRs, without running ahead too much, it can be mentioned that although longer loop lengths result in an optimised SBS threshold, the latter is limited by a correspondingly increased losses, associated with the increased length. Bearing in mind the foregoing discussion on OFRR finesse, resonators of loop lengths less than 10 m were subsequently fabricated, in order to ensure maximum possible finesse.

In the course of these experiments, two effects, previously unreported, were observed. The extra dips on either side of the main dip make the laser source appear multimode, and are in fact due to the deviation from the linear ramp variation of the piezo-electric transducer[25], and are evident in high finesse resonators at comparatively low triangular ramp frequency (< 200 Hz) and applied voltage (< 20 V peak-to-peak). This effect can be explained by resonator intensity output with a *linear* ramp variation of path length but with an *additional low level sinusoidal modulation* superimposed, describing the PZT deviation from linear operation with frequency. Figure 5.11(b) shows clearly the main resonator dip with extra resonances which are discernible on figure 5.11(a). The levels of the side dips vary with drift in phase offset of the ramp (that is in the optical path), and depend on the temperature or the frequency drift of the laser. And in this case the linewidth of the resonator was approximately 200 KHz (FSR/*F*). No such spurious nulls were observed with sinusoidal modulation. The result of the theoretical simulation[25] of this effect is shown in figure 5.12. Resonance occurs at a certain phase delay, corresponding to an integer number of 2π. When in simulation a low level of sinusoidal modulation is superimposed on the linear ramp, the phase condition for resonance is approached on the either side of the resonance dip. The level of this effect, thus, depends on the frequency content of the driving voltage. This effect is important, since it indicates that in all experiments, modulation at high frequency should be avoided.
For comparison, the transmission of the resonator using a multi-mode He-Ne source (with three modes spaced over 1085 MHz) is shown in fig. 5.13. Three modes are clearly observed, and a sinusoidal variation is applied to the PZT to avoid nonlinearities.

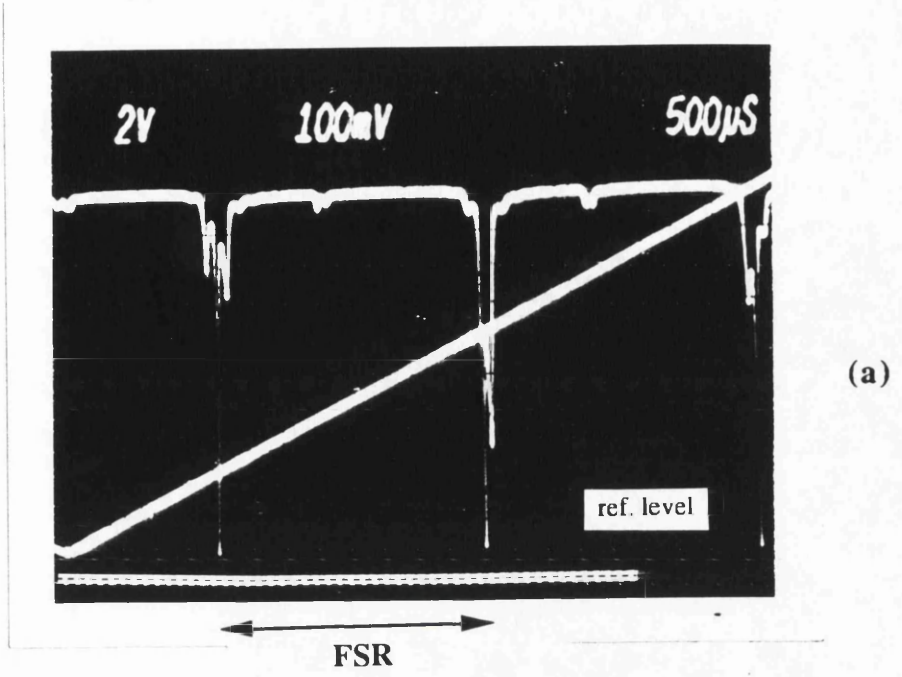

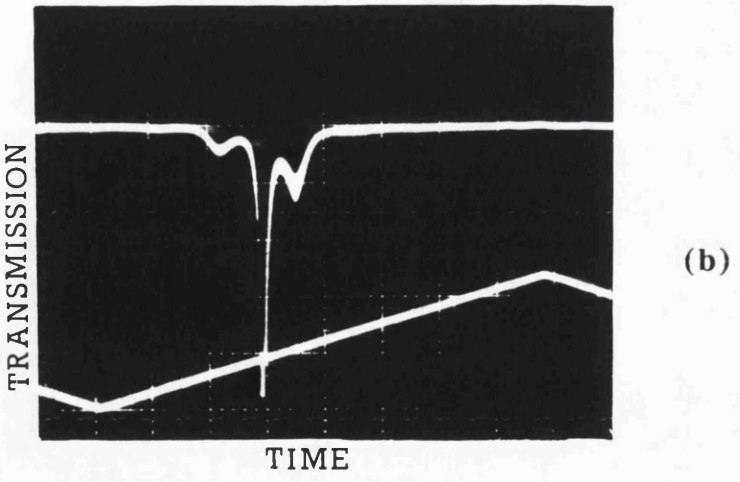

Figure 5.11. (a) Resonator transmission response for the 10 m resonator for a single mode He-Ne laser at 633 nm: L = 10 m, finesse = 97; (b) showing one resonance dip: the spurious resonance dips either side of the main dip are due to PZT nonlinearity.

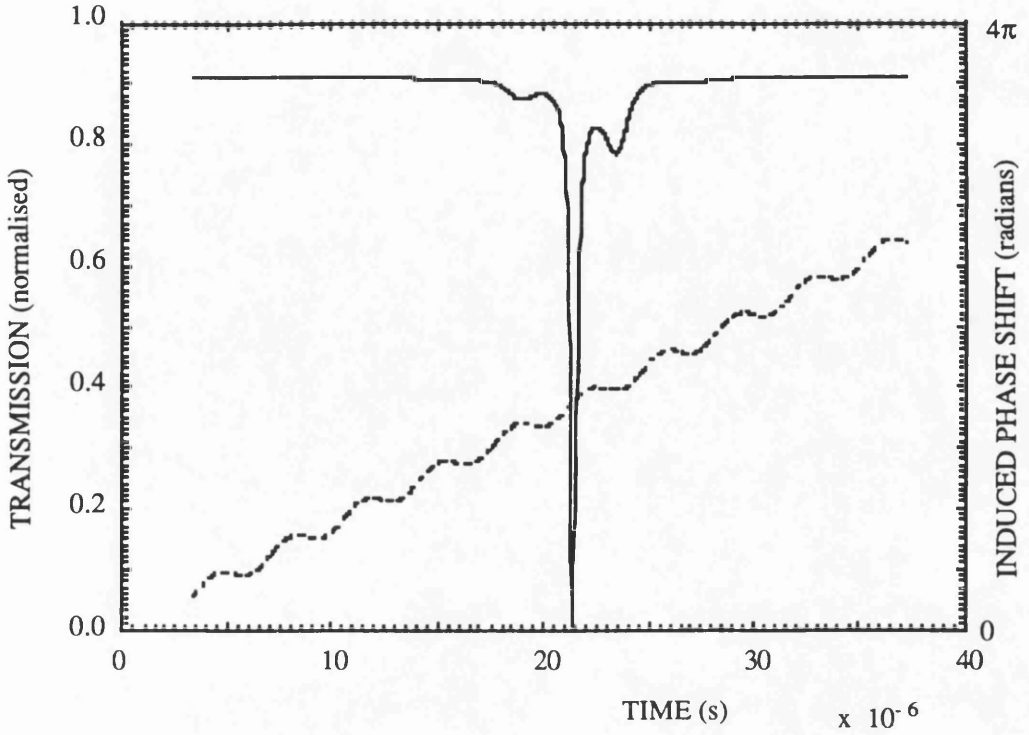

Figure 5.12. Computer simulation of the PZT nonlinearity obtained by superimposing a sinusoidal variation on the linear phase ramp[25].

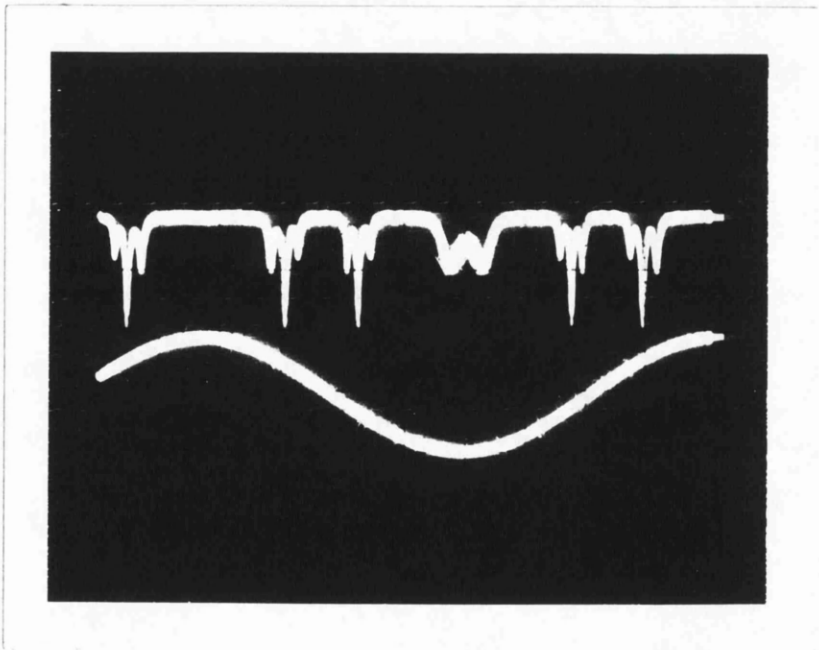

Figure 5.13. Response of the 10 m resonator using a multimode He-Ne source with three modes.

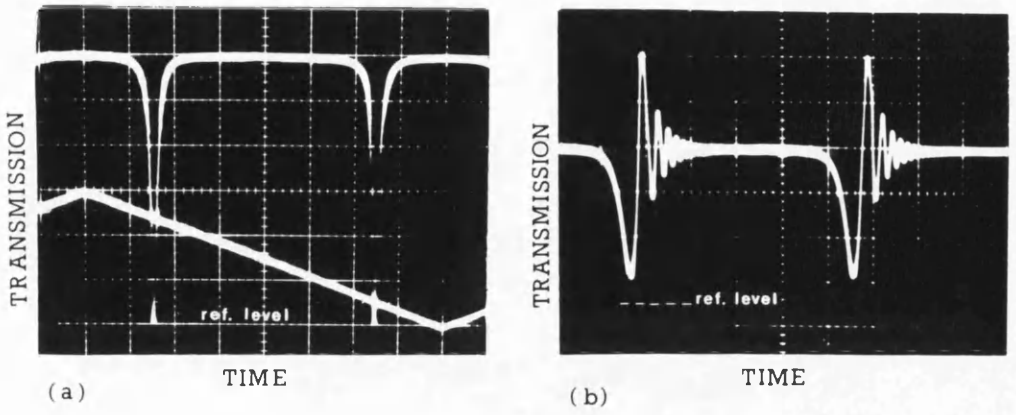

Figure 5.14. Experimental results showing the effect of ringing in the dynamic response of the resonator: (a) linear response; (b) ringing - scale: 1 unit = 200 ns.

The second new effect observed was that of 'ringing' apparent in the dynamic response of the resonator when driven either (or both) at high frequency (> 1000 Hz) or amplitude of the ramp voltage (> 15V peak-to-peak) applied to the PZT. This ringing is illustrated in figure 5.14. It can be seen that the transmitted power does not reach zero at resonance and the resonance minima appear to be shifted compared to the steady state response. Moreover, each resonance is followed by an overshoot, resulting in a decaying oscillatory structure of increasing frequency. Such dynamic characteristics can be explained by considering the multi-circulation nature of the OFRR deviation of the loop phase delay in the dynamic case from that at steady state This phase deviation is shown to become significant in the case of high finesse resonators, and presents another reason for operating the resonator at very low values of ramp frequency[26]. Generally, a high amplitude of the applied voltage is necessary (except in resonators of very long loop lengths) to be applied in order to be able to scan the resonator response across at least one FSR. For 1 m OFRR the voltage amplitude of 40 V peak-to-peak to scan over 1 FSR was necessary. The importance of this effect will also be realised at the end of next chapter, and with reference to the Chapter 3, as it effectively rules out the possibility of suppression of SBS in high finesse resonators by high frequency modulation of the pump wave.

Although the fabrication of OFRRs out of polarisation maintaining fibre is more complex, there is no need to use polarisation controllers, and as will be shown in chapter 6, the threshold power in the SBS process is reduced by a factor of 2 in this case. The fabrication is more complicated because both halves of the directional coupler have to be accurately aligned on the same birefringence axes prior to polishing. In addition, alignment of the fibre principal axes must be themselves accurately aligned with certain device axes to avoid undesirable polarisation cross-coupling[27-30].

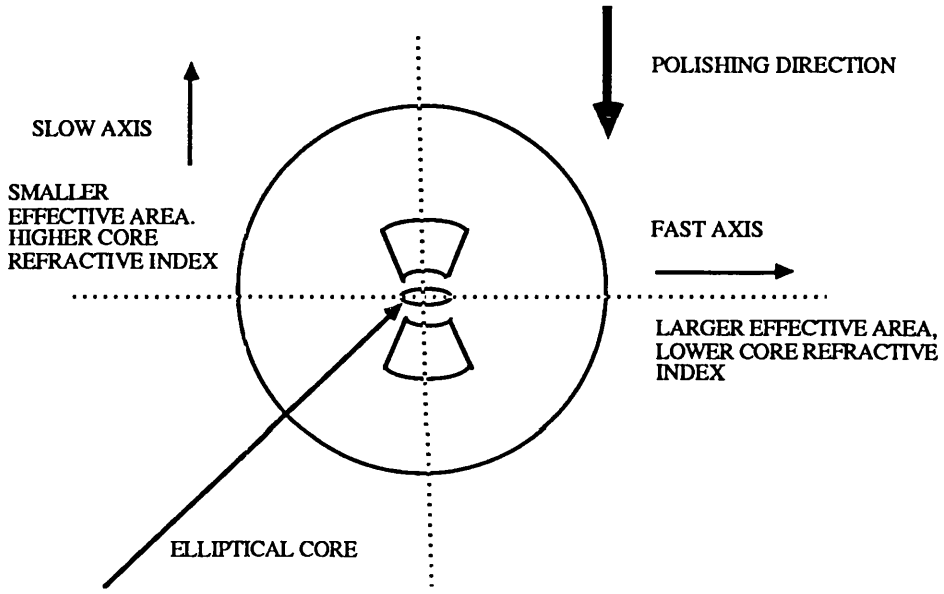

Figure 5.15. The cross-section profile of the bow-tie polarisation maintaining fibre (with elliptical core) used in experiments.

The elasto-optic alignment technique to ensure accuracy was initially proposed by Carrara et al.[27]. The technique consists of applying an external force by squeezing the fibre (say, at an angle θ to one of the principal axes) which induces an external birefringence proportional to the elasto-optic coefficient. If linearly polarised light is launched along either of the principal axes at the input to the fibre, with analyser aligned to transmit light in the orthogonal direction, it can be shown that the output power measured after the analyser, becomes zero when the external stress is along either of the principal birefringent axes. Moreover, it turns out that the minimum along the slower axis is sharper and narrower than that of the fast axis. This is explained by the fact that squeezing the fibre parallel to the fast axis increases the net birefringence, while along the slow axis, the intrinsic and applied birefringence tend to cancel, resulting in a more sensitive dependence on θ, as the net

birefringence approaches zero. This allows one to distinguish the two birefringence axes, and provides a better resolution for the alignment on the slow axes. The cross-section profile of the elliptical core bow-tie birefringent fibre is shown in fig. 5.15. During polishing one half of the bow is removed (along the direction of the slow axis) to reach the core. Through continual improvement of the technique developed in the Fibre Optics Group at UCL[28], fabrication of couplers with better than -25 dB polarisation cross-coupling was achieved throughout this work.

The finesse of the OFRR made of polarisation maintaining fibre with a loop length of 1 m (fibre loss 10 dB/km) was initially 600 (giving a coupler loss of 0.4% (0.02 dB)), but within a few days decreased to 300, coupler loss 0.8% (0.03 dB), FSR of 200 MHz and a linewidth of approximately 600 KHz. Indeed, it has been observed in the process of this work that the finesse might often be degraded with time. The exact reasons for this are not known. However, the most likely reason is that the index matching oil used used between the two halves of the coupler is absorbed in the epoxy with which the fibres are secured in the slots of the glass blocks, and forces the fibres 'up' increasing the losses on coupling.

The behaviour of this resonator was found to follow the results described above except that different losses were observed for light launched along the orthogonal polarisation directions. The polarisation directions of the fibre were identified by examining the cleaved launch end under a microscope. The bow-tie profile could be easily identified, and the principal axes directions were marked on the fibre chuck, with accuracy to 1^{o}. It is interesting to note that *different* finesses were observed for the light launched along the slow axis, compared with that for the fast axis. For all values of finesses, this difference was approximately 4 - 6% of the higher finesse value. The resonator had to be retuned for each measurement for the optimum finesse ($F = 310$) to be obtained for each polarisation axis. These results imply differential coupling coefficients for the two axes or additional losses between the fibre losses, either incurred through polishing or due to the inherent index difference of the two fibre modes. It seems that the differential coupling coefficients are most likely because of the different effective refractive indices, and hence phase velocities along the two directions, resulting in differential losses in the two directions.

Incidentally, it was found that the coupler losses are very sensitively dependent on the refractive index of the index matching oil used between the coupler halves. As the refractive index of the Corning oils used varies with temperature, this affected which

particular oil was used, depending on the ambient conditions. It was found that the oil with the refractive index of 1.58 resulted in minimum coupler losses at room temperature (approx. 23° C).

5.2.2.2. Experiments at 830 nm

The next stage in the work was to investigate the resonator behaviour using a shorter coherence semiconductor laser source.

Equation (5.16) shows that the highest cavity finesse F is achieved for the values of k_{res} which approach unity, and as will be shown in Chapter 6 the Brillouin threshold power is reduced for longer resonator loop lengths. However, as can be seen from equation (5.8), a longer loop lengths leads to a lower finesse due to higher corresponding fibre loss. Resonator operation in the near infra-red region of the spectrum both reduces the fibre losses, and makes this device more compatible with the current optical fibre technology.

The laser source chosen was a temperature controlled, Hitachi HLP 1400 GaAlAs single mode semiconductor laser, operating at a wavelength of approximately 830 nm, output power > 15 mW at 110 mA drive current. At the time of this work, this was the only commercially available, narrow linewidth (less than 10 MHz at maximum output power) with relatively high power output (with reference to its use as a pump for generation SBS in ring resonators). The divergent beam from the laser diode was collimated using an anti-reflection (AR) coated Newport collimating lens.

Although the fibre losses at this wavelength are still comparatively high (2 - 4 dB/km for York 800 nm fibre), the choice of source wavelength was governed by the availability of the source - fibre - detector combination for this work.

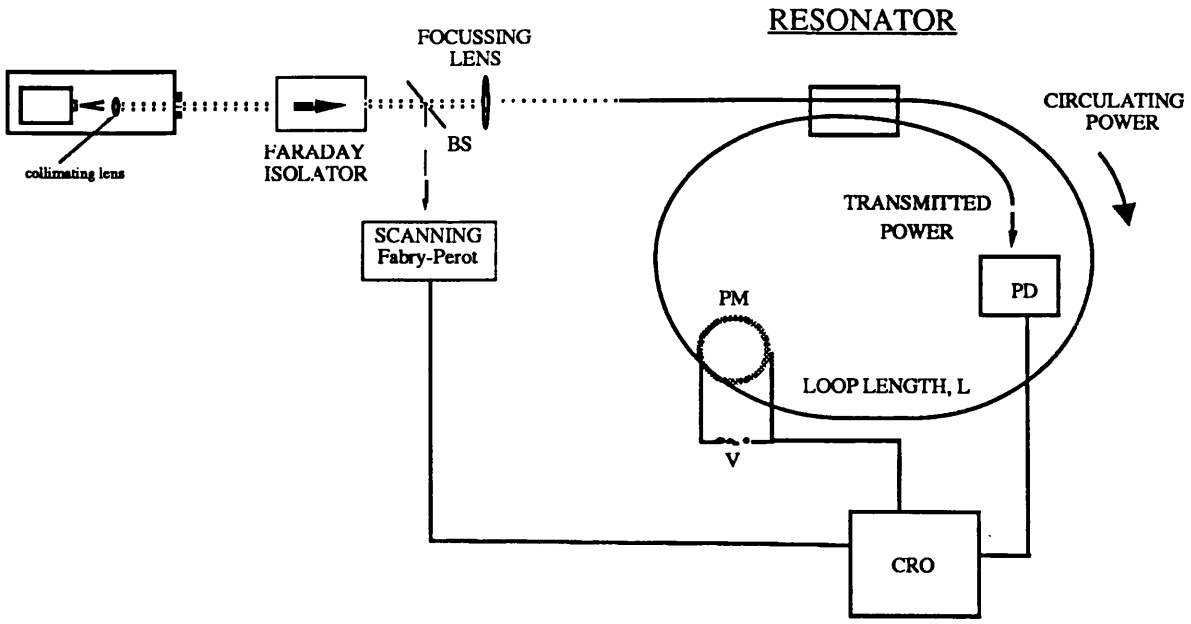

Fig. 5.16. Experimental set-up used investigation of the operation of OFRR using a semiconductor laser source.

The experimental conditions in this case were somewhat different to those described above, and the experimental set-up used is shown in fig 5.16. Associated with semiconductor laser sources are the broader spectral linewidth, and fluctuations in the output frequency. As shown in section 5.3, this results in a lower re-circulating power and 'effective finesse'. In fact, it was shown in ref. [13] that the lower source coherence is equivalent to having a higher coupler loss. Moreover, the semiconductor laser sources are very susceptible to optical feedback into the laser cavity, and it was found that good isolation (better than 25 - 30 dB) is essential between the fibre and the laser. The Faraday isolator used was a 30 dB Hoya isolator, mounted on a micrometer controlled, rotatable mount. All the optical components were AR coated.

When the resonator length is scanned, at resonance, when most of the power is stored in the loop, a large level of backscattered signal is fed back in the direction of the laser. This causes severe mode hopping and a significant broadening of the laser linewidth. Even with 30 dB isolation, 10 mW of laser out power can result in several microwatts of optical power backscattered into the laser. Depending on the phase of this backreflected signal, it can cause a significant increase in the laser intensity noise[31-36]; this area has formed a subject of much theoretical and experimental study, since a reflection of an appropriate amplitude and phase can in fact lead to a dramatic *decrease* in the output linewidth. It is

extremely difficult to evaluate the amplitude and phase of the reflection necessary to result in linewidth narrowing of a semiconductor laser[33,36]. However, after carrying out some careful measurements it was found out that the isolator, positioned appropriately can act as an effective external cavity, reducing the output linewidth of the HLP1400 to approximately 2 MHz from the specified 10 MHz. Because the output linewidth is inversely proportional to the output power, the isolator had to be adjusted between measurements to optimise the back-reflected signal. A series of careful experiments ensured repeatable and temporally stable (> 2-3 minutes) output linewidth.

The need to use two lenses for coupling the laser output into the fibre reduces the launch efficiency to a maximum of about 40%. The lens used to focus the light into the fibre was an AR coated 4.5 mm focal length plano-convex lens, which has a numerical aperture (NA $\approx$ 0.1) which matches that of the fibre. Although a graded index (GRIN) rod lens or a 'lensed' section of fibre for launching would ensure a higher launch efficiency (maximum coupling between a semiconductor laser and a single mode fibre using a GRIN lens reported[37] was 1.0 dB (79%) and 70% (1.5 dB) for a 'lensed' fibre[38]), this would mean that the direct access to the source would be lost; for example, for linewidth monitoring and/or control, and for access to the backscattered (Rayleigh or Brillouin) signal, as can be seen later.

Two resonators were fabricated at 830 nm. A 2 m OFRR made of ordinary single mode York 800 nm fibre (loss 2.5 dB/km), and a 3.8 m resonator made of polarisation maintaining fibre (loss 4.0 dB/km). When the isolator was used the resonator transmission was quite stable. An optimum transmission finesse of approximately 35 (giving an equivalent coupler loss of approximately 5%) was measured for both resonators, and a typical transmission response is shown in figure 5.17; The laser noise, clearly evident from in figure 5.17(b) makes accurate measurements difficult. It was estimated, using a narrow-linewidth, frequency-stabilised He-Ne laser that the actual cavity F was significantly higher in both cases, with approximately 85 for the 2 m OFRR and 95 for the 3.8 m OFRR. Because in this case, the 'effective' finesse was governed by the source linewidth, differential finesses for the two polarisation directions were not observed. For the same reason, the extra resonance effects resulting from PZT nonlinearity were not observed. 'Ringing' (as described above) was seen to be significant above 500 Hz for 20 V peak-to-peak. It was also found that it was much harder to tune the resonators for

V peak-to-peak. It was also found that it was much harder to tune the resonators for optimum coupling at this wavelength, and a higher refractive index oil (n_{oil} = 1.460) had to be used.

The experimental results of observation of stimulated Brillouin scattering in OFRRs are described in Chapter 6.

5.2.3. Stabilisation Electronics

The resonator response is very susceptible to temperature drifts (of an order of 100 rad/°C m (refs [39, [40]), and acoustic vibrations so that active stabilisation must be employed to 'lock' the loop length to the resonant value. The principle of the employed technique is to apply a small ac signal at frequency f_{ac}. The transmission is modulated symmetrically about the resonance dip if the length is locked to resonance which produces an even harmonic output at frequency $2f_{ac}$, as shown in fig. 5.18 (a). When the fibre length drifts say due to temperature or acoustic vibrations, the transmission is no longer modulated symmetrically about the resonance dip, and a first harmonic is generated, as shown in fig. 5.18 (b) .The role of the stabilisation electronics is to minimise the first harmonic correcting the fibre length to its resonant value.

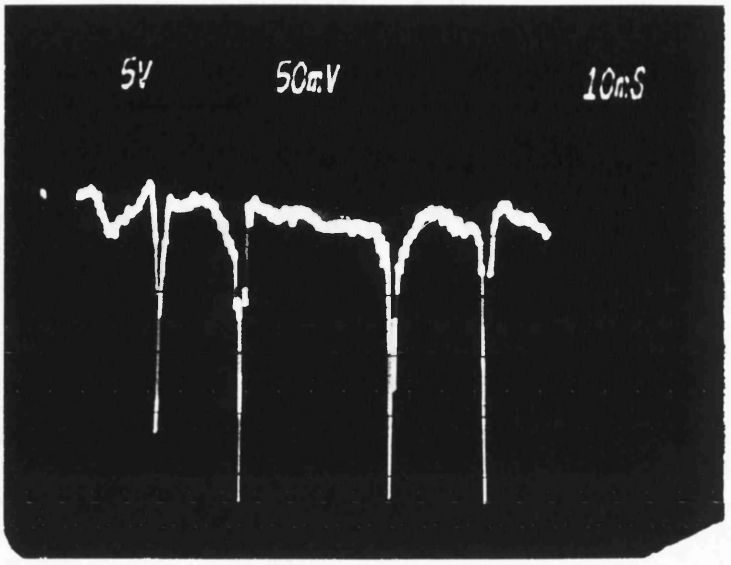

(a)

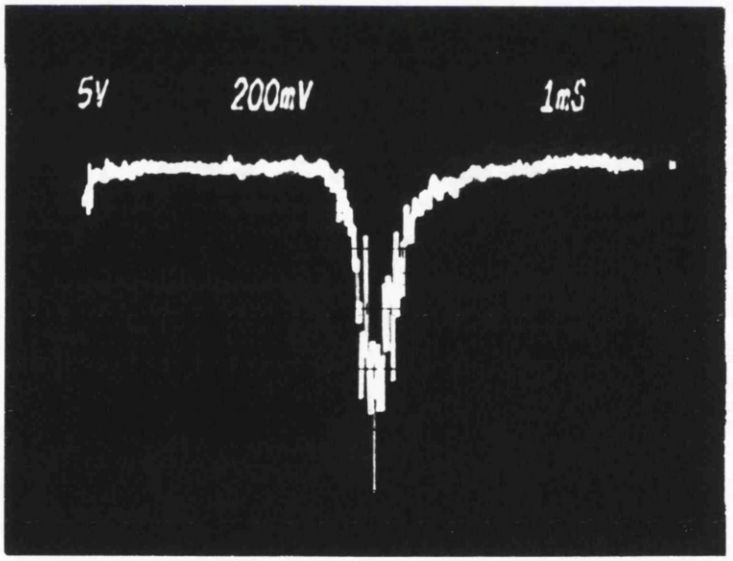

(b)

Figure 5.17. (a) Resonator transmission response at 830 nm: L = 3.8 m, F≈ 40; (b) showing single resonance in which laser intensity noise is evident.

The block diagram of the adopted control circuit is shown in fig. 5.19. The detected resonator response is fed into the lock-in amplifier and compared with a local oscillator signal at frequency f_{ac}, and if the two voltages are different, the error proportional to the difference is amplified and applied to the PZT to appropriately correct for the drifts in length. Whether positive or negative feedback is applied (and hence the sign of the correction voltage) is determined from the phase value, measured by the lock-in amplifier. The lock-in amplifier incorporated a low-pass filter which limited the close loop response to low frequencies which are characteristic of the slow temperature variations.

The results showing the operation of the stabilisation electronics are given in figure 5.20. Figure 5.20 (a) shows the transmission of the resonator dip with the second harmonic output indicating the resonator length locked to its resonant value. The spectrum analyser output and the 20 dB suppression of the first harmonic is shown in figure 5.20 (b).

Although the system above allowed 'locking' (with > 20 dB suppression of the first harmonic) of the fibre length for up to several minutes for a finesse of 90, there are a number of problems with this type of circuit unacceptable in practical application where a stable, drift-free operation would be required[14]. From fig. 5.11 (a), the phase sensitivity per volt is 1.6 rad/volt. With approximately 9.5 m of fibre wound on the PZT of diameter 125 mm, the amplifier ±18 V supply rails allow approximately ± 25 rad compensation for thermal drifts. Given the optical phase sensitivity of light propagating in the fibre is approximately 100 rad/^{o}C m, implies stabilisation in temperature to not better than a minute fraction (0.05) of a degree (it would be necessary to apply several hundred volts to stabilize the length to, say, within half a degree). In addition, if the ramp voltage necessary to scan the length over one spectral range is 4V, then for F = 100, the electronics has to track a 40 mV (0.06 rad) wide transmission dip (which will be narrower for higher finesses).

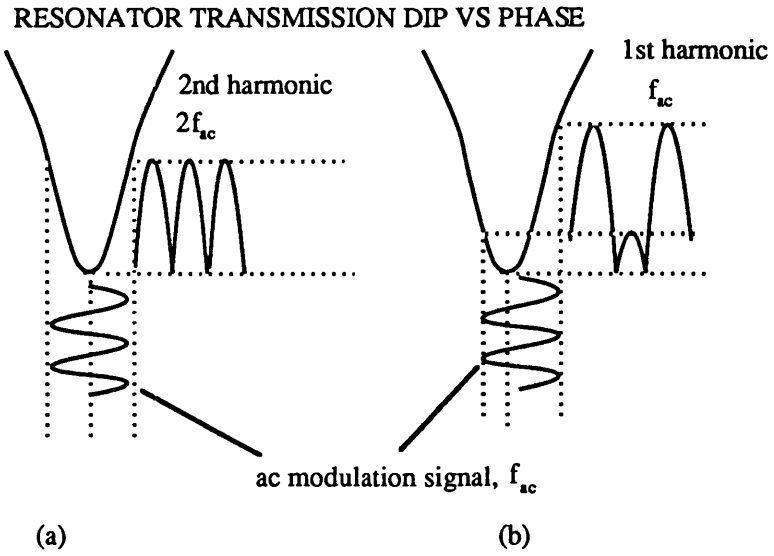

Figure 5.18. Transmission of resonator dip against phase (a) with resonator length 'locked to resonance; (b) resonator - off resonance.

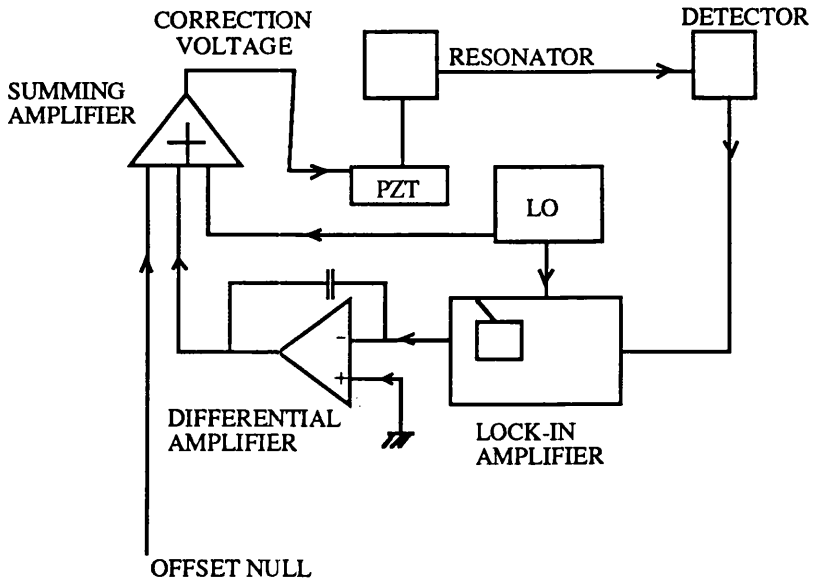

Figure 5.19. Block diagram of the stabilisation electronics.

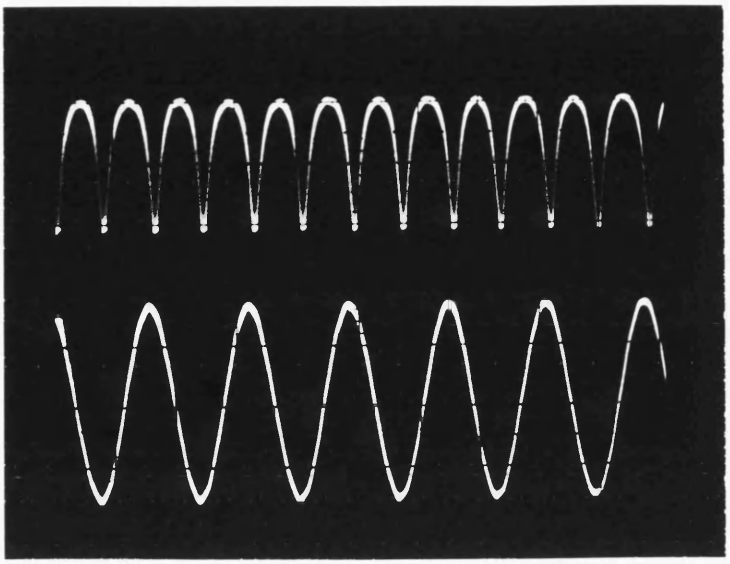

(a)

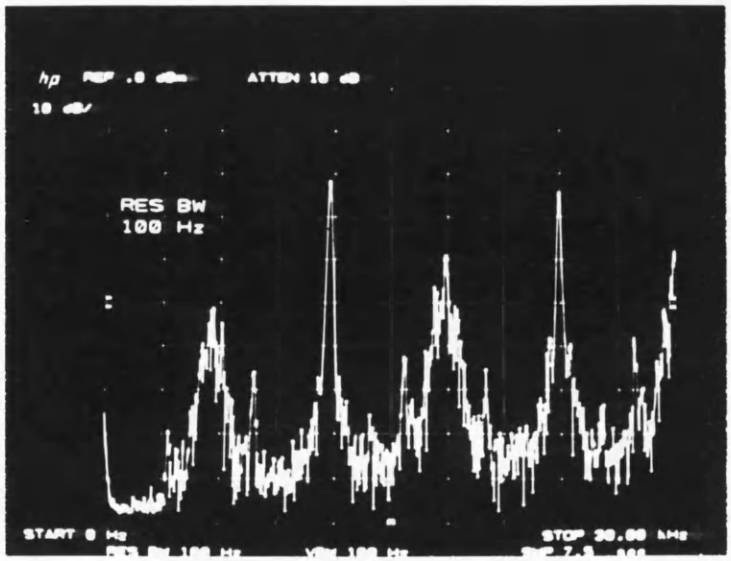

(b)

Figure 5.20. (a) Transmission of resonance dip vs time (phase) with resonator length locked to resonance - the lower trace shows the ac correction voltage, scale: 0.2 V/cm; (b) spectrum analyser output showing 20 dB suppression of the first harmonic f_{ac}; f_{ac} = 6 kHz.

5.3. Summary and conclusions

In this chapter we have described the results of a detailed evaluation of high finesse single mode all-fibre ring resonators, including fabrication, alignment, and characterisation. The important resonator parameters such as the finesse, free spectral range, and resolution were defined, and their dependence on the fibre and coupler losses, and the coupling coefficient were discussed. The coupling coefficient is seen as the most important resonator parameter. For resonance operation the coupling coefficient must be tuned so as to equal coupler and fibre losses. Hence the resonator finesse is dependent on the resonant coupling coefficient. It was shown that the resonator loop length must be carefully chosen for optimum finesse. In the cases of very low coupler losses, the finesse is limited by the fibre loss , and if the latter is high, a reduction in the the resonator length would result in a higher finesse. Similarly, if the coupler loss is relatively high, a longer loop length will not degrade the finesse (and in addition, as will be shown in the next chapter, will lead to a reduction in the Brillouin threshold).

We have successfully fabricated and tested a number of high finesse ring resonators, both using standard and polarisation maintaining fibre, at wavelengths of 600 and 800 nm. Fabrication of the resonator from polarisation maintaining fibre is more complex, as both coupler halves have to be aligned on the same axes, but this removes the necessity of having in-loop polarisation controllers. The effects of PZT nonlinearity and ringing, evident in high finesse OFRRs were identified, and the corresponding constraints on the linear operation of OFRRs were outlined.

It was also shown that while the use of a semiconductor laser means lower fibre losses and increased compatibility with current fibre systems, its short coherence length compared with a stabilised single frequency He-Ne laser (or other stabilised, narrow frequency gas or solid state laser), results in a lower circulating intensity and a lower effective 'finesse'.

5.4. References for Chapter 5

1 B. S. Kawasaki, K. O. Hill, and R. G. Lamont, 'Biconical taper single mode coupler', Opt. Lett. **6**, 327 (1981)

2 M. Kawachi, B. S. Kawasaki, K. O. Hill, and T. Edahiro, 'Fabrication of single-polarisation single mode fibre couplers', Electron. Lett. **18**, 963 (1982)

3 R. A. Bergh, H. C. Lefevre and H. J. Shaw, 'Single mode fibre-optic directional coupler', ibid. **16**, 454 (1980); 'Single mode fibre-optic polariser', Opt. Lett .**5**, 479 (1980); M. J. F. Digonnet and H. J. Shaw, 'Analysis of a tunable single mode optical fibre coupler', IEEE J. Quantum Electron. **QE-18**, 746 (1982)

4 L. F. Stokes, M. Chodorow, and H. J. Shaw, 'Sensitive all-single-mode resonant ring interferometer', J. Lightwave Tech, **LT-1**, 110 (1983)

5 M. Brierley and P. Urquhart, 'Transversely coupled fibre Fabry-Perot resonators: performance characteristics', Appl. Opt. **26**, 4841 (1987)

6 P. Barnsley, P. Urquhart, C. Millar, and M. Brierley, 'Fibre Fox-Smith resonators: application to single-longitudinal-mode operation of fibre lasers', JOSA A **5**, 1339 (1988)

7 P. Urquhart, 'Compound optical fibre based resonators', ibid., page 803

8 G. Y. Yue, J. D. Peng, Y. P. Liao, and B. K. Zhou, 'Fibre ring resonator with finesse 1260', Electron. Lett. **24**, 622 (1988)

9 R. Kadiwar, P. Bayvel, and I. P. Giles, 'SBS in polarisation maintaining all-fibre ring resonators', presented at SPIE conference 985 on Fibre Optics and Laser Sensors VI', Proc. SPIE **985**, 338 (1988)

10 R. E. Meyer and S. Ezekiel, 'Passive fibre-optic ring resonator for rotation sensing', Opt. Lett. **8**, 644 (1984)

11 R.A. Bergh , H. C. Lefevre and H. J. Shaw, 'An overview of fibre-optic gyroscope', J. Lightwave Tech. **LT-2**, 91 (1984)

12 K. Iwatsuki, 'Eigenstate of polarisation in a fibre ring resonator and its effect in an optical passive ring-resonator gyro', Appl. Optics **25**, 2606 (1986)

13 Y. Ohtsuka, 'Analysis of fibre-optic passive loop-resonator gyroscope: dependence on resonator parameters and light-source coherence', J. Lightwave Tech. **LT-3**, 378 (1985)

14 L. Stokes, 'Single mode optical fibre resonator and application to sensing', PhD Thesis, Stanford 1983

15 S. P. Smith, F. Zarinetchi, and S. Ezekiel, 'Fibreoptic ring laser gyroscope', Proc. Conference on Optical Fibre Sensors (OFS'89), postdeadline paper Tu10-6, pp 48 - 53

16 S.Tai, 'Applications of fibre optic ring resonators using laser diodes', Opt. Acta **33**, 1539 (1986);

17 W. V. Sorin, M. Nazarathy, and S.A. Newton, 'Kilohertz laser linewidth measurements using fibre ring resonators', Session WC5, OFC '88 Technical digest, volume 1

18 J. E. Bowers, S. A. Newton, and H. J. Shaw, 'Single mode fibre recirculating delay line', Proc. SPIE **326**, 108 (1982)

19 J. E. Bowers, S. A. Newton, and H. J. Shaw, 'Filter response of single mode fibre recirculating delay line', Electron. Lett. **18**, 110 (1982)

20 E. Desurvire, M. Digonet, and H. J. Shaw, 'Theory and implementation of a Raman active delay line', J. Lightwave Tech. **LT-4**, 426 (1986)

21 B. Crosignani, B. Daino, P. Di Porto, and S. Wabnitz, 'Optical multistability in a fibre-optic passive-loop resonator', Opt. Comms. **39**, 309 (1986)

22 R. M. Shelby, M. D. Levenson, and S. H. Perlmutter, 'Bistability and other effects in a nonlinear fibre-optic ring resonator', JOSA B **5**, 347 (1988)

23 M. Tur, B. Moslehi, and J. W. Goodman, 'Theory of laser phase noise in recirculating fibre-optic delay lines', J. Lightwave Tech. **LT-3**, 20 (1985)

24 A. Yariv, "Optical Electronics", 3rd ed., CBS College Publ., New York, 1985, Chapter 2

25 Z.K. Ioannidis and I. P. Giles, 'Nonlinear phase modulation in optical fibre ring resonators', Letters to Appl. Opt. **27**, 3058 (1988)

26 Z.K. Ioannidis, P. Radmore, and I. P. Giles, 'Dynamic response of an all-fibre ring resonator', Opt. Lett. **13**, 422 (1988)

27 S. L. A. Carrara, B. Y. Kim, and H. J. Shaw, 'Elasto-optic alignment of birefringent axes in polarisation holding fibre', Opt. Lett. **11**, 470 (1986)

28 I. P. Giles , M. Farhadiroushan, S. Markatos, A. Kerr, M. N. Zervas, and R. Kadiwar, 'Polarisation maintaining fibre components for advanced sensor applications systems', Proc. EFOC/LAN'88, Amsterdam, July 1988, IGI Europe publ., 274 (1988)

29 E. Shafir, A. Hardy, and M. Tur, 'Polarisation maintaining fibre couplers with misaligned birefringent axes', Electron. Lett. **24**, 754 (1988)

30 Z.K. Ioannidis, R.Kadiwar, and I. P. Giles, 'Polarisation mode coupling in highly birefringent optical fibre ring resonators', Opt. Lett. **14**, 520 (1989)

31 M. Tamburrini, P. Spano, and S. Piazzola, 'Influence of external cavity on semiconductor laser phase noise', Appl. Phys. Lett. **43**, 410 (1983)

32 M. W. Fleming and A. Mooradian, 'Fundamental line broadening of single mode GaAlAs diode lasers', ibid. **38**, 511 (1981)

33 L. Goldberg, H. F. Taylor, A. Dandridge, J. F. Weller, and R. Miles, 'Spectral characteristics of semiconductor lasers with optical feedback', IEEE J. Quantum Electron. **QE-18**, 555 (1982)

34 K. Kikuchi and T. P. Lee, 'Spectral stability analysis of weakly coupled external cavity

semiconductor lasers', J. Lightwave. Tech. **LT-5**, 1269 (1987)

35 E. M. Strzlecki, D. A. Cohen, and L. A. Coldren, 'Investigation of tunable singlr frequency diode lasers for sensor applications', ibid. **LT-6**, 1610 (1988)

36 C. Henry, 'Theory of linewidth of semiconductor lasers', IEEE J. Quantum Electron. **QE-18**, 259 (1982)

37 H. Honmou, R. Ishikawa, H. Ueno, and M. Kobayashi, '1.0 db low-loss coupling of laser diode to single mode fibre using a planoconvex graded index rod lens', Electron. Lett. **22**, 1122 (1986)

38 W. Bludau and R. H. Rossberg, 'Low loss laser-to-fibre coupling with negligible optical feedback', J. Lightwave Tech. **LT-3**, 294 (1985)

39 W. Eickoff, 'Temperature sensing by mode-mode interference in birefringent optical fibres', Opt. Lett. **6**, 204 (1981)

40 A. J. Harris and L. J. Auchterlonie, Novel means of detecting microwave power using optical fibres', Electron. Lett. **22**, 1179 (1986)

Chapter 6

STIMULATED BRILLOUIN SCATTERING IN RING RESONATORS: SBS LASERS

As we saw in the overview discussion in Chapter 3, most of the studies in this area have been primarily qualitative, and the state of research on SBS in resonators could be described as somewhat sketchy. In all the work on Brillouin lasers, the absence of any theory describing the generation of SBS in a resonator is conspicuous. There is no description of the conversion efficiency, pump saturation, and the Stokes output power as a function of resonator parameters (loop length, L, coupling coefficient k^2, the fibre and the coupler losses), whereas as was described in the previous chapter, the resonator operation is sensitively dependent on the optimisation of these parameters. And yet, it is interesting to point out that the Raman laser, and Raman amplifier both based on the optical fibre recirculating delay line have been well characterised, theoretically and experimentally, including the case of pump depletion[1-5].

The main difficulties of solving the SBS equations were already discussed in detail in Chapter 4. Significant additional complications result from attempting to describe the generation of SBS in a resonator. The reason for this is due to the difficulty of finding solutions to equations (2.24) for a resonant cavity - which demands the coherent addition of fields, while the Raman scattering is effectively an incoherent process. That is, both the linewidths and frequency shifts are order(s) of magnitude greater in SRS than in the corresponding Brillouin process. Consequently, the main complication arises from the fact that in a Brillouin laser it is not possible to add the fields after each circulation for the Stokes wave (as given in eqns (G.1) and (G.3) in the transient resonator analysis in Appendix G), since the transmission coefficient will include the growing Stokes intensity in addition to the fibre losses, and which in this case will not be constant for each circulation. Full numerical solutions which include the depletion of the pump wave are also difficult to obtain since it is necessary to know both the phases of the pump and the Stokes

electric fields as they are propagated in the resonator. Indeed we shall consider numerical solutions in the next chapter to describe the transient operation of the Brillouin laser and amplifier.

However, some relatively simple analysis which would describe the variation of the output Stokes intensity with pump intensity, as a function of resonator parameters, would be invaluable as it would enable some design and optimisation of Brillouin laser operation, as well as providing some insight into the physics of the operational limits of this device. In view of this it was felt that that a derivation of such an analysis was the first step in the evaluation of all-fibre Brillouin lasers. An analytical steady state theory which describes the operation of a Brillouin laser has been developed and is presented in Section 6.1. This theory can be used to predict the threshold lasing power, optimum conversion efficiency, cavity gain and saturation regime in terms of the resonator parameters, at steady state. When considering the high conversion efficiency of Brillouin lasers and amplifiers it is necessary to take into account the depletion of the pump by the counter propagating Stokes wave, and this theory takes into account the depletion of the pump. The justifications of the assumptions made in arriving at the mathematical description of operation of the Brillouin laser are outlined in Section 6.2, and the results of the experimental investigation of Brillouin laser action in OFRRs using a He-Ne and a semiconductor laser pumps are described in Section 6.3. Section 6.4 presents a discussion describing possible applications of the Brillouin laser in optical generation and distribution of microwave signals, and a comparison with existing techniques.

6.1. Theory of operation of single mode all-fibre Brillouin laser

In this section we going to derive analytical expressions describing the performance parameters of single mode all fibre Brillouin lasers, at steady state. The starting point of the analysis are the equations describing the variation of the intensities of the pump and the Stokes waves in a length of optical fibre:

$$\frac{dI_p(z)}{dz} = - g_B I_p(z) I_S(z) - 2\alpha_o I_p(z) \qquad (6.1)$$

and,

$$\frac{dI_S(z)}{dz} = -g_B I_p(z) I_S(z) + 2\alpha_o I_S(z) \tag{6.2}$$

where I_p and I_S are the pump and the Stokes intensities, respectively, g_B is the Brillouin gain coefficient. As in the last chapter we continue with the convention of $2\alpha_o$ representing the linear intensity attenuation coefficient. As outlined in Chapters 2 and 4, g_B is maximum when the pump and Stokes waves are polarisation matched. This is true in the case of a resonator fabricated from polarisation preserving fibre. In the case of non-polarisation preserving fibre, as in the analysis carried out in Chapter 4, g_B is reduced to $g_B/2$ for 45^o polarisation scrambling. Reduction in the gain due to finite pump linewidth can also be contained in the expression for g_B, while the rest of the analysis is unaffected.

We make the following approximation in this analysis to arrive at analytical solutions. The validity of this approximation is discussed in the next section. In general, the resonators are fabricated with relatively short loop lengths L (less than 15 metres) to optimise the resonator finesse. This means, that at the pump powers of interest, the total Brillouin gain over one loop transit is small. Therefore, the above equations can effectively be *decoupled*, and the expression for the pump intensity transmission coefficient in the loop, T_L^2 can be obtained by integrating eqn (6.1) to give:

$$I_p(L)/I_p(0) = T_L^2 = \exp - [2\alpha_o + g_B I_S(0)]L \tag{6.3}$$

It can be noted that equation (6.3) now accounts for pump depletion.
Providing the pump wave is at resonance of the ring, Brillouin lasing will occur when the Stokes wave is also resonant, that is the round trip phase delay is 2π, and the resonant pump mode falls within the Brillouin gain curve. In this case the generation of SBS introduces only an additional *loss*, and does not affect the *phase* of the transmission coefficient.

The threshold circulating power can similarly be obtained by integrating eqn (6.2) to give:

$$I_S(0) = I_S(L) \exp [- 2\alpha_o + g_B I_p(0)]L \tag{6.4}$$

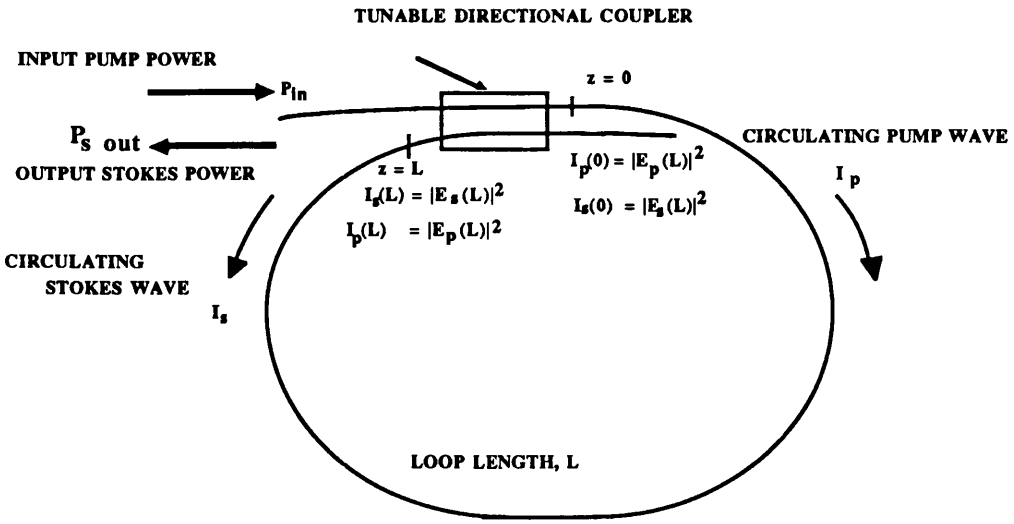

Fig 6.1. Schematic diagram showing propagation of the pump and Stokes waves in a single mode all-fibre ring resonator.

By considering propagation of the pump and Stokes fields around the resonator loop, at steady state (with reference to fig. 6.1), it can be seen that:

$$E_s(L) = jk\,(1 - 2\gamma_o)^{1/2} E_s(0) \qquad (6.5)$$

where E_S is the Stokes field, $2\gamma_o$ is the coupler radiation loss and k is the field coupling coefficient. Squaring eqn (6.5) and combining with eqn (6.4) gives:

$$1 = k^2(1 - 2\gamma_o)\exp[-2\alpha_o + g_B I_p(0)]L \qquad (6.6)$$

This equation in fact represents the familiar threshold condition for lasing which occurs when the losses are compensated by gain. In the case of high finesse resonators where $k^2 > 0.94$ ($F > 50$), we can make the approximations that $k^2 = \exp - [2\alpha_k L] \approx 1 - 2\alpha_k L$ where $2\alpha_k L$ is the coupling loss, and $\exp[-2\alpha_o + g_B I_p(0)]L \approx \{1 - (2\alpha_o - g_B I_p(0)L\}$. The error introduced into the analysis through these approximations is less than 1% for $k^2 > 0.87$ ($F > 23$), with 1% uncertainty in k^2 resulting in the accuracy of the finesse of

approximately 5% at the lower end of k^2, and better than 1.5% at values of k^2 higher than 0.97 ($F > 100$).

The above approximations, therefore, yield an expression for the threshold pump intensity circulating in the loop as:

$$I_p(0) = I_p = 2[(\alpha_o + \alpha_k)L + \gamma_o]/g_B L \qquad (6.7)$$

Clearly I_p represents both a limiting and a threshold value of the circulating intensity. This is understandable, since the circulating intensity, at steady state, can not fall *below* its threshold value. As we saw in the solutions of the SBS equations in Chapter 4, the pump intensity saturates after the Brillouin threshold has been exceeded, at approximately its value at threshold. Any additional pump above the threshold intensity is completely converted into the counter propagating Stokes intensity.

The cavity finesse, F, is proportional to $[(\alpha_o + \alpha_k)L + \gamma_o)^{-1}$, and at resonance $\alpha_k L = \alpha_o L + \gamma_o$ from equation (5.8). In addition, using equation (5.16) we can see that $F = \pi(1 - \alpha_k L)/2\alpha_k$ which after rearranging gives:

$$\alpha_k L = \frac{1}{1 + \frac{2F}{\pi}}$$

so that equation (6.7) can be directly related to the finesse of the resonator. Thus equation (6.7) demonstrates the importance of having a low loss, high finesse cavity in order to minimise the pump threshold power. In fact, for $2F/\pi >> 1$, equation (6.7) reduces to the expression for the threshold circulating intensity $I_{th} = 2\pi/(g_B L F)$ derived by Stokes[7].

From the theory of the optical fibre resonator the equation for the circulating power at resonance (eqn (5.10)):

$$I_p = I_{in} \frac{(1 - 2\gamma)(1 - k^2)}{[1 - k(1 - \gamma_o)T_L]^2} \qquad (6.8)$$

Where I_{in} is the input pump intensity. By equating equations (6.8) and (6.7) and substituting the expression for the pump intensity transmission coefficient from eqn (6.3),

we obtain an expression for the output Stokes intensity as:

$$I_{S,\,out} = T_{out} I_p \left[\sqrt{\frac{I_{in}}{I_0}} - 1 \right] \tag{6.9}$$

where T_{out} is the output intensity transmission coefficient - $\{(1 - k^2)(1 - 2\gamma_o)\}$ and I_0 is the input pump threshold intensity where

$$I_0 = [(\alpha_o + \alpha_k)L + \gamma_o]^3/[(1 - 2\gamma_o)\alpha_k g_B L^2] \tag{6.10}$$

From equation (6.10) we see the importance of having the coupling coefficient as close to unity as possible, that is α_k tending to zero, as well as having a long length of low loss fibre.

We can now define the conversion efficiency of the Brillouin laser, as:

$$\eta = I_{S,\,out}/I_{in} \tag{6.11}$$

so that,

$$\eta = T_{out} I_p \left[\frac{1}{\sqrt{I_0 I_{in}}} - \frac{1}{I_{in}} \right] \tag{6.12}$$

Differentiating η with respect to I_{in} we find that the maximum conversion efficiency, η_{max}, is obtained when $I_{in} = 4I_0$. Physically, this represents complete conversion of circulating pump power above threshold into the Stokes power and represents the saturation of the gain. At maximum conversion efficiency the threshold power for the second order Stokes signal with a double Brillouin shift will be reached. The second-order Stokes wave will propagate co-directionally with the pump. By substituting the expressions for T_{out}, I_p, and I_0, we obtain an explicit expression for η_{max} in terms of the resonator parameters: the coupling coefficient and the losses:

$$\eta_{max} = \frac{(1 - 2\gamma)^2 (\alpha_k L)^2}{(\alpha_k L + \alpha_o L + \gamma_o)^2} \tag{6.13}$$

If the coupling constant is tuned to its resonant value, in the absence of SBS, (from resonator theory) $\alpha_{k,\,res}L = \alpha_0 L + \gamma_0$, maximum conversion efficiency at resonance can be calculated as 25%. The conversion efficiency can be increased by undercoupling ($\alpha_k > \alpha_{k,\,res}$), at the expense of an increased lasing threshold. This is illustrated in figure 6.2, which shows the variation of the conversion efficiency η with pump power for different coupling coefficients, plotted for a resonator with parameters equal to the 1 m resonator described in the previous chapter. The increase in the conversion efficiency for the undercoupling case is a result in the increase in the output intensity transmission coefficient, T_{out}. As k^2 is increased, more power can be coupled *out* of the resonator.

The graphs of the output Stokes power vs input pump power for different loop lengths with fibre loss of 10 dB/km are shown in Fig 6.3. From this figure it can be seen that although longer loop length can be used to reduce the lasing threshold, this decreases the finesse as a result of a higher fibre loss. Consequently there is a trade off between the reduction in the lasing threshold associated with a longer interaction length, and the corresponding reduction in finesse owing as a result of an increased fibre loss. For comparison, the variation of the threshold lasing power vs loop length for a relatively high fibre loss of 10 dB/km is shown on figure 6.4.

Figure 6.5 in which we plot the input power threshold (plotted on $\log_{10}$ scale) against fibre loop length, L, for different fibre losses clearly illustrates that for extremely low fibre losses, the resonator length can be efficiently increased. It should be noted that this dependence of the threshold lasing power on the fibre length and losses is exactly equivalent to the behaviour of Brillouin threshold power with L_{eff} in the case of straight lengths of fibre; of course the product $[g_B I_0 L_{eff}]$ is considerably higher in the case of straight fibres as compared to $[g_B I_p L]$ (where because of very low loop losses, $L_{eff} \approx L$) in resonators. For example, for the case of a 1 m resonator with fibre loss of 10 dB/km and a coupler loss of 1 %, $g_B I_p L$ can be calculated from equation (6.7) as ≈ 0.01 or $2\alpha_k L$ compared to $g_B I_0 L_{eff} \approx 18$ at threshold in straight fibres with no feedback.

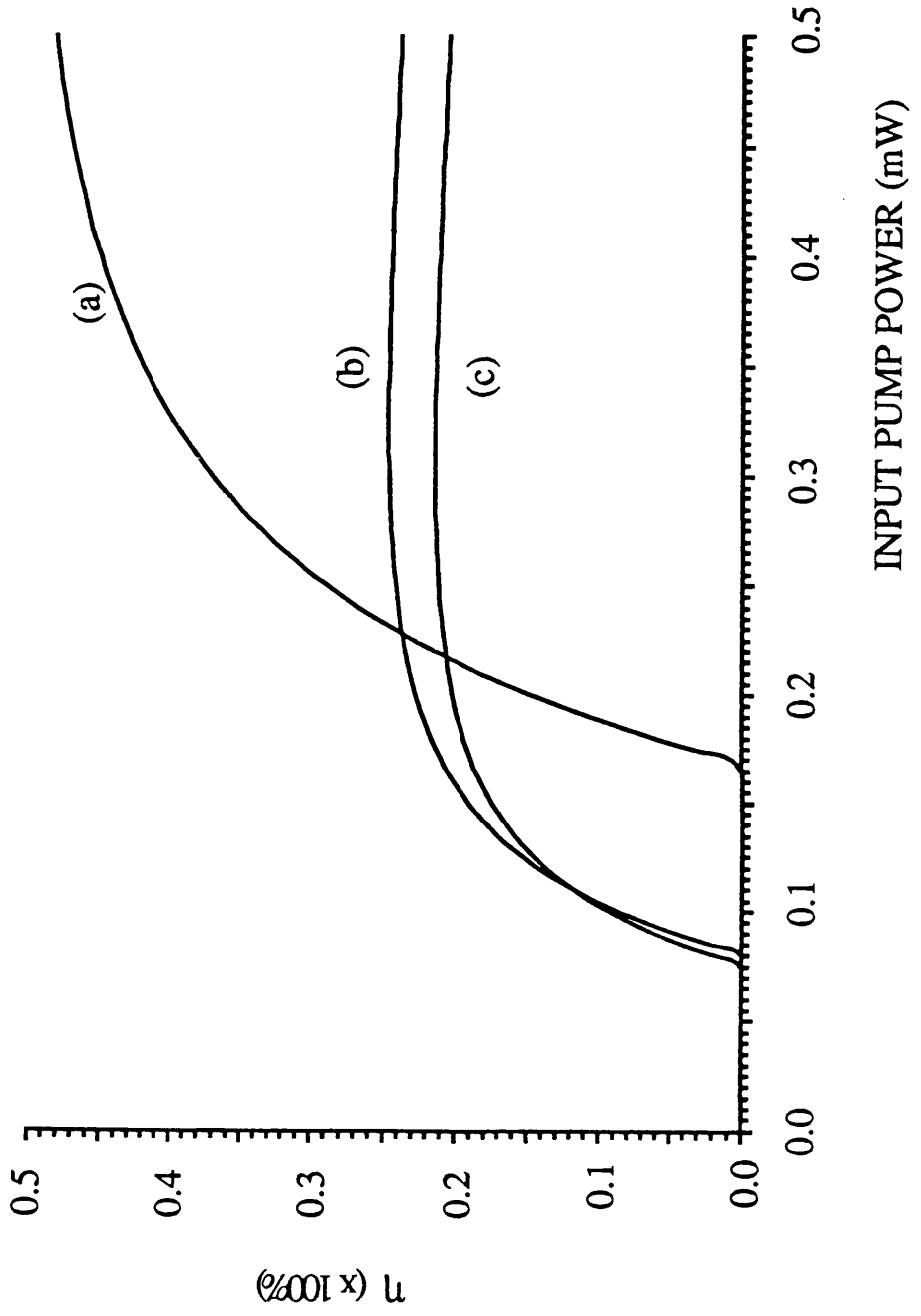

Figure 6.2. Conversion efficiency vs input pump power for different values of the coupling coefficient k^2: (a) $k^2 = 0.9750$ (less than resonant coupling coefficient); (b) $k^2 = 0.9897$ (= resonant coupling coefficient); (c) $k^2 = 0.9905$ (greater than resonant coupling coefficient). Fibre loss = 10 dB/km; coupler loss = 1%, and L = 1 m.

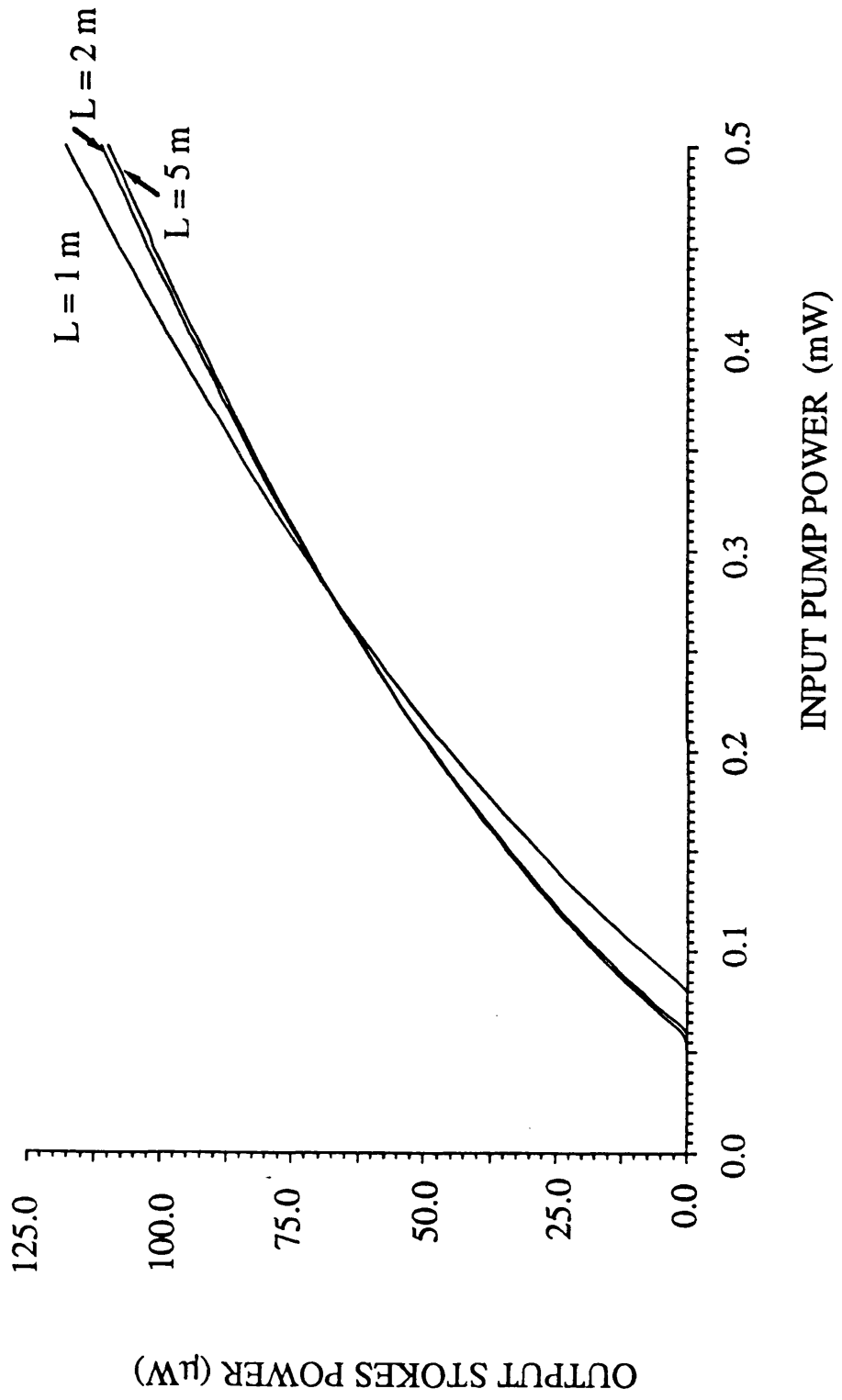

Figure 6.3. Theoretical plot of the output Stokes power vs input pump power for different values of resonator loop length; resonator parameters as in fig. 6.2.

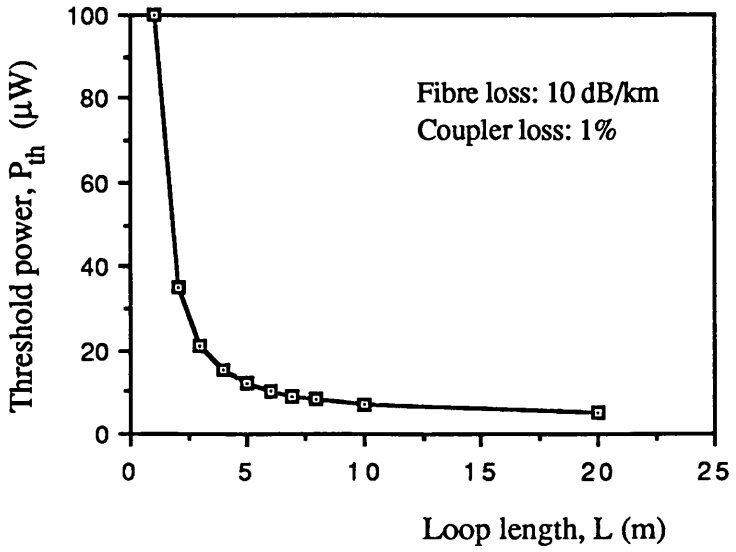

Figure 6.4. Variation of the threshold lasing power with length in a resonator; fibre loss = 10 dB/ km, and coupler loss = 1%.

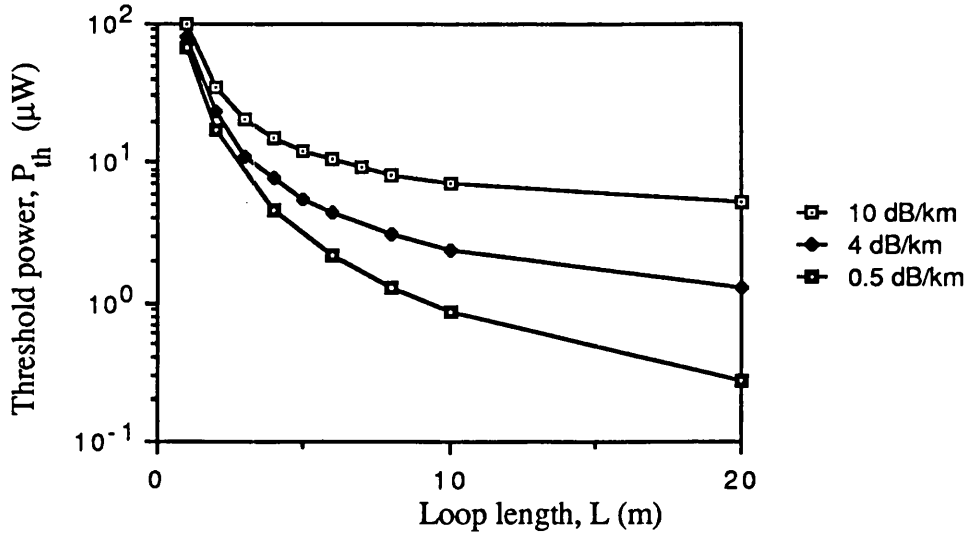

Figure 6.5. Variation of the threshold lasing power vs length for different fibre losses; coupler loss = 1%.

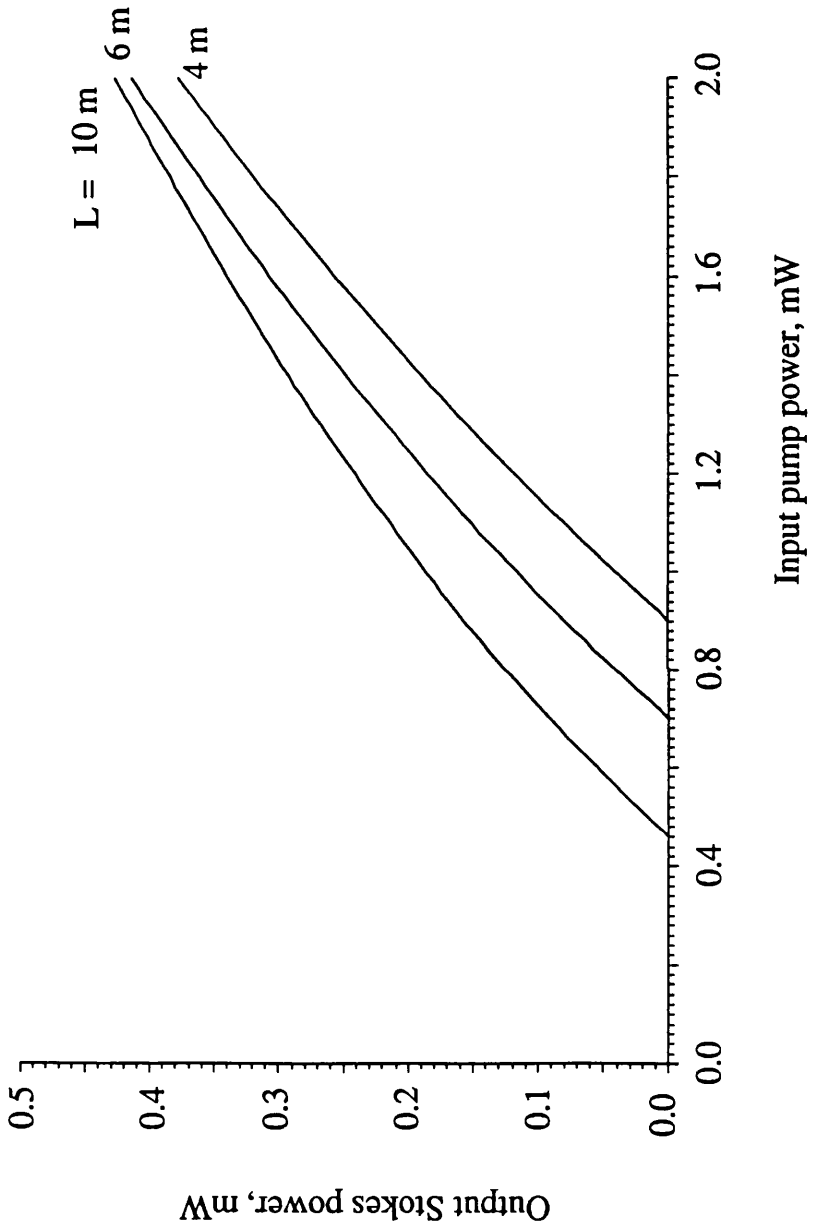

Figure 6.6. Output Stokes power vs input pump power for different resonator loop lengths. Coupler loss = 7%, fibre loss = 4 dB/km.

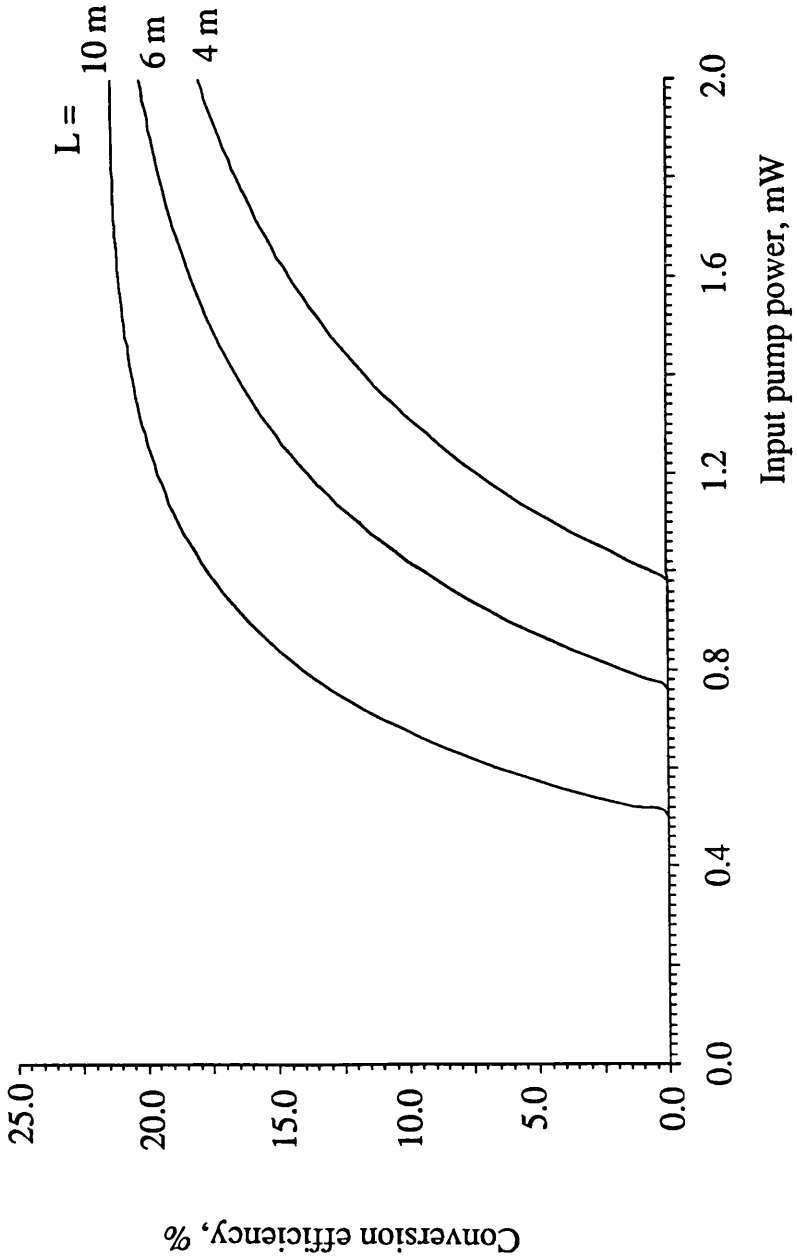

Figure 6.7. Conversion efficiency vs input pump power corresponding to fig. 6.6.

For comparison, figures 6.6 and 6.7 show the variations of the output Stokes power, and conversion efficiency for a resonator with similar parameters to the one fabricated from the 800 nm polarisation maintaining fibre for the investigation of SBS generation with semiconductor laser pumping. It can be seen that in this case the lasing threshold is considerably higher, corresponding to a lower value of finesse, coupled with a considerably lower conversion efficiency over the same range of input powers as above. In addition, over this range of input powers, the cavity detuning from the finesse of 38 wasmuch less dramatic, calculated as approximately 31 at the input pump power of 2 mW for the 4 m resonator.

As mentioned above, the counterpropagating Stokes wave introduces an additional loss in the resonator. As the pump power is increased, the coupling constant is no longer equal to its value for resonant operation [as given by eqn (5.8)] since for resonance (equivalent to zero output power) $\alpha_{k,\,res} \neq (\alpha_o L + \gamma_o)$, but differs from it by the amount given by equation 6.3 as $\approx [1 - g_B I_S L/2]$, which represents the depletion of the pump. If the coupling coefficient is optimised at its resonant value, the increase in the Stokes intensity has the effect of 'detuning' the resonator cavity from resonance through progressive overcoupling, thus reducing the finesse and the modulation depth. This leads to a non-zero resonator output and can limit the performance of devices using single mode optical fibre resonators, for example, fibre gyroscopes. Figure 6.8 shows cavity detuning from resonant values due to the build up of the counterpropagating Stokes wave, calculated with the help of resonator equations for non resonant coupling coefficient [eqns (5.17b) and (6.9)].

For input powers above the SBS threshold, the coupling coefficient in the loop can be optimised to give zero output power at resonance, by retuning the resonator to take account of the loss associated with a specified Stokes level. Because of the effective additional loss due to pump depletion, this results in a reduced finesse. Subsequent reduction of the input power to below threshold will, therefore, result in undercoupling, which actually means that more power than required to overcome the round-trip losses is coupled into the loop. This behaviour is illustrated in figure 6.9 which shows the variation of output power from resonator with input pump power (= counterpropagating Stokes power) for different values of the coupling coefficient (calculated using eqns (5.17b) and (6.9)).

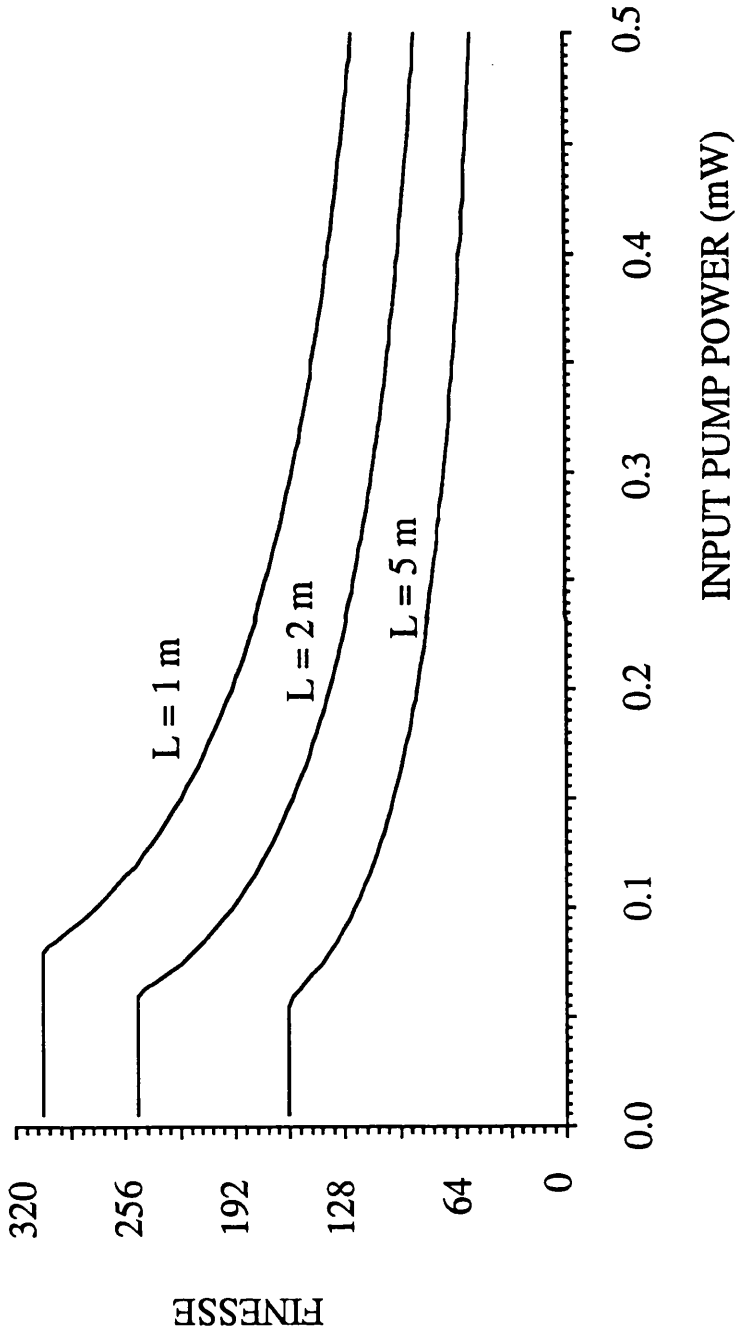

Figure 6.8. Finesse vs input pump power (corresponding Stokes power and resonator parameters of figs 6.2 and 6.3.

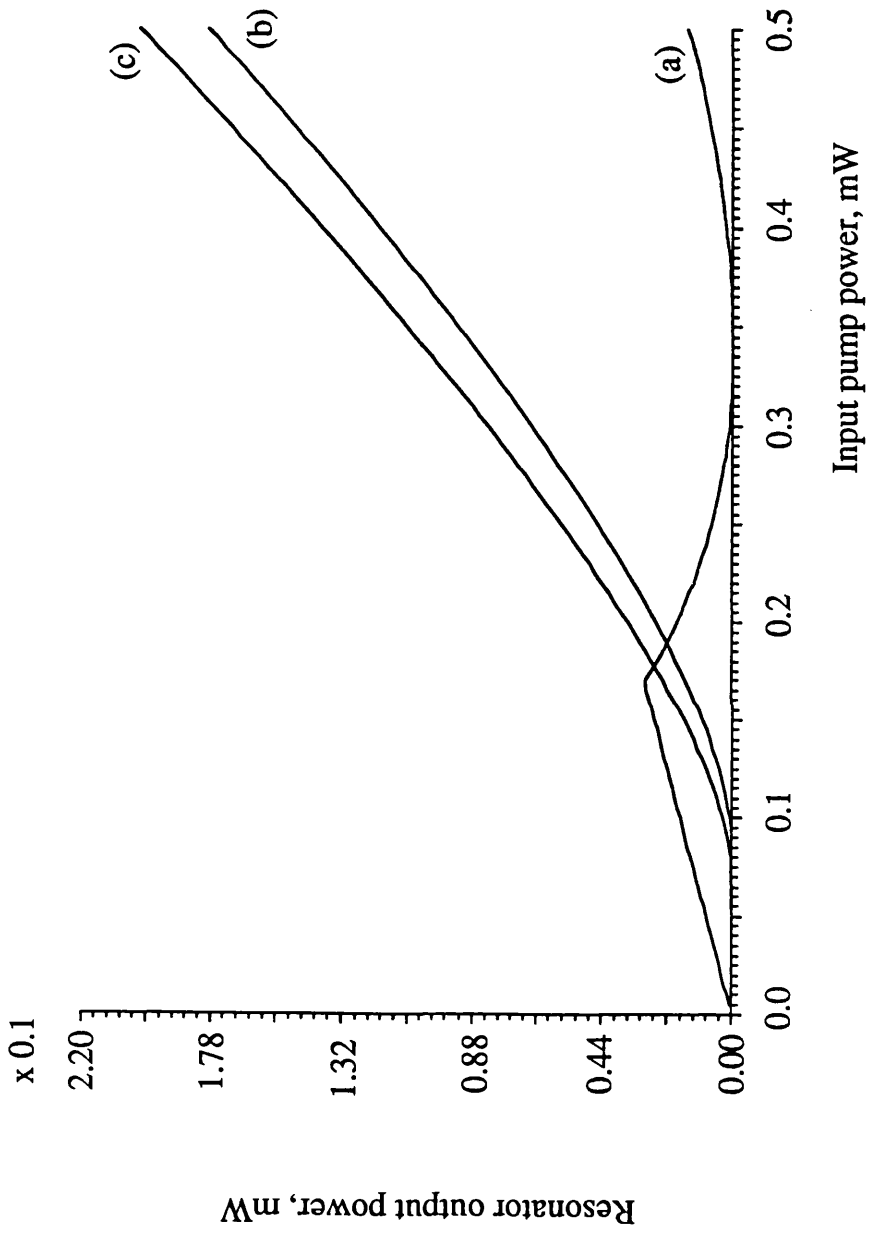

Figure 6.9. Variation of output power from resonator with input pump power for different coupling coefficients (corresponding to the output Stokes power given in figs. 6.3). (a) - (c) corresponding to (c) - (a) of fig. 6.2. Resonator parameters as in figs 6.2, 6.3 and 6.8.

6.3. Justification for using the small signal approximation in the analysis of the SBS in an OFRR

The validity of the approximations used in arriving at eqns (6.3) and (6.4) can be verified by expressing the solutions of eqns (6.1) and (6.2) as series expansions in L:

$$I_p(L) \approx I_p(0)\{1 + a_1L + a_2L^2 + ...\}$$
$$I_S(L) \approx I_S(0)\{1 + b_2L + b_2L^{2+} ...\} \qquad (6.14)$$

where $I_p(0) = I_p$ and $I_S(0) = I_S$ are the steady state pump and Stokes circulating powers as before. a_n and b_n are the coefficients in the series expansion of $I_p(L)$ and $I_S(L)$. Equations (6.14) are substituted into eqns (6.1) and (6.2). For the first equation of (6.14) and (6.1) we have:

$$I_p(a_1 + 2a_2L) = -\{2\alpha_o + g_BI_S(1 + b_1L + b_2L^2 + ..).\{I_p(1 + a_1L + a_2L^2 + ..)\}$$

If terms higher than L^2 are ignored as insignificant, and we equate the coefficients of L^n, the coefficients a_n and b_n are obtained as:

L^0: $\quad a_1 = -(2\alpha_o + g_BI_S) \qquad b1 = 2\alpha_o - g_BI_S$

L^1: $\quad 2a_2 = -\{2\alpha_o a_1 + g_BI_S(a_1 + b_1)\} \qquad 2b_2 = \{2\alpha_o b_1 - g_BI_p(a_1 + b_1)\}$

where $a_1 + b_1 = -g_B(I_S + I_p)$.

The practically important case to take is when $I = I_S$, that is the case of 100% internal conversion efficiency, since as the cavity is detuned above threshold, there is no longer zero output power from the resonator. Further increase of input pump power leads to partial conversion into the Stokes power, and a fraction of the circulating power will leave the resonator. Graphs of figs 6.10 and 6.11 show the relative magnitudes of the above coefficients as a function of the resonator length, for a fibre loss of 10 dB/km and coupler losses of 1% and 2%, respectively. It can be verified that a_2 and b_2 are sufficiently small (less than 10 %) compared with a_1 and b_1 respectively, to warrant the approximations used. In fact the approximation is most accurate for shorter loop lengths (10 m and less). If the parabolic correction terms are ignored, examination of eqn (6.14) shows that they are identical to eqns (6.3) and (6.4). For comparison we also plot the a_n and b_n coefficients for a resonator with finesse of 40 and a coupler loss of 7%, in figure 6.12. It can be seen

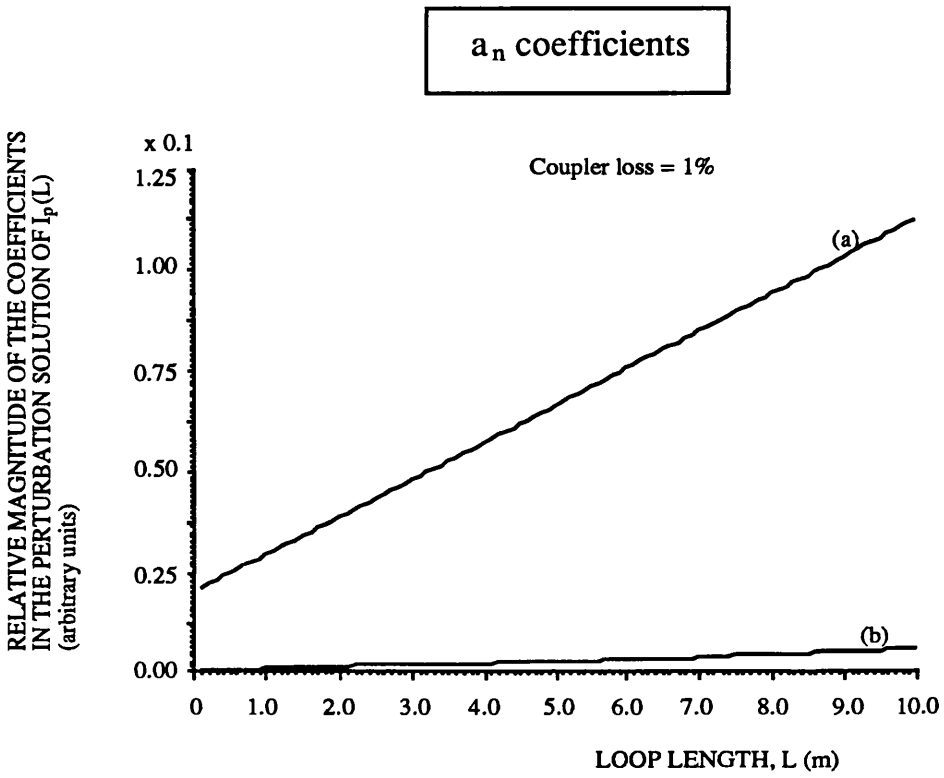

Figure 6.10 (i)

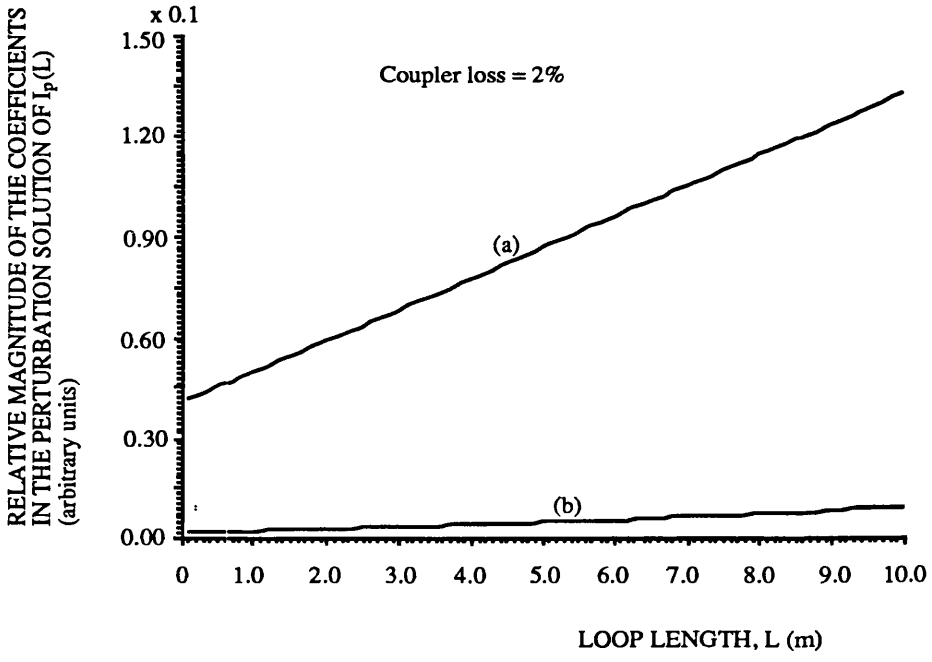

Figure 6.10 (ii)

Figure 6.10. Relative magnitude of the coefficients in the series solution of pump intensity: (a) a_1L; (b) a_2L^2 vs loop length; fibre loss = 10 dB/km.

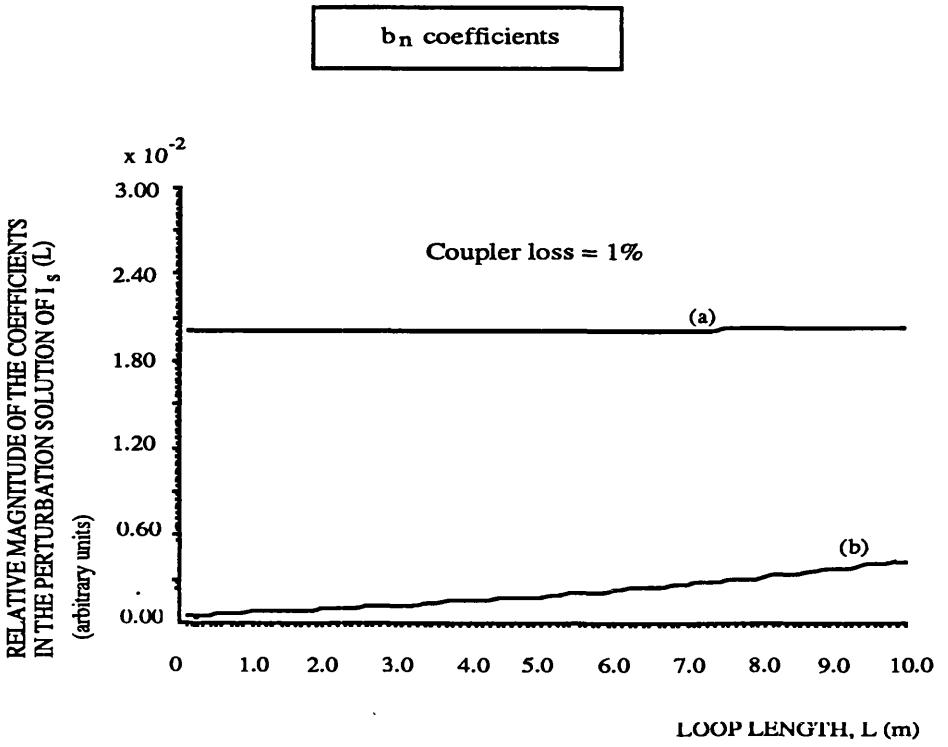

Figure 6.11 (i

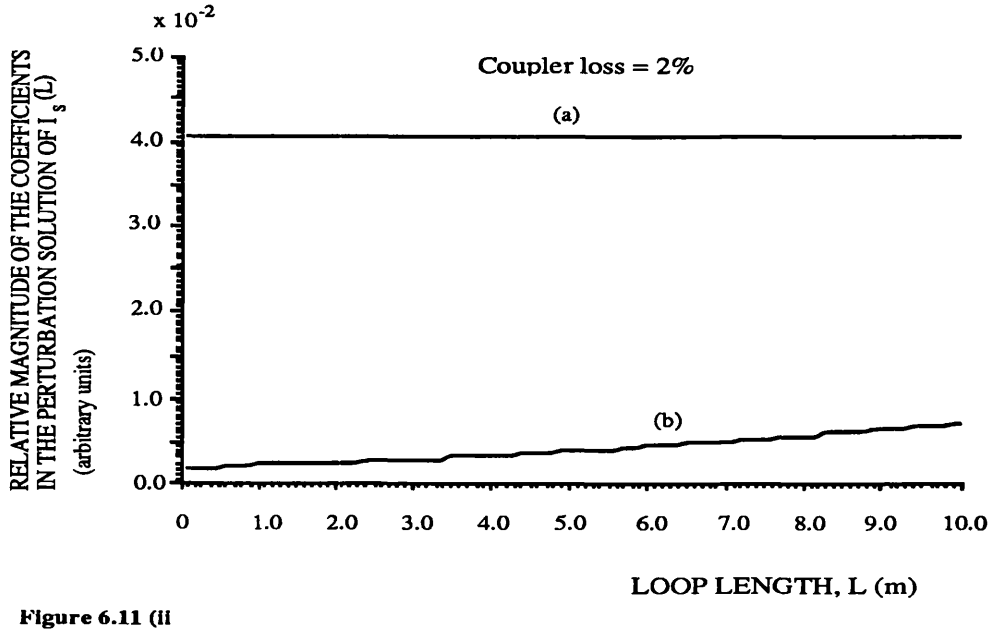

Figure 6.11 (ii

Figure 6.11. Relative magnitude of the coefficients in the series solution of Stokes intensity: (a) b_1L; (b) b_2L^2 vs loop length corresponding to fig. 6.10.

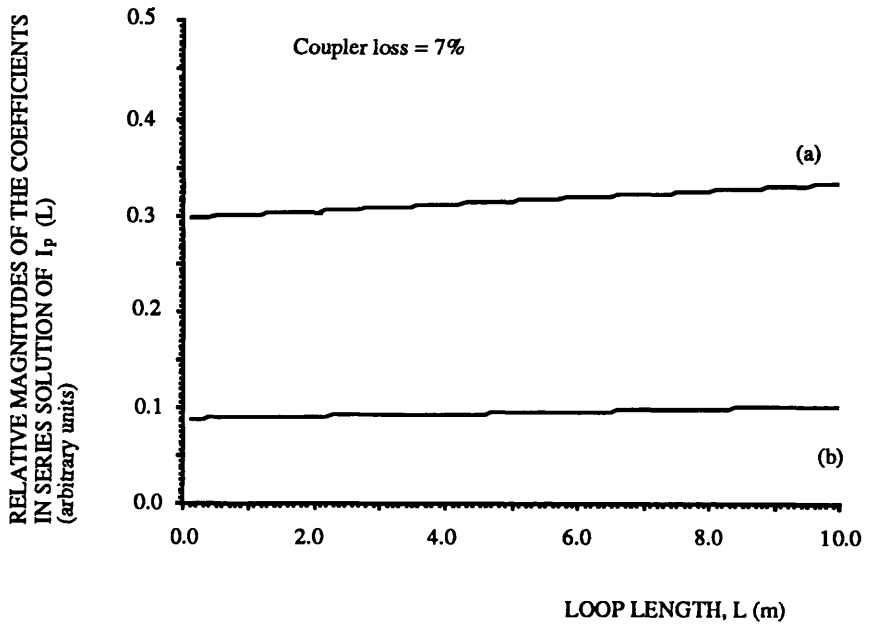

Figure 6.12 (i)

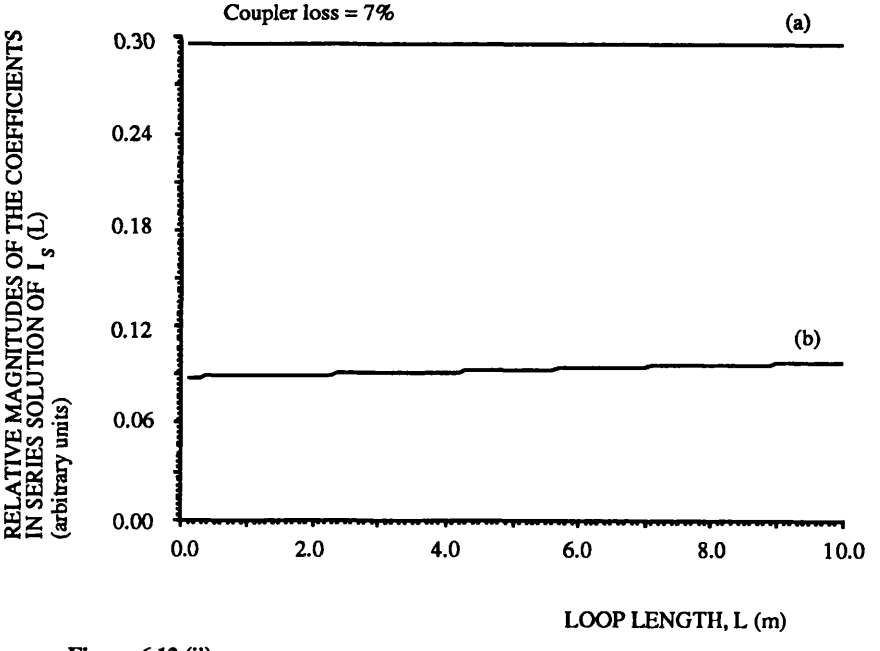

Figure 6.12 (ii)

Figure 6.12. Relative magnitude of the coefficients in the series solution of (i) pump intensity: (a) a_1L; (b) a_2L^2 (ii) Stokes intensity: b_1L; (b) b_2L^2 vs loop length; fibre loss = 4 dB/km.

that the ratios of a_1L/a_2L^2 and b_1L/b_2L^2 are correspondingly higher, approaching 25 -30% for longer loop lengths. [The errors in this case are somewhat more significant, particularly for the pump intensity solution, as the depletion per loop can no longer be considered negligible. However, because the absolute magnitudes of a_2 and b_2 are small (less than 0.1), the errors involved in using the small gain per loop approximation need not preclude the use of this very convenientapproximation for resonators with short loop lengths. The errors simply have to be evaluated in each particular case]. This means that this approximation would also not be valid in the case of resonators with low finesse, such that the gain per loop is large, and also in the case of resonators with a long loop length, L. For neither of the above cases do analytical solutions exist, and the numerical method has to be adopted, by evaluating the Stokes field amplitude or intensity over each loop L as in Chapter 3, circulation by circulation, until steady state is reached, similar to the analysis carried out in the next chapter. For simplicity, however, we shall only concern ourselves with the small gain per loop case which is justified for most cases dealt with in this work.

6.3. Experimental investigation of SBS in OFRRs

6.3.1. Experiments at the pump wavelength of 633 nm

Initially SBS was investigated at 633 nm using a Barr & Stroud frequency stabilised single mode laser in OFFRs described in Chapter 5. The experimental set up used is shown in fig. 6.13. The backscattered Stokes signal was deflected by a 50/50 beamsplitter and detected on the confocal Fabry-Perot with a FSR of 7.5 GHz and on a silicon photodetector by considering the backscattered signal power. The choice of the 50/50 beamsplitter ratio was chosen since it optimised the magnitude of the backscattered Stokes power. Consider a beamsplitter with an arbitrary splitting ratio, M. The output Stokes power, P_S is proportional to the pump power coupled into the resonator through $f(M)$ such that

$$f(M) = P_{in} M (1 - M) \tag{6.15}$$

Differentiating $f(M)$ and equating to zero yields the result that the maximum Stokes power is obtained when $M = 1/2$. In fact, the splitting ratio was not exactly 50/50 at 633 nm, and was measured to be 48/52.

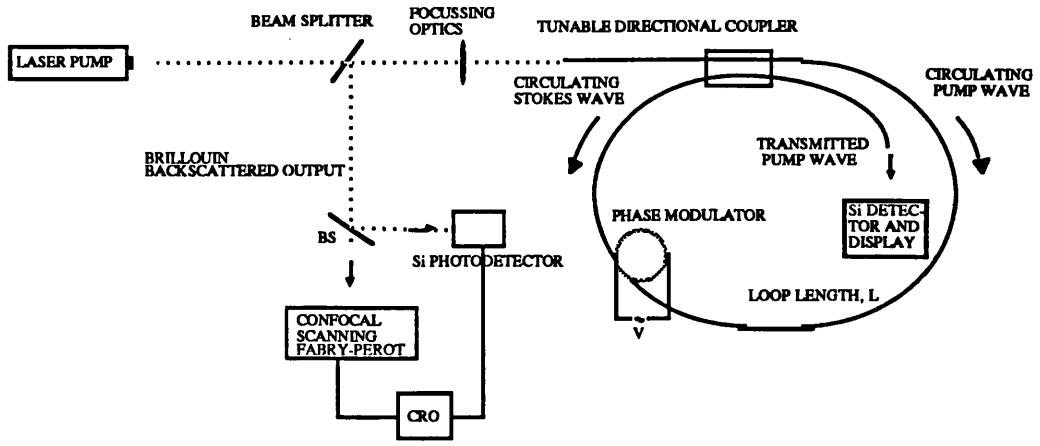

Fig. 6.13. Experimental set-up used in investigating the generation of SBS in an OFRR using a frequency stabilised single mode He-Ne laser as a pump.

The launch efficiency of the input pump power into the fibre was found by measuring the output power from the resonator, off resonance, and accounting for the fibre and coupler radiation losses, as, off resonance, the input power is totally transmitted through the resonator. This could be done by empirically adjusting the coupling coefficient for resonance, and measuring the finesse which allowed the calculation of the coupler loss, from resonator theory of Chapter 5. The coupling coefficient was then tuned to an off-resonance value and the output power from resonator measured. This method was also verified by separating the coupler halves, cleaning them of the index matching oil, and re-measuring the power transmitted through the resonator. The pump power was measured using a precalibrated silicon diode power meter (Coherent, model 212) with a screw-on light shield to block out external light, and having switchable ranges from 100 nW to 100 mW (full scale deflection).

Light from another He-Ne laser was launched into the resonator at the output end, and its spectrum was observed on the Fabry-Perot. This method allowed accurate positioning of the Fabry-Perot cavity, so that only the backscattered light was detected. The Brillouin threshold was evident as a sharp increase in the 4% backreflection signal which is proportional to the incident pump power. Rayleigh backscattering is also proportional to the input power, and could, therefore, be easily differentiated from SBS which increases nonlinearly with input power once the threshold has been exceeded. The backscattered Stokes power could then be found by subtracting the linearly varying power from the total

backscattered signal power.

The Fabry-Perot response was calibrated with a He-Ne laser, and the Stokes power was calculated by measuring the height of the Stokes peak in the spectrum of the backscattered light. Although the FSR of the Fabry-Perot was 7.5 GHz, the measurement of the Stokes shifted signal (Brillouin shift of 20 - 34 GHz at 830 - 514.5 nm) could be made unambiguously by interpreting the Stokes shift as the measured frequency shift plus the appropriate number of free spectral ranges.

For the 10 m resonator, $F = 95$, the Brillouin threshold was observed at 0.26 mW ± 15 μW in the fibre (74% launch efficiency, 52% power deflected by the beamsplitter). This is significantly higher than the theoretically calculated threshold of 0.12 mW (from eqn (6.10)). This is probably due to fibre birefringence causing the pump and Stokes waves to be mismatched in polarisation, as described in Chapters 3 and 4. Since the pump power available from the He-Ne is only very marginally above the threshold power, no accurate measurements of the continuous variation of Stokes output power with variation with the input pump power could be made. The Brillouin shift measured from the Fabry-Perot was calculated to be 27.8 GHz ± 75 MHz (5.3 GHz + 3 free spectral ranges). This figure is in good agreement with the theoretical 27.6 GHz calculated using eqn (2.8) with $v_a = 5990$ m/s, $n_{core} = 1.46$.

More accurate measurements could be taken with the 1 m resonator, F of approximately 300 ($k^2_{res} = 0.9897$, coupler loss = 0.8%, power enhancement of circulating power over input power of 96!!) made of polarisation maintaining fibre. The pump light was polarised and initially aligned to one of the axes of the fibre (slow axis, effective core area $A_{eff} = 1.5 \times 10^{-11}$ m^2, measured at the GEC Hirst Fibre Optics Division).

The graph in fig. 6.14 shows the variation of output Stokes power against the pump power (these measurements were taken by R. Kadiwar, Optical Fibre Group, UCL) for different values of finesse. The lasing threshold for $F = 310$ was measured as 65.5 ± 3.5 μW and the conversion efficiency of 23% was measured, while for $F = 290$, the threshold was 77.0 ± 4.0 μW and the conversion efficiency of 22% over the the experimental range of input pump powers. This compares extremely well with the theoretical values calculated from the analytic solutions, which are 64.1 μW (23.5%) and 73.6μW (22.4%)

respectively.

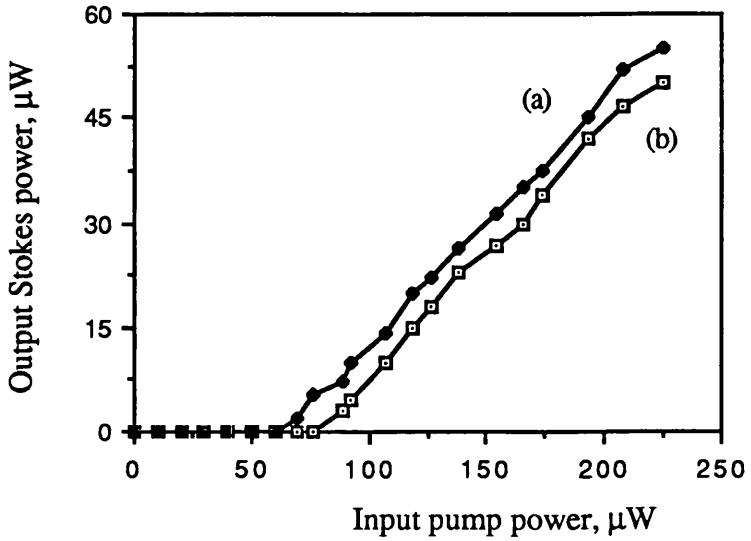

Figure 6.14. Typical experimental graph of the variation of output Stokes power with input pump power as a function of cavity finesse *F*: (a) 310; (b) 290.

The threshold for the $F = 300$ was considerably lower than for the 10 m resonator, measured as 70 μW (-11.5 dBm) ± 3.5 μW (-24.6 dBm). This is in close agreement with the values predicted in eqn (6.10) of 67.9 μW. Progressive detuning of the cavity finesse of $F = 303$ to $F = 190$ for the increase of input pump powers of 70μW to 225 μW was observed, due to the depletion of the pump by the counterpropagating Stokes wave, and is shown in figure 6.15. This is in excellent agreement with the theoretically predicted results of fig. 6.3. The maximum conversion efficiency was measured as 23% which is again in very good agreement with theory (see fig. 6.2).

The Stokes shift was measured as 26.3 GHz ± 75 MHz, giving v_a of 5690 m/s somewhat lower than expected. This could perhaps be accounted for by the stress-induced birefringence leading to a decrease in the Young's modulus and a higher density in the core, resulting in a reduced acoustic velocity (where v_a is given by $[Y/\rho_0]^{1/2}$, and Y is Young's modulus).

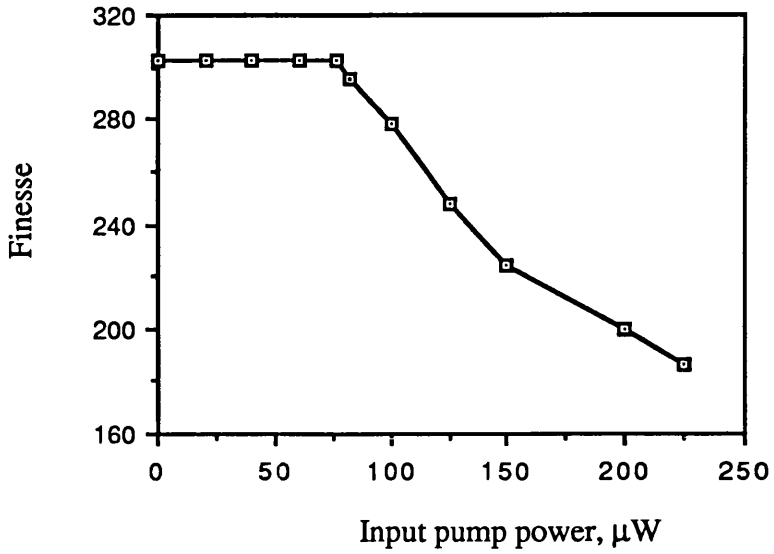

Figure 6.15. Typical graph showing the variation of finesse with input pump power; coupler loss = 0.8%. (The corresponding theoretical curve is shown in figure 6.8).

6.3.2. Experiments at the pump wavelength of 830 nm

The experimental set-up used in investigating the operation of the Brillouin laser using a semiconductor laser (Hitachi HLP 1400, wavelength 830 nm) as a pump is essentially the same as for 633 nm, with the addition of an Faraday isolator between the pump and the beam splitter as shown in fig. 6.16.

The experimental conditions in this case were quite different to those described in the experiments with the He-Ne laser. This is because the semiconductor laser is very susceptible to feedback as described in Chapter 5. Contrary to the case of a He-Ne laser, above the Brillouin threshold, the backscattered Stokes signal is within the semiconductor laser gain bandwidth, and high isolation is necessary to prevent the Stokes signal being fed back into the laser cavity. Although a 30 dB Hoya magneto-optic (Faraday) isolator was used (insertion loss 1 dB), inevitably some power was still fed back into the cavity.

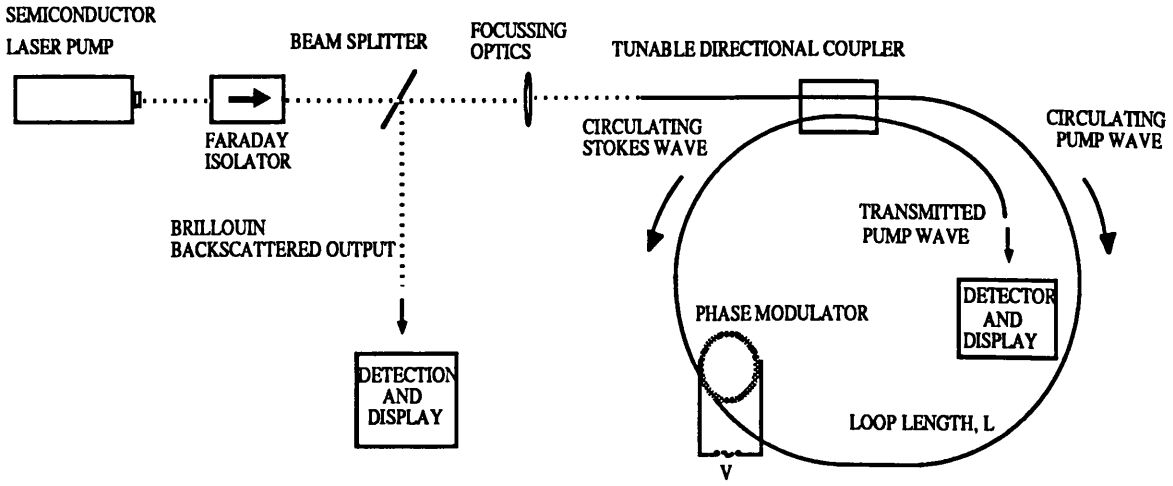

Fig. 6.16. Schematic of the experimental set up of the all-fibre Brillouin laser with semiconductor laser pumping.

As described in the previous chapter, this feedback had either a favourable effect in narrowing the output laser linewidth, or conversely, resulted in some considerable instabilities of the output power and frequency. All the possible causes of the the instabilities such as electrical noise, mechanical or acoustic vibrations and temperature variations were investigated, and as many as possible minimised or isolated. The entire experimental set up was mounted on an anti-vibration optical table, and the resonator was enclosed in an insulated perspex box which helped to minimise the effect of mechanical and acoustic vibrations. After careful investigations, it was found that there was no appreciable noise from the power supply or the laser drive electronics. However, the intensity noise (measured on the spectrum analyser) was found to decrease significantly when the sources of optical feedback were blocked. This made the measurements of the SBS rather difficult, since the resonator could not be properly stabilised, and the Stokes power was generated only when the pump frequency was stable and resonant.

The measurements were made on the resonators described in Chapter 5. The SBS threshold could not be reached in the resonator made out of ordinary fibre. The series of measurements described below were carried out using the 3.8 m polarisation maintaining resonator. The resonator transmission finesse, F', was measured as approximately 35, although the actual cavity finesse F was estimated to be approximately 90. The transmission coefficients of all the optical components before the fibre were carefully

measured, and the launch efficiency optimised. The maximum power which could be launched into the fibre was 1.25 mW (having taken into the account the transmission coefficients of the various optical stages and the launch efficiency of 40%).

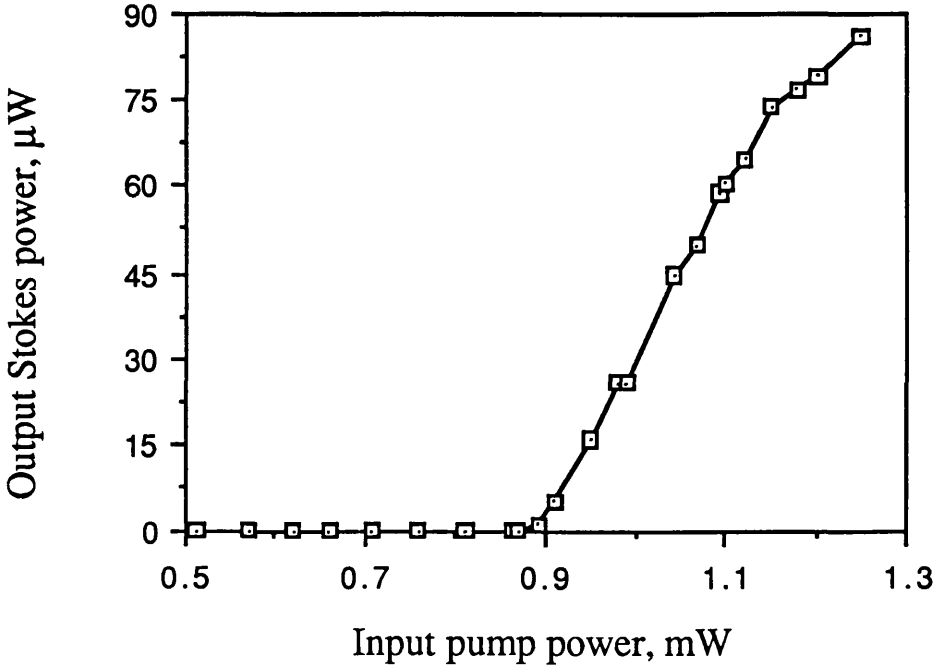

Figure 6.17. Typical graph of output Stokes power vs input pump power for 3.8 m HI-BI resonator; fibre loss = 4 dB/km; coupler loss = 6%; A_{eff} = 1.6 x 10^{-11} m^2.

Initially, the polarised laser output was aligned to the slow axis of the fibre (smaller area, higher core refractive index) by rotating the fibre holder on which the axes directions were marked. The Stokes power was measured in two ways: by monitoring the Stokes frequency component on the confocal Fabry-Perot, and by measuring the level of the backscattered signal on the photodetector. The Fabry-Perot was carefully calibrated with the HLP1400 pump laser. The Brillouin threshold was measured at 0.89 mW ± 20 μW of optical power in the fibre, and a typical experimental curve of output Stokes power against input power is given in fig. 6.17. [The corresponding theoretical graphs of the Stokes output power and conversion efficiency against the input pump power were shown in figs. 6.6 and 6.7 , and it can be seen that there is close agreement between the two.]. The output power of the laser was varied by means of precalibrated neutral density filter plates, while monitoring the resonator output response. An alternative method is to vary the drive

current to the laser and waiting several minutes between measurements for the temperature and frequency to stabilize. Clearly, such a method is not ideal, since the spectral characteristics of the pump change slightly on the corresponding measurements. It is interesting to observe that no significant cavity detuning was obtained, since in this case the resonator transmission is determined by the laser linewidth of approximately 2 MHz. The state of polarisation of the backscattered Stokes signal was measured and was found to be linear, in the same direction as the pump. The conversion efficiency was measured as approximately 7% at the maximum input pump power of 1.25 mW.

The Stokes wave was shifted from the pump wave by 20.2 GHz ± 75 MHz, as measured from the confocal Fabry-Perot (see fig. 6.18). This figure is in very good agreement with the theoretical figure of 20.6 GHz for the Brillouin shift, and with the results of the 633 nm measurements, in conjunction with the λ_p^{-1} dependence of the Brillouin shift.

Next, the fibre holder was rotated, to launch the pump along the fast birefringence axis. The pump power was varied from zero to the laser output maximum of 1.25 mW, but no Brillouin threshold was obtained, while the transmission finesse was the same. The reason for this is thought to be that because the core of the York HI-BI fibre is inherently elliptical, with the diameters typically in the ratio of ≈ 4:6 μm [measured in the GEC Hirst Fibre Optics Division using a SIRA refractive index profiler based on the refracted near-field scan technique[11a]; the core ellipticity could also be verified by examining the fibre under the microscope]. Hence the power density in the effective area of the fast axis of 3.0×10^{-11} m^2 compared with $1.6 \times 10^{-11} m^2$ (from GEC fibre measurements) for the slow axis is nearly 1.9 times lower. Thus the threshold predicted for the fast axis is approximately 1.6 mW, which is higher than the maximum power of the laser.

To verify this, in another experiment, the fibre holder was rotated, so that each time a small percentage of pump power was launched along the fast axes of the total power was launched along the direction of the fast axis, and the measurement of the output Stokes power with pump power was repeated for each.

The graph showing these results are given in fig. 6.19. In this case the nonlinear increase in the backscattered power was observed only on the inverted resonance peak corresponding to the resonance of the slow axis, when the threshold was exceeded. It can

be seen that a considerably higher lasing thresholds were measured in this case, ranging from 0.9 mW to 1.1 mW as the percentage of the total power launched into the fast axis was increased from 0 up to approximately 22.5%, over the range of input power used. The output Stokes power, however, followed the same dependence in each case, with a clearly defined threshold, and progressively lower conversion efficiency for a given power.

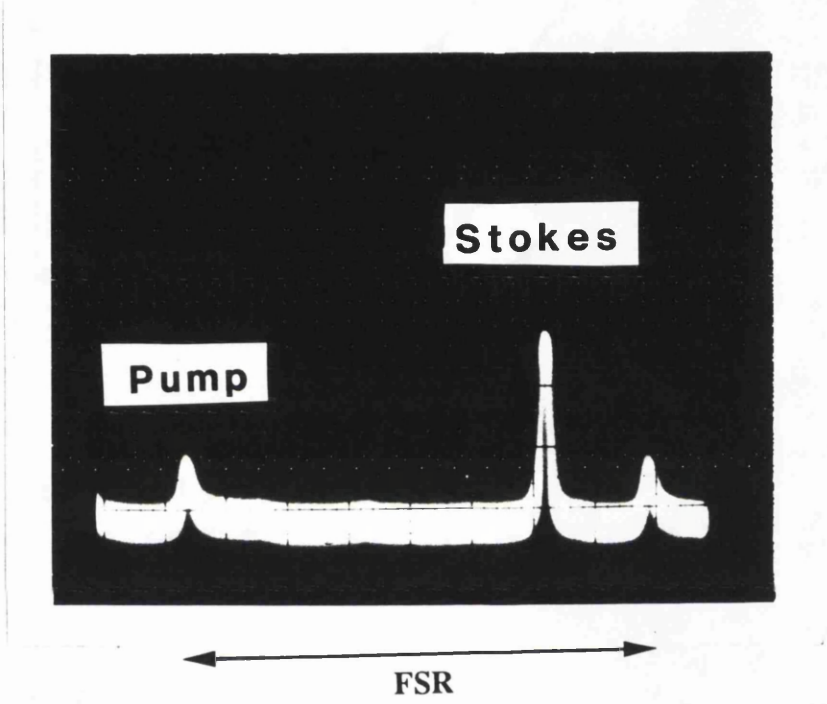

Figure 6.18. The output of the scanning Fabry-Perot showing the residual pump (small peak) and the Stokes frequencies. The Brillouin shift is calculated to be 3 x FSR (7.5 GHz) plus the difference between the pump and Stokes frequencies as 20.2 GHz.

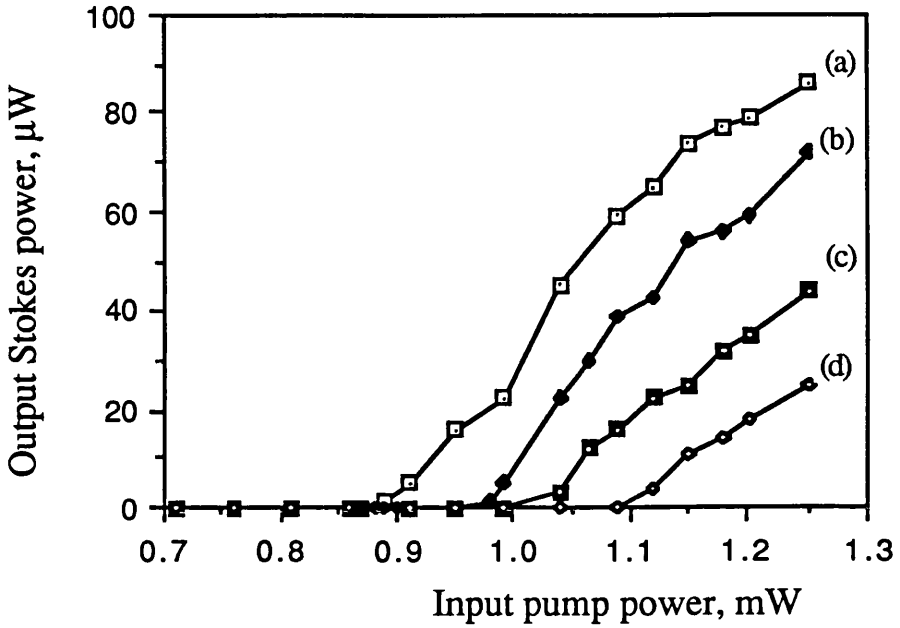

Figure 6.19. Output Stokes power vs input pump power as a function of the percentage of total pump power launched in the slow axis: (a) 100%; (b) 90%; (c) 85%, (d) 78%.

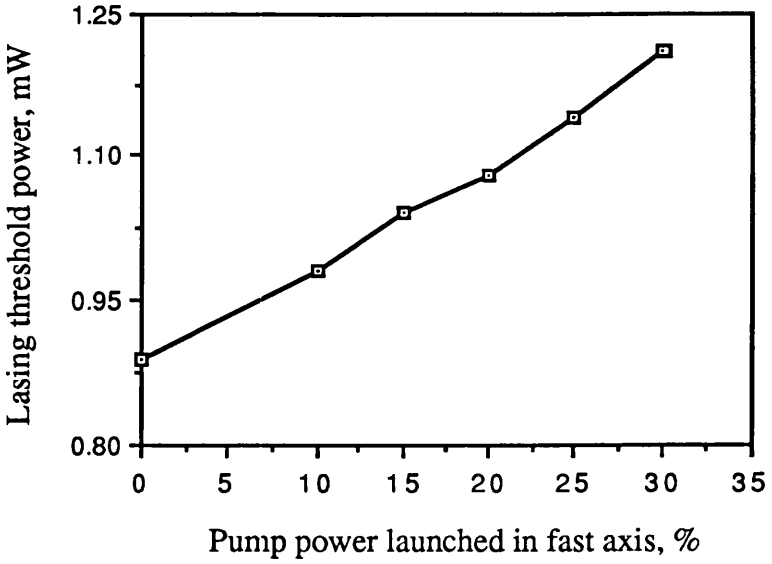

Figure 6.20. Showing the increase in measured threshold for Brillouin lasing as a function of % of total pump power launched in the direction of the fast axis (A_{eff} = 3.0 x 10^{-11} m^2).

The polarisation of the Stokes wave in this case was also linear, in the same direction as the

pump. However, the output of the resonator was elliptically polarised, due to some power having been launched into both modes. These results are very important for a number of reasons. Firstly, it confirms that maximum gain occurs when the pump and the Stokes waves are polarisation matched. Secondly, this means that since the two polarisation axes have different lasing thresholds, and if the Brillouin laser is biased at a particular operating point, below the higher threshold, this will ensure that the output of the Brillouin laser will be linearly polarised.

It was also discovered (for the case of all the pump power launched into the the slow axis) that the resonator response for the backscattered signal has a narrower resonator response peak than the transmitted pump wave. This is illustrated in fig. 6.21. [The laser intensity noise is evident in the transmitted and backscattered signals is due to the reflection of some *pump* power (mainly from the isolator, as was already described in section 5.2.2.2 and illustrated in fig. 5.7) into the laser cavity].

A best linewidth narrowing of approximately a factor of 2.8 was obtained for a conversion of approximately 8%, pump power 1.25 mW. This corresponds to a finesse of 88 which approaches the cavity finesse of the resonator. Measurements were repeated to ensure that real linewidth narrowing was being measured, and not incidental linewidth narrowing due to feedback into the laser. It is thought, that as the generation of SBS in the ring resonator is considered as a lasing action, and since the Stokes wave is generated inside the ring it will have the spectral characteristics of the cavity. In this way, the backscattered Brillouin laser output has the linewidth which is a function of the resonator linewidth, providing the resonator linewidth is smaller than the pump linewidth. This again is a very significant result, since Brillouin lasing could be used as a means of linewidth narrowing. It is thought that better linewidth narrowing could be achieved for higher conversion efficiency, since the output linewidth decreases with gain as $[g_B I_p L]^{-1/2}$ [7,8]. Indeed, the Stokes signal exhibits most significant linewidth narrowing where the circulating pump intensity is the highest, as can be seen from figure 6.21.

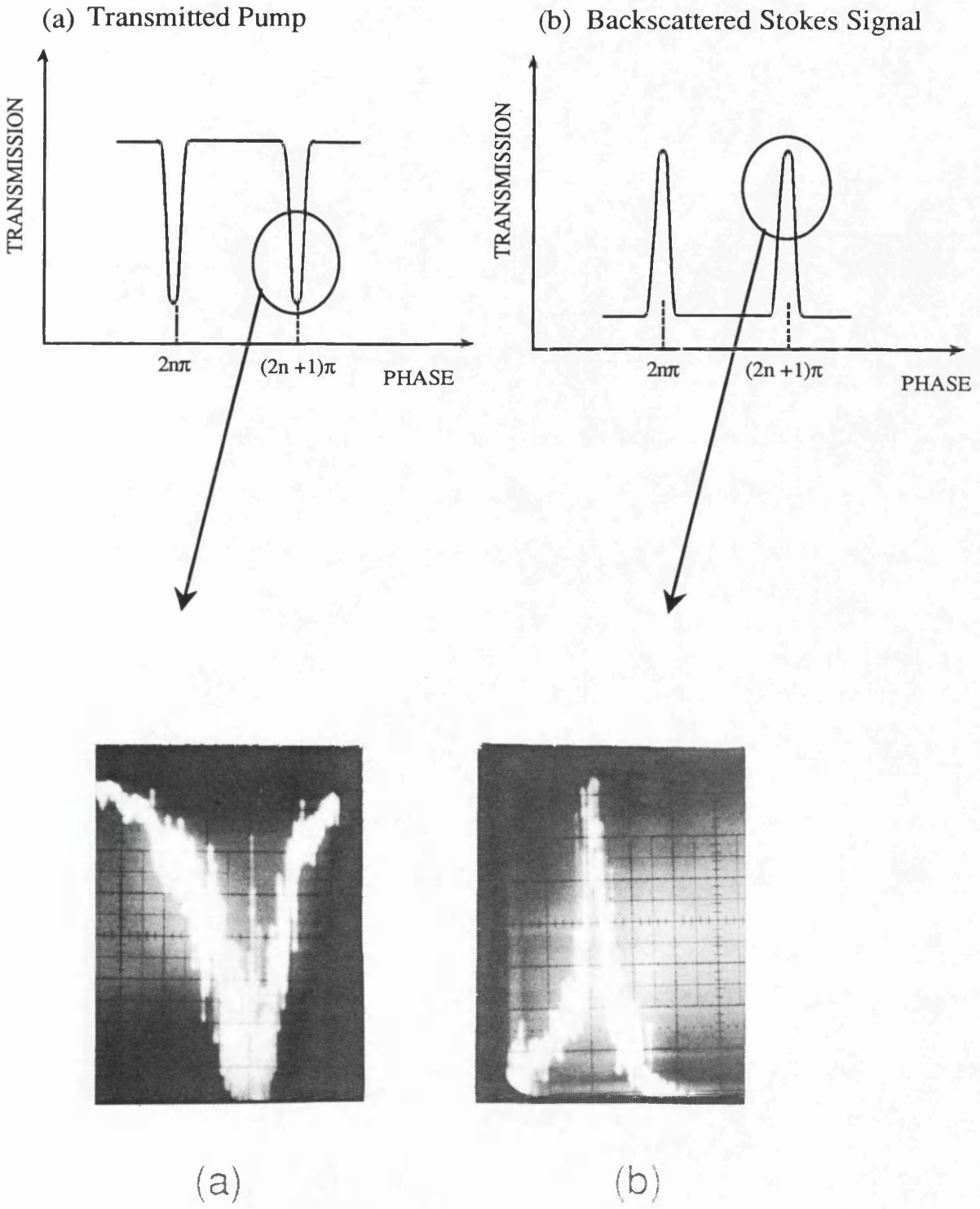

Figure 6.21. Resonator response (a) for transmitted pump wave; (b) resonance peak for the backscattered Stokes wave [same scale for both]. The Stokes wave exhibits clear linewidth narrowing.

At first sight it might appear that the resonator linewidth, as determined by the resonator finesse, is the limiting factor in output linewidth of Brillouin laser. In actual fact, the limiting factor as in all lasers[9,10] is the phase noise associated with the circulating laser field which is due to quantum mechanical fluctuations, and it can be shown[10] that the output spectral width of the laser output Δf_{out} is proportional to $\{hf_{out}(\Delta f_{las})^2 P_{out}^{-1}\}$, where f_{out} is the output frequency of the laser (in our case, the semiconductor laser pumped Brillouin laser) and is the result of the weighted average of the two frequencies, f_B and f_{res} as shown in figure 6.22.

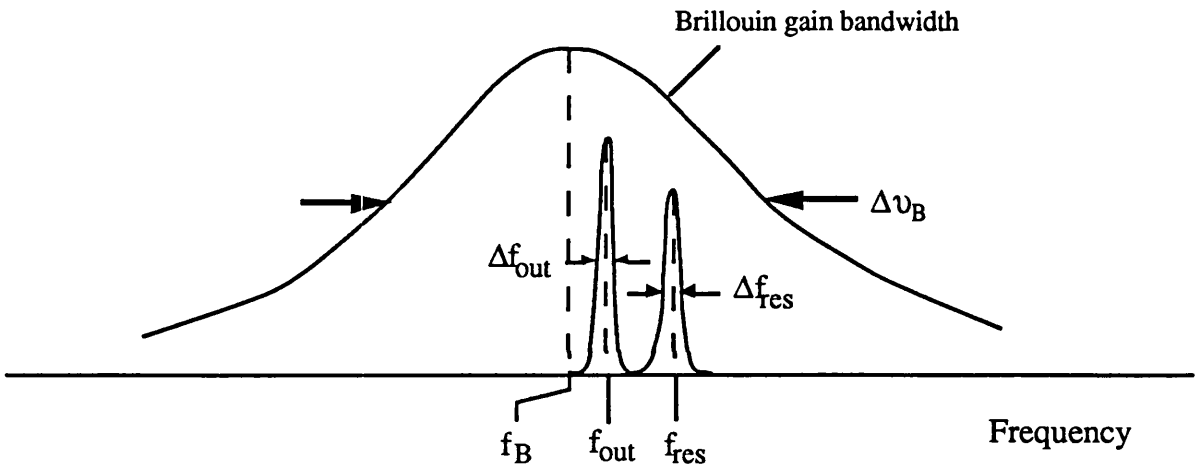

Figure 6.22. Brillouin gain curve, resonator (cavity) mode, and the Brillouin laser output: f_B is the frequency at the peak of the Brillouin gain curve, f_{res} is the frequency of the resonant mode falling within the Brillouin gain curve, and f_{out} is the resultant output frequency of the Brillouin laser.

This figure shows the resonant curves of both the Brillouin gain (centred on f_B and of width $\Delta\upsilon_B$) and of the resonator mode (centred on f_{res} and of width Δf_{res}). In the case when the resonant mode does not necessarily coincide with the peak of the gain curve, it can be shown that f_{out} will be in some intermediate position between f_{res} and f_B which means that f_{out} may not be coincident with f_{res} but may be 'pulled' towards the centre of the Brillouin gain curve. [This phenomenon of mode-pulling is well known in laser theory and discussed in texts such as ref. 10, for example]. When mode pulling occurs, the output frequency of the Brillouin laser f_{out} is given by:

$$f_{out} = \frac{(f_B/\Delta\upsilon_B) + (f_{res}/\Delta_{f_{res}})}{(1/\Delta\upsilon_B) + (1/\Delta f_{res})} \qquad (6.16)$$

Now, as in our case $\Delta f_{res} << \Delta\upsilon_B$ we can simplify the above equation to yield the value of the output frequency of the Brillouin laser $f_{out} \approx f_{res}$, and differentiation also leads to the result that $\Delta f_{out} \approx \Delta f_{res}$. This means that for very small output powers the value of the output laser linewidth predicted by the phase noise relationship is so small that in practice other spectral broadening mechanisms dominate in establishing the actual laser linewidth. In fact, the actual linewidth is limited by the stability of the resonant cavity , since any fluctuations in the resonant frequency Δf_{res} will lead to the fluctuations in the Stokes output Δf_{out} resulting in a broadened linewidth. So that if the cavity length is properly stabilised, the resultant Brillouin laser output linewidth should be extremely narrow - *not limited* by the pump or cavity linewidths. This is an extremely valuable property of this device, and its possible applications will be discussed in the next section.

In order to observe possible modelocking of the Brillouin laser, as described in Chapters 2 and 3, we measured the output of the Brillouin laser using a fast photodetector (reverse biased silicon p-i-n diode, Antel AR-S2, risetime (10 - 90%) of 35 ps and pulse response (FWHM) of 60 ps. The output was displayed on a Tektronix (7704) digital fast oscilloscope. However, the expected train of stable SBS pulses at the repetition frequency of approximately 18 ns (given by the = c/nL), arising as a result of passive modelocking associated with these devices, was not obtained. However, this is not surprising when we consider the Brillouin laser characteristics of the experimental device with regard to the cavity length used. For the 3.8 m resonator, the FSR of the device of approximately 54 MHz is comparable to the intrinsic Brillouin gain bandwidth at the experimental wavelength of 830 nm. This means that because the Brillouin laser is homogeneously broadened, it can not operate cw on more than one mode. Although this property does *not* prevent instabilities (such as mode competition) which can lead to oscillation on several modes, resulting in steady oscillations (or passive modelocking), this can *only* occur if $1/\Delta\upsilon_B$ is much greater than the cavity transit time, since the pulsewidth of the resultant pulse train is limited to the inverse of the gain bandwidth of the lasing medium[8,11]. However, in our case, only one cavity mode can oscillate near the peak of the gain curve, and even very

weak, low-modulation oscillations are not expected. It is suspected that some low-modulation oscillation will be obtained by increasing resonator loop lengths, but short pulses are not expected until the condition of FSR << $\Delta\upsilon_B$ is fulfilled by dramatically increasing the resonator length[8,12,13].

6.3.3. Measurement of the Brillouin gain coefficient, g_B.

It is perhaps of interest to consider the value of the Brillouin gain coefficient, g_B. So far the value of g_B adopted in all calculations was equal that of fused silica. However, the results of the measurements of the Brillouin shift lead to the assumption that the polarisation maintaining York HI-BI fibre used in experiments has a higher core density and a reduced Young's modulus (as compared to values for fused silica), and the specified refractive index of the core (1.462) is higher than that of fused silica (1.457) at 830 nm. In view of the discussion on the dependence of g_B on material parameters, we have, therefore, undertaken measurements to determine the value of g_B in a length of single mode optical fibre. Because the threshold in straight lengths of fibre are considerably higher than in resonators, neither of the sources used for pumping in the resonator experiments could be used. The only available suitable source was the argon pumped, cw tunable Styryl 9 dye laser, with an intracavity etalon to provide single frequency operation at approximately 860 nm. The spectral linewidth was measured on a confocal Fabry-Perot interferometer with a FSR of 300 MHz and a resolution of 2 MHz as 40 MHz. The maximum output power was 90 mW, and the maximum power which could be coupled into the fibre was approximately 28 mW(having taken into account the the transmission coefficient of the beamsplitter (0.52) and the coupling efficiency (60%). The measurements were carried out on a 1 km straight length of York HI-BI 800 nm fibre with beat length of 1.2 mm and loss of 6 dB/km. The experimental set up used was the one normally used for Brillouin scattering measurements and sketched in figure 3.1, Chapter 3. The Stokes power was measured as in resonator experiments on a confocal Fabry-Perot with FSR of 7.5 GHz and resolution of 40 MHz, and the nonlinear increase in the level of backscattered power was measured on a silicon photodetector. The launch end of the fibre was positioned so that the linearly polarised output of the laser was aligned along the slow axis of the fibre having an effective core area of 1.6×10^{-11} m^2. Typical experimental graphs showing the variations of the output Stokes power and the transmitted pump power vs pump power are shown in figures 6.23 and 6.24.

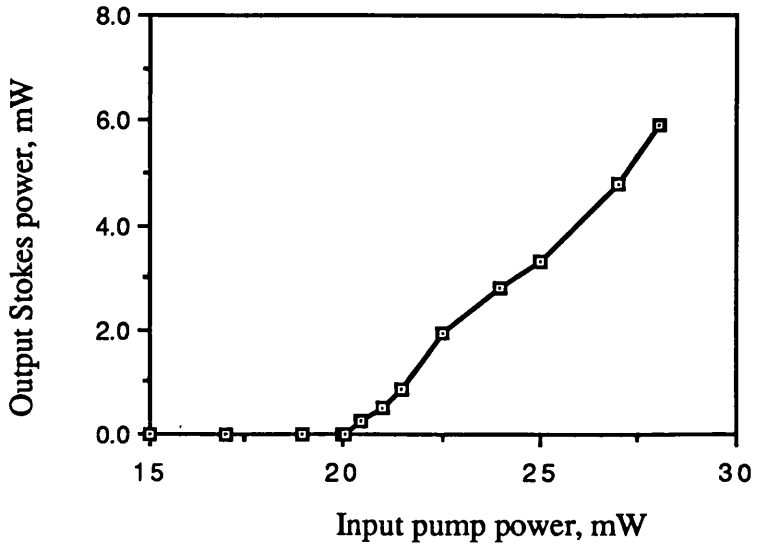

Figure 6.23. Output Stokes power vs input pump power for 1 km length of York HI-BI fibre.

The measured Brillouin threshold was measured as approximately 20.1 mW of pump power in the fibre, and the maximum conversion efficiency was approximately 22%.

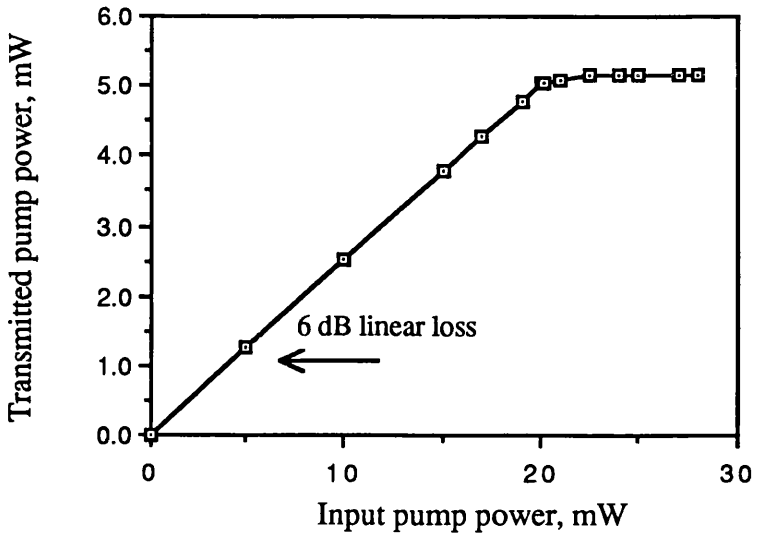

Figure 6.24. Transmitted power vs input pump power corresponding to figure 6.23.

We used the analysis in Chapter 4 to evaluate the Brillouin gain coefficient in the following

way. For the given attenuation of 6 dB/km, the linear attenuation of the fibre $2\alpha_0 L = 1.3$. For this value of loss, the Brillouin gain $g_B I_0 L$ at threshold is 33.0. From above values of threshold power of 20.1 mW, A_{eff} of 1.6×10^{-11} m^2, and L of 1 km, this yields the value of g_B as 2.6×10^{-11} m/W. The assumption that in the absence of guided acoustic mode interaction, the intrinsic Brillouin linewidth varies as the square of the pump wavelength gives the value of the Brillouin linewidth as 58 MHz. Given that the pump linewidth was 40 MHz, and assuming Lorentzian profiles, deconvolution yields the value of Brillouin gain coefficient as 4.7×10^{-11} m/W. This value is indeed approximately equal (within the limits of the experimental error of ± 5%) to the value of the gain coefficient in fused silica.

The Brillouin shift was measured as 19.9 GHz ± 50 MHz. The calculated value for fused silica is (from eqn (2.8)) 20.3 GHz at the experimental wavelength of 860 nm. Taking into account the difference in the core refractive index of the HI-BI fibre, the acoustic velocity is less in this fibre by a factor of approximately 0.96 as compared with fused silica. Since the acoustic velocity is varies as $(\rho_0)^{-1/2}$, it can be seen from equation for g_B, that it is approximately proportional to $[n^7/(\rho_0)^{1/2}]$. In this case, the Brillouin gain coefficient is approximately unchanged from its value for fused silica, in agreement with the above result.

The Brillouin threshold could not be observed when the pump power was launched in the direction of the fast axis. This can again be explained by the fact that the effective area for the fast axis is 1.9 times that for the slow axis, which means that the expected threshold of approximately 38 mW is above the maximum output pump power which can be launched into the fibre (even when the increased coupling efficiency of 65% has been taken into account). However, the graphs of the output Stokes power when 10% and 20% of the total pump power were in turn launched along the direction of the fast axis are shown in figure 6.27. Similar result as in the case of the Brillouin laser have been obtained with the brillouin threshold increasing with the decrease of the total pump power in the slow polarisation axis. The threshold was measured at 22.3 mW of pump power in the fibre for the case of 90% of the total pump power in the slow axis, and 24.6 mW for 80%, in good agreement with theory.

Once again, the polarisation state of the Stokes light was measured and was found to be in the same direction as the pump.

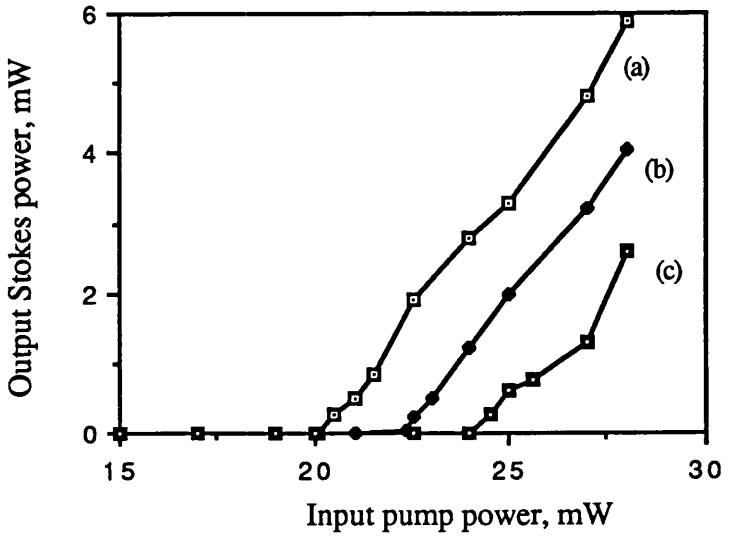

Figure 6.25. Output Stokes power vs input pump power as a function of the percentage of the total pump power launched in the slow axis:(a) 100%; (b) 90%; (c) 80% for the 1 km of York HI-BI fibre.

6.4. Application of the Brillouin laser to microwave frequency generation and distribution

6.4.1. Optical techniques for microwave signal distribution in phased arrays

One of the possible and very interesting applications of the work on the Brillouin laser is in the all-optical signal distribution in phased arrays. A phased array is a form of a microwave antenna in which the radiating aperture comprises a number of radiating elements[14]. The resultant radiation pattern is determined by the relative amplitudes and phases of the currents at the elements. Accurate control of these parameters can configure the radiation pattern to give a number of functions, including the rapid scanning of radiated beams, the formation of multiple beams, and adaptive nulling of sources of interference. Indeed, the beam agility and adaptive antenna pattern control made possible by the electronically scanned phased array antenna has been shown to be of great importance in coping with the high demands placed on future radars. In the past, however, comparatively few phased array radars have been constructed, with the main limitation being their enormous cost. Recent advances in the development of the microwave

monolithic integrated circuits (MMIC) offers the prospect of reduced element cost in active element phased arrays, and so the signal distribution network is likely to become an important limitation in the array cost requirement. Conventional arrays use precision waveguides and coaxial cable or space-feeds which are lossy, bulky, and expensive. For this reason optical fibres which are compact, lightweight, immune to interference, and have extremely low losses coupled with wide bandwidth, have attracted considerable interest from the microwave and optics fraternities, particularly for applications in signal distribution in phased arrays[15-18].

With a modular approach to array hardware, each element will need to be interfaced with a variety of signals which will generally include a microwave phase reference, receive (or transmit), and control and monitoring signals. The phase reference signal is at microwave frequency which is mixed with the incoming microwave receive signal to generate a signal at the intermediate frequency (IF) which can then be processed (similarly the transmitted signal is at IF which is mixed with the microwave reference signal to generate a microwave transmit signal). However, the demands placed on the distribution system are quite severe because of the stringent inter-element phase error requirements. It is for the generation and distribution of this microwave phase reference that the optical fibre solution has been proposed[15].

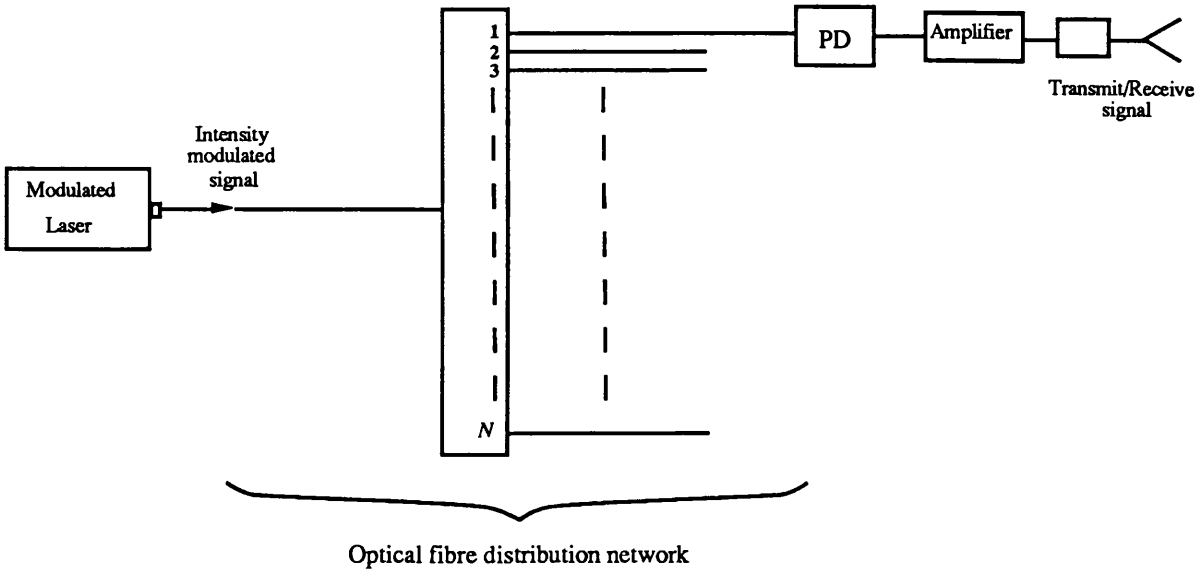

Figure 6.26. Optical network for distribution of microwave signals.

Optical fibre signal distribution systems will generally use single mode fibre to minimise

modal noise and single mode semiconductor laser sources between 830 nm - 1.5 μm. The schematic diagram of such a system is shown in figure 6.26, where an optical source is intensity modulated at the microwave reference frequency, by one of the methods described below, and summarised in figure 6.27. The modulated signal passes through a distribution network which may include phase shifting for beam forming purposes, to a fast photodetector, for detection, demodulation, and amplification. The amplified signal can then be used as a local oscillator for transmission or reception.

The optical output power of the semiconductor laser can be modulated either by direct intensity modulation of the drive current or using an external modulator, for example, lithium niobate, so that the modulated power is proportional to the laser output power for a given modulating signal. Although lasers with modulation bandwidths of about 30 GHz have been demonstrated[17], microwave modulation of semiconductor lasers at appreciable modulation depths still presents practical difficulties and can perturb the laser characteristics, particularly through the increase of the relative intensity noise (RIN) of the device, and breakdown into multimode operation[15]. Because the modulation bandwidth varies as the square root of the bias point of the laser, high frequency operation requires the drive current to be set to a high level, close or at the limit of the laser linear operation. Such operation can result in harmonic distortion at the output, as well as reduction in the device lifetime[17,19].

Lithium niobate electro-optic modulators with bandwidths of up to 40 GHz have been fabricated, but these require considerable electrical driving power of greater than 100 mW[17]. The electrical power requirements can be reduced considerably by using multiple quantum well modulators which have been shown to be capable of high-contrast, low voltage operation, at frequencies of up to 5.5 GHz[20]. However, the maximum optical power which can be applied to both conventional and multiple quantum well modulators is limited by the exciton bleaching effects (which reduce absorption] to about 1 kW/cm^2 [17], while modulator size controls the modulator bandwidth.

Alternatively, microwave frequency generation can also be achieved using the optical heterodyne system. The principle of this system is to combine two optical frequencies of slightly different frequencies which can be simply represented by $E_1 \cos \omega_1 t$, $E_2 \cos \omega_2 t$ on a square-law photodetector to generate the beat signal (using the fact that 2cosAcosB = cos

(A + B) + cos (A - B)):

$$|E_1 \cos \omega_1 t + E_2 \cos \omega_2 t|^2 = |E_1^2| \cos^2 \omega_1 t + |E_2^2| \cos^2 \omega_2 t + E_1 E_2 \{\cos (\omega_1 + \omega_2)t + \cos (\omega_1 - \omega_2)t\} \quad (6.17)$$

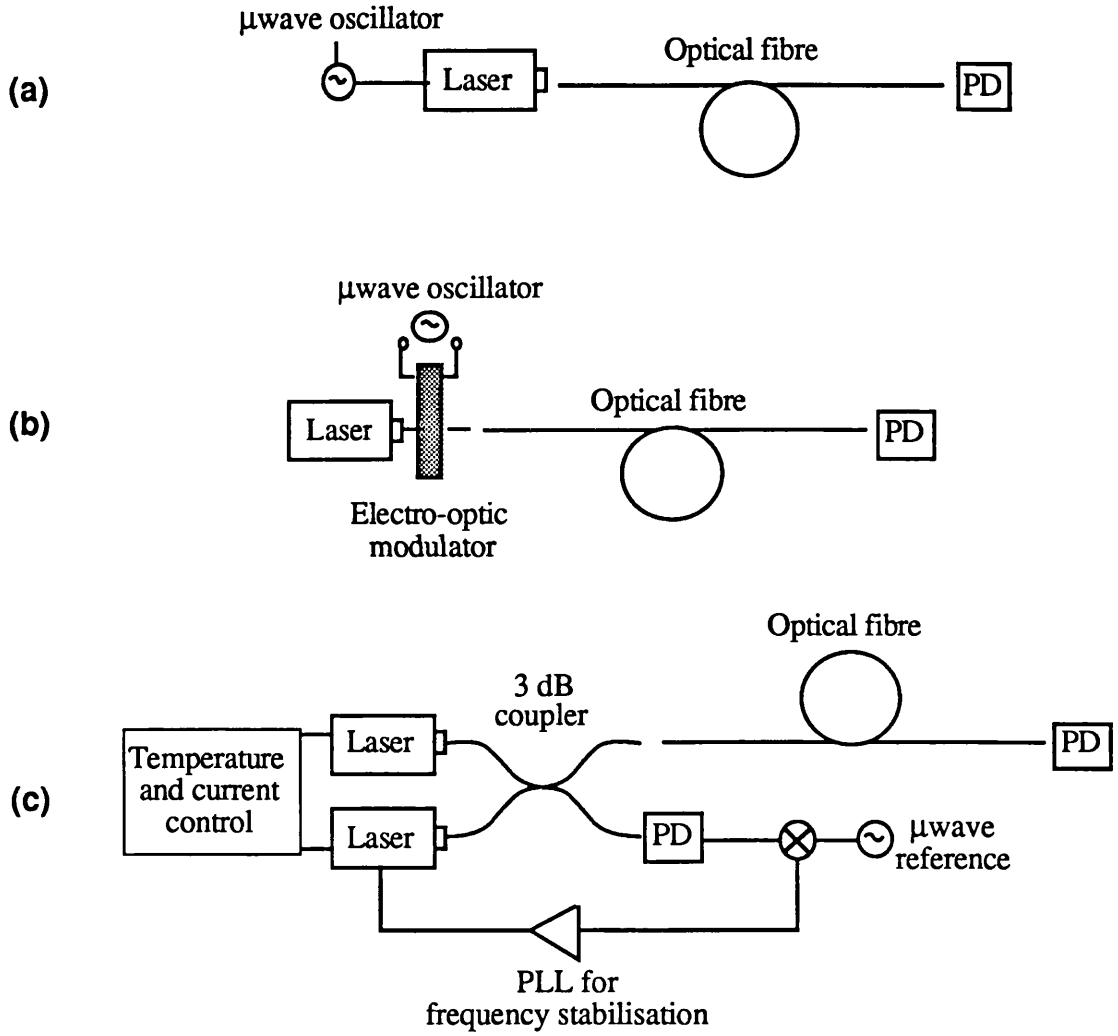

Figure 6.27. Optical techniques for generation of an intensity modulated signal at μwave frequencies: (a) direct modulation; (b) external modulator (c) heterodyne system

where the first two terms represent the unmodulated intensity components. Assuming that the detector bandwidth is less than $(\omega_1 + \omega_2)$ but greater than $(\omega_1 - \omega_2)$, the sum frequency term will be filtered out yielding a beat frequency at the difference frequency $(\omega_1 - \omega_2)$

with a modulation index m given by:

$$\frac{2E_1E_2}{|E_1^2| + |E_2^2|} \qquad (6.18)$$

This approach is simplistic because it assumes monochromatic signals. In order to calculate the full dependence of the detected photocurrent spectrum on the phase fluctuations of the interfering signals complicated statistical treatment of complex fields has to be invoked, as for example in reference [21]. We can however simplify the analysis by assuming that spectral linewidth of the heterodyne signal is given by the convolution of the two linewidths (as given by eqn (2.26)) which for Lorentzian lineshapes is just their sum.

Practical systems would employ semiconductor lasers whose wavelength can simply be tuned by several nanometers by varying the temperature and drive current. This would result in a beat frequency Δf, ($\Delta f = c\Delta\lambda/\lambda^2$) of greater than several hundred gigahertz at λ = 830 nm, where a change in the wavelength of 0.1 nm represents a change in frequency of approximately 40 GHz, so that the maximum heterodyne frequency which can be generated would, in principle, be limited by the photodetector frequency response. However, the technical limitations in implementing a stable practical heterodyne systems are due to the same factors which make such systems potentially very attractive: the easy variation of laser characteristics with temperature, drive current and optical feedback. Because of the very high sensitivity of the output laser frequency to variations in temperature ($\approx$ 30 GHz/K) and drive current ($\approx$ 1 GHz/mA), very accurate control of the laser temperature and drive current is necessary. Generally a phase-lock loop (PLL) would be used where the heterodyne signal is compared with a microwave reference signal to control the laser frequency by feedback. This task is further complicated by the necessity of controlling *two* sources, one with reference to the other. In addition, recent calculations[22] have indicated that for stable operation where the PLL would not lose lock, the PLL bandwidth must be significantly greater than the laser linewidth. In practice such performance is very difficult to achieve. For a commercially available semiconductor lasers (with linewidths of 10 - 20 MHz) at 830 nm, the loop delay time, both electrical and optical, would have to be much less than 1 ns, requiring very stringent and compact loop design.

Indeed, although the principle of optical heterodyning has been demonstrated[16,23], a stable,

long-term, high frequency, all-semiconductor laser system has yet to be reported.

6.5.2. Brillouin laser for microwave signal distribution and generation

As we saw from the preceding discussion, the existing optical signal generation and distribution techniques are still at the research stage with a number of outlined technological problems which have yet to be solved. It is therefore believed that the Brillouin laser as a means of microwave signal generation and distribution can offer an interesting and promising alternative to the above techniques. This section is therefore devoted to a discussion of the feasibility of this method.

As was shown in the first part of this chapter that Brillouin lasing is fully compatible with semiconductor laser technology. As will be described in Chapter 8, Brillouin enhanced four wave mixing can be used to generate several Stokes and anti-Stokes orders which can be combined on a square law photodetector to result in very high frequency beat signals. However, even considering the first order Stokes laser it is clear that combining the pump and the Stokes waves on a square law photodetector, as illustrated schematically in figure 6.28, will result in an automatically intensity modulated beat signal at a frequency given by the Stokes shift, which at 830 nm is approximately 21 GHz, and varies as λ^{-1} (as described in Chapter 2).

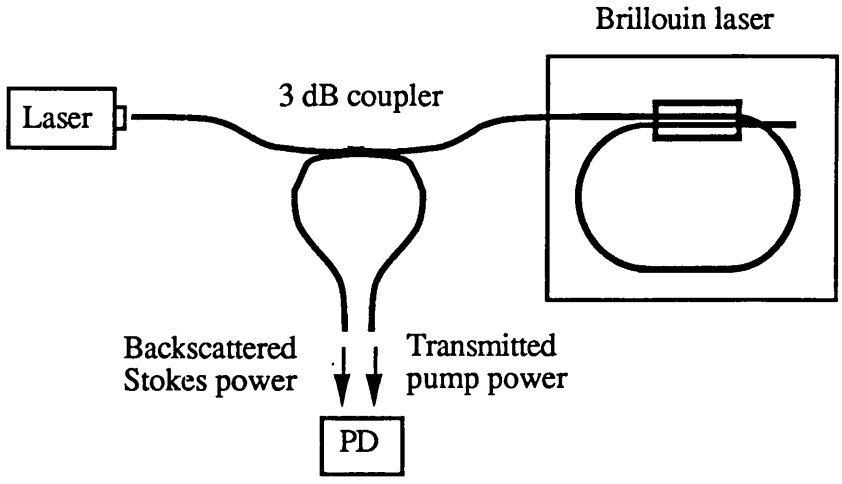

Figure 6.28. Schematic diagram of microwave frequency generation using an all-fibre Brillouin laser. [Not shown is an optical isolator which is necessary in all optical fibre systems to prevent undesirable feedback into the laser cavity].

In fact, the Brillouin shift in this technique will then determine the absolute working frequency. An important system consideration, particularly for military radar applications is the frequency range over which this frequency can be tuned. In this case (from eqn 2.8) $f_B = 2nv_a/\lambda$, so that the tunability range can be expressed as $\Delta f_B/f_B$ where $\Delta f_B = 2nv_a\Delta\lambda/\lambda^2$. Assuming that the pump wavelength can be tuned by say 10 nm, the tunability in this case is limited to approximately 1 - 2% about f_B. Although this tunability range is somewhat limited, this feature of this particular technique will also guarantee outstanding stability of the microwave signal as a drift in the laser frequency of even as much as 100 GHz (corresponding to several K and mA in drive current) would correspond to microwave signal stability of better than 0.01%. Thus the need for complex stabilisation electronics would be eliminated, as well as the necessity for an external microwave signal generator, as in the cases of the PLL for the heterodyne system, as well as both types of intensity modulated systems. The frequency of operation in the case of the Brillouin laser could also be varied by the appropriate choice of pump wavelength (830 nm - 1500 nm).

Another crucial factor in systems consideration is the electrical output power which can be detected, as it determines the efficiency of the system, but even more importantly, the signal-to-noise ratio (SNR). SNR in turn determines the number of array elements, N which can be controlled using the optical system.

We can calculate the electrical power which could be detected for the resonator at 830 nm as described in the first part of this chapter. For operation of the Brillouin laser at resonant coupling, the peak conversion efficiency which could be achieved is 25%. From figures 6.6 and 6.7, this would be at a pump power of 2 mW. The detected electrical power is proportional to m^2 which we can calculate [by squaring eqn (6.18)] from the expression

$$m^2 = \frac{I_{in}/I_{S,out}}{[(I_{in}/I_{S,out}) + 1]^2} \qquad (6.19)$$

to be 0.16 (or m = 0.4). Then the peak photocurrent can be expressed as $m\Re(P_{out})$ where P_{out} is the output optical power given by $(P_{in} + P_{S,out})$ and $\Re$ is the detector responsivity. Then the rms electrical power which is dissipated in a load R_{out} is:

$$P_{out}^{elec} = \frac{1}{2}[m\,\Re\,P_{out}^{opt}]^2 R_{out}$$

(where a factor of 1/2 arises because we are calculating the rms value of electrical power) and where

$P_{out|_{opt}} = 2.4$ mW

$R_{out} = 50\Omega$

$m = 0.4$

$\Re = 0.4$ A/W [GEC high frequency GaAs photodiode]

which gives the value for the rms electrical power as:

$$P_{out}^{elec} = 3.7\ \mu W \text{ or } -24.3\ dBm$$

we can now work out the output SNR for a network of N elements which is given by[17]:

$$SNR_{out} = \frac{P_{out}^{elec}}{2B[N_L(\eta P_{out}^{opt})^2 + 2N\eta P_{out}^{opt} + 4N^2 kT_{eff}/R]} \qquad (6.20)$$

where B is the bandwidth and N_L is the ratio of detected laser intensity noise and detected optical power per unit bandwidth (for commercially available lasers $N_L \approx -130$ dB/Hz), T_{eff} is the effective noise temperature for the photodiode and amplifier (≈ 580 K), and k is Boltzmann's constant. It is clear from equation (6.20) that the three terms in the denominator represent the main sources of noise, which are, respectively: laser intensity noise, shot noise in the photodetector, and Johnson noise for detector and amplifier, and their relative magnitudes depend on the number of array elements, N which can be fed by the electrical power available from the network. As the number of elements is increased, detector and amplifier thermal noise will dominate, and become the limiting factor in the SNR. Using a conservative estimate of the SNR required at each array element as 100 dB (1 Hz bandwidth), we can calculate the number of elements as N as approximately 100. This figure compares very well with that calculated in reference [17] for $N \approx 90$ for the intensity modulated laser where the output optical power was analogously calculated by considering the system losses (coupling and splitting losses) which are approximately 70 - 80% and a modulation index of no greater than 0.7 to avoid excess RIN and mode-hopping at the output.

In the case of the Brillouin laser, the spectral linewidth of the heterodyne signal will be limited by the pump linewidth, since as was described earlier, the Stokes signal will always be linewidth narrowed above the lasing threshold. The lasing power and hence the heterodyne output power is also dependent on the pump linewidth, and the number of elements which can be fed can be increased by using a linewidth narrowed external cavity semiconductor laser[24,25]. The main advantage of the Brillouin laser method over the conventional two-laser heterodyne method is the generation of the second signal within the fibre, and thus the elimination of the need for the second laser and PLL. As already mentioned, this removes the necessity for complex stabilisation circuitry, and significantly improves the stability of the output microwave signal - possibly removing the need for an external microwave signal generator, required in both the intensity modulated and heterodyne systems. Additionally, in the heterodyne system polarisation controllers must be provided to ensure that both signals are polarisation matched - a condition which is automatically fulfilled in the case of the Brillouin laser. The advantage over the external modulator solution is in the fact that the Brillouin laser operation power is not limited by modulator characteristics.

6.5. Summary and conclusions

In this chapter we have considered theoretically and experimentally the operation of all-fibre Brillouin ring lasers. In the first part of this chapter the analytical theory which describes the steady-state operation of the Brillouin laser was derived, in terms of the resonator parameters. This theory enables the design of resonator cavities for optimisation of device operation in given applications. Detailed experimental investigation of Brillouin laser operation was carried out, with particular emphasis on the semiconductor laser pumping. Experiments on Brillouin lasing in resonators fabricated from ordinary and polarisation maintaining fibre, using a He-Ne laser at 633 nm and the first operation of the semiconductor laser pumped all-fibre Brillouin laser at 830 nm, with a submilliwatt threshold were described. The experiments confirmed the reduction in the Brillouin threshold in polarisation maintaining fibres by a factor of 2 as compared to ordinary fibres. Very good agreement between the experiments and the developed theory was observed in all cases. The Stokes wave was polarised, and exhibited linewidth narrowing, measured as approximately a factor of 3. It is expected, however, that the Stokes output spectral width,

as in gas or solid-state laser systems, is limited in principle by phase noise, and in practice by fluctuations in the resonator linewidth due to drift in the cavity length. Hence, proper stabilisation of the resonator would result in a stable, narrow-linewidth output signal.

No temporal variation in the laser output were observed, and the reason for this was thought to be because the cavity length was too short, and hence the laser operation is believed to be single mode and cw. The measurement of the Brillouin gain coefficient was carried out in 1 km length of York polarisation maintaining (HI-BI) fibre and g_B measured for the slow axis of the York fibre was found to be approximately equal to that of pure fused silica, as calculated in section 3.5. It is thought that the value for g_B for fast axis would differ very little from this, primarily through the effect of slightly different refractive indices for the two axes. However, an investigation of the frequency spectrum of g_B, as well as possible acoustic guidance phenomena (as discussed in section 3.5) would be valuable for conclusive material evaluation of the fibre.

The obvious applications of this work lie in the area of narrow linewidth all-fibre lasers and local oscillator applications for coherent optical fibre systems. However, it is also believed that the Brillouin laser can provide a very promising alternative to the existing optical techniques for microwave signal generation and distribution in phased arrays. Although the tunability range of this device is limited, the stability of the output frequency and the efficiency in this technique, as well as the pump wavelength and power flexibility, compare very favourably with both intensity modulated and heterodyne systems. It was shown on the basis of the results of the Brillouin laser operation described in this chapter that optical signal generation and distribution to an array of approximately 100 elements using a single commercially available AlGaAs laser at 830 nm, is feasible, at a frequency of approximately 21 GHz. However, effective isolation between the semiconductor laser and the resonator, and proper resonator stabilisation are expected to be necessary for application in practical systems to significantly reduce the intensity noise evident in the Brillouin laser output. A detailed study of Brillouin laser noise properties would be necessary for conclusive remarks to be made.

6.6. References for Chapter 6

1 E. Desurvire, M. Digonet, and H. J. Shaw, 'Theory and implementation of a Raman

active delay line', J. Lightwave Tech. **LT-4**, 426 (1986)

2 E. Desurvire, M. Tur, and H. J. Shaw, 'SNR in Raman active fibre systems: application to recirculating delay lines', ibid., 560 (1986)

3 E. Desurvire, A. Imamoglu, and H. J. Shaw, 'Low-threshold synchronously pumped all-fibre ring Raman laser', ibid., **LT-5**, 89 (1987)

4 K. Mochizuki, N. Edagawa, and Y. Iwamoto, 'Amplified spontaneous Raman scattering in fibre Raman amplifiers', J. Lightwave Tech. **LT-4**, 1328 (1986)

5 R. H. Stolen, 'Fibre Raman lasers', Fibre and Integr. Opt. **3**, 21 (1979)

6 L. Stokes, 'Single mode optical fibre resonator and applications to sensing', PhD Thesis, Stanford, 1983

7 C. L Tang, 'Stokes emission in the stimulated Brillouin process', J. Appl. Phys. **37**, 2945 (1966)

8 R. Stolen, AT&T Bell Laboratories, personal communication, 1989

9 G. H. B. Thompson, "Physics of semiconductor laser devices", John Wiley & Sons Ltd, 1980

10 O. Svelto, "Principles of lasers", transl. by D. C. Hanna, 2nd ed., Plenum Press, New York, 1982, Chapter 5

11 G. C. New, 'Generation of ultra short laser pulses', Rep. Prog. Phys. **46**, 877 (1983)

11a. S. Robertson, GEC Hirst Fibre Optics Division: personal communications

12 I. Bar-Joseph, A. A. Friesem, E. Lichtman, and R. G. Waarts, 'Steady and relaxation oscillations of stimulated Brillouin scattering in single mode optical fibres', JOSA B **2**, 1606 (1985)

13 J. Botineau, C. Leycouras, C. Montes, and E. Picholle, 'Stabilisation of stimulated Brillouin fibre laser by strong pump modulation', ibid. **6**, 300 (1989)

14 "Phased array antennas", Proceedings of 1970 Phased Array Antennas Symposium, A. A. Onliner and G. H. Knittel eds., Artech House, 1972, Section II: 'Types and applications of phased array antennas'

15 J. R. Forrest, F. P. Richards, A. A. Salles, and P. Varnish, 'Optical fibre networks for signal distribution and control in phased array radars', Proc. Int. Conf. Radar'82, London 1982, p. 408

16 A. J. Seeds, I. D. Blanchflower, N. J. Gomes, G. King, and S. J. Flynn, 'New developments in optical control techniques for phased array radar', IEEE MTT-S Symposium Digest, 905 (1988)

17 A. Seeds, 'Optical techniques in phased arrays', IEE Tutorial Meeting on 'Phased array radar', September 1989, paper 4

18 J. R. Wallington and J. M. Griffin, 'Optical techniques for signal distribution in phased arrays', GEC J.Research **2**, 66 (1984)

19 D. L. Switzer and S. P. James, 'A dc - 20 GHz externally modulated fibreoptic link', IEE Colloquium on "Optical control and generation of microwave and millimetre wave signals, Digest No. 1989/61; I. A. Wood and N. J. Parsons, 'A dc - 20 GHz modulated optical source at 1.3 μm', ibid.

20 G. D. Boyd, J. E. Bowers, C. E. Soccolich, D. A. B. Miller, D. S. Chemla, L. M. F. Chirovsky, A. C. Gossard, and J. H. English, '5.5 GHz multiple quantum well reflection modulator', Electron. Lett. **25**, 558 (1989); M. Whitehead, A. Rivers, G. Parry, J. S. Roberts, and C. Button, 'Low voltage multiple quantum well reflection modulator with on:off ratio > 100', ibid. 984

21 M. Nazarathy, W. V. Sorin, D. M. Baney, and S. A. Newton, 'Spectral analysis of optical mixing measurements', J. Lightwave Tech. **LT-7**, 1083 (1989)

22 I. D. Blanchflower, R. Ramos, Department of Electrical Engineering, UCL: personal communication

23 R. C. Steele, 'Optical phased-lock loop using semiconductor laser diodes', Electron. Lett. **19**, 69 (1982)

24 J. Mellis, S. A. Al-Chalabi, K. H. Cameron, R. Wyatt, J. C. Regnault, W. J. Devlin, and M. C. Brain, 'Miniature packaged external cavity lasers for coherent communications', Proc. ECOC'88, Conf. publ. **292**, Part 1, 219 (1988)

25 Y. C. Chung, 'Frequency-locking of 1.3 μm DFB laser using a miniature argon glow lamp', IEEE Phot. Tech. Lett. **1**, 135 (1989)

Chapter 7

TRANSIENT AND STEADY STATE CHARACTERISTICS OF A BRILLOUIN AMPLIFIER BASED ON AN OPTICAL FIBRE RING RESONATOR (OFRR)

So far we have considered the steady state response, operation and applications of the all-fibre Brillouin ring laser. In the last chapter we have described the demonstration of low threshold Brillouin lasing using a commercially available AlGaAs laser at 830 nm, making this device compatible with current coherent fibre systems. In this chapter we consider another application of the generation of Brillouin scattering in an OFRR - for amplification.

With rapid development of the coherent fibre communications systems, there has been a considerable interest in optical amplification[1]. Substantial theoretical and experimental research efforts have been invested in the investigation of semiconductor amplifiers[2-4], and more recently modified vapour-phase techniques for fibre fabrication have led to the realisation of the rare earth doped fibre amplifiers[5-7]. Due to inherent index and mode-matching, the all-fibre geometry offers the advantage of low insertion loss and direct splicing into an all-fibre system. The uses of gain in the nonlinear Raman[8-11], and as we have already seen in Chapter 3, Brillouin scattering processes for amplification have also received much attention in recent years.

All-fibre amplifiers based on scattering processes are attractive because they require a minimum of additional components, essentially only a pump source. The principle of operation of scattering amplifiers is to amplify an external signal, by coupling into the fibre a certain amount of the pump power (below lasing threshold) which provides a distributed gain at the signal wavelength. Considerable amount of work has been directed towards the investigation of Raman gain and noise characteristics both theoretically and experimentally in fibre transmission systems[8-11], as well as in low-loss, all-fibre recirculating delay lines[12]. We shall be discussing the differences and trade-offs between different optical amplifiers towards the end of this chapter, but it can be briefly mentioned here that fibre

Raman amplifiers have a very broad bandwidth (approximately 12 THz), but require substantial amounts of pump power. Moreover, when using Raman amplifiers in long-haul coherent systems, various schemes for suppression of stimulated Brillouin scattering (SBS) which causes pump depletion, have to be employed[10]. And yet, in Chapter 4 (and reference [13]) it was shown that SBS threshold dramatically decreases in the presence of linear gain (which serves to cancel linear fibre loss) - provided by the Raman process in this case.

By operating the Brillouin laser below threshold, a signal at the Stokes frequency can be amplified. However, the amplification applications require knowledge of the transient characteristics of this device to enable evaluation of amplifier response time and speed. In this chapter we present the calculations for Brillouin amplifier parameters of a device configuration based on an all-fibre ring resonator. Initially we present the analysis and results of a theoretical model which describes the transient operation of an all-fibre Brillouin ring laser in section 7.1. The model which accounts for pump depletion, describes the build up of the amplified spontaneous scattering (ASS) and calculated the lasing thresholds as a function of the number of circulations and cavity parameters. Then, the theoretical evaluation of the Brillouin amplifier is presented in section 7.2, with the signal gain, signal-to-noise ratio (SNR), time response of the device, and the limits on the gain and the output signal power due to saturation are calculated in terms of the cavity parameters. It is shown that the transient Stokes intensity in the ring can significantly exceed the steady-state value and that there is a good agreement between the model and experimentally obtained lasing thresholds and steady-state values. The different methods available for optical amplification are compared in Section 7.3.

7.1. Transient operation of the Brillouin laser

7.1.1 Theoretical description

The schematic diagram of the device which can operate as a Brillouin laser (above the Brillouin lasing threshold) or as a Brillouin amplifier (below Brillouin lasing threshold) based on the all-fibre ring resonator is shown in figure 7.1. Initially we consider the operation of the Brillouin laser, in the absence of an external Stokes signal, S_{in}. The pump field E_{in} circulates in the resonator to amplify the counterpropagating spontaneous Stokes

noise. To describe the coherent build-up of SBS we start off with the coupled equations for the slowly varying complex *amplitudes* of the pump and Stokes waves: pump and Stokes rate equations [(2.24)]:

$$\frac{dE_p^{m+1}}{dz} = -\frac{1}{2}[\gamma + g_B|E_S^m|^2]E_p^{m+1} \tag{7.1}$$

$$\frac{dE_S^{m+1}}{dz} = \frac{1}{2}[\gamma - g_B|E_p^{m+1}|^2]E_S^{m+1} \tag{7.2}$$

where E_p and E_S are the pump and Stokes field amplitudes, and g_B is the peak Brillouin gain coefficient in m/W, as before.

The pump light propagates in the +z direction: from z = 0 to z = L in the loop. The Stokes light travels in the opposite direction (from z = L to z = 0). The index m (where m = 1, 2, 3...) refers to the number of pump and Stokes circulations the number of circulation around the loop, that is the integer number of transit periods, where $\tau = nL/c$, where L is the loop length, n is the refractive index, and c is the speed of light in a vacuum. The propagation of the field once around the loop is considered as 1 circulation, where we assume that the time taken for the light to propagate the length of the directional coupler is insignificant compared to the length of the loop. Thus the build up of the pump and Stokes fields as a function of the number of circulations effectively gives us the transient response of the device.

In eqns (7.1) and (7.2), $\gamma = 2(\alpha_o + j\beta)$ where $(2\alpha_o)$ is the intensity attenuation coefficient and β is the propagation coefficient of the pump and Stokes fields. We assume that both pump and Stokes waves are resonant (as given by the resonance condition of eqn (5.7)). That is, providing the pump wave is at resonance, Brillouin lasing will occur when the Stokes wave is resonant (ie whenever a resonant mode falls within the Brillouin gain curve, as discussed in the last chapter). [This assumption can be justified if we consider that the FSR of a 10 m resonator (≈20 MHz) is some three orders of magnitude smaller than the Brillouin shift (≈20 GHz at 830 nm), ensuring a resonant Stokes mode]. In this case, the round-trip phase delay $\beta L/2$ will be equal to 2π for both pump and Stokes waves. We shall return to this point later in this section.

Because the pump and the Stokes waves propagate in opposite directions, the boundary conditions for them have to be applied on the opposite boundaries. As we have already discussed, this means that the equations (7.1) and (7.2) have no analytical solutions, and generally the numerical calculations are carried out using the assumption that pump depletion is negligible. However, as was already seen in Chapters 4 and 6, pump depletion is an important factor in the calculation of the lasing threshold and conversion efficiency of Brillouin lasers, and in the evaluation of SNR and gain of Brillouin amplifiers. In addition, the fact that we are considering the coherent addition of fields inside the resonator further complicates the solutions, necessitating numerical analysis of considerable complexity[14,15], while the results for amplification for this configuration have not been previously calculated.

We adopt the same approach as for the analytic solutions of the Brillouin laser, derived in the previous chapter, by using the small gain per loop transit approximation. Although this approximation is valid for the cases considered in this work, in general, as shown in the previous chapter, its range of validity has to be carefully evaluated. In cases of longer resonator loop lengths, and lower finesses, where the accuracy of the small gain per loop approximation is considered insufficient, the numerical method of calculating the pump and Stokes intensity per loop of length L can be adopted. Considered in detail in Chapter 4, this method has been shown to yield excellent accuracy and stability, and can be applied to the following analysis as a relatively straightforward extension. However, for simplicity we limit the analysis below to the small gain per loop approximation.

In this case we can directly integrate equations (7.1) and (7.2) wrt z from 0 to L.
We obtain, for the pump:

$$E_p^{m+1}(L) = E_p^{m+1}(0) \exp - \{ \frac{1}{2}[\gamma + g_B |E_S^m(0)|^2]L \} \tag{7.3}$$

The factor $g_B|E_S^m(0)|^2L$ in the exponential now accounts for the pump depletion.

Similarly, for the Stokes wave, integration of (7.2) yields:

$$E_S^{m+1}(L) = E_S^{m+1}(0) \exp\{\frac{1}{2}[\gamma - g_B |E_p^{m+1}(0)|^2]L\} \tag{7.4}$$

To simplify the mathematics, in this case, we have implicitly accounted for the coupler radiation loss by including it as a lumped loss in the expression for the coupling coefficient.

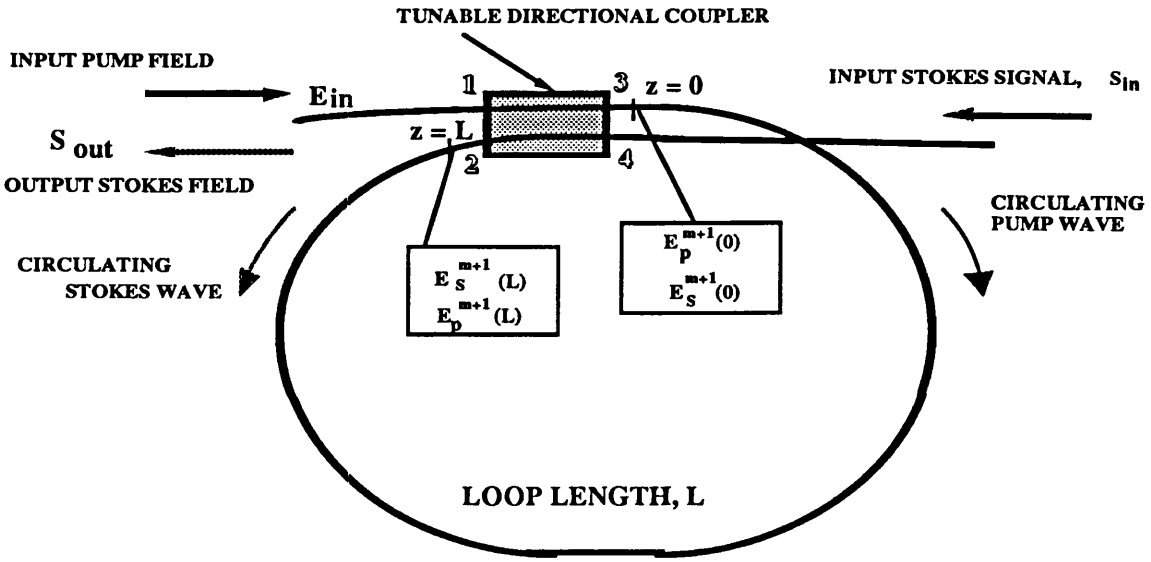

Figure 7.1. Propagation of the pump and Stokes fields in an all-fibre ring resonator; field transmission coefficients: $T_{13} = T_{24} = (1 - k^2)^{1/2}$
$T_{14} = T_{23} = jk$

From figure 7.1, it can be seen that the boundary conditions are, for the pump wave:

$$E_p^{m+1}(0) = jkE_p^m(L) + (1 - k^2)^{1/2}E_{in} \tag{7.5}$$

k is the field coupling coefficient, as shown in figure 7.1.

Rearranging eqn (5), we obtain:

$$E_p^m(L) = \frac{\{E_p^{m+1}(0) - E_0\}}{jk} \tag{7.6}$$

where $E_0 = (1 - k^2)^{1/2}E_{in}$, and k includes the coupler radiation loss - γ_o, with $(1 - \gamma_o)$ being transmitted through the coupler, as before.

The inclusion of all the losses is important to make the calculations practical, and applicable in experimental situations. This is necessary, because as discussed previously, the cavity finesse or quality factor is determined by the losses in the ring. In the passive resonator (that is in the absence of SBS) the losses consist of the coupler loss ($2\gamma_o$), and fibre loss ($2\alpha_o$). It was shown in Chapter 5, which described the resonator theory, that for resonance the coupling coefficient, k^2 should be equal to $\{(1 - 2\gamma_o)\exp[- 2\alpha_o L]\}$, as derived in eqn (5.8). The resonator finesse, which determines the sharpness of the resonant dip, and is given by the ratio of free spectral range, c/nL and the FWHM width of the resonator dip, Δf, is proportional to $k/(1 - k^2)$. Analogously to the Fabry-Perot cavity - the finesse determines the enhancement of the circulating field over the input field. In addition, the important parameter - the cavity decay time or damping coefficient is also determined by the losses, and hence by the cavity finesse.

Now, in the absence of an external signal at the Stokes frequency, the boundary condition for the Stokes noise present in the ring is given by:

$$E_S^{m+1}(L) = jkE_S^m(0) \tag{7.7}$$

Next, substituting (7.6) into (7.3) and simplifying, we obtain:

$$E_p{}^{m+1}(L) - E_p{}^m(L) = E_p{}^{m+1}(0)[\exp - \frac{1}{2}\{\gamma + g_B |E_S^m\ (0)|^2\}L - \frac{1}{jk}] + \frac{E_0}{jk} \tag{7.8}$$

Equation (7.8) effectively gives us the incremental change of the pump field E_p with each circulation or $dE_p(L)/dm$.

In a similar manner, we want an expression for the Stokes wave, $E_S{}^{m+1}(0)$, and combining (7.7) and (7.4) we get:

$$E_S^{m+1}(0) - E_S^m(0) = E_S^{m+1}(L)\{\exp\frac{1}{2}(\gamma - g_B |E_p^{m+1}(0)|^2)L - \frac{1}{jk}\} \quad (7.9)$$

Equations (7.9) and (7.10) give the variation of the pump and Stokes waves in terms of $E_p^{m+1}(0)$ and $E_S^{m+1}(L)$, respectively. We do, however, require to obtain the change in the pump and Stokes fields per circulation as a function of their values from the previous circulation, to enable as to calculate the *change* in the pump and Stokes field amplitudes *per circulation*, so as to give their effective temporal variations. So we make use of equations (7.6) and (7.7) again.

Substituting (7.6) into (7.8), we obtain for the pump wave:

$$E_p^{m+1}(L) - E_p^m(L) = \{jkE_p^m(L) + E_0\}\{[\exp - \frac{1}{2}(\gamma + g_B |E_S^m(0)|^2)L - \frac{1}{jk}] - \frac{E_0}{jk} \quad (7.10)$$

Equation (7.10) can be re-arranged to give the 'new' value of the pump field circulating in the loop on the (m+1)th circulation in terms of the previous m-th value:

$$E_p^{m+1}(L) = jkE_p^m(L)\{\exp - \frac{1}{2}[\gamma + g_B |E_S^m(0)|^2]L\} + E_0\exp - \frac{1}{2}[\gamma + g|E_S^m(0)|^2]L \quad (7.11)$$

Now, similarly for the Stokes wave; Using (7.7) and (7.9) we get:

$$E_S^{m+1}(0) = jkE_S^m(0)\{\exp - \frac{1}{2}[\gamma - g_B |E_p^{m+1}(0)|^2]L\} \quad (7.12)$$

Equations (7.11) and (7.12) completely describe the evolution of the fields of the pump and spontaneous Stokes noise per circulation (pass) around the ring: in terms of the resonator and fibre parameters. Because each of the above expressions represents the change of the pump and Stokes field amplitudes over *one loop transit*, then if we now iteratively solve the above coupled equations, we will obtain the transient build up of the pump and Stokes

fields as a function of the integer number of circulations in the ring. It can also be noted from (7.9) and (7.10) that the difference $E_S^{m+1}(0) - E_S^m(0)$ grows with each circulation as the Stokes field is amplified on each circulation. And consistently, $E_p^{m+1}(L) - E_p^m(L)$ decreases with each circulation - due to depletion by the counterpropagating Stokes.

The following points confirm the validity of the model. It can be verified that in the absence of any Stokes components, equation (7.11) reduces to the transient resonator response for the passive case, as derived in Appendix G. Setting both equations (7.11) and (7.12) to zero, that is $E_p^{m+1}(L) = E_p^m(L)$ and $E_S^{m+1}(0) = E_S^m(0)$, yields the steady-state SBS equations which describe the all-fibre Brillouin ring laser, as derived in the previous chapter.

Equations (7.11) and (7.12) were solved numerically with the following initial conditions.

For the pump wave,

$$E_p^m(L)|_{m=1} = E_0 \exp[\gamma/2] \qquad (7.13)$$

The initial Stokes field in the absence of an external Stokes signal is due to the spontaneous Stokes emission, as in the straight fibre case. For a single mode fibre, the effective input Stokes intensity is given by eqn (3.2): where we again use the approximation that the summation of amplified spontaneous Brillouin scattering weighted by the relative gain over the length L is approximately equal to the fictitious injection of 1 Stokes photon per mode.

As stated earlier, we assume that the build up of Stokes noise starts after the pump wave has traversed the ring once, although final results are not very sensitively dependent on the exact initial value of the Stokes field amplitude, a behaviour which is not dissimilar to the straight fibre case, considered in Chapter 3.

The Stokes noise $E_S^{m+1}(0)|_{m=1}$ can be evaluated over the length of the ring L from eqn (3.2). Using practical values for loop lengths between 1 and 15 metres and for a ranges of input pump powers of 1 - 5 mW, the input Stokes power intensity at room temperature

approximately equals $\approx 10^{-9}$ times the input pump intensity, $|E_{in}|^2$. The other parameters used in the calculations are listed in Table 7.1.

In solving equations (7.11) and (7.12) we have assumed, for simplicity, that the pump and Stokes waves are resonant, and therefore, the roundtrip phase delay $\beta L/2$ is 2π. This assumption is justified on two counts. Firstly, the coupler is not very strongly frequency dependent, and in addition, the frequency difference in the pump and Stokes waves is negligible in terms of the optical frequency. Therefore, the difference in the roundtrip phase delay for both the pump and Stokes waves is correspondingly negligible to allow us to consider it to be the same for both. The second justification is concerned with the fact that Brillouin lasing will occur when the lasing threshold is exceeded, a situation, which is clearly optimised at resonance. Therefore, any frequency detuning of the pump from resonance, will simply result in a significantly reduced Brillouin gain.

Brillouin gain coefficient, g_B	4.6×10^{-11} m/W
Brillouin shift, Δf_B	27 GHz at 633 nm 20.5 GHz at 830 nm
Brillouin gain bandwidth, $\Delta \upsilon_B$	$\approx$ 90 MHz at 633 nm $\approx$ 50 MHz at 830 nm
Typical fibre parameters (York fibre):	
Fibre loss, $2\alpha_o$	10 dB/km at 633 nm 4.0 dB/km at 830 nm
Fibre core refractive index, n	1.462
Effective core area, A_{eff} (slow axis, Hi-Bi fibre)	1.6×10^{-11} m^2
Coupler loss	2% (0.03 dB)

Table 7.1. Coupler and fibre parameters used in the calculations.

In addition, it is interesting to note that since the phase change experienced by the pump and Stokes waves in traversing the directional coupler (jk) is $\pi/2$, and as we are solving the equations for the pump and Stokes waves at opposite boundaries, the phases of the pump and Stokes waves are in quadrature. That is, the phases of $E_S^{m+1}(0) = E_S^{m}(0)$ and $E_p^{m+1}(L) = E_p^{m}(L)$ differ by $\pi/2$.

It should also be noted that the additional loss due to the recirculating Stokes wave which serves to deplete the pump - does not affect the resonant phase delay (or - 'detune' the cavity) - only the optimum coupling coefficient, which no longer will allow zero output power. This last point is consistent with the steady state analysis carried out previously.

7.1.2. Transient characteristics of the Brillouin laser - results and discussion

The results of above calculations giving the evolution of the circulating Stokes field with the number of circulations as a function of loop length, L, for different values of the pump intensity ranging from 1.0×10^6 W/m^2 to 25.0×10^6 W/m^2 (corresponding from Table 7.1, to pump powers from 70 μW to 0.4 mW) are presented in figures 7.2 (i) - (iv).

As mentioned above, the build up of the Stokes noise represents the amplified spontaneous emission and it can be seen that initially (fig. 7.2(i)) the Stokes noise level is small, and the fibre loss exceeds the Brillouin gain. However, for higher input pump intensity, the circulating Stokes wave starts to build up and deplete the pump wave - as the threshold for stimulated scattering is reached, and Brillouin lasing starts. it should be noted that in this context the threshold is defined as that pump power (or intensity) at which the roundtrip Brillouin gain just exceeds the roundtrip system (fibre and coupling) losses.

From figs 7.2(iii) and 7.2(iv) it can be seen that the transient Stokes intensity significantly exceeds the steady-state value. The corresponding curves for the circulating pump intensity are shown in figure 7.3, plotted for a loop length L = 2 m. Figures 7.3 (a) and (b)

correspond to the pump intensity being below threshold, and hence undepleted - and are analogous to the transient response of the circulating intensity for the passive resonator case, described in Appendix G). It can be seen that the transient peak in the Stokes

intensity (curves (a) in figs. 7.2(iv) and 7.2(v)) exactly corresponds to a minimum in the pump intensity (7.3(c) and 7.3(d)). This, in fact, represents the depletion of the pump by the counterpropagating Stokes wave and is a characteristic feature of the stimulated scattering processes operating in a high conversion efficiency regime. Figure 7.4 illustrates this in showing the variation in the resonator finesse for different values of the input intensity corresponding to figure 7.3. It can be seen that, initially, below the Brillouin threshold (figs. 7.4(a), (b)), the finesse remains unchanged. However, the cavity is detuned for higher pump intensity representing the depletion of the pump by the growing counter-propagating Stokes wave (figs. 7.4(c) and (d)).

The effect of a longer loop length is to reduce the Brillouin threshold, since longer loop length results in a higher loop gain $g_B|E_p^m(0)|^2L$. However, longer loop length also has the effect of reducing cavity finesse as a result of a higher fibre loss, and consequently results in a lower level in the Stokes intensity circulating in the ring, at steady-state (Figs 7.2(iv) and (v)). Again this behaviour is consistent with the steady state analysis carried out in the previous chapter.

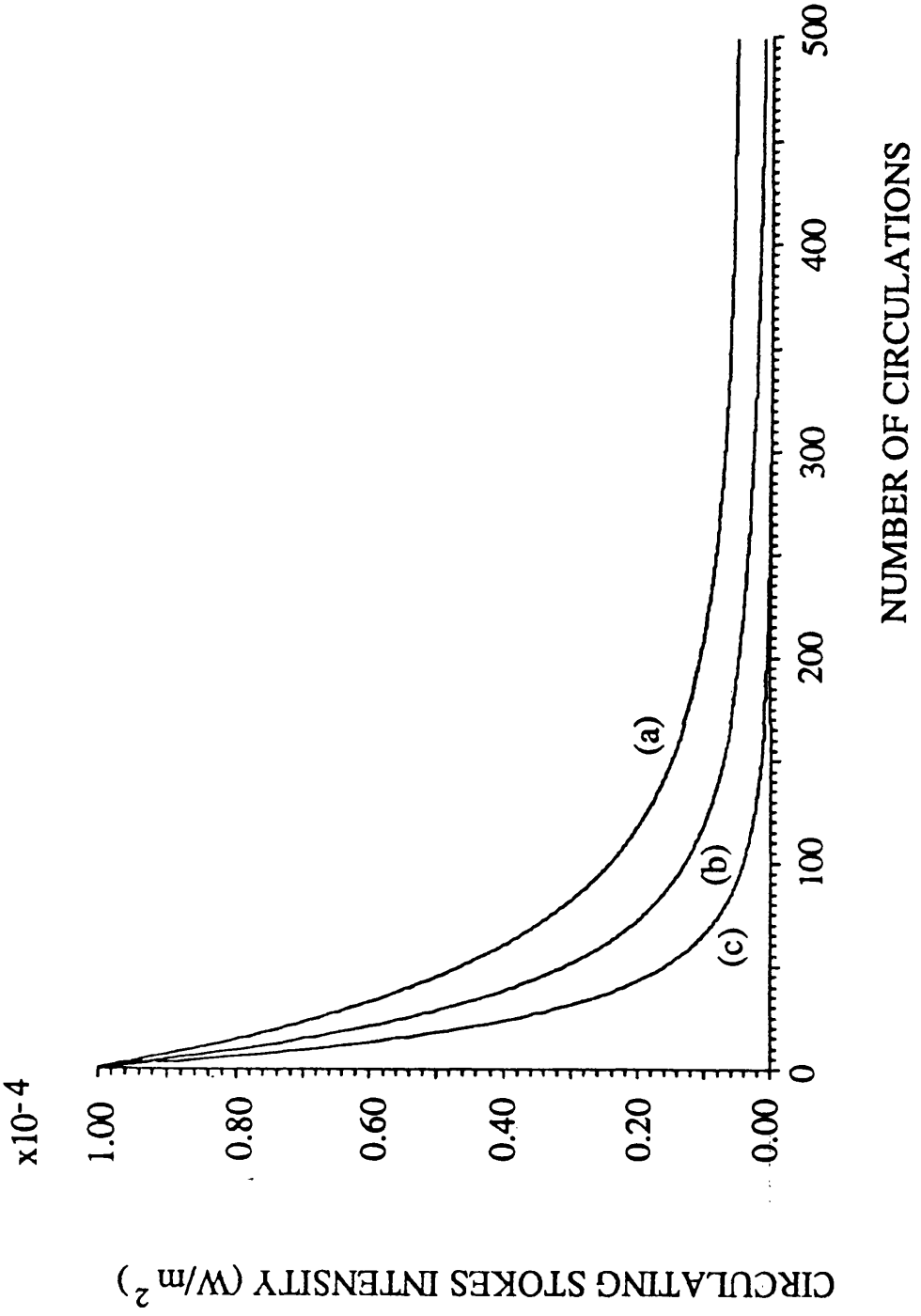

Figure 7.2 (i)

Figure 7.2. Evolution of Stokes circulating intensity, $|E_S(0)|^2$ vs number of loop circulations, m, as function of loop length L for different pump intensities $|E_{in}|^2$: (i) 1.0 x 10^6 W/m^2 (P_0 = 18 μW or -17.5 dBm);
(ii) 4.0 x 10^6 W/m^2 (P_0 = 72 μW ; - 11.5 dBm);
(iii) 9.0 x 10^6 W/m^2 (P_0 = 0.16 mW; - 8.0 dBm);
(iv) 25.0 x 10^6 W/m^2 (P_0 = 0.45 mW; - 3.5 dBm)
(a) L = 2 m; (b) L = 5 m; and (c) L = 10 m

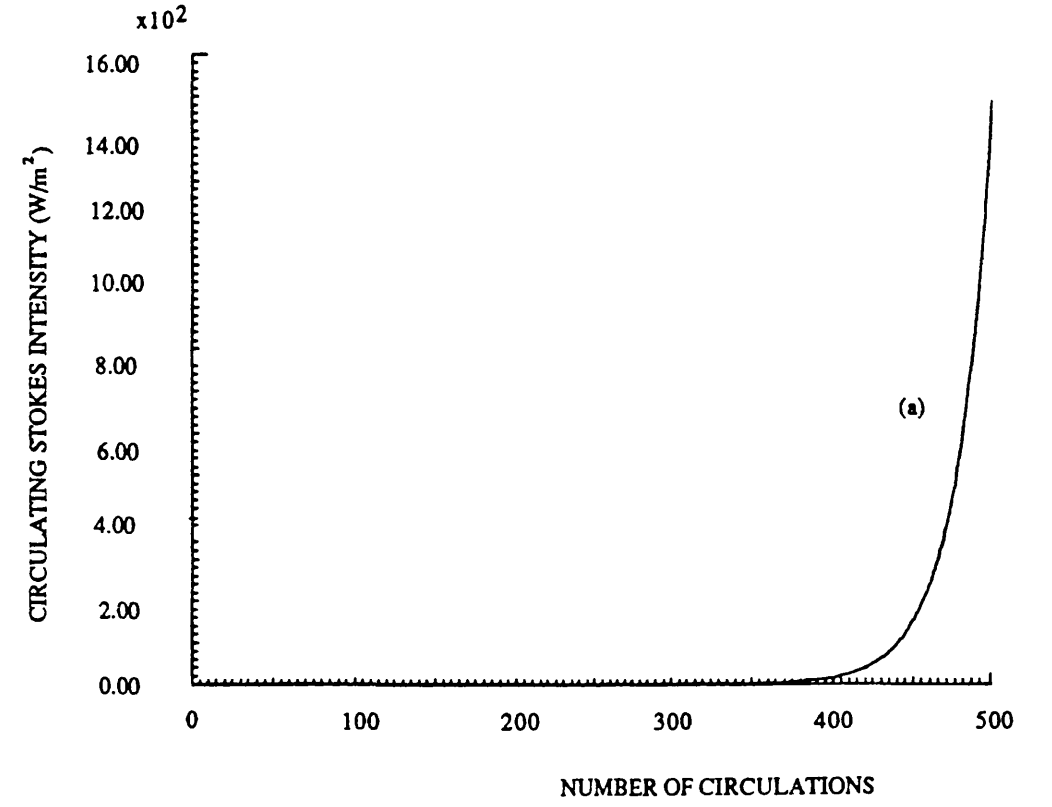

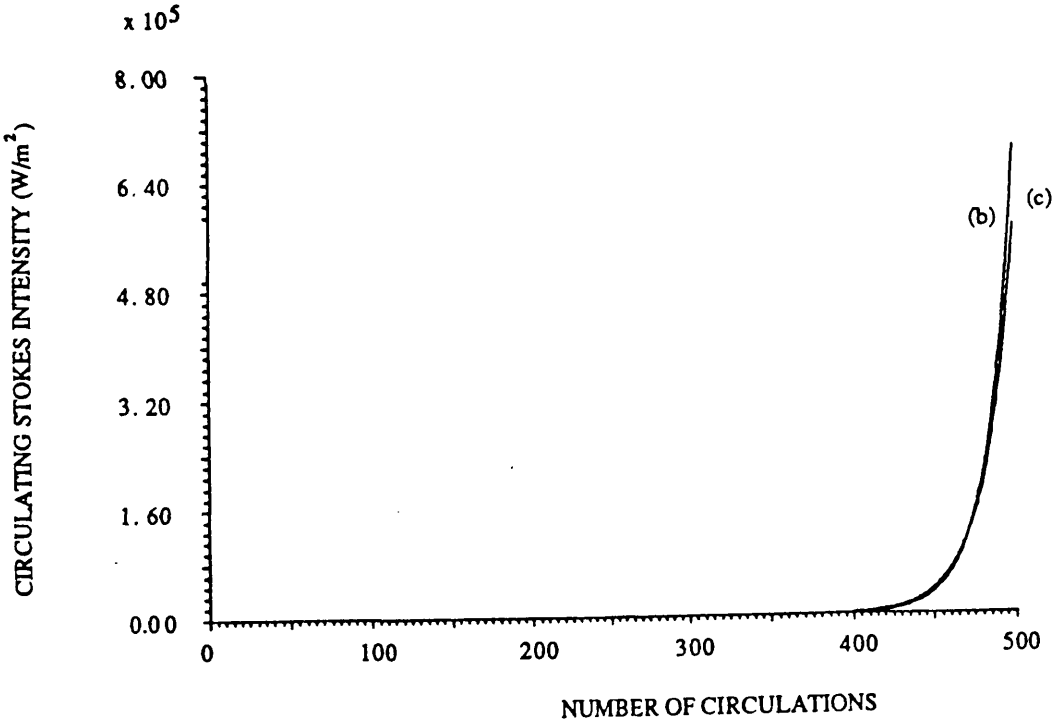

Figure 7.2 (ii)

Figure 7.2. Evolution of Stokes circulating intensity, $|E_S(0)|^2$ vs number of loop circulations, m, as function of loop length L for different pump intensities $|E_{in}|^2$: (i) 1.0 x 10^6 W/m^2 (P_0 = 18 μW or -17.5 dBm);
(ii) 4.0 x 10^6 W/m^2 (P_0 = 72 μW ; - 11.5 dBm);
(iii) 9.0 x 10^6 W/m^2 (P_0 = 0.16 mW; - 8.0 dBm);
(iv) 25.0 x 10^6 W/m^2 (P_0 = 0.45 mW; - 3.5 dBm)
(a) L = 2 m; (b) L = 5 m; and (c) L = 10 m

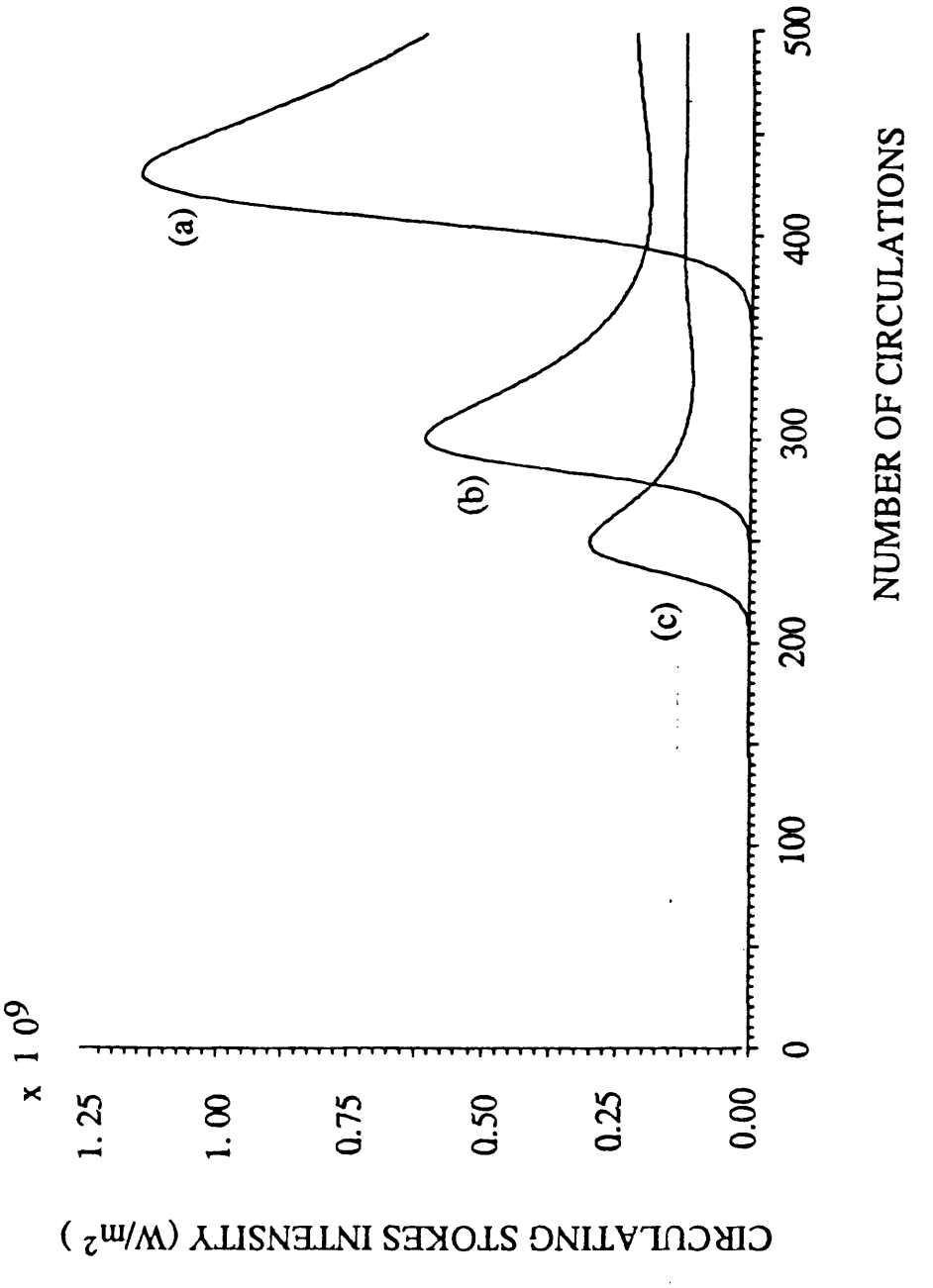

Figure 7.2 (iii)

Figure 7.2. Evolution of Stokes circulating intensity, $|E_S(0)|^2$ vs number of loop circulations, m, as function of loop length L for different pump intensities $|E_{in}|^2$: (i) 1.0 x 10^6 W/m^2 (P_0 = 18 μW or -17.5 dBm);
(ii) 4.0 x 10^6 W/m^2 (P_0 = 72 μW ; - 11.5 dBm);
(iii) 9.0 x 10^6 W/m^2 (P_0 = 0.16 mW; - 8.0 dBm);
(iv) 25.0 x 10^6 W/m^2 (P_0 = 0.45 mW; - 3.5 dBm)
(a) L = 2 m; (b) L = 5 m; and (c) L = 10 m

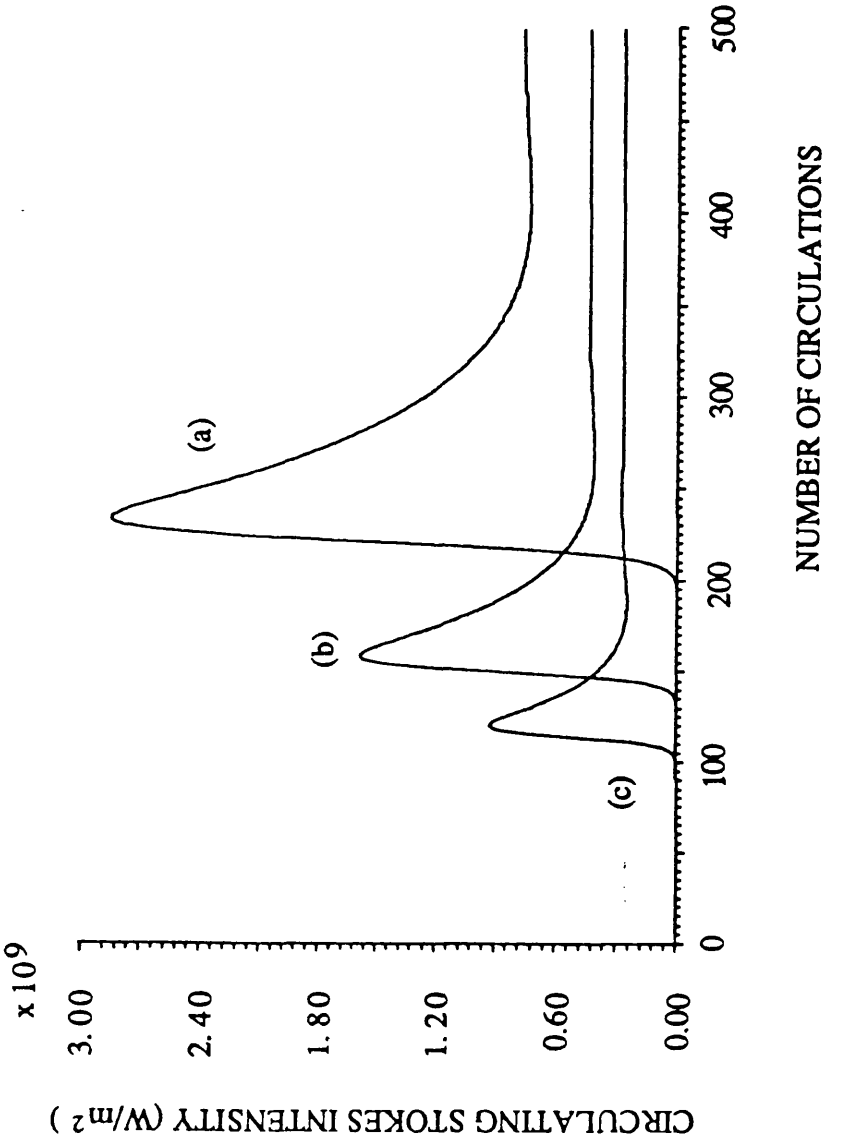

Figure 7.2 (iv)

Figure 7.2. Evolution of Stokes circulating intensity, $|E_S(0)|^2$ vs number of loop circulations, m, as function of loop length L for different pump intensities $|E_{in}|^2$: (i) 1.0 x 10^6 W/m^2 (P_0 = 18 μW or -17.5 dBm);

(ii) 4.0 x 10^6 W/m^2 (P_0 = 72 μW ; - 11.5 dBm);

(iii) 9.0 x 10^6 W/m^2 (P_0 = 0.16 mW; - 8.0 dBm);

(iv) 25.0 x 10^6 W/m^2 (P_0 = 0.45 mW; - 3.5 dBm)

(a) L = 2 m; (b) L = 5 m; and (c) L = 10 m

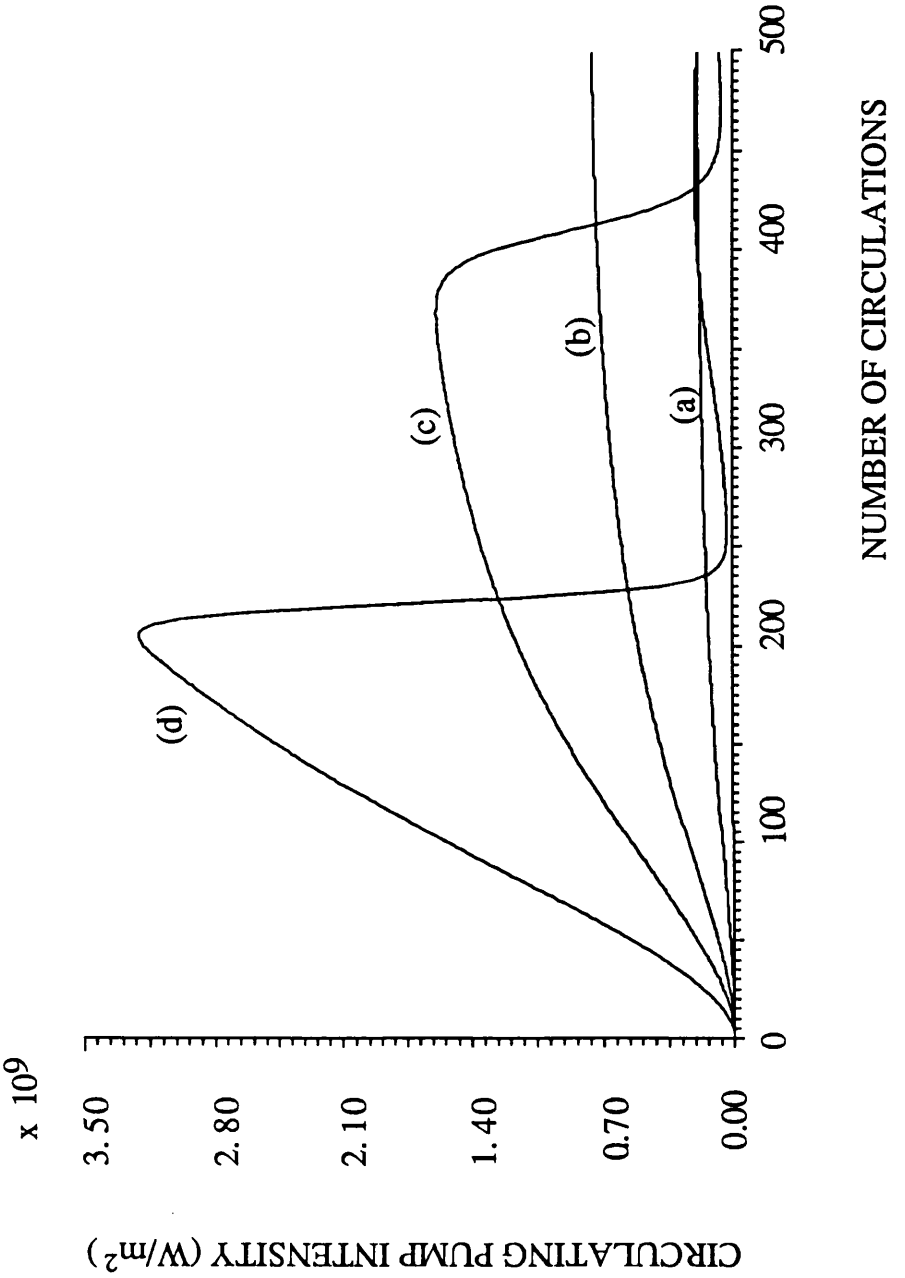

Figure 7.3. Pump circulating intensity, $|E_p(L)|^2$ vs number of circulations as function of the input pump intensity $|E_{in}|^2$: Curves (a) - (d) correspond to 7.3 (i) - (iv) above; L = 2 m.

The additional effect of higher cavity losses caused by a longer loop length is in, effectively, increasing the damping coefficient in the resonant system. This decreases the response time of the device, that is the time delay taken for the circulating pump and Stokes intensities to reach their steady-state values. For example, at the pump intensity of 25.0 x 10^6 W/m^2, the time delay for a 5 m loop length corresponds to approximately 200 circulations (i.e. 200 times the loop transit time $\tau = nL/c$ or ≈ 5 μs) compared with approximately 400 circulations for a 1 m loop. Indeed, these time delays govern the time response of this device, and as can be seen limit the operating speeds of practical devices.

In all the above calculations, for simplicity, the coupling coefficient k was taken to be at its optimum value for a resonant operation, in the absence of SBS; that is k was set equal to the roundtrip loop loss comprising of the fibre and coupler losses. Detuning the cavity (by setting the coupling coefficient to a non-resonant value) simply leads to a higher Brillouin threshold, for a particular value of the input pump intensity, as discussed in the previous chapter, and in the description of the OFRR in Chapter 5.

It is interesting to note that the above solutions are very similar to those calculated in references [14] and [15] giving the temporal behaviour of SBS in optical fibres and fibre lasers, using considerably more complex analysis and numerical calculations. The difference lies in the fact that in since both [14] and [15] calculated the variation of the pump and Stokes intensities explicitly with time, their solutions exhibit the characteristic relaxation oscillations of stimulated Brillouin scattering. The period of these oscillations is equal to the mode spacing of the SBS laser cavity or the loop transit time τ, and are due to the periodic depletion of the pump in the Brillouin medium. Described earlier (Chapters 2, 3 and 6), this gain modulation causes locking of the modes. Because in our analysis the variation of the pump and Stokes intensities is given in terms of an integer number of loop circulations, no oscillatory behaviour can be expected.

However, it must be pointed out that the calculations in [14] and [15] were carried out for fibre loop lengths sufficiently long (greater than 50 m) so that a number of Brillouin laser modes within the Brillouin gain bandwidth could be supported. In our case, the analysis

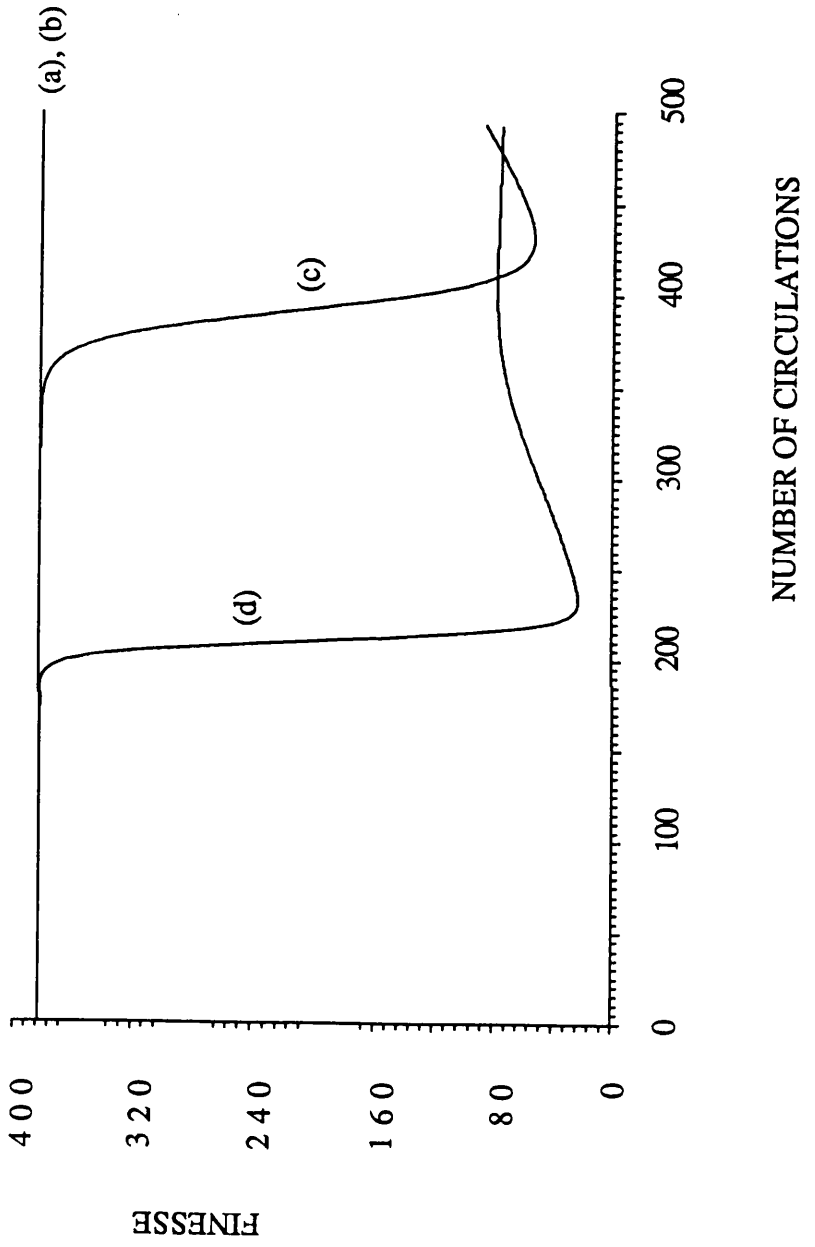

Figure 7.4. Variation of the resonator finesse with the number of circulations as a function of input pump intensity: (a) - (d) as in fig. 7.3.

deals with all-fibre resonators of loop lengths less than 10 m corresponding to a mode spacing of c/nL of greater than 40 MHz. Since this is approximately equal to the Brillouin gain bandwidth at 633 nm and 830 nm, the situation in our case concerns a single mode cw

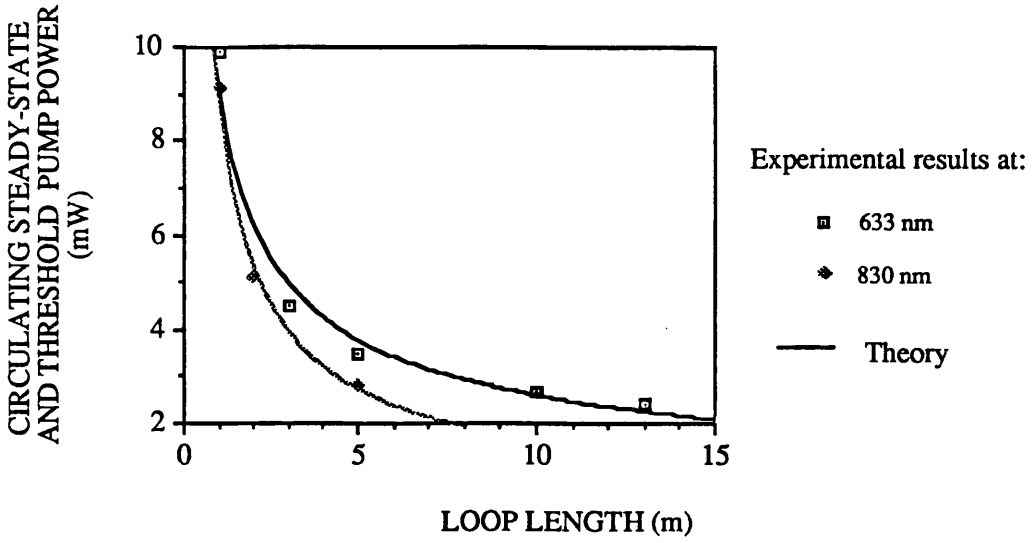

Figure 7.5. Comparison of theoretical and experimental results for Brillouin lasing threshold at pump wavelengths of 633 nm and 830 nm.

operation of the Brillouin laser. Indeed, this is in agreement with the experimental results described in the previous chapter, where the passive modelocking was not observed, andfollowing earlier discussion, it seems that no useful additional information can be gained by increasing the complexity of the analysis to incorporate the explicit time dependence.

As a further test of the validity of the model, the steady-state values from our transient model were compared with all recent published experimental results, both obtained in this work and described in the previous chapter, and those published by other workers[16-19]. [No comparison of the transient characteristics could be made as no transient experimental data on Brillouin lasing was available]. In figure 7.5 we show the experimental data obtained for Brillouin lasing thresholds for resonators of different loop lengths plotted together with theoretically predicted curve using the above model. We have plotted these curves in terms of powers to relate the theory to experimental values. It can easily be verified that the variation of the output steady-state power with input pump power for different loop lengths is also in agreement with the experimental values described in the previous chapter. The solid lines represent the theoretical curves, and the points - experimentally obtained data. It can be seen that there is a very good fit between the theory and the experimentally measured values. The predicted reduction in threshold with increased loop length is evident. The reduction in resonator finesse with an increase in the

circulating Stokes intensity which was discussed in the previous chapter is again in excellent agreement with the results from the model developed here and with the steady state analysis.

7.2. Transient and steady-state characteristics of the Brillouin amplifier

It is now possible to consider the characteristics of the Brillouin amplifier based on the OFRR. When operated below threshold - the Brillouin laser can act as an amplifier. In this case, analogously to the Raman amplifier, a small signal at the Stokes frequency is input at the (pump) output end of the resonator, as shown in figure 7.1. We make the assumption that this input signal has the correct phase to be resonant and that the amplified Stokes noise present in the ring is also resonant. (In practice it was found out that the phase of the input Stokes signal has no effect on the results of the numerical calculations). In this case, the circulating Stokes noise and signal amplitudes can be simply added, so in exactly the same way as above we arrive at the Brillouin amplifier equations:

$$E_S^{m+1}(0) - E_S^{m}(0) = jkE_S^{m}(0)\{\exp -\frac{1}{2}[\gamma - g_B |E_p^{m+1}(0)|^2 L] - \frac{1}{jk}\} + S_0 \exp -\frac{1}{2}[\gamma - g_B |E_p^{m+1}(0)|^2 L \tag{7.16}$$

where $E_S^m(0)$ is now the total Stokes field which is the sum of the spontaneous Brillouin noise (calculated as above) and the external Brillouin signal - evaluated at $z = 0$ in the loop; $S_0 = (1- k^2)^{1/2} S_{in}$. In this case we are considering polarisation maintaining fibre, and hence the Brillouin gain coefficient g_B is equal to its peak value. However, care must be taken when considering the amplification in resonators fabricated from ordinary polarisation non-preserving fibre, where the twofold gain reduction, each by a factor of 2, due to the depolarisation must be taken into account: both between the pump and the Stokes wave, as well as between the distributed Brillouin gain and the external Stokes signal to be amplified. This is exactly equivalent to the Brillouin amplification as discussed in Chapter 3 with respect to straight fibres.

The output Stokes field is found by combining the circulating Stokes with the 'straight through' component of the input signal:

$$S_{out} = jkS_{in} + (1 - k^2)^{1/2} E_S^{m+1}(0) \qquad (7.17)$$

The amplifier optical power gain G can now be defined as the ratio of $|S_{out}|^2/|S_{in}|^2$, for a particular pump intensity. The amplifier noise at a particular pump power is found by setting the input signal to zero - this gives the noise due to the amplified spontaneous scattering (ASS) - and is in fact the same as the value calculated above for the Brillouin laser biassed at a pump power below threshold power. From this the SNR of the Brillouin amplifier can be evaluated as the ratio of the output Stokes signal and the amplified spontaneous emission for a particular value of the pump intensity.

7.2.1. Results and Discussion

We have solved equations (7.11), (7.16), and (7.17) for a range of values of the input Stokes signal and pump intensities. The results of these calculations are shown in figures 7.6 - 7.9. In fig 7.6, we have plotted the steady state gain G in dB's ($10\log_{10}G$) as a function of the input pump intensity for different values of input Stokes signal and loop lengths. From figure 7.6 (i)-(iii) it can be seen that the gain is dependent on pump intensity, and as would be expected in a power dependent process, the gain is most linear at low input Stokes signal levels. It can also be noted that although the largest gain is obtained at high pump intensity values, this is accompanied by rapid gain saturation (as can be seen from 7.6 (a) - (e)). Gain saturation also means that for a particular value of the input pump intensity, the saturated gain is lower for an amplifier with a longer loop length (figs. 7.6 (ii) and (iii)). In fact there is also a clear trade-off between the gain and the linearity: although the higher input pump intensity increases the gain , the high gain saturates rapidly as the Brillouin lasing threshold is approached. Indeed, the range of signal intensities which can be amplified in this type of amplifier can be quite high by decreasing the pump intensity used for higher signal intensities - to avoid pronounced gain saturation. It should also be remembered that in these calculations the steady state values of the gain in the loop have been used and the transient Brillouin gain is considerably higher than the steady-state value.

SNR is plotted in figure 7.7 in the bandwidth equal to B_{eff}. In fact it can be verified that the output SNR is practically independent of the detection bandwidth higher than B_{eff}[7].

This accounts for the fact that after a sufficiently large number of circulations, both the Stokes signal and the noise spectra are narrower than the detection bandwidth. It can be

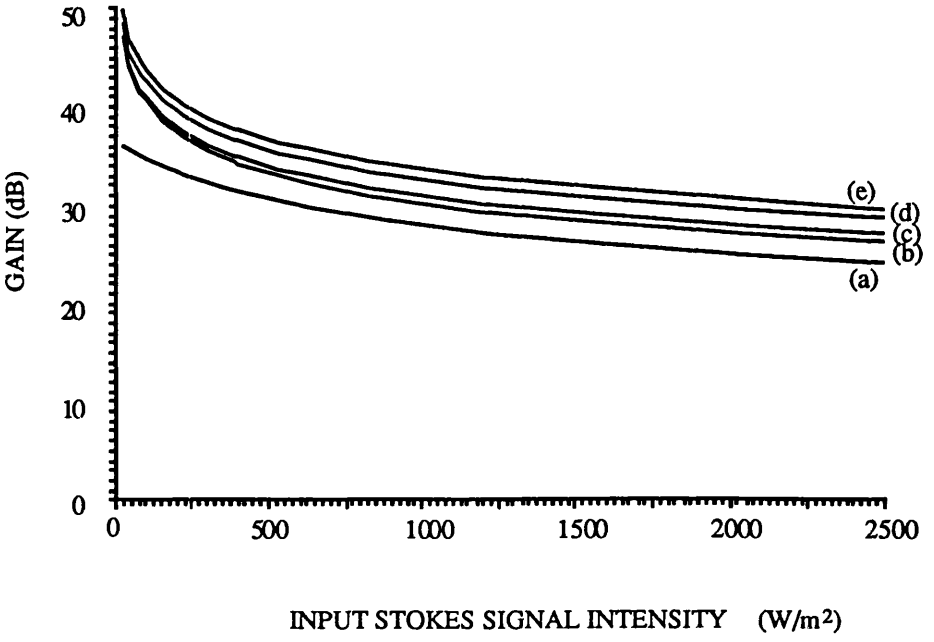

Figure 7.6 (i)

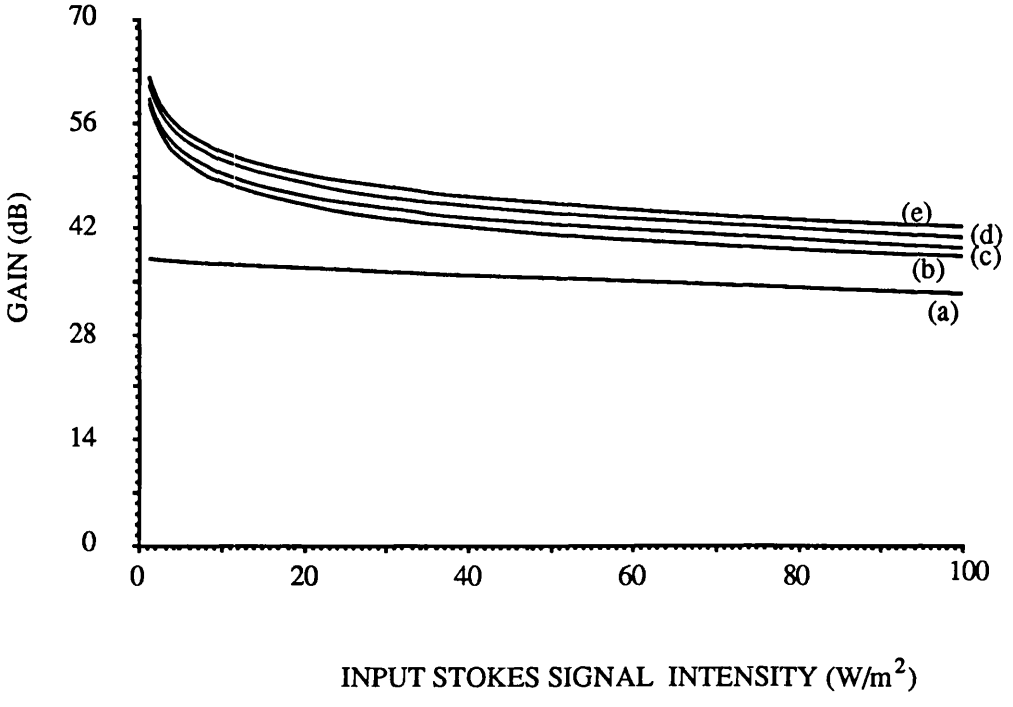

Figure 7.6 (ii)

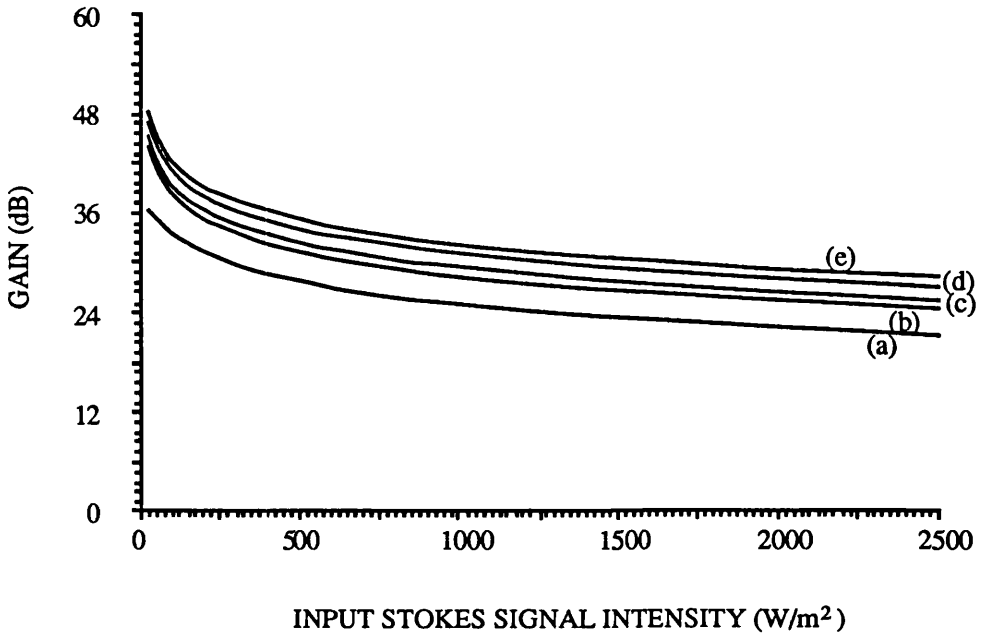

Figure 7.6 (iii)

Figure 7.6. Signal gain vs input Stokes signal intensity as function of input pump intensity $|E_{in}|^2$: (a) 1.4 x 10^6 W/m^2 ; (b) 2.0 x 10^6 W/m^2; (c) 2.3 x 10^6 W/m^2; (d) 2.9 x 10^6 W/m^2; 3.6 x 10^6 W/m^2; (i) L = 2 m; (ii) L = 5 m; (iii) L = 5 m.

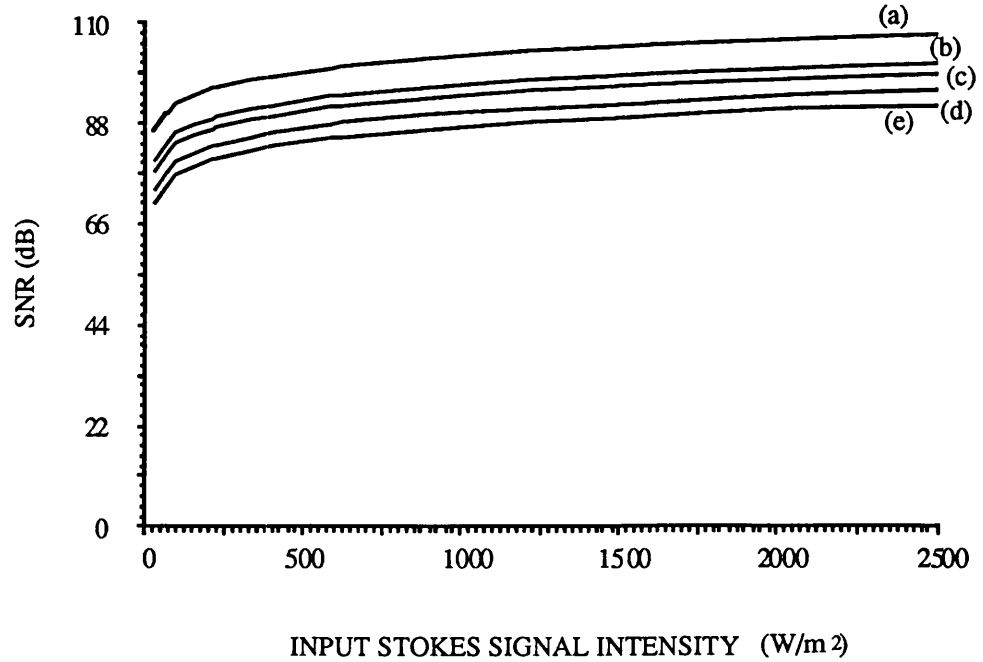

Figure 7.7 (i)

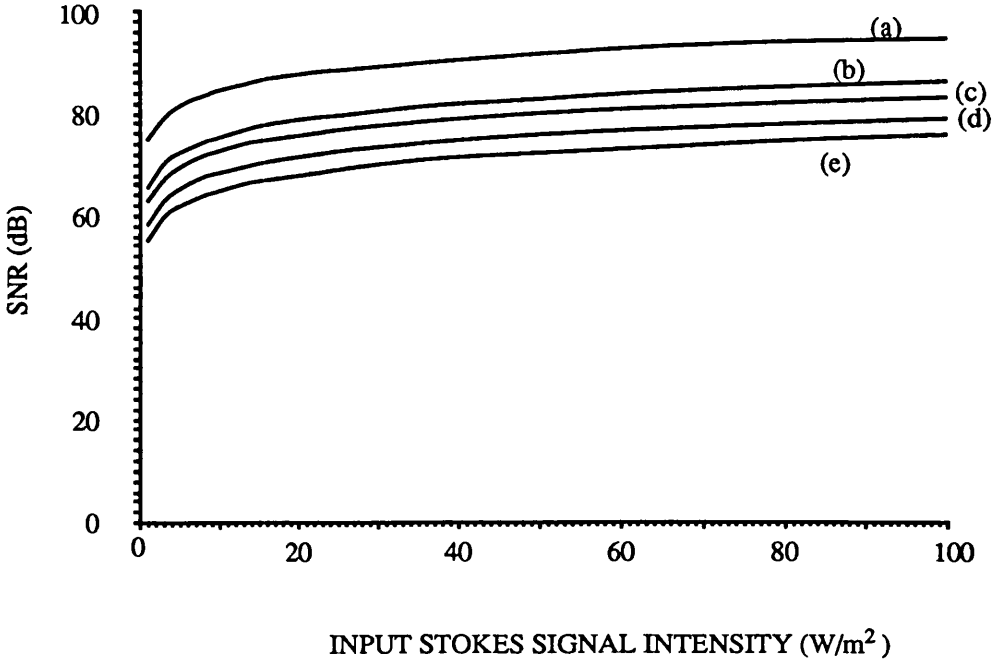

Figure 7.7 (ii)

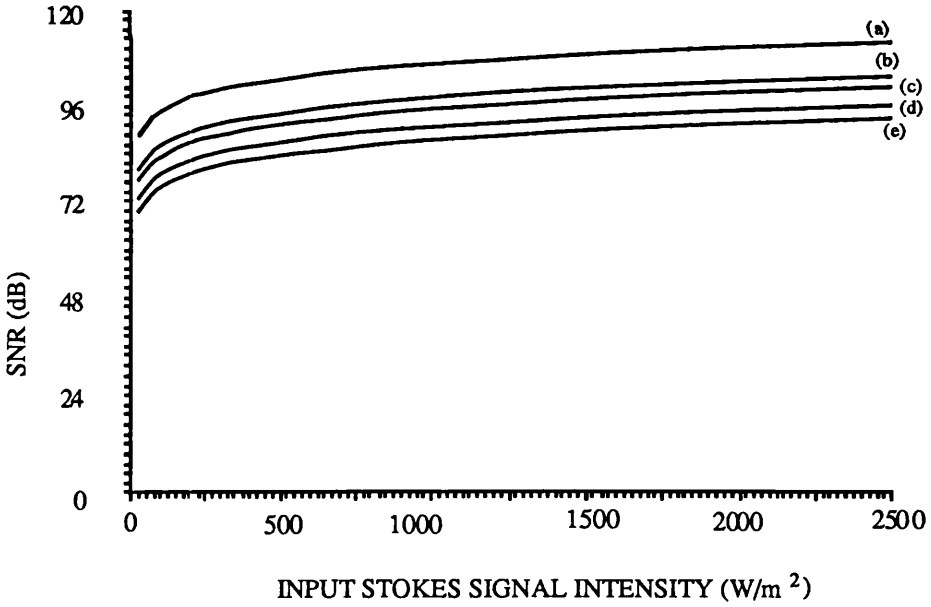

Figure 7.7 (iii)

Figure 7.7. SNR against input Stokes signal as function of input pump intensity $|E_{in}|^2$: (a) - (e) and (i) - (iii) as in fig. 7.6.

seen that a very high SNR is predicted which increases with increasing input pump intensity as the lasing threshold is approached. This is expected as the ASS decreases with increasing Stokes input signal intensity owing to gain competition. Similarly, it should also be noted that the SNR improves with increasing amplifier loop length where gain saturation is more pronounced - analogously to the noise build-up in rare earth doped fibre amplifiers[33]. In order to help relate these results to practical system parameters, we have replotted the steady state gain G and SNR of figures 7.6 and 7.7, as a function of the input pump power in dBm: -55 dBm to - 35 dBm, covering the range of powers of 3 nW to 0.3 μW in figures 7.8 and 7.9.

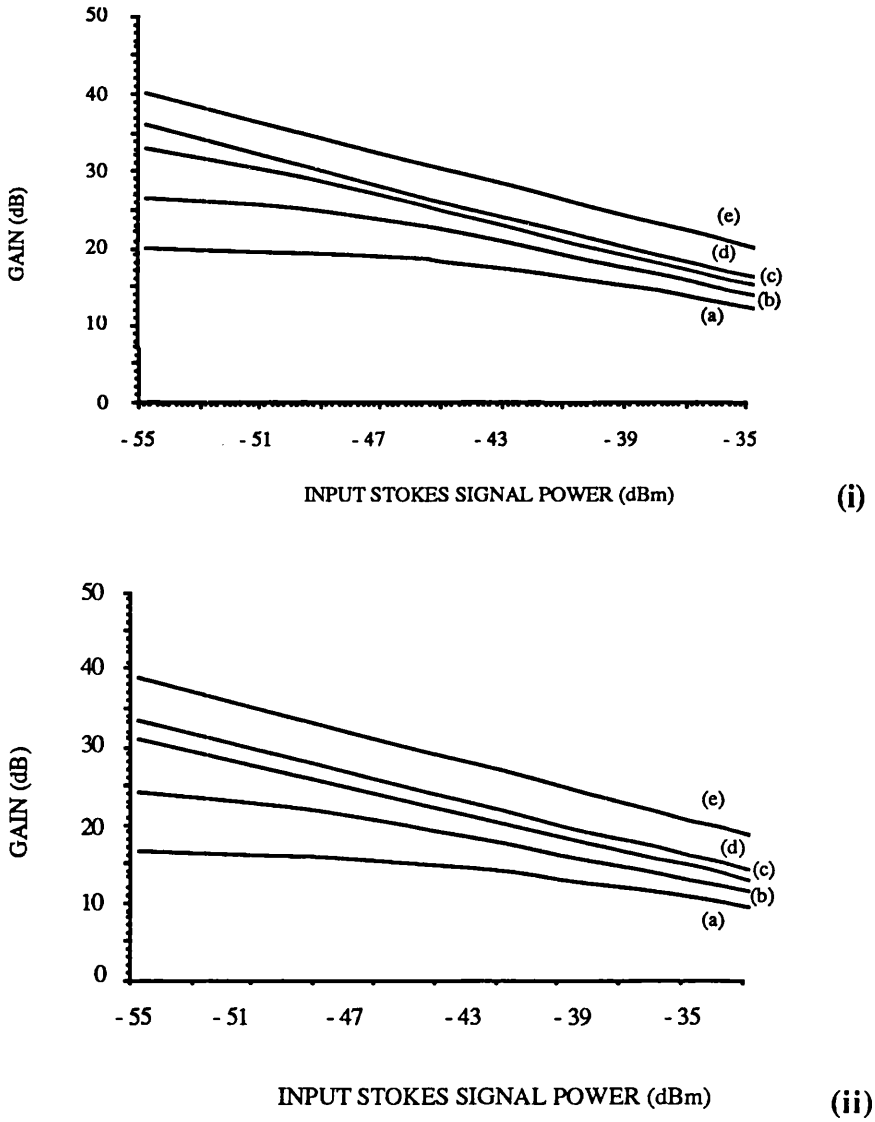

Figure 7.8. Signal gain vs input Stokes signal power as function of input pump power: (a) - 16.8 dBm; (b) - 15.2 dBm ; (c) - 14.6 dBm; (d) - 13.6 dBm; (e) -12 .7 dBm. (i) L = 2 m; (ii) L = 5 m.

From these graphs, the power dependent gain characteristics are evident, as is the fact that best linearity (albeit coupled with a lower gain) is obtained at lowest signal levels.

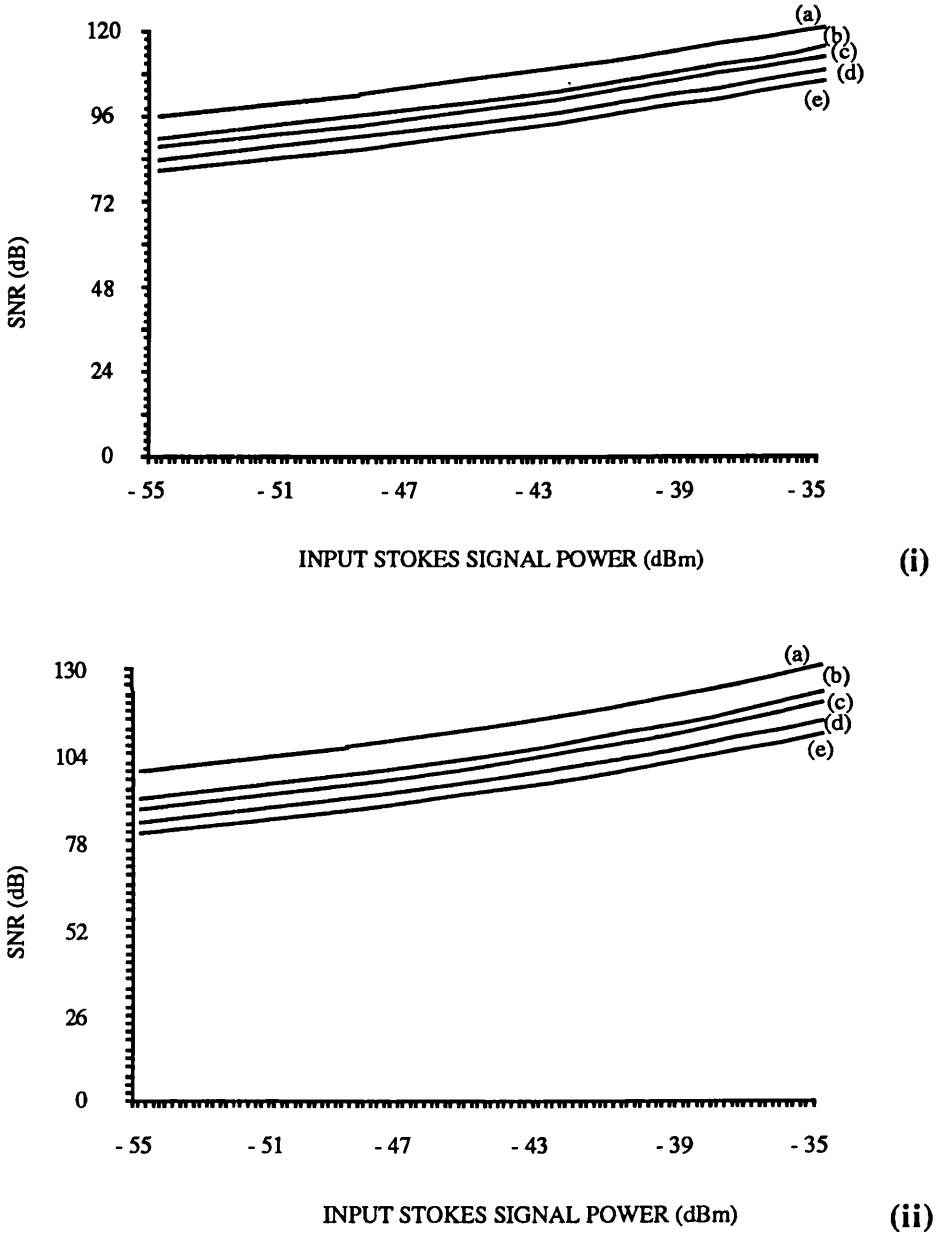

Figure 7.9. SNR vs input Stokes signal power as function of input pump power corresponding to fig. 7.8.

Conversely, it is thought that if gain variation as a function of signal power is acceptable, and can be accomodated by calibration, this characterisitic need not represent a shortcoming of this type of amplifier. The variation of the output Stokes signal is plotted vs the number of circulations is plotted in figure 7.10 as a function of the input

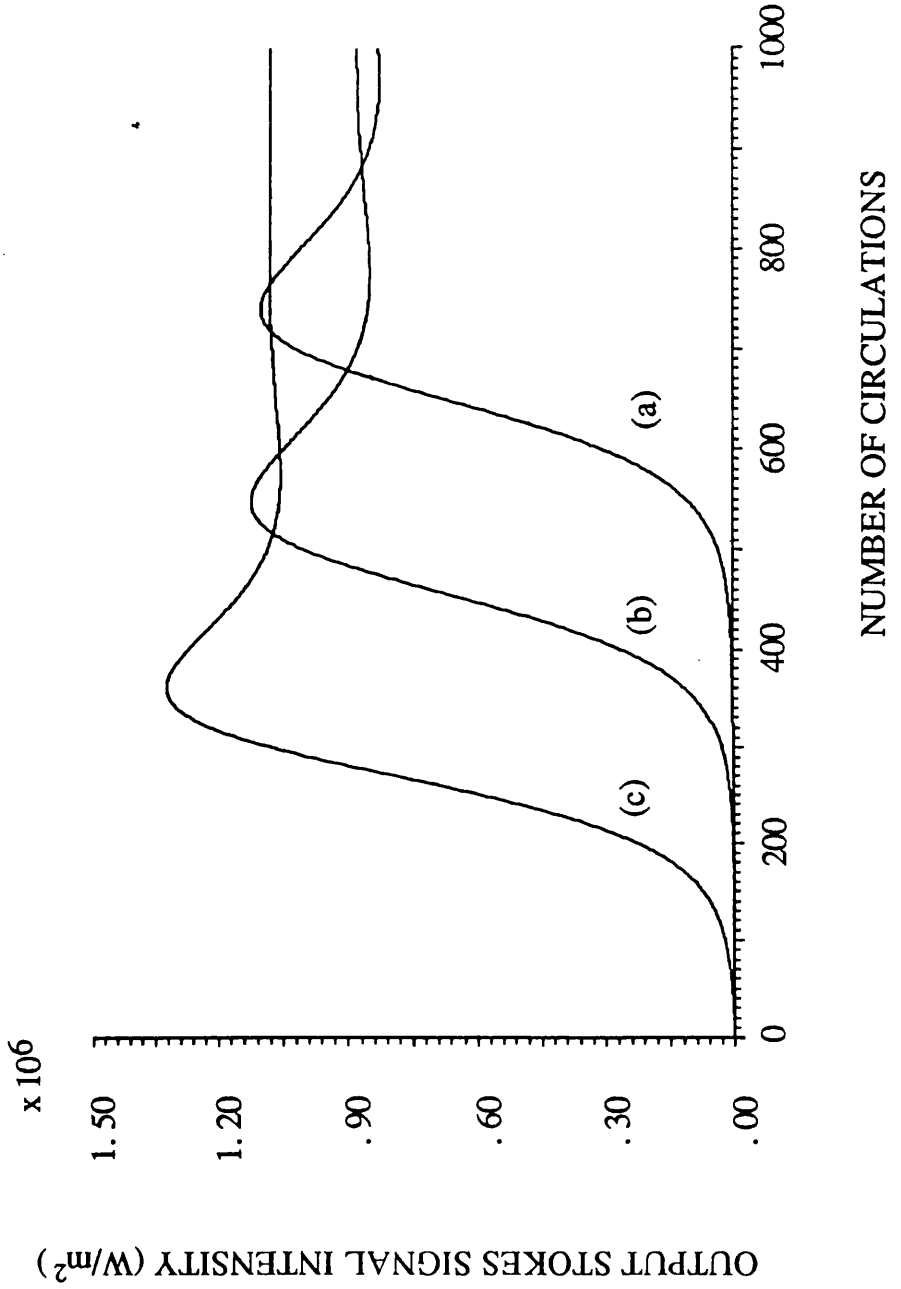

Figure 7.10. Output (amplified) Stokes signal vs no of circulations as a function of input Stokes signal intensity $|S_{in}|^2$:
(a) 1.0 W/m^2; (b) 100.0 W/m^2; (c) 1.0 x 10^4 W/m^2 for: L = 5 m and $|E_{in}|^2$ = 2.3 x 10^6 W/m^2.

Stokes signal. As expected, the time response of the amplifier is considerably less for a higher Stokes input level, which results in a more rapid saturation. As explained earlier, the peak transient output Stokes intensity is again higher than its steady-state value.

7.3. Comparison with other optical amplifiers

As was indicated in the introductory section to this chapter, much research effort has been invested into the field of optical amplification. The important device criteria which have to be considered in assessing amplifier performance parameters are the pump power requirement for sizeable signal gain (greater than 10 dB), noise characteristics, gain bandwidth, required fibre length, sensitivity to polarisation, and operating signal wavelength. A full comparison of these in the context of system requirements, and a review of their advantages and limitations taking into account the current state of research has not been carried out, but a number of qualitative comparative statements can be made which identify in general sense the potential role for Brillouin amplifiers.

Although the optical semiconductor amplifier technology has matured significantly since the realisation of the first GaAs laser diodes, with best reported facet reflectivities around 10^{-6} - 10^{-5}, gain of approximately 30 dB, and saturation output powers of ≈ 5 - 8 dBm at 1.3 - 1.5 μm[3,4], the outlook for the future is not without problems. One of the major tasks which has yet to be realised is the design and fabrication of an optical amplifier that is polarisation independent, as even the best state-of-the-art amplifiers have several dBs gain difference for the TE and TM polarised light, with both the facet reflectivity and internal gain being polarisation dependent[21]. Another potential problem is that of crosstalk in amplifiers due to presence of several transmitted channels, particularly through gain saturation and four-wave mixing. This can present considerable restraints on channel spacing, and maximum output power from the amplifiers. An inherent disadvantage of this type of amplifier is also in the fact that some 10 dB of gain are lost (≈ 5 dB insertion loss per facet) on light coupling to and from the fibre - a figure which is unlikely to be reduced in the near future[21].

The two main single mode fibre amplifier types are nonlinear scattering amplifiers (Raman and Brillouin) and doped fibre amplifiers (primarily erbium doped), all being polarisation

insensitive. For SRS, gains in the range of 30 - 40 dB can be achieved with high power cw or pulsed lasers, at pump powers above 1 W which are clearly not practical for communication applications, although low gain for fibre loss compensation can be achieved using a high power semiconductor laser[22]; this means that practical applications of SRS to optical communications (if any) seem to be limited to signal boosting and distributed gain for loss compensation in very-long-haul links, which is also amenable with soliton propagation, and has been demonstrated for 4000 km link using 300 mW of optical power[24].

High gain (> 30 dB) and low noise have been demonstrated in high bandwidth (≈ 1 THz) erbium doped fibre amplifiers, several metres long, at approximately 30 mW of pump power with saturation powers of around 10 dBm. However to date best performance have has been obtained using impractical argon and dye laser pump sources at wavelengths of 514 and 660 nm, while similar performance has yet to be demonstrated with more realistic solid-state lasers[6,23,25]. Potential pump-bands in the erbium absorption spectrum exist at wavelengths 520 nm, 670 nm, 807 nm, and 980 nm, as well as the recently demonstrated in-band pumping at 1.48 μm. Research indicates that a phenomenon of excited-state absorption (ESA) which drains the pump power and limits the available gain affects the most practical pump band at 807 nm where multi-stripe laser diodes are available, while the other bands at 520, 670 and 980 nm are relatively clear of ESA. Very recently, the operation erbium doped fibre fibre amplifier at 1.48 μm using high power laser diodes was demonstrated by several authors, with best performance of 20 dB gain, at 30 mW pump power and approximately 3 dBm saturation output power[26]. However, the noise characteristics have not been analysed for this pump wavelength, and further work is required to assess the practical feasibility of this solution[25].

In contrast to both of the above, Brillouin amplifiers (the existing results on amplification in long fibres were summarised in Chapter 3), have the advantage of the high gain capability (up to 40 dB in ordinary fibre) at low pump powers (≈ 10 mW) and complete flexibility in the choice of the pump wavelength, and thus are fully compatible with semiconductor laser pumping. Indeed, the pump power levels required in the case of the Brillouin amplifier based on the OFRR as calculated above, are the only ones which comply with the inherent laser safety standards for Class 1 laser as specified by British Telecom and British Standard (BS4803) (approximately - 2.7 dBm of optical power in the fibre at 1.3 μm). The noncompliance with the laser safety standards could ostensibly be permitted in submarine

systems, but in land-based systems it may preclude distributed (remote) amplifier pumping.

Because of the narrow bandwidth SBS gain, which limits the signal bit rate, which in the case of the OFRR based device is also limited by the transient response, it is thought that the most promising application for the SBS amplifier is in densely packed wavelength division multiplexed (WDM) systems or coherent multi-channel systems (CMC) such as the one illustrated in figure 7.11.

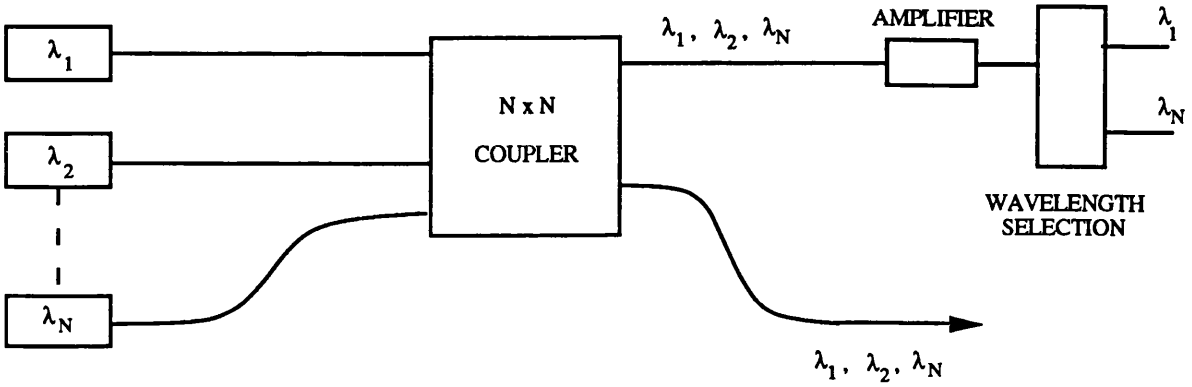

Figure 7.11. Schematic diagram of a coherent multi-channel (CMC) system making use of a Brillouin amplifier.

Indeed, Tkach et al.[27] have demonstrated system capability of a network operating with channel spacing as small as 1.5 GHz (or approximately 3.5 picometers) with 1000 channels at 250 Mbits/s, using commercially available AlGaAs lasers. In comparison, even the most optimistic researchers quote channel spacing of greater than 1 nm (greater than 150 GHz) for the conventionally multiplexed/ demultiplexed WDM systems using DFB lasers at 1.3 -1.5 μm, consisting of typically 16 channels[28]. However the penalty paid in the case of Brillouin amplification within WDM networks is the need for a pump laser per channel. Alternatively, a better utilisation of the Brillouin amplifier would be in CMC applications where N-channels are transmitted along a single fibre, and at the receiver end, the amplifier can than be tuned (by tuning the pump frequency) to select one of the channels, as shown in figure 7.11. In such a case, if the channels are closely spaced, and the amplification covers the transmission bandwidth, a single pump source would be sufficient[28]. Another application of the Brillouin amplifier which exploits its inherent narrow bandwidth is the selective amplification of the carrier component of the received signal in self-homodyne coherent transmission. In applications where modest data rates

would be acceptable, additional benefits could also be achieved by utilising OFRR based Brillouin amplifiers, which could be fabricated from differently doped fibres to provide different Brillouin shifts. [Following the same principle, if operated above threshold, such OFRRs could be used to generate different Brillouin frequencies for applications as local oscillators, using just one pump laser].

Overall, the comparison of different methods of optical amplification reveals that it is unlikely that any method will provide a universal solution, applicable to all types of optical fibre systems. The particular application of any of the amplifier types described will need careful consideration of the system requirements. It has been shown that the OFRR based Brillouin amplifier has the lowest pump power requirements, coupled with favourable noise characteristics. It seems, therefore, that in some applications it may find a niche amongst other fibre amplifiers. However, to be able to assess accurately the advantages and limitations of Brillouin amplifiers, both in long fibres and OFRRs, it would be necessary to carry out a systematic and comprehensive investigation to characterise these device in terms of gain, saturation, and noise parameters: both theoretically (particularly in the case of the former) and experimentally, taking into account gain variation due to depolarisation finite pump linewidth, and modulation.

7.4. Summary and conclusions

In conclusion, a simple model which describes the transient operation of an all-fibre Brillouin laser and amplifier has been developed. The model accounts for pump depletion, and describes the build up of the amplified spontaneous Brillouin noise. The model can be used to predict the Brillouin threshold intensity, cavity gain and saturation - in terms of practical fibre resonator parameters, specifically cavity loop length and the coupling coefficient. It was shown that the transient Stokes intensity in the ring can significantly exceed the steady-state value, and that the steady-state solutions are in agreement with existing steady-state model of the Brillouin laser. Moreover, the theoretically predicted values are in good agreement with all experimentally obtained data on Brillouin thresholds and steady-state values.

It was shown that by pumping the resonator below the Brillouin lasing threshold, it can act as an effective amplifier of signals at the Stokes frequency. The amplifier

calculations yielded a number of important results. Firstly, a high intensity gain is predicted - for a range of very low pump intensities (less than 0.1 mW), and resonators with short loop lengths. Although, the gain is intensity dependent due to the nature of the Brillouin scattering effect, this need not be a shortcoming. By varying the pump intensity to take account of gain saturation, a wide range of signal levels can be amplified, including signals at extremely low power levels (as low as fractions of nanowatts). The corresponding output signal-to-noise ratio is very high (greater than 55 dB), even for very small signals, and improves with increasing signal intensity and loop length.

It was pointed out that there is a trade-off between the time delay of this device and the cavity losses, and consequently, the Brillouin threshold intensity. This means that for resonators with highest finesse - the time delay is longest, approximately 0.1 - 1 μs for a resonator with finesse of 200 and loop length 5 m. This relatively slow time response effectively limits the uses of such an amplifier to applications as a low-frequency power booster for amplification of low intensity signals - with very low pump powers, and in closely spaced WDM or CMC systems. However, further analysis and experimental investigation are necessary to evaluate the usefulness of these devices in this context.

7.5. References for Chapter 7

1 Y. Yamamoto,'Characteristics of AlGaAs Fabry-Perot cavity-type laser amplifiers', IEEE J. Quantum Electron. **QE-16**, 1047 (1980)

2 T. Saitoh and T. Mukai, '1.5 μm GaInAs travelling-wave semiconductor laser amplifier', ibid., 1010 (1987

3 J. C. Simon, 'GaInAs semiconductor laser amplifiers for single mode fibre communications', J. Lightwave Tech. **LT-5**, 1286 (1987)

4 N. A. Olsson, 'Lightwave systems with optical amplifiers', ibid. **LT-7**, 1071 (1989)

5 L. Reekie, R. J. Mears, S. B. Poole, and D. Payne, 'Tunable single mode fibre lasers', ibid. **LT-4**, 956 (1986)

6 D. N. Payne and L. Reekie, 'Rare earth-doped fibre lasers and amplifiers',ECOC'88 conference proc. Part 1, IEE Conf. Publ. 292, 49 - 53 (1988)

7 C. R. Giles, E. Desurvire, J. R. Talman, J. R. Simpson, and P. C. Becker, '2Gbit/s

signal amplification at $\lambda = 1.53$ μm in an erbium-doped single mode fibre amplifier', J. Lightwave Tech. **LT-7**, 356 (1989)

8 K. Mochizuki, 'Optical fibre transmission systems using stimulated Raman scattering: theory', ibid. **LT-3**, 688 (1985)

9 Y. Aoki, 'Properties of fibre Raman amplifiers and their applicability to digital optical communication systems', ibid. **LT-6**, 1225 (1988)

10 Y. Aoki, S. Kishida, and K. Washio, 'Stable cw backward Raman amplification in optical fibres by stimulated Brillouin scattering suppression', Appl. Opt. **25**, 1056 (1986)

11 G. N. Brown, 'Raman fibre amplifier characteristics for use in optical transmission systems', Br. Telecom. Technol. J. **5**, 45 (1987)

12 E. Desurvire, M. J. F. Digonnet, and H. J. Shaw, 'Theory and implementation of a Raman active delay line', J. Lightwave Tech. **LT-4**, 426 (1986); E. Desurvire, M. Tur, and H. J. Shaw, 'SNR in Raman active fibre systems: application to recirculating delay lines', ibid., 560 (1986)

13 A. N. Pilipetskii and V. V. Shkunov, 'Calculation of the threshold and the efficiency of conversion by stimulated Brillouin scattering', Sov. J. Quantum Electron. **15**, 284 (1985)

14 I. Bar-Joseph, A. A. Friesem, E. Lichtman, and R. G. Waarts, 'Steady and relaxation oscillations of stimulated Brillouin scattering in single mode fibres', JOSA B **2**, 1606 (1985)

15 J. Botineau, C. Leycouras, C. Montes, and E. Picholle, 'Stabilisation of a Brillouin fibre laser by strong pump modulation'ibid. **6**, 300 (1989)

16 P. Bayvel, J.M. Halley, R. Kadiwar, and I. P. Giles, 'Theoretical and experimental investigation of an all-fibre Brillouin laser', ECOC'88 conference proc. Part 1, IEE Conf. Publ. 292, pp 189 - 192

17 P. Bayvel and I.P. Giles, 'Linewidth narrowing in a semiconductor laser pumped, single mode all-fibre Brillouin laser', Electron. Lett. **25**, 261 (1989)

18 M. Kemmler, K. Kempf, and W. Schroeder, paper WBB6 in OFS'85 Technical Digest, pp 121-122

19 R. M. Shelby, M. D. Levenson, and S. H. Perlmutter, 'Bistability and other effects in a nonlinear fibre-optic ring resonator', JOSA B **5**, 347 (1988)

20 R. I. Laming, P. R. Morkel, D. N. Payne, and L. Reekie, 'Noise in erbium-doped fibre amplifiers', ECOC'88 conference proc. Part 1, IEE Conf. Publ. **292**, pp 54 - 57

21 N. A. Olsson, AT&T Bell Laboratories (Murray Hill): personal communication, 1989

22 Y. Tamura, S. Shikii, H. Maeda, E. Nishimura, and K. Kawahara, 'Fibre Raman amplifier module with semiconductor laser pump source', ECOC'87, Conf. proc. 62 - 65

(1987)

23 R. I. Laming, M. C. Farries, P. R. Morkel, L. Reekie, D. N. Payne, P. L. Scrivener, F. Fontana, and A. Righetti, 'Efficient pump wavelengths of erbium-doped fibre optical amplifier', Electron. Lett. **25**, 12 (1989)

24 L. F. Mollenauer and K. Smith, 'Demonstration of soliton transmission over more than 4000 km in fibre with loss periodically compensated by Raman gain', Opt. Lett. **13**, 675 (1988)

25 E. Desurvire, AT&T Bell Laboratories (Crawford Hill): personal communication, 1989

26 P.C. Becker, J. R. Simpson, N. A. Olsson, and N. K. Dutta, 'High gain and high efficiency diode laser pumped fibre amplifier at 1.56 μm', IEEE Phot. Tech. Lett. **1**, 267 (1989)

27 R. W. Tkach, A. R. Chraplyvy and R. M. Derosier, 'Performance of a WDM network based on stimulated Brillouin scattering', Phot. Tech. Lett. **1**, 111 (1989)

28 Ayman El-Fatatry, Optical Fibre Division, GEC Hirst Research Laboratories: personal communication, 1989

Chapter 8

FOUR WAVE MIXING PROCESSES IN BRILLOUIN LASERS

As briefly described in the chapter on the overview of work in optical fibres, Brillouin lasers have attracted much interest for frequency generation. Generation of several Stokes and anti-Stokes components by four wave mixing (FWM) process have been shown in long (greater than 20 m) hybrid bulk/fibre cavities at pump powers of hundreds of milliwatts[1-3]. Potentially, as in the case of the Brillouin laser discussed in Chapter 6, this could be a very useful technique for optical generation of very high frequencies by mixing Stokes and anti-Stokes optical frequency components on a square-law photodetector, particularly if this could be shown at low pump powers. For example, the Brillouin shift at the pump wavelength of 830 nm is 20 GHz. Thus, heterodyning just the 2nd order Stokes and first order anti-Stokes components will result in the generation of a spectrally narrow signal at 60 GHz, and higher at shorter pump wavelengths because of the λ^{-1} dependence of the Brillouin shift.

In this chapter we describe the experiments carried out to observe the nondegenerate FWM in a single mode OFRR. In this process, the signal at the anti-Stokes frequency (disallowed in the normal SBS process because of phase matching restrictions) was generated by mixing the pump and the first two Stokes Brillouin shifted frequencies, at low pump powers. In the second half of this chapter we describe the process known as Brillouin enhanced four wave mixing (BEFWM), observed for the first time in fibres in this work. BEFWM has been shown to be tremendously promising as a phase conjugation technique in which a very high reflectivity is achievable. The physics of the process shall be discussed, and we shall show that BEFWM in fact represents an extension of the type of FWM process described in Section 8.3.

8.2 Theory of the nondegenerate FWM

In the nondegenerate FWM process[4,5], frequency ω_4 can be generated by mixing of frequencies, ω_1, ω_2, and ω_3:

$$\omega_4 = \omega_1 + \omega_2 - \omega_3 \qquad (8.1)$$

through the real part of the third order electronic susceptibility χ_3. Physically, the FWM process can be explained as follows. When two intense light beams beams of ω_2 and ω_3 propagate in an optical fibre, the fibre refractive index is modulated at the beat frequency (ω_2 - ω_3) and this periodic index variation (or a grating) in turn modulates a third signal at ω_1, so that $\omega_4 = \omega_1 + (\omega_2 - \omega_3)$. In degenerate FWM $\omega_2 = \omega_1$, and $\omega_4 = 2\omega_1 - \omega_3$. Conservation of momentum is necessary for most efficient frequency generation, so that: $\mathbf{k}_4 = \mathbf{k}_1 + \mathbf{k}_2 - \mathbf{k}_3$. In general, no power threshold is necessary for observation of FWM.

Although in single mode fibres material dispersion prevents complete phasematching, approximate phase matching can be attained over significant lengths of fibre for small frequency shifts. The field intensity at the output frequency ω_4 strongly depends on the phase mismatch, ΔkL, expressed in terms of the coherence length, $L_{coh} = \pi/\Delta k$. Efficient FWM at low pump powers requires long coherence lengths, and it can be shown that[4],

$$L_{coh} = \frac{4\pi^2 c^2}{2\lambda(\Delta\omega)^2 D(\lambda)} \qquad (8.2)$$

where $\Delta\omega$ is the frequency difference between the components being mixed, λ is the wavelength, and $D(\lambda) = \lambda^2 d^2n/d\lambda^2$ is the material dispersion function which equals 0.08 at 514.5 nm[4]. The power of the signal generated via the FWM process follows the dependence[4,5]: $P_4 \propto \chi_3^2 P_1 P_2 P_3 L_{eff}^2$, where L_{eff} is the effective interaction length, $L_{eff} = (1 - \exp - 2\alpha_o L)/2\alpha_o$, and $(2\alpha_o)$ is the fibre attenuation coefficient.

8.2. Experimental observation of FWM in an OFRR

The experimental set up used to investigate the FWM process is shown schematically in figure 8.1.

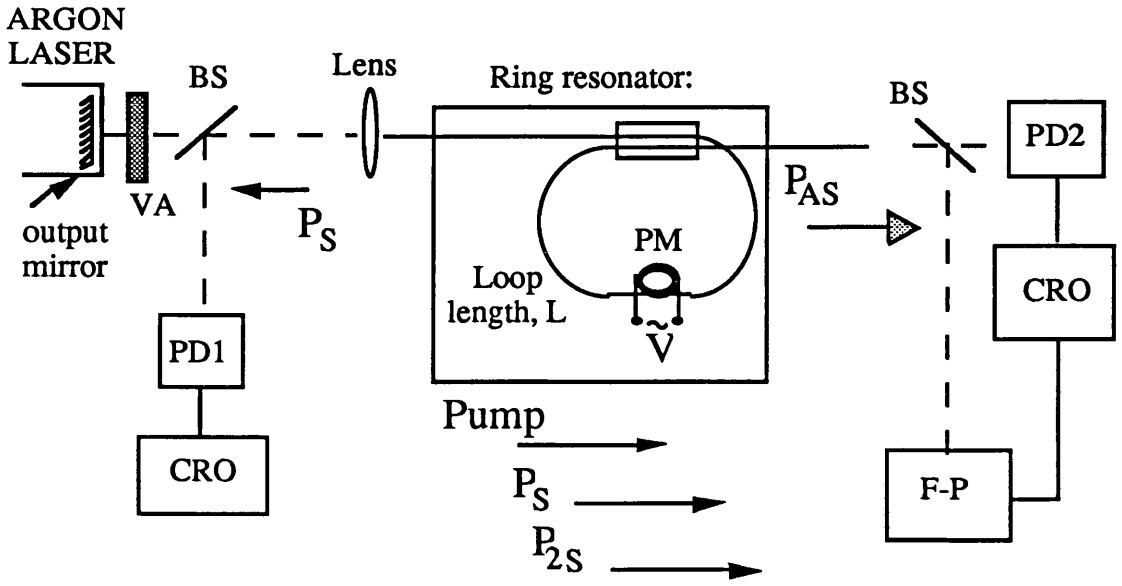

Figure 8.1. Schematic diagram of the experimental set up used for observation of FWM: PM - phase modulator; F-P - scanning Fabry-Perot, VA - variable attenuator.

A cw argon-ion laser with an intracavity étalon to provide single frequency operation at 514.5 nm was used as the pump. The spectral linewidth of the laser was approximately 1 MHz at output powers of up to 2 W. The ring resonator used was fabricated from York polarisation maintaining single mode fibre at 600 nm, with measured attenuation loss of 22 dB/km at 514.5 nm, loop length 4 m and a measured finesse of ≈ 30. The launch efficiency was approximately 60%. As before, the nonlinear increase in the level of the first-order backscattered Stokes power was monitored by the photodiode PD_1, and displayed on a CRO. In the absence of an isolator between the input fibre end and the laser, the Stokes signal was reflected by the output mirror of the argon laser (reflection coefficient of approximately 70%) and coupled back into the fibre. The output power from the resonator is detected on a photodiode, PD_2 and a scanning

Fabry-Perot to monitor the spectral content of transmitted light. Because the magnitude of the Brillouin shift is considerably larger the gain bandwidth (≈ 5 GHz) of the argon laser, the counterpropagating Stokes signal coupling into the argon-ion laser cavity does not significantly perturb the oscillating mode, as was confirmed experimentally.

Initially, the polarised laser output power was aligned along the direction of the slow axis, and the variation of the backscattered Stokes power with pump power was measured on the confocal Fabry-Perot; the Brillouin threshold for the first Stokes component was measured at 2.4 mW of optical power in the fibre. This is in agreement with the value of 2.26 mW calculated using the theory of SBS lasing as derived in Chapter 6. The Stokes shift, $\Delta\omega_B$ was measured as 33.8 GHz, and is in good agreement with the calculated figure of 34 GHz. The confocal Fabry-Perot was then aligned for measurement of the output power of the resonator. As the pump power was increased (using a variable attenuator), the circulating Stokes power builds up until the threshold for second order Stokes is reached, and for powers of above 12.2 mW in the fibre, second order Stokes component, propagating in the forward direction, was detected. This value is threshold power is somewhat higher than the predicted value of 9.1 mW. The reason for this is that the resonator was detuned for high conversion efficiency, so that the finesse, and the corresponding enhancement of the pump power circulating in the loop over the input power in was reduced for with increase in the pump power, through pump depletion by the growing Stokes power. Almost concurrently, the generation of a forward propagating anti-Stokes component was detected, in conjunction with eqn (8.1),

$$\omega_{AS} = \omega_P + (\omega_P - \Delta\omega_B) - (\omega_P - 2\Delta\omega_B) = \omega_P + \Delta\omega_B \qquad (8.3)$$

where ω_p and ω_{AS} are the pump and anti-Stokes frequencies, respectively.

The Fabry-Perot spectra of the resonator output, measured at just above the pump power of 12.5 mW are shown in figure 8.2. The variation of the output powers for the detected frequencies with input pump power is shown in fig. 8.3. Significantly above the threshold

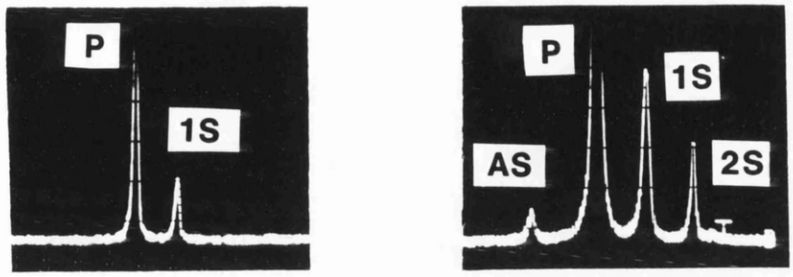

(a) (b)

re 8.2. Output spectra from the ring resonator for a range of input ers: (a) below 12.5 mW; (b) above 12.5 mW, showing the pump, xes, and anti-Stokes frequencies. The Brillouin shift is 33.8 GHz.

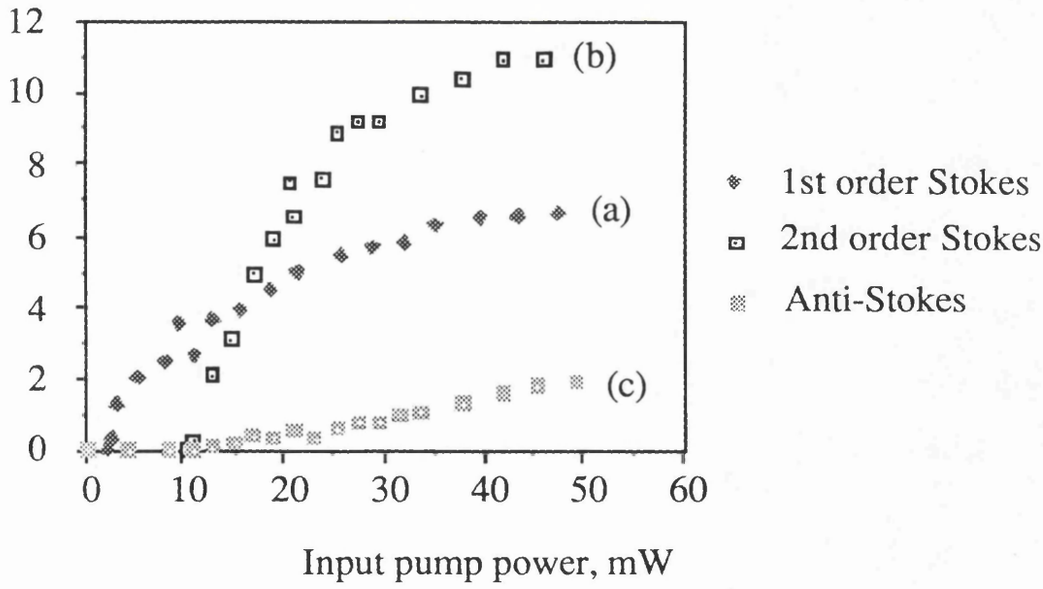

Figure 8.3. Typical variation of the powers for the frequencies output from the ring resonator as a function of the input pump power: (a) 1st order Stokes; (b) 2nd order Stokes; (c) Anti-Stokes. All the power launched in the direction of the slow axis (smaller A_{eff}).

for the second order Stokes, it can be seen that the level of the first order Stokes power is lower than the second order Stokes, since the former is scattered backwards.

The generation of the anti-Stokes power exhibited a threshold, in agreement with the FWM power dependence, that is, starting only after the threshold for the second order Stokes has been exceeded. [It must be pointed out, however, that in this case the constant of proportionality is not the *electronic* susceptibility χ_3 (for fused silica $\approx 0.6 \times 10^{-33}$ Cm/V^3, or in the esu system still used in much of the literature: $\approx 0.5 \times 10^{-14}$ cm^3/erg) which is used to describe the fast nonlinearities, such as degenerate FWM in optical glasses, as explained below]. The conversion efficiencies of the pump power into the first-, second order Stokes, and anti-Stokes signals at the maximum input pump power of 50 mW were measured to be approximately 24% (in the direction counter to the pump), 21%, and 5% respectively. Clearly, a higher conversion efficiency can be expected, and will be observed at lower pump power, for resonators with a higher finesse. The fibre input end was then rotated to launch the pump power along the orthogonal fast axis, having a larger effective core area, A_{eff}, as already described in Chapter 6. The measurements were repeated, and as expected, higher thresholds for the 1st order Stokes, and 2nd order Stokes, and correspondingly anti-Stokes powers were observed. For the same launch efficiency of 20%, the threshold for the first-order Stokes generation was measured at 4.4 mW of pump power in the fibre - approximately a factor of 1.8 higher than for the case of slow axis, implying that the ratio of the effective areas for the two principal axes was approximately 1.8; the second-order Stokes (together with the anti-Stokes) threshold power was measured a 22.1 mW. It can be verified from figure 8.4 that the variation of the respective output powers follows the same dependence as for the case of the 100% of the pump power launched along the direction of the slow axis. Over the correspondingly higher range of input powers, similar conversion efficiencies were measured for the three waves, as 23%, 20.5%, and 4%, respectively for the 1st- order, 2nd-order Stokes, and the anti-Stokes waves.

As the level of the input pump power is relatively high, the high intensity in the fibre was accompanied by significant heating, which presented two experimental difficulties.

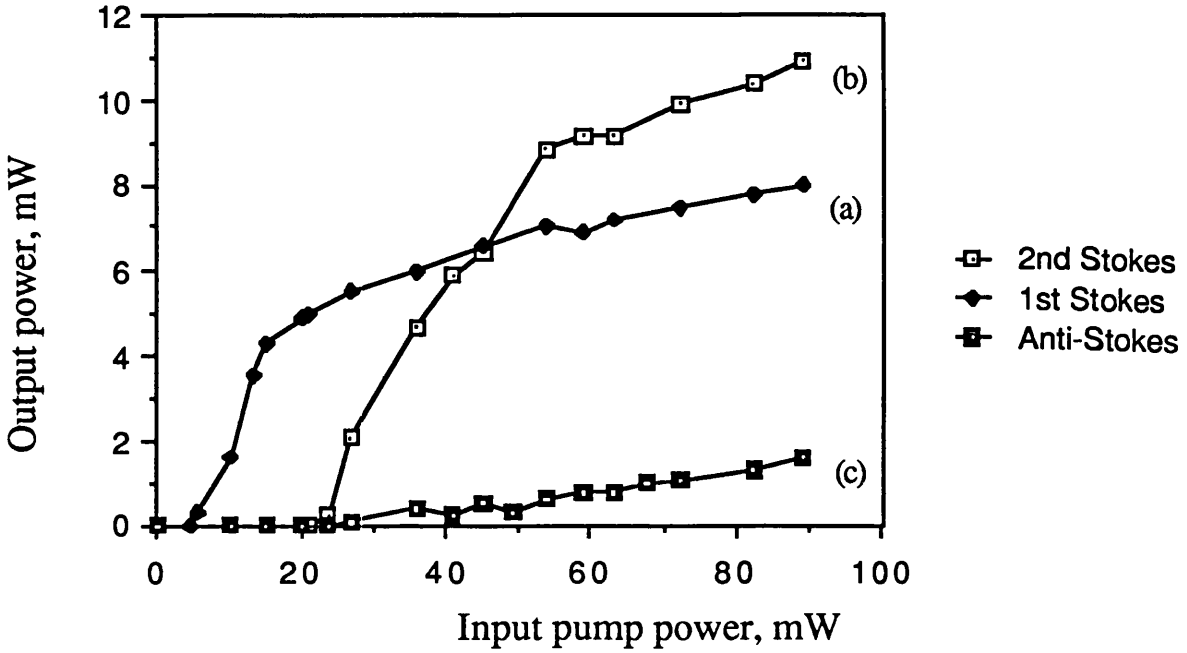

Figure 8.4. Typical variation of the powers for the frequencies output from the ring resonator as a function of the input pump power: (a) 1st order Stokes; (b) 2nd order Stokes; (c) anti-Stokes. All the power launched in the direction of the fast axis (larger A_{eff}).

Firstly, the approximate finesse of 30 results (from resonator theory, Chapter 4) in the enhancement of the circulating pump power over the input pump power of approximately a factor of 10. At lower levels of the input pump power, the heating in the coupler due to the high level of the circulating intensity resulted in the heating of the index matching oil, changing its refractive index (according to temperature dependence of the refractive index of dn/dT of $\approx$ - 0.0005/^{o}C), and necessitating retuning of the coupler, and as the pump power was further increased, the change of oil to a higher index one. Secondly, in earlier experiments the heating associated with the high circulating intensity resulted in the destruction of the coupler in a resonator with similar characteristics to the one above at a pump power of approximately 60 mW in the fibre (launched along the direction of the slow axis), corresponding to the circulating power of greater than 0.5 Watt!! After the examination of the coupler under the microscope, severe nonuniformities and buckling of the fibre in the interaction region were observed, which were thought to be due to the possible melting of the epoxy , and resulting in the

deformation, and subsequent buckling of fibre, particularly susceptible to strains in the polished region. Indeed, these constraints present another motivation for using high finesse resonators and low pump powers in practical devices. Governed by this the input pump power was not increased above 50 mW for the slow axis (and 90 mW for the fast axis).

Over the range of applied input powers, only two Stokes orders and one anti-Stokes order were detected, but it is thought that in principle (provided the destruction of the coupler could be prevented) a number of anti-Stokes orders can be detected at higher pump powers[1-4]. This, however, may not be immediately obvious from the simple consideration of the phase matching. In a ring resonator, the coherence length can not be compared directly to the actual loop length because of the multiple recirculations in the loop. However, the effective length, L_{eff} is limited by the fibre attenuation and coupler losses in the loop. From transient resonator theory of the passive resonator (as derived in Chapter 7) and for the Brillouin laser, described in Chapter 6, the number of circulations is calculated as approximately 100, leading to $L_{eff} \approx 400$ m (a similar result is arrived at by assuming the fibre attenuation being the dominant factor and letting $L_{eff} = 1/2\alpha_o \approx 400$ m for the fibre used). A comparable figure is arrived at for the coherence length calculated from eqn (8.2) with $\Delta\omega = \Delta\omega_B = 2\pi$ x 33.8 GHz (rads). Hence, initially, it is possible to conclude that anti-Stokes lines of higher than first order can not be efficiently generated due to phase mismatching. Indeed, this reasoning was originally suggested by Hill et al[4] to explain the early results on frequency generation by FWM in optical fibres. However, a closer examination of the physics of this process reveals that the phase matching mechanism in this FWM process, and the process itself, are different to conventional nondegenerate FWM process as observed, for example in optical glasses or liquids[4-9].

Primarily, it should be pointed out that the proportionality constant for the generation of new frequencies as a result of four wave mixing is not the *electronic* susceptibility χ_3, as already mentioned above. The reason for this is that the electronic susceptibility is generally used to describe fast nonlinearities ($\approx$ picoseconds), where the polarisation adiabatically follows the electric field such as formation of gratings in optical glasses and liquids, and the term *electronic* refers to the fact that the refractive index variation (or the resultant grating) is due to the redistribution of electrons caused by the modulating field[10,11]. In our case, the formation of a grating is not governed by the electronic

distribution, but rather by density variation, or the process of electrostriction. Indeed, because the frequency separation of the three waves (pump, 1st Stokes, and 2nd Stokes) that generate the anti-Stokes is by integer multiples of the Brillouin shift, then there is *resonant* coupling to the acoustic phonon field. One can, in fact, think of the interference grating being formed between the 1st and 2nd Stokes components, at the acoustic frequency, and propagating counter to the pump field (in contrast to the acoustic field which results from the scattering of the pump field into the 1st Stokes , which propagates in the same direction as the pump field). A pump field photon then scatters from this acoustic grating gaining the energy from the acoustic phonon to become an anti-Stokes phonon. The process is then pseudo phase-matched as in eqn 8.3.

In other words, the mechanism by which the anti-Stokes wave is generated is effectively the same, *once the 1st and 2nd Stokes are present*, to the SBS process by which the Stokes components are generated, both in conversion efficiency and power level requirements[12], which is confirmed by the anti-Stokes generation starting almost concurrently with the threshold for the 2nd order Stokes. It is thought that the waves not separated in frequency by integer multiples of the Brillouin shift would not be as efficient at generating the first order anti-Stokes wave equivalent because of the absence of resonance with the acoustic field. In this sense, higher powers are required to observe the non-resonant (electronic) four wave mixing[6] than in this resonantly enhanced process. The proportionality constant governing the power dependence in our case, would then be some complex function of the third order nonlinear susceptibility χ_3' (written in *italics* to differentiate it from the electronic susceptibility), resonantly enhanced through the coupling to the acoustic field[11]. This same mechanism is exploited in the Brillouin enhanced four wave mixing process which is described in the next section.

8.3. Brillouin enhanced four wave mixing (BEFWM) in an all-fibre ring resonator

8.3.1. Theory of BEFWM

As we saw in the previous section, Brillouin nonlinearity can enhance the process of frequency generation through FWM. In this section we describe the experimental

observation of a different four wave mixing process in all-fibre ring resonators at low pump powers. It is believed that this particular four wave mixing process represents the fibre equivalent to the process observed in liquids and known as the Brillouin enhanced four wave mixing (BEFWM)[13-17], and is the first observation of this process in optical fibres. The principal difference between the BEFWM process reported here and the frequency generation associated with the FWM process described in the last section, is in the fact that in the latter, the three waves being mixed are all generated *within* the resonator, whereas in the BEFWM process, the mixing can occur between waves, with one or more of which can be *externally* generated, and having appropriate (Brillouin)frequency shifts, as described below. In a way, the BEFWM process represents an extension of the resonantly enhanced FWM process described above.

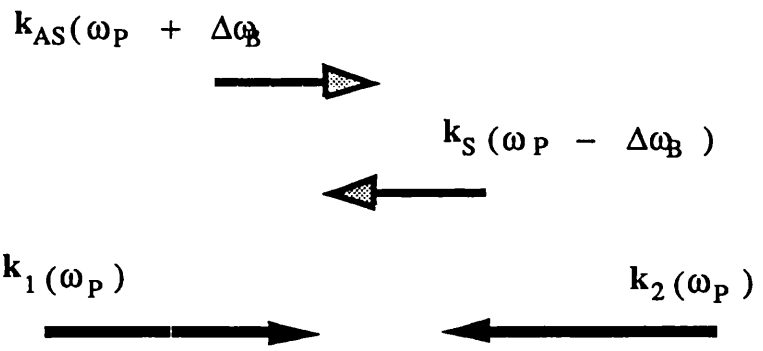

Figure 8.5. Propagation of the four waves in the BEFWM process. $\underline{k}_1$ and $\underline{k}_2$, are the wave vectors of pump beams 1 and 2; $\underline{k}_S$ is the wave vector of the Stokes shifted wave, and and $\underline{k}_{AS}$ - of the anti-Stokes wave conjugate wave. The acoustic grating in the process propagates co-directionally with $\underline{k}_1$.

BEFWM is a technique which has recently been receiving considerable attention because of its ability to achieve phase conjugation with extremely high reflectivities (up to 10^5 - 10^6) using high power pulsed lasers. The advantage of this technique over the conventional SBS method of phase conjugation as described in Chapter 2, is that in the latter the reflection coefficient is limited to 1 (or 100%). In addition, it has been suggested that this method has advantages over the conventional FWM in a number of respects, primarily because the conditions required to produce high reflectivities in the BEFWM process are considerably relaxed as compared to the FWM process, where the

fulfillment of extremely precise conditions and and high quality beams are necessary[6,13,16].

The technique is a form of nearly-degenerate four wave mixing in which the four waves are coupled by the Brillouin nonlinearity. In this process (schematically illustrated in figure 8.5) the incoming signal beam, wave vector $\mathbf{k}_S$ (frequency, ω_S) has a Brillouin frequency shift, $\Delta\omega_B$ ($\omega_S = \omega_P - \Delta\omega_B$) with respect to one of the pump beams, wave vector $\mathbf{k}_1$, (frequency - ω_P), so that the interference pattern they produce moves at close to the acoustic velocity and drives an acoustic wave. This moving acoustic grating scatters the incoming second pump beam $\mathbf{k}_2$ (ω_P) to form the conjugate beam, which will have a frequency,

$$\omega_{AS} = \omega_P + \omega_P - \omega_S = \omega + \Delta\omega_B \tag{8.4}$$

that is, it will have an anti-Stokes shift relative to the pump frequency. Alternatively, the generation of the anti-Stokes wave can be viewed as the second pump P2 acquiring a positive Doppler shift through being scattered by the acoustic grating moving towards it. With reference to the above discussion, the signal beam can either be generated through the SBS process within the mixing medium, or input externally.

Clearly, this process is not phase matched since the two wave vectors $\mathbf{k}_{AS}$ and $\mathbf{k}_S$ have different magnitudes, and the magnitude of the phase mismatch, $\Delta\mathbf{k}L$, is given by:

$$|\Delta\mathbf{k}L| = \frac{n}{c}\{\omega_P + \omega_S - \omega_P - \omega_{AS}\}L = \frac{2n}{c}\Delta\omega_B L \tag{8.5}$$

where L is the length of the interaction region. The described configuration, in which a Stokes shifted signal is used, has the advantage over an analogous BEFWM configuration which uses an anti-Stokes shifted signal (to result in a Stokes shifted conjugate) in providing the maximum sensitivity in a BEFWM mirror, - thus allowing the conjugation of very small signals. For further details, the reader is referred to a very thorough and comprehensive review of BEFWM given by Scott and Ridley (Ref. 16).

Generally, experimental studies of BEFWM has been carried out in highly multimode

glass waveguide cells filled with CS_2 with a Brillouin shifted beam generated in a separate cell. Because the BEFWM cell is very short (approximately 10 cm) pulsed lasers with very high pump powers (peak powers greater than 1 MW) have to be used. However, because of much smaller interaction areas and increased interaction lengths, the use of optical fibres will allow the Brillouin nonlinearity to develop at considerably lower powers. On the other hand, longer interaction lengths result in a higher phase mismatch, which has the effect of reducing the acoustic coupling, and hence, the conjugate reflectivities achievable. Bearing this in mind, the demonstration of BEFWM in optical fibres gives a very useful indication of physical limits of this process.

8.3.2. Experimental observation of BEFWM

The schematic diagram of the experimental set up used is shown in figure 8.6. The same cw argon-ion laser with an intracavity etalon to provide single frequency operation at 514.5 nm, as above was used as the pump. The ring resonator used was made from York polarisation maintaining single mode fibre at 600 nm with loss of 22 dB/km at 514.5 nm, loop length 1 m, with finesse of approximately 25 at this wavelength. We used this particular resonator as it had the shortest available loop lengths, in order to minimise the phase mismatch. The second pump beam was provided by reflecting the transmitted pump (P1) by the mirror M. The level of P_2 was monitored on a photodetector PD1. The Stokes wave was generated in the resonator, and detected on a photodetector and a scanning Fabry-Perot. Indeed, this configuration of the Stokes shifted signal beam propagating counter to the strong pump beam has been shown to have the advantage of maximum sensitivity in the BEFWM process[16].

An isolator comprising of a polariser and a $\lambda/4$ plate was inserted to minimise back reflections into the laser. The fibre launch was misaligned - in order to prevent the coupling of the Stokes and pump light into the laser cavity, and being reflected and re-injected back into the resonator, resulting in 'conventional four-wave mixing', as described in the earlier section. This, however, had the effect of reducing the launch efficiency to approximately 20%. The $\lambda/4$ plate (equivalent to $\lambda/2$ after double pass) in front of the mirror M is used to vary the polarisation state of the pump beam, P2 in order to verify that the process observed was indeed BEFWM. The forward propagating phase conjugate anti-Stokes signal was deflected by a beamsplitter onto a photodetector

PD2 and a scanning Fabry-Perot which was used to measure its frequency shift.

Its polarisation state was also monitored by an additional λ/4 plate and a polariser. The use of polarisation maintaining fibre prevented polarisation scrambling, allowing accurate measurement of the transmitted state of polarisation.The Brillouin threshold for the first Stokes component was measured at approximately 12 mW of optical power in the fibre. This figure is in good agreement with theoretically calculated figure of 11.54 mW calculated using equations derived in Chapter 6. As the pump power was increased to 100 mW in the fibre, an output conversion efficiency (ie the ratio of the input pump power, P_1, and the output Stokes power P_S) of approximately 18% was obtained. The internal conversion efficiency is somewhat higher, since only $(1 - k^2)$ of the Stokes power circulating in the ring couples out, where k^2 is the resonator coupling coefficient as before, and is approximately equal to 0.9 for F = 25.

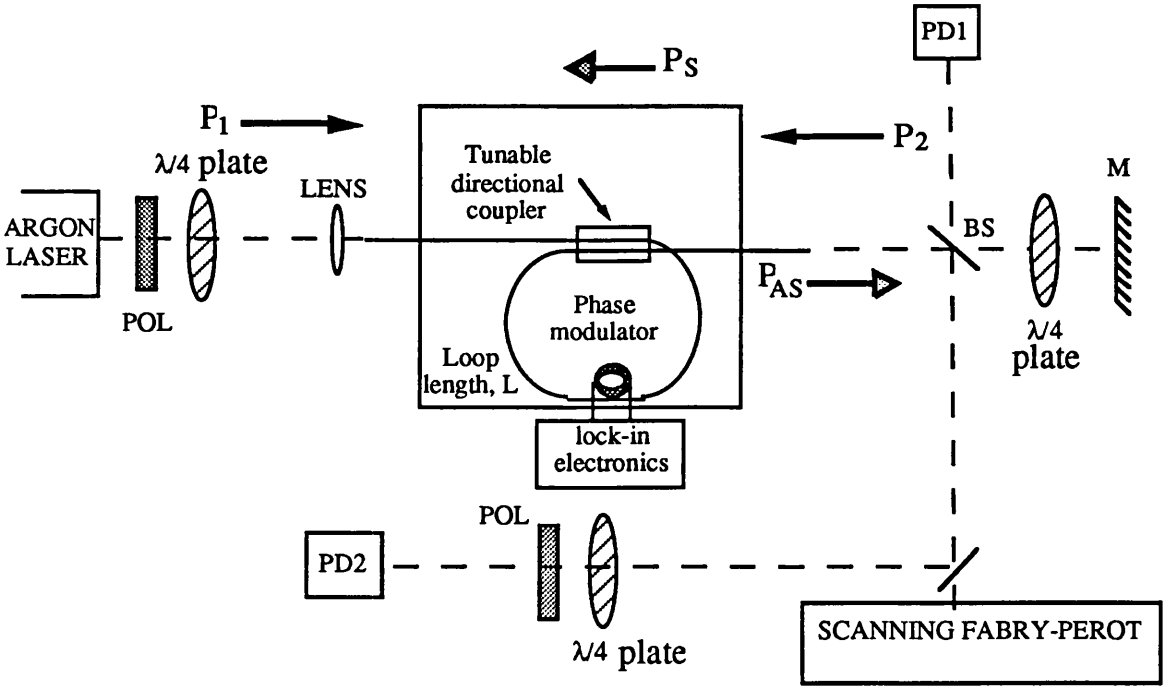

Figure 8.6. Schematic diagram of the experimental set up used for the observation of BEFWM in an OFRR; POL - polarizer, BS - beamsplitter, M - mirror.

The measured variation of the Stokes output power with input pump power is shown in fig. 8.7 (a).

Although the resonator response was electronically locked to the transmission minimum, the increase in the Stokes level represents an additional loss, and tends to detune the cavity. This detuning varies the level of the transmitted pump power, $P_{1,\,out}$, and hence P_2, and was continually monitored. Over the range of pump powers used $P_2 \approx 0.05$ - 0.1 x P_1. There was no significant variation in the measured reflection coefficient with these values of P_2. It should be pointed out that the level of P_2 is below the Brillouin threshold.

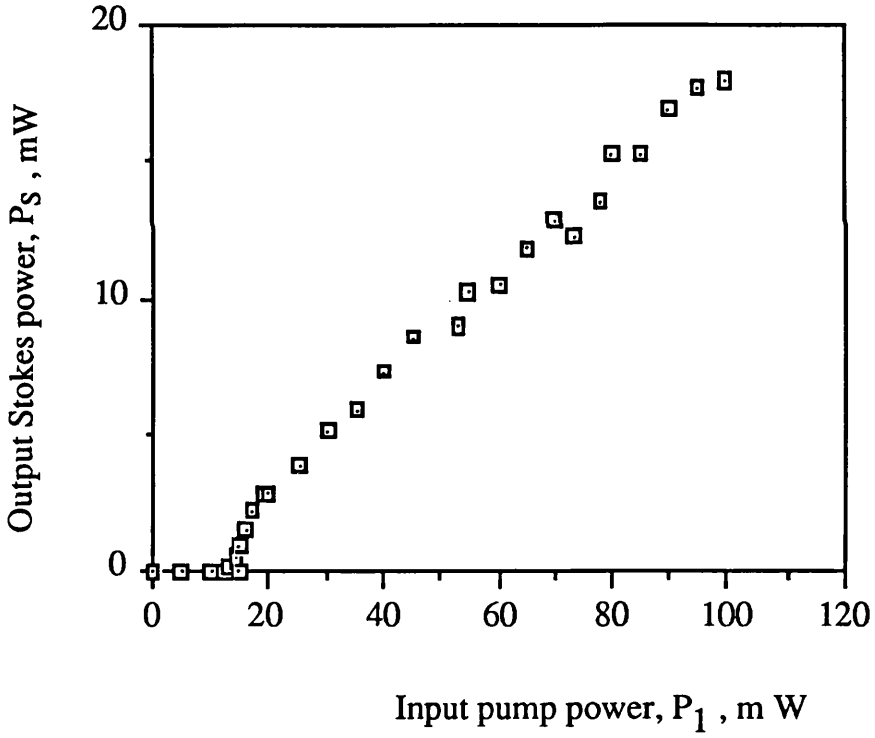

Figure 8.7 (a). Typical variation of the output Stokes power with pump power, P_1.

As the pump power was further increased, at approximately 40 mW of input pump power in the fibre, the start of the anti-Stokes generation was detected. The variation of the anti-Stokes signal output power with input pump power was measured , and is

shown in figure 8.7 (b).

It can be seen that the growth of the anti-Stokes conjugate signal also exhibits a well-defined threshold. This is expected, since the conjugate intensity, $|E_{AS}|^2 \propto |E_{P1}|^2|E_{P2}|^2|E_S|^2$, and the generation of the anti-Stokes component starts when $|E_S|^2$ is significantly above threshold. The constant of proportionality in this case is also, as discussed earlier, some complex function of the third-order susceptibility χ_3.

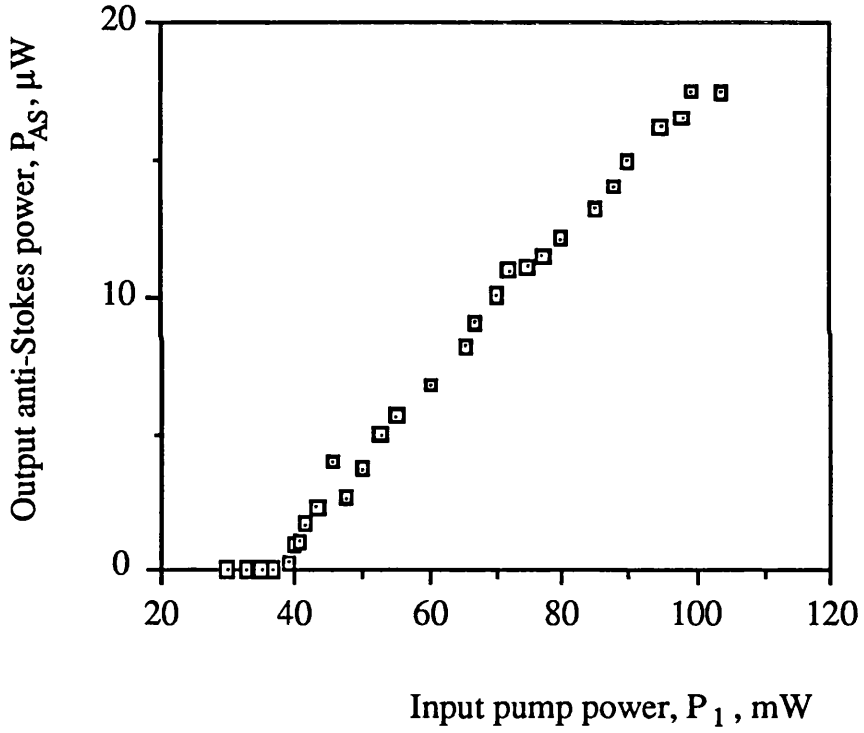

Figure 8.7 (b). Variation of the conjugate anti-Stokes output power with input pump power, P_1.

It was experimentally verified that the polarisation state of the anti-Stokes signal was the same as that of the weak pump P_2. Because the polarisation maintaining fibre used was linearly birefringent, it was not possible to perform experiments to measure unambiguously the ellipticity of the anti-Stokes signal. Ideally, it would be desirable to establish the handedness of the anti-Stokes signal by varying the ellipticity of the

polarisation of the input pump, P_1. Since a phase conjugate mirror behaves just like a conventional mirror by reversing the handedness of circular and elliptical polarisation[16], polarisation measurements are used to indicate the quality of the phase conjugation process.

The spectral characteristics of the resonator output were analyzed on the Fabry-Perot and are shown on figure 8.8. The Fabry-Perot trace shows the transmitted pump, residual Stokes (reflected by the fibre end), and the conjugate anti-Stokes signal. The Stokes shift was measured to be approximately 33.8 GHz which is in good agreement with the value measured in FWM experiments, described in section 8.2.

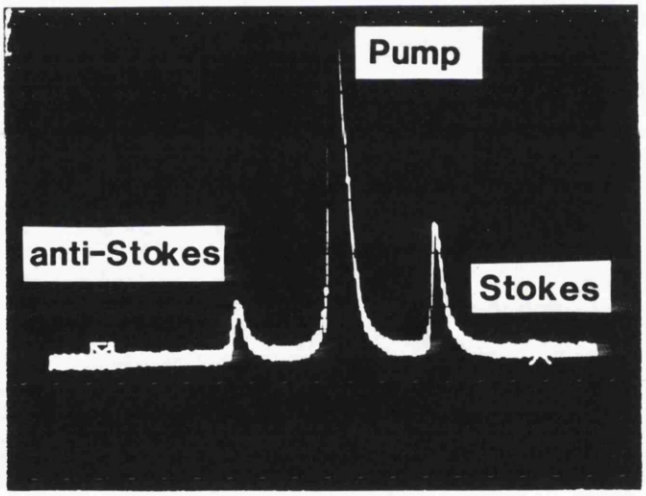

Figure 8.8. Output spectra from the scanning Fabry-Perot showing the transmitted pump, residual Stokes and the conjugate anti-Stokes frequencies.

The reflection coefficient, $R = |E_{AS}|^2/|E_S|^2$ can be deduced from the above graphs to be approximately equal to 0.001. This result for the reflectivity needs some further discussion. In general, the reflectivity in the BEFWM process must be computed.

Following Scott's approximations[17], at low intensities $g_B|E_{P1}|^2L$, $g_B|E_{P2}|^2L << 1$,

$$R = g_B^2|E_{P1}|^2|E_{P2}|^2L^2\mathrm{sinc}^2\{\frac{\Delta kL}{2}\} \tag{8.6}$$

where g_B is the peak Brillouin gain coefficient equal to 4.6×10^{-11} m/W. Using our values this yields a reflection coefficient of the order of 10^{-6}, since the phase mismatch over one resonator loop, $L - \Delta kL$, is very high (approximately $600\ \pi$). However, since the intensity of the strong pump is high, resulting in $g_B|E_{P1}|^2L > 1$ (typically between 1 and 5), a more useful indication of the maximum steady state reflectivity may be the expression $|E_{P1}|^2/|E_{P2}|^2$ (ref. [17]) which however assumes a very small phase mismatch ($< \pi$). In our case, since the $|E_{P1}|^2 \approx 0.05 - 0.1\ |E_{P2}|^2$ so that the maximum reflection coefficient would be 10 - 20.

In our case, a reflection coefficient of 0.001 was obtained. This is considerably higher than would be expected on the basis of the above estimate with a very high phase mismatch. This can be explained by the fact that the build up of the acoustic wave, and the scattering off it takes place over a distance much shorter than the total interaction length, since maximum coupling occurs when the acoustic and Stokes waves have reached their maximum intensity. This would tend to occur over a much shorter distance, at the front end of the resonator (since the Stokes wave propagates counter to the strong pump, P_1). In this way, the effective phase mismatch which corresponds to this shorter interaction length and would therefore be considerably reduced, particularly at higher pump (P_1) intensity, and for resonators with higher finesse. The foregoing discussion just provides an additional explanation of the apparent pseudo phase matching associated with this process in which the frequency generation is enhanced by the Brillouin nonlinearity through the resonant coupling to the acoustic field[18].

In fact, the highest reflectivities reported in the BEFWM process have been explained to be the result of an instability in which the conjugate intensity grows exponentially in time until pump depletion prevents further growth. This will be true providing the pump beams exceed a certain intensity ($g_B|E_{P1}|^2L > 25 - 30$), and are of long enough duration (in the case of pulsed lasers). However, since in our case the scattering occurs below this instability threshold, this fact (in addition to the high phase mismatch) will contribute to the low value for the reflection coefficient.

8.4. Summary and conclusions

We have observed FWM in an all-fibre ring resonator for the first time. The threshold for the generation of anti-Stokes component was approximately 12 mW which is an order of magnitude lower than previously demonstrated, and expected to be considerably lower for resonators with higher finesse. The phase matching and efficiency in the FWM process of several Brillouin orders were discussed, and the difference between this process and the conventional FWM process resulting from fast nonlinearity governed by the electronic susceptibility, was explained. Specifically the former process is more efficient (and thus can be observed at lower optical powers) as the proportionality constant governing the frequency generation is resonantly enhanced through the acoustic field coupling. The potential application of this process is in an all-fibre generation of very high microwave frequencies, at low pump powers.

A four wave mixing process believed to be the BEFWM process below the instability threshold has been observed in an all-fibre ring resonator. This is believed to be the first observation of BEFWM in optical fibres. The fibre resonator allows the use of significantly lower pump powers than previously measured. The Stokes shifted signal was generated in the ring, and the threshold for generation of the conjugate anti-Stokes signal was measured at 40 mW. Despite a very high phase mismatch associated with the long interaction length and high Brillouin shift, a reflection coefficient of 0.001 was measured, and it is expected that a much higher reflection coefficient would be achievable at higher pump powers and higher resonator finesse. These experiments give a useful insight into the absolute physical limits associated with this process. In optical fibres, phase conjugation through BEFWM can be used, for example, in image transmission[19,20] using an all-fibre phase conjugator. However, further investigations into the physics of the process, and particularly measurements of phase conjugation fidelity, are necessary.

8.5. References for Chapter 8:

1 B. S. Kawasaki, D. C. Johnson, Y. Fujii, and K. O. Hill, 'Bandwidth-limited operation of a mode-locked Brillouin parametric oscillator', Appl. Phys. Lett.. **32**, 429 (1978)

2 K. O. Hill, D. C. Johnson, and B. S. Kawasaki, 'cw generation of multiple Stokes and anti-Stokes Brillouin shifted frequencies', ibid. **29**, 185 (1976)

3 J. Botineau, C. Leycouras, C. Montes, and E. Picholle, 'Stabilisation of a stimulated Brillouin fibre ring laser by strong pump modulation', JOSA B, **6**, 300 (1989)

4 K. O. Hill, D. C. Johnson, B. S. Kawasaki, and R. I. MacDonald, 'cw three wave mixing in single mode optical fibres', J. Appl. Phys. **49**, 5096 (1978)

5 R. H. Stolen, 'Phased-matched stimulated four-photon mixing in silica fibre waveguides', IEEE J. Quantum Electron. **QE-11**, 100 (1975)

6 H. H. Yaffe, R. G. Waarts, E. Lichtman, and A. A. Friesem, 'Multiple-wave generation due to four wave mixing in a single mode fibre', Electron. Lett. **23**, 42 (1987)

7 D. M. Pepper, 'Nonlinear optical phase conjugation', Opt. Eng. **21**, 156 (1982)

8 A. Yariv and P. Yeh, "Optical waves in crystals", John Wiley & Sons, New York, 1984

9 R. W. Hellwarth, 'Theory of phase conjugation by four wave mixing in a waveguide', IEEE J. Quantum Electron. **QE-15**, 101 (1979)

10 J. AuYeung, D. Fekete, D. M. Pepper, A. Yariv, and R. K. Jain, 'Continuous backward wave generation by degenerate four wave mixing in optical fibres', Opt. Lett. **4**, 42 (1979)

11 Kenneth O. Hill, Communications research centre, Ottawa, Canada: personal communication

12 Martin W. McCall, Physics Department, Imperial College: personal communication

13 N. F. Andreev, V. I. Bespalov, A. M. Kiselev, A. Z. Matveev, G. A. Pasmanik, and A. A. Shilov, 'Wavefront inversion of weak optical signals with a large reflection coefficient', JETP Lett. **32**, 626 (1980)

14 W. A. Shroeder, M. J. Damzen, and M. H. R. Hutchinson, 'Studies of single frequency stimulated Brillouin scattering phase conjugate Nd:YAG laser oscillator', JOSA B **6** (1989) 171; 'Polarisation decoupled Brillouin enhanced four wave mixing', IEEE J. Quantum Electron. **QE-25**, 460 (1989)

15 A. M. Scott and M. S. Hazell, 'High efficiency scattering in transient Brillouin enhanced four wave mixing', IEEE J. Quantum Electron. **QE-22**, 1248 (1986)

16 A. M. Scott and K. D. Ridley, 'A review of Brillouin enhanced four wave mixing', IEEE J. Quantum Electron. **QE-25**, 438 (1989)

17 A. M. Scott, 'Efficient phase conjugation by Brillouin enhanced four wave mixing', Opt. Commun. **45**, 127 (1983)

18 Andrew M. Scott, Royal Signals Research Establishement, Malvern: personal comminication

19 G. J. D Dunning and R. C. Lind, 'Demonstration of image transmission through fibres by optical phase conjugation', Opt. Lett. **7**, 558 (1982)

20 Y. Tomita, R. Yahalom, K. Kyuma, A. Yariv, and N. Sze-Keung Kwong, 'Polarisation and spatial information by modal dispersion and phase conjugation: properties and applications', IEEE J. Quantum Electron. **QE-25**, 315 (1989)

Chapter 9

SUMMARY AND CONCLUSIONS

This thesis has been concerned with the investigation of stimulated Brillouin scattering (SBS) in single mode optical fibres and all-fibre ring resonators. The project had two specific aims. Firstly, the identification and study of the deleterious effects of SBS in coherent optical fibre systems and devices, and secondly, the investigation of the wide range of potential applications utilising the nonlinear Brillouin gain. In particular, attention focussed on the investigation of the Brillouin lasers, four wave mixing (FWM), and to a lesser extent, amplifiers.

SBS is a very important nonlinear process as it is the first nonlinear effect to be observed as the optical power is increased. Despite this, a detailed and systematic review of the existing theoretical and experimental research in this area has revealed that a number of important characteristics of SBS have not been fully investigated, both in terms of the numerical as well as the experimental treatment. Primarily, it was shown that the numerical treatment must consider full solutions of a system of coupled equations which describe the generation of SBS. Having established that the approximations adopted by most authors have, in general, a limited range of validity, we proceeded to solve the SBS equations numerically. The method has been shown to yield stable and accurate solutions, and the comparison of the numerical solutions with the exact (analytical) solutions for the pump and Stokes equations available for the case of zero fibre loss, has revealed an excellent agreement. The results of the calculations for non-zero loss provide a valuable insight into the process of SBS generation, particularly into the energy exchange process between the counterpropagating pump and Stokes intensities. The calculations allow the exact evaluation of the SBS threshold, the value of Stokes intensity, and the degree of pump depletion for a given input pump power, fibre length, and losses. The importance of including the fibre loss term in calculating the evolution of the pump and Stokes intensities was clearly demonstrated, with higher fibre loss leading to a higher Brillouin threshold and

lower conversion efficiency at a given input pump intensity. These calculations are significant as they have implications to practical long haul fibre links and fibre amplifiers, with the results easily related to practical values and experimental parameters. *All* the system information, such as the bit rate, transmitter linewidth, and depolarisation effects can be included in the value for the Brillouin gain coefficient g_B. The flexibility and the ease of use of this particular method are extremely valuable, allowing easy estimation of the power budgets for a given link length and loss. Although previously it had been thought that pump depletion in the SBS process is a limiting factor in fibre transmission systems, it was shown that Brillouin backscattering below the SBS threshold can be damaging to system operation through increasing the RIN of the transmitter laser.

A comprehensive comparison of our results with published data on systems and amplifier experiments was undertaken, showed that good agreement was obtained for both. The Brillouin gain coefficient g_B was calculated using this method, from the measurements carried out in a 1 km length of York polarisation maintaining (HI-BI) fibre at 860 nm, and was found to be 4.7×10^{-11} m/W - approximately equal to that of pure fused silica.

The operation of an all-fibre Brillouin laser was considered. In addition to the difficulties in solving the SBS equations in a straight length of optical fibre, the description of SBS generation in a resonator is more complex, requiring a coherent addition of circulating pump and Stokes fields. Using a small gain-per-loop approximation - justified in the case of short (less than 10-15 m) resonator lengths, a steady-state analytical theory was derived. This theory takes into account pump depletion, and can be used to predict the threshold lasing power, optimum conversion efficiency, cavity gain and the saturation regime, as well as giving a continuous variation of the output Stokes power with input pump power - in terms of the resonator parameters. A comparison of the theoretical and experimental results described in this thesis has confirmed an excellent agreement in all cases, and it was shown how the results of this theory can be used to design or optimise the fibre cavity by finding the loop length and coupling coefficient for optimum conversion efficiency, threshold power, and operating conditions.

A numerical model which describes the transient operation of an all-fibre Brillouin laser and amplifier was also developed. The model accounted for pump depletion, and described the build up of the amplified spontaneous Brillouin noise, with the theoretically predicted values in good agreement with all experimentally obtained data on Brillouin thresholds and

the steady-state values. It was suggested for the first time in this work, that by pumping the Brillouin laser below threshold, it can act as an effective amplifier of signals at the Stokes frequency. The amplifier calculations were carried out, and showed the resonator-based Brillouin amplifier would have the lowest pump power requirements of all fibre amplifiers, coupled with a high gain and favourable noise characteristics. This relatively slow time response, however, effectively limits the uses of such an amplifier to applications as a low-frequency power booster for amplification of low intensity signals and coherent multi-channel systems.

From a comparison of various methods of optical amplification - all currently at the research stage - it can be concluded that it is unlikely that any one method of optical amplification will provide a unique and universal solution which would be applicable to any type of optical system. A careful evaluation of the particular system requirements is necessary to identify the particular type of amplifier most suitable for a given application. The application of the nonlinear Brillouin gain is in all-fibre amplification is promising, mainly because of the low pump power requirements, as compared with other optical fibre amplifiers, namely Raman and rare-earth doped fibres. The results of the numerical method developed yielded the value of the achievable gain as approximately 90 dB, and it was outlined how the described method could be extended to enable complete calculations of the achievable gain, noise and saturation characteristics, as well as gain reduction due to depolarisation and finite pump linewidth. This analysis and the associated experimental investigations should be carried out to consider the the usefulness of this method of amplification. Indeed a full and accurate assessment of the advantages and limitations of Brillouin amplifiers in systems context, both in long fibres and ring resonators, is required. It is thought further work in this field would undertake systematic systems experiments, as well as further theoretical evaluation of the performance characteristics of these devices.

The study of SBS in all-fibre ring resonators included a detailed theoretical and experimental evaluation of high-finesse all-fibre ring resonator operation, and involved device fabrication and characterisation. (This work formed part of an intensive component fabrication programme carried out in the UCL's Fibre Optics Group.) A number of high finesse resonators were fabricated using both standard and polarisation maintaining fibre, at wavelengths of 600 and 800 nm.

The important resonator parameters such as the finesse, free spectral range, and resolution, and their dependence on the fibre and coupler losses, and the coupling coefficient were considered. It was shown that the employed fabrication technique allowed the achievement of very low coupler losses. In such cases, the resonator finesse is limited by the fibre loss, and if the latter is high, a reduction in the resonator length would result in a higher finesse, and a greater enhancement of the circulating power over the input power. In connection with this, the experimental results showed that while the use of a semiconductor laser means lower fibre losses and increased compatibility with current fibre systems, its short coherence length compared with a stabilised single frequency He-Ne laser (or other stabilised, narrow frequency gas or solid state laser), results in a lower circulating intensity and a lower effective 'finesse'.

We have described the experimental investigation of Brillouin laser operation carried out, with particular emphasis on the semiconductor laser pumping. We have described and compared the experiments on Brillouin lasing in high finesse resonators fabricated from ordinary and polarisation maintaining fibre, using a He-Ne laser at 633 nm, and a commercially available GaAs semiconductor laser at 830 nm. A number of interesting and novel features have characterised this work. Brillouin lasing in resonators fabricated from polarisation maintaining fibre has not been demonstrated prior to this work. The first experimental observation of Brillouin lasing using semiconductor laser pumping and having a submilliwatt threshold was also achieved. These results are particularly significant as they establish the compatibility of this device with semiconductor laser technology and current fibre systems.

Notably, the measured Brillouin thresholds of 70 μW at 633 nm and 0.89 mW at 830nm represent the lowest experimentally demonstrated values, while the conversion efficiencies of 23% (at 0.22 mW) and 8% (at 1.25 mW), respectively, are the highest reported. These results also represented the first experimental confirmation of a factor of 2 reduction in Brillouin threshold in polarisation maintaining fibres. However, the high conversion efficiencies were shown to be accompanied by cavity detuning due to the build up of the counterpropagating Stokes wave in the resonator cavity - an effect which has been observed for the first time, and can limit the performance of all-fibre resonator-based devices. In the case of the semiconductor pumped Brillouin laser, several additional interesting results were obtained. The Stokes wave was polarised, and exhibited linewidth narrowing. It is expected, however, that the Stokes output spectral width, as in gas or

solid-state laser systems, is limited in principle by phase noise, and in practice by fluctuations in the resonator linewidth due to drift in the cavity length. Consequently, proper stabilisation of the resonator cavity can establish this aspect of Brillouin lasing as a means for narrowing the linewidth of semiconductor lasers for applications in coherent systems.

The applications of this work lie in the area of narrow linewidth all-fibre lasers and local oscillator applications, as well as Brillouin laser gyroscopes. In addition, a potential application of the Brillouin laser in microwave frequency generation and distribution in phased arrays has been suggested. From the comparison of the existing optical techniques for microwave signal generation and distribution it is thought that the Brillouin laser can provide a very promising alternative to the existing optical techniques. Although the tunability range of this device is limited, the stability of the output frequency and the efficiency in this technique compare very favourably with both intensity modulated and heterodyne systems. On the basis of the results of the Brillouin laser operation it was shown that optical signal generation and distribution to an array of approximately 100 elements using a single commercially available AlGaAs laser at 830 nm and currently available components is feasible, at the frequency of approximately 21 GHz. These calculations were performed using the data for currently commercially available components and based on results obtained with a relatively broad pump source. It is expected that the development of lower noise amplifiers, high speed detectors with better efficiency, and most importantly, stable, narrow linewidth, high power lasers will render this method particularly attractive. In the meantime, future work should focus on the experimental demonstration and development of a system based on the all-fibre Brillouin laser for stable, narrow linewidth microwave generation and distribution.

We have also observed FWM in an all-fibre Brillouin laser for the first time. The threshold for the generation of anti-Stokes component was approximately 12 mW obtained in a resonator with a relatively modest finesse. This figure is more than an order of magnitude lower than previously demonstrated in bulk/fibre cavities, and expected to be considerably lower for resonators with higher finesse. A possible application of this process is in all-fibre generation of very high microwave frequencies, extending the possible range of frequencies achievable with a Brillouin laser emitting only a first order Stokes frequency. To realise the considerable potential offered by this technique, this process should be demonstrated using a semiconductor laser. It is expected, however, that considerable

advances in the development of the high power semiconductor technology, and continuing improvement in component fabrication will allow the observation of semiconductor laser pumped FWM process.

The experimental investigation of Brillouin enhanced four wave mixing process resulted in the first observation of this process in optical fibres, which, in addition, represent the first observation of all-fibre phase conjugation. It could be concluded, that this process represents an extension to the FWM process in so much as it allows the mixing of internally generated and *externally input* waves. The Stokes shifted signal was generated within the ring, and the threshold for generation of the conjugate anti-Stokes signal was measured at 40 mW. The fibre resonator allows the use of significantly lower pump powers than previously measured and even lower powers are predicted for higher finesse resonators. Despite a very high phase mismatch associated with the long interaction length and high Brillouin shift, a reflection coefficient of 0.001 was measured, and it is expected that a much higher reflection coefficient would be achievable at higher pump powers and higher resonator finesse. These experiments provided a valuable and fascinating insight into the physical limits associated with this process which is of interest in optical fibres for phase conjugation applications, although it is thought that a considerable amount of further research is necessary to establish the practicality of this technique.

In conclusion, it is expected that future work will focus on further development and optimisation of the applications considered in this thesis. In addition, it is worthwhile to point out that there is a considerable scope for a systematic investigation of the effects of fibre dopant concentration and type on the gain and bandwidth in the Brillouin process. The results of such an investigation would enable further device optimisation in the context of this thesis.

APPENDIX A

Interference and diffraction view of SBS

As we have seen in Chapter 2, the density variation $\Delta\rho$, which arises in the SBS process produces a proportional variation in the dielectric permittivity, given by:

$$\delta\varepsilon = \frac{\partial\varepsilon}{\partial\rho}\Delta\rho \qquad \text{(A.1)}$$

and leads to the appearance of a travelling volume diffraction grating in the permittivity. As we have seen the scattering of the pump wave (eqn (2.8)) occurs with a frequency shift $\omega_p \rightarrow \omega_S$ and gives rise to polarisation at frequency ω_S while the scattering produces a wave with the spatial dependence exp ($j\mathbf{k_S}.\mathbf{r}$) corresponding to the signal direction - that is the Bragg phase matching condition for travelling gratings is automatically satisfied.

This in fact is a general property of the third order susceptibility[1] which appears in the expression of the polarisation of the medium, as given in equation (2.12). However, the appearance of a component proportional to exp $j[\mathbf{k_S}.\mathbf{r} - \omega_S t]$ in the polarisation (or displacement) does not necessarily mean the transfer of energy in the direction of of the Stokes wave from the pump wave caused by the grating $\delta\varepsilon \propto \exp - j[\mathbf{q}.\mathbf{r} - \Omega t]$. In fact, there is already a wave at the Stokes frequency present in the medium (which arose as a result of spontaneous scattering], and therefore, the additional field excited by the nonlinear polarization interferes with the initial field E_S. The result of the interference depends on the relation of these two contributions and may lead either to an increase (reinforcement) or attenuation of the initial field, or to an additional phase shift. The additional term in the electric displacement vector at the Stokes frequency can be written as (from equations (A.1) and (2.22)):

$$\begin{aligned}\delta D_S &= (\delta\varepsilon)E_P(z)\ \exp j[k_p z - \omega_p t] \\ &= \delta\varepsilon_{eff}(\omega_S)E_S(z)\exp j[k_S z - \omega_S t]\end{aligned}$$

$$\text{and } \delta\varepsilon_{eff}(\omega_S) \propto \rho_0[\partial\varepsilon/\partial\rho]^2|E_p(z)|^2 \qquad \text{(A.2)}$$

This result can be explained that as far as the Stokes wave is concerned, the interaction

with the pump leads only to the change in permittivity by an amount $\delta\epsilon_{eff}(\omega_S)$. It should also be emphasised that the result of the interference of the pump wave E_p with the Stokes wave E_S depends on the phase of the field E_p, whereby (from 2.22)):

$$\delta\epsilon(z, t) \propto E_p(z)E_S^*(z) \exp j[qz - \Omega t] \tag{A.3}$$

However, the result of the scattering of the pump wave by the interference grating created,

$$\begin{aligned}\delta D &\propto E_p(z)\delta\epsilon(z, t) \\ &\propto |E_p(z)|^2 E_S(z) \exp j\,[k_S z - \omega_S t]\end{aligned} \tag{A.4}$$

does not depend on the phase of E_p and is *only* determined by the pump intensity $|E_p|^2$.

The amplitude of the pump wave $E_S(z)$ varies in space as:

$$\begin{aligned}E_S(z) &\propto \exp\left[j\frac{\omega_S}{c}z\epsilon_S^{1/2}\right] \\ &\propto \exp\left[j\frac{\omega_S}{c}z\epsilon_0^{1/2} + j\frac{\omega_S}{2c}z\frac{\delta\epsilon_{eff}}{\epsilon_0^{1/2}}\right]\end{aligned} \tag{A.5}$$

where the permittivity $(\epsilon_0)^{1/2}$ represents the refractive index of the material assumed to be the same for both pump and Stokes waves. In this way, the intensity for real ϵ_0, is then :

$$E_S(z) \propto \exp\left[-\frac{\omega_S}{c}\frac{\text{Im}\,(\delta\epsilon)}{\epsilon_0^{1/2}}\right] = \exp\,[-\alpha z] \tag{A.6}$$

where α is the coefficient of additional attenuation (m^{-1}) of the intensity. This equation is very interesting as it describes quantitatively the effect of phase relationships on the energy exchange between the waves. In fact, equation (A.2) describes the variation of

the Brillouin gain for the case of the Stokes and anti-Stokes scattering.That is when $\Delta\omega_B > 0$ (ie Stokes scattering), Im $(\delta\varepsilon) < 0$ and the signal is amplified. The amplification and hence, the Brillouin gain is maximum when $\omega_p - \omega_s = \Omega$, when the phase matching condition is met precisely, and the phase shift between the electrostriction pressure $\Delta\rho$ and the density is equal to $\pi/2$. On the contrary, when $\omega_p - \omega_s < 0$, that is for anti-Stokes scattering, Im $(\delta\varepsilon) > 0$ and the anti-Stokes signal is attenuated, as described in Chapter 2. In this case the Stokes wave E_S plays the part of the pump with respect to E_p.

---

[1] B. Ya. Zeldovich, N. F. Pilipetskii, and V. V. Shkunov, "Principles of phase conjugation", Springer-Verlag, Berlin, 1985

APPENDIX B

Polarisation properties of the SBS process

In the foregoing discussion it has been tacitly assumed so far that for maximum Brillouin gain the polarisations of the interacting waves are linear and coinciding with each other. The effects on situations of this not being so are considered here. As we have seen, in SBS, the scattering mechanism is the build up of a scalar parameter of the medium, viz., its density. The part of the density perturbation $\Delta\rho$ which is of interest builds up due to the interference term is proportional to $E_p^*(z)E_S(z)$. In an isotropic medium the scalar parameter $\Delta\rho$ can be proportional only to the *scalar product* of the fields

$$\Delta\rho \propto \boldsymbol{E_p}^*(\mathbf{r})\boldsymbol{E_S}(\mathbf{r}) \exp - j[\mathbf{q}.\mathbf{r} - \Omega t] \qquad (B.1)$$

The perturbation of the dielectric susceptibility tensor is also of scalar form

$$\delta\varepsilon = (\frac{\partial\varepsilon}{\partial\rho})\Delta\rho \qquad (B.2)$$

The scattering of the pump field $\mathbf{E_p}$ by the perturbation $\delta\varepsilon$ gives rise to the dielectric displacement vector:

$$\delta\mathbf{D_S} \propto \boldsymbol{E_p}(\boldsymbol{E_p}^*.\boldsymbol{E_S}) \qquad (B.3)$$

In fact, the stimulated scattering processes with the nonlinear dielectric displacement are called scalar mechanisms. In SBS, $\delta\mathbf{D_S}$ from (B.3) immediately satisfies the condition of being orthogonal to the wave vector. The shortened equation (without linear loss) for $\boldsymbol{E_S}$ is of the form:

$$\frac{d\boldsymbol{E_S}}{dz} = -\frac{1}{2}g_B\boldsymbol{E_p}(\mathbf{r})[\boldsymbol{E_p}^*(\mathbf{r}).\boldsymbol{E_S}(\mathbf{r})] \qquad (B.4)$$

If we let the pump field be completely polarised, so that $\boldsymbol{E_p} = \mathbf{e_1}E_p$, where $\mathbf{e_1}$ is a unit polarisation vector. It is convenient to project the field $\boldsymbol{E_S}$ onto $\mathbf{e_1}$ and another unit vector $\mathbf{e_2}$ defined by the condition, $\mathbf{e_1}^*.\mathbf{e_2} = 0$:

$$E_S(z) = s_1(z)\mathbf{e_1} + s_2(z)\mathbf{e_2} \qquad (B.5)$$

Then,

$$E_S(z) = s_2(0)\mathbf{e_2} + s_1(0)\exp[(g_B|E_p(z)|^2)/2]\mathbf{e_1} \qquad (B.6)$$

This means that the orthogonal component $s_2\mathbf{e_1}$ of the Stokes field *does not* interfere with

the pump, or in other words, it does not build up a perturbation in density and the pump is not scattered into this orthogonal component. In contrast, the component $s_1(z)\mathbf{e_1}$ with coinciding polarisation is amplified in full. Therefore, in scalar type stimulated scattering, and SBS in particular, the Stokes wave tends to reproduce the polarisation unit vector of the pump. It should also be pointed out that the circularly polarised pump is reflected into the Stokes wave as if from a conventional mirror, i.e. a right-hand circularly polarised photon of the pump is converted into a left-hand circularly polarised photon of the counterpropagating Stokes wave. As the light waves are transverse, the dielectric displacement , for non colinear $\mathbf{k_p}$, $\mathbf{k_S}$, should be projected onto a plane, perpendicular to the direction of $\mathbf{k_S}$, and then the solution becomes rather more complicated than in eqn (B.6). It is important that in this case the Stokes wave polarised orthogonal to the pump is not amplified either[1].

In optical fibres, because of long interaction lengths, polarisation scrambling may lead to polarisation mismatch between the pump and the Stokes wave, and hence to a reduction of the Brillouin gain coefficient g_B, which in this case should be multiplied by a factor P which varies between 0 and 1 (this is further discussed in the context of practical systems in the Chapter 4). This factor characterises the degree of polarisation matching between the pump and the Stokes waves - 0 for completely mismatched polarisations to 1 (for pump and Stokes with identical polarisation). P is generally taken as 1/2 for ordinary fibre. In order to minimize the polarisation mismatch, polarisation maintaining fibre can be used in which P equals 1.

---

[1] B. Ya. Zeldovich, N. F. Pilipetskii, and V. V. Shkunov, "Principles of phase conjugation", Springer-Verlag, Berlin, 1985

APPENDIX C

Derivation of the exact solution to the SBS equations: α_o case

As derived in Chapter 2, the SBS equations with zero loss are:

$$\frac{dI}{dz} = - g_B BI \qquad \text{and} \qquad \frac{dB}{dz} = - g_B BI \tag{C.1}$$

where for simplicity, $I_p(z) = I$ and $I_S(z) = B$, and $0 \le z \le L$.

Subtracting the equations, we get:

$$\frac{dI}{dz} - \frac{dB}{dz} = 0, \text{ and therefore, } I - B = k, \text{ constant} \tag{C.2}$$

$$\text{Thus,} \quad \frac{dI}{dz} = - g_B I(I - k) \text{ , so that,:} \quad \int \frac{dI}{I(I - k)} = -g_B z + C$$

$$\text{giving:} \quad -\frac{1}{k}\int \{\frac{1}{I} - \frac{I}{I - k}\} dI = - g_B z + C$$

$$-\frac{1}{k}\{\ln I - \ln (I - k)\} = - g_B z + C, \text{ where: } \ln\{\frac{I}{I - k}\} = k g_B z + E \qquad [E = \text{const}]$$

which gives:

$$\frac{I}{I - k} = K e^{k g_B z} \qquad [K = \text{const}]$$

and rearranging, yields for the pump intensity:

$$I = \frac{kKe^{g_B kz}}{Ke^{g_B kz} - 1} \tag{C.3}$$

Similarly, for the Stokes intensity, eqns (C.2) and (C.3) give:

$$B = I - k = \frac{k}{Ke^{g_B kz} - 1} \qquad (C.4)$$

where I(0)/B(0) = K. As in Section 4.1 (Chapter 4), these equations can be normalised by defining new variables $\zeta = z/L$, where $0 \le \zeta \le 1$, and $\sigma = g_B I_0 L$, with I_0 being the input pump intensity at $\zeta = 0$, as before. Then the equations (C.3) and (C.4) can simply be re-written as

$$P(\zeta) = \frac{kKe^{\sigma k\zeta}}{Ke^{\sigma k\zeta} - 1} \qquad (C.5)$$

and

$$S(\zeta) = \frac{k}{Ke^{\sigma k\zeta} - 1} \qquad (C.6)$$

where k = P - S, K = P(0)/S(0), and P(0) = 1.

The known boundary conditions are then: P(0) = 1 and S(1) = b ($\approx 10^{-9}$), as before. Applying these, eqn (C.5) then gives, for the pump:

$$P(0) = 1 = \frac{kK}{K - 1} \qquad \therefore K = \frac{1}{1 - k} \qquad (C.7)$$

and for the Stokes, using eqns (C.6) and (C.7):

$$S(1) = b = \frac{k(1 - k)}{e^{\sigma k} - (1 - k)} \qquad (C.8)$$

Multiplying through by the denominator in (C.8) and rearranging, yields a transcendental equation in k:

$$b(e^{\sigma k} - 1) + (b - 1)k + k^2 = 0 = f(k) \qquad (C.9)$$

Clearly, $e^{\sigma k} = 1$, and k = 0 are trivial solutions, and the function can be represented graphically by fig. C.1

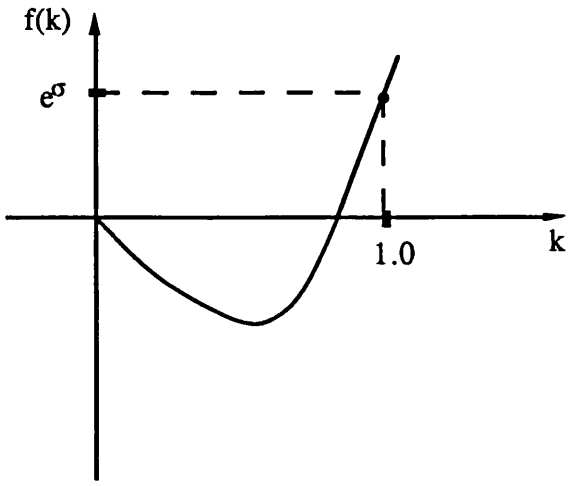

Figure C.1 Schematic representation of the function f(k).

It can be seen that the root must lie somewhere in the range $0 \leq k \leq 1$, and can be simply calculated by Newton's method:

$$k_{n+1} = k_n - \frac{f(k)}{f'(k)}$$

where f'(k) is from (C.9):

$$f'(k) = b\sigma e^{\sigma k} + b - 1 + 2k$$

The value of k can then be substituted back into eqns (C.5) and (C.6) to evaluate the pump and Stokes intensities.

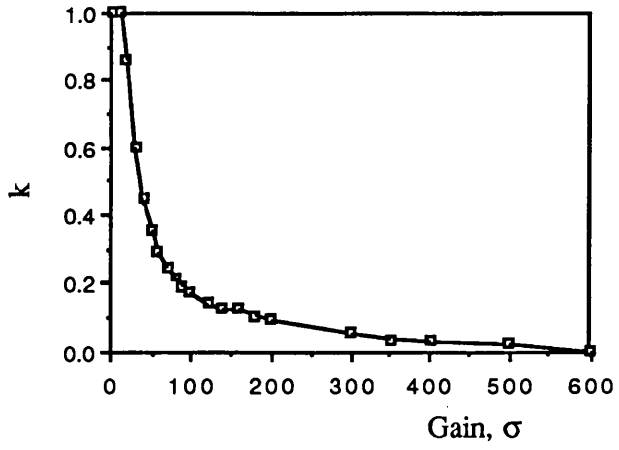

Figure C.2. Graph of k (= I - B) vs gain; k represents pump depletion.

Figure C.2 shows the plot of k with $\sigma = g_B I_0 L$, varying from 0 to 600. It can be seen that

the effect of increasing σ results in the decrease of k. Physically, this represents the growth of the conversion efficiency of pump intensity into the Stokes intensity as the gain is increased. In other words k also represents the amount of pump depletion, where for low values of gain, the pump intensity I is virtually unaffected by the Stokes intensity, with $I \approx 1$. However as the gain is increased, the growth in the counterpropagating Stokes intensity B results in more severe pump depletion.

APPENDIX D

Analytical solution to the SBS equations

In this appendix we are going to illustrate the problems with finding the analytical solutions to the SBS equations[1]. Specifically, although analytic solutions are derived, it is shown that their range of validity is limited.

From Chapter 2, the nonlinear coupled SBS equations including loss terms which we are trying to solve are (eqn (2.24)):

$$\text{Pump: } \frac{dI}{dz} = -gIB - \alpha I \qquad \text{Stokes: } \frac{dB}{dz} = -gIB + \alpha B \tag{D.1}$$

where, for simplicity $I_{p,S}(z) = I, B$, and $g = g_B$, and $\alpha_0 = \alpha$; and $0 \le z \le L$.
Subtracting the above equations, we obtain:

$$I' + \alpha I = B' - \alpha B \tag{D.2}$$

where ' indicates the derivative
In the light of the discussion in Chapter 2, it seems logical to assume that the solutions to (D.2) will be some exponential functions of z, and as a first approximation we try the substitutions of:

$$I = I_0 \exp -[kz] \quad \text{and} \quad B = B_0 \exp -[Kz] \tag{D.3}$$

where I_0 is the input pump intensity, and B_0 is the output Stokes intensity, at $z = 0$. k and K are constants or <u>slowly</u> varying functions of z.
Substituting these into (D.2), we get:

$$-k I_0 \exp -[k z] + \alpha I_0 \exp -[k z] = -K B_0 \exp -[K z] - \alpha B_0 \exp -[K z] \tag{D.4}$$

Now, it can be seen that <u>only</u> the condition $k = K$ will lead to a solution. [This is reasonable as it implies that the rate of growth of the Stokes wave is equal to the rate of attenuation (or depletion) of the pump wave, a result which was obtained in Appendix C while solving these equations for the case of $\alpha_0 = 0$. In this case, simplification of equation (D.3) results in the following expressions giving the spatial dependence of the pump and Stokes intensities:

$$I = I_0 \exp - [k\, z] \qquad \text{and} \qquad B = I_0 \left[\frac{K - \alpha}{K + \alpha} \right] \exp -[K\, z] \tag{D.5}$$

Since we would like the solution for the Stokes intensity, $B \geq 0$, the condition $K \geq \alpha$ clearly signifies threshold for the onset of SBS. Correspondingly substituting (D.4) into the pump equation of (D.1) yields:

$$- K\, I_0 \exp -[K\, z] = - g I_0^2 \left[\frac{K - \alpha}{K + \alpha} \right] \exp -[2K\, z] - \alpha I_0 \exp -[K\, z] \tag{D.6}$$

Simplifying (D.5) results in:

$$K = g I_0 \exp -[K\, z] - \alpha \tag{D.7}$$

where K is the function defining the rate of growth of the Stokes intensity with distance z in the - z direction - or attenuation in the +z direction (and the rate of the depletion of the pump intensity by it in the + z direction].

The values of K can then be analysed easily for the following cases (where only $K > 0$ is a physical solution, as K must decrease in the + z direction):

(a) when $z = 0$: $K = g I_0 - \alpha$, indicating that maximum pump depletion or Stokes amplification occurs at $z = 0$.

(b) when $z \rightarrow \infty$: the only possible solution is $K \rightarrow 0$. [That is, if we assume that $K = \varepsilon$ where ε is very small, and assuming that z is very large, we get, $K = g I_0 \exp -[\varepsilon z] - \alpha$ with $K > 0$; it can then be seen that $\varepsilon = g I_0 \exp -[\varepsilon z] - \alpha$ is satisfied for a very small ε where $\ln \varepsilon|_{z \rightarrow \infty} = 0$ or $\varepsilon z \rightarrow 1$]

(c) when $K = \alpha$: from (D.4), $B = 0$ which as before gives the threshold condition for the onset of SBS. Therefore the pump intensity necessary for threshold is then obtained from the condition, $g I_0 - \alpha \geq \alpha$, or:

$$I_0 \geq \frac{2\alpha}{g} \tag{D.8}$$

Note that this is twice the threshold (as defined by Brillouin gain exceeding linear loss) value obtained from the undepleted pump approximation as derived in Chapter 3. At this value of K, the pump intensity, from (D.4) is $I = I_0 \exp -[\alpha z]$, meaning that at

threshold, the pump intensity is attenuated only through the linear attenuation term. These cases are schematically is illustrated on figure D.1.

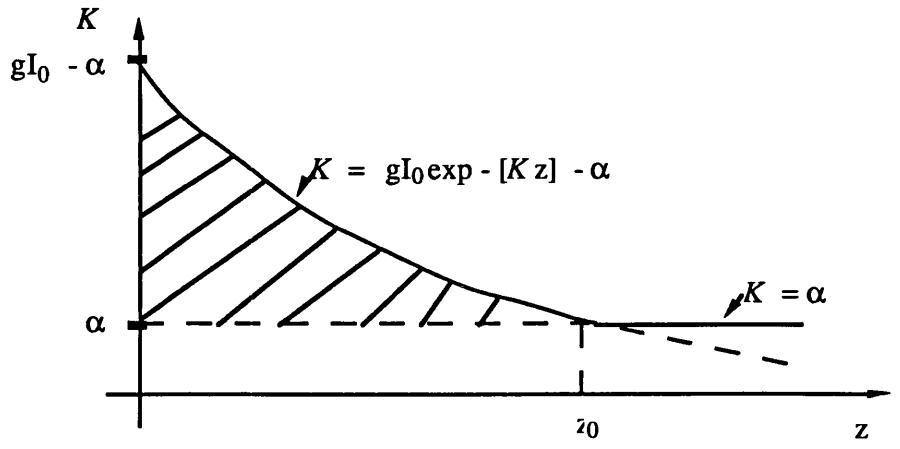

Shaded area: $B > 0$ for $z < z_0$

Figure D.1. Schematic variation of *K* with z.

In summary, we have obtained complete analytic solutions for the variation of the pump and Stokes intensities with distance. Moreover, these calculations show that, providing I_0 is not too large compared with $2\alpha/g$,and K is a slowly varying function of z, the Stokes intensity B is zero below threshold (given by $I_0 = 2\alpha/g$); the pump and Stokes dependences are given by (D.4). The transcendental equation (D.6) giving the variation of K can be solved very simply using a graphical or numerical method.

Range of validity

Although the simple ansatz of (D.2) yielded analytic solutions to the SBS equations, it is necessary to investigate their range of validity. The solutions of (D*) are valid, providing that K varies slowly such that:

$$\frac{d(\exp -[K\,z]}{dz} = -\,K \exp -[K\,z] \qquad (D.9)$$

and if K is a function of z, that:

$$\frac{d(\exp -[K\,z]}{dz} = -\exp -[K\,z].\{K + z\frac{dK}{dz}\} \qquad (D.10)$$

with $|zdK/dz| << K$. Substituting the expression for K (eqn (D.6)) into (D.10) we

get:

$$\frac{dK}{dz} = - gI_0 \exp -[K\, z].\{K \; + z\frac{dK}{dz}\} \qquad (D.11)$$

Making use of (D.6) again to give $gI_0 \exp -[K\, z] = (K + \alpha)$ equation (D.11) requires that:

$$\left|z\frac{dK}{dz}\right| = \frac{K\,(K\; + \alpha)z}{1 + (K\; + \alpha)z} << K \qquad (D.12)$$

Clearly, this will always be fulfilled for $z = 0$, so that our solution for K is valid for such z that:

$$z < \frac{1}{(K\; + \alpha)} \qquad (D.12)$$

with $K = gI_0 - \alpha$ at $z = 0$, from above, so that

$$z < \frac{1}{gI_0} \qquad (D.13)$$

Indeed, for a full solution, we have to calculate the value of z, say z_0, where $K = \alpha$, i.e. at point of Brillouin threshold. Then (from (D.6), $\alpha = gI_0 \exp -[K\, z_0] - \alpha$ we obtain the value for z_0, the point of threshold as:

$$z_0 = \frac{1}{\alpha} \ln\left[\frac{gI_0}{2\alpha}\right] \qquad (D.14)$$

From (D.12) we get that $z_0 < 1/2\alpha$ as $K = \alpha$, and combining with (D.14) we obtain, after simplification, that the input pump intensity must fulfill

$$I_0 < 3.2\,\frac{\alpha}{g} \qquad (D.15)$$

for a full solution for all z, where the factor 3.2 is equal to {2exp[0.5]}.

To try and estimate the range of input intensities covered by (D.15), consider 1 km length of fibre with attenuation of say, 1 dB/km (0.23/km), the Brillouin gain coefficient of 4.6×10^{-11} m/W, and core area, A of 5.0×10^{-11} m^2. Substituting these values into (D.15), we obtain that P_0 (= I_0/A) must be less than ≈ 0.8 mW. Now, Smith's threshold criterion for the fibre with above parameters gives the threshold

power, P_{th} as $\approx$ 25 mW. This means that the range of validity for these solutions is limited to significantly below the threshold. They, therefore, do not provide any significant new information as compared to the undepleted pump approximation. However, this solution might nevertheless be of some use to amplifier calculations since the pump power in amplifier applications is kept below threshold.

---

[1]P. C. Klipstein, Physics Department, Imperial College: personal communication

APPENDIX E

The Runge-Kutta algorithm

The equations which have to be solved numerically are:

$$\frac{dP}{d\zeta} = -\sigma SP - \beta P \quad \text{or} \quad P' = f(P, S) \tag{E.1}$$

and

$$\frac{dS}{d\zeta} = -\sigma SP + \beta S \quad \text{or} \quad S' = g(P, S) \tag{E.2}$$

As with many numerical methods for solving differential equations, the interaction length is divided into n steps, with step size h whose value depends on the desired accuracy of the approximate values.

In the Runge-Kutta algorithm, four auxillary quantities are computed at each step[1]:

$$a_1 = hf(P_n, S_n)$$
$$b_1 = hg(P_n, S_n)$$

$$a_2 = hf(P_n + \frac{a_1}{2}, S_n + \frac{b_1}{2})$$
$$b_2 = hg(P_n + \frac{a_1}{2}, S_n + \frac{b_1}{2})$$

$$a_3 = hf(P_n + \frac{a_2}{2}, S_n + \frac{b_2}{2})$$
$$b_3 = hg(P_n + \frac{a_2}{2}, S_n + \frac{b_2}{2})$$

$$a_4 = hf(P_n + a_3,\ S_n + b_3)$$

$$b_4 = hg(P_n + a_3,\ S_n + b_3)$$

And then the new values:

$$P_{n+1} = P_n + \frac{1}{6}(a_1 + 2a_2 + 2a_3 + a_4)$$

$$S_{n+1} = S_n + \frac{1}{6}(b_1 + 2b_2 + 2b_3 + b_4)$$

and so on for n steps.

In our case, the starting values P_n and S_n are P(0) = 1, and $S_n(0)$ which is unknown, and a 'guess' is made. The solutions are calculated at the other boundary, to give P(1), and S(1), which is known - being the value of the input Stokes noise. If the algorithm yields the correct value of S(1), then the initial 'guess' was correct. Alternatively, another 'guess' is made, until the correct end value is reached. The stability of the algorithm can be checked by noting the effect of varying the initial values.

The step size, h, is chosen to guarantee a sufficient accuracy of the method, since the truncation error in this method is of the order of h^5. The choice of the number of steps is a trade off between the desired accuracy and the computation (CPU) time. As the end value S(1) which we are trying to calculate is of the order 10^{-9}, the minimum number of steps necessary is 1/h = 100. In fact, it is thought that h = 0.002 (500) steps would generate reasonably accurate solutions.

---

[1] E. Kreyszig, "Advanced engineering mathematics", John Wiley & Sons Inc, New York, 1962

APPENDIX F

Proof of the energy balance condition for the OFRR

So far it has been assumed that in a resonator the circulating power will grow until the power dissipated by the losses equals the input power. Below it is proved that the condition:

$$P_{in} = P_{loss} + P_{out}$$

is indeed fulfilled.

The power lost to the system as heat has two contributions:

$$P_{loss} = P_{\alpha} + P_{\kappa} \qquad \text{(F.1)}$$

where P_{α} represents the fibre loss and P_{κ} - the loss in the coupler.

(i) Power loss in the fibre: is the difference between the power at z = 0, and the power leaving at z = L. That is if $2\alpha_0$ is the attenuation coefficient as before,

$$P(L) = P(0) \exp - 2\alpha_0 L$$

so that: $$P_{\alpha} = P(0) - P(L) = (1 - e^{-2\alpha_0 L})AI_3 \qquad \text{(F.2)}$$

where I_3 is the circulating intensity as before, and A is the fibre cross-section area. Substituting for I_3 from eqn (5.10), we obtain the expression for power loss in the fibre as:

$$P_{\alpha} = \frac{(1 - T)\, A\, D\, I_1}{1 + F \sin^2\phi}$$

$$D = \frac{(1 - k^2)(1 - 2\gamma_o)}{(1 - k[(1 - 2\gamma_o)T_L]^{1/2})^2}; \qquad F = \frac{4[k(1 - 2\gamma_o)T_L]^{1/2}}{(1 - k[(1 - 2\gamma_o)T_L]^{1/2})^2} \qquad \phi = (\beta L + \frac{\pi}{4})$$

(F.3)

and $T = \exp - 2\alpha_0 L$.

(ii) Coupler losses: The power lost as heat in the coupler is the difference between the entrant and the exit powers.

$$\Delta P = P_k = A\{|A_1|^2 + |B_1|^2 - |A_2|^2 - |B_2|^2\} \qquad \text{(F.4)}$$

where A_1, A_2, and B_1, B_2 are the field amplitudes entering and exiting the coupler, respectively, as shown in figure F.1.

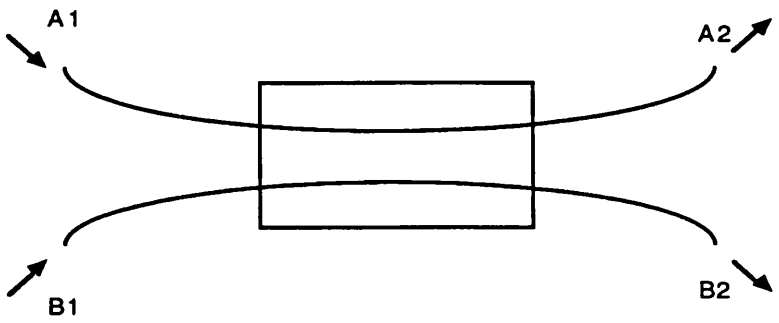

Figure F.1. Showing the fields entering and exiting the coupler

and where:

$$A_2 = (1 - 2\gamma_o)^{1/2}\{(1 - k^2)^{1/2}A_1 + jkB_1\}$$
$$B_2 = (1 - 2\gamma_o)^{1/2}\{(jkA_1 + (1 - k^2)^{1/2}B_1\}$$
and
$$|A_2|^2 + |B_2|^2 = (1 - 2\gamma_o)\{|A_1|^2 + |B_1|^2\} \qquad \text{(F.5)}$$

Thus the proportion of power lost in the coupler is simply $2\gamma_o$ of the total entrant power as stated in Chapter 5 (Section 5.1).

Then, the power loss in the coupler is:

$$P_{k.} = 2\gamma_o\{P_{in} + P_3\}$$
$$P_k = A\,2\gamma_o\{I_1 + T_L I_3\}$$

and using eqns (5.10) and (F.5) above:

$$P_k = A2\gamma_o I_1\{\ 1 + \frac{T_L D}{1 + F\sin^2\phi}\ \} \qquad \text{(F.6)}$$

Thus substituting expressions (F.3) and (F.6) into (F.1) to find P_{loss}:

$$P_{loss} = AI_3\left[2\gamma_o + \frac{\{2\gamma_o T_L + (1 - T_L)\}D}{1 + F\sin^2\phi}\right] \qquad \text{(F.7)}$$

Having related B_1, B_2, and A_1, it remains to find the relationship between A_1 and A_2, that is the difference in the input and output powers.

$$P_{in} - P_{out} = AI_1\left[1 - (1 - 2\gamma_o)\frac{C + F\sin^2\phi}{1 + F\sin^2\phi}\right]$$

$$C = \left[\frac{[T_L(1 - 2\gamma_o)]^{1/2} + k}{1 - k[(1 - 2\gamma_o)T_L]^{1/2}}\right]^2 \qquad \text{(F.8)}$$

where eqn (5.6) for the output field has been used.

If the second expression inside the [] of eqn (F.8) is re-arranged, so that $1 + F\sin^2\phi$ appears only in the denominator (by adding and subtracting 1 from the numerator), we have:

$$P_{in} - P_{out} = AI_1\left[2\gamma_o + \frac{(1 - 2\gamma_o)(1 - C)}{1 + F\sin^2\phi}\right] \qquad \text{(F.9)}$$

This should be exactly balanced by the power losses in the fibre and coupler. Equating eqns (F.7) and (F.9), we have:

$$AI_1\left[2\gamma_o + \frac{D(2\gamma_o T_L + (1 - T_L)}{1 + F\sin^2\phi}\right] = AI_1\left[2\gamma_o + \frac{(1 - 2\gamma_o)(1 - C)}{1 + F\sin^2\phi}\right] \qquad \text{(F.10)}$$

LHS represents the total losses (fibre + coupler) and RHS the power difference between input and output power. This will be true only if the numerators of the RHS and LHS are equal, ie:

$$D[2\gamma_0 + (1 - T_L)] = (1 - 2\gamma_0)(1 - C)$$

Substituting expressions for C and D, it is found that

$$\text{LHS} = \text{RHS} = 1 - T_L(1 - 2\gamma_0) \qquad \text{Q.E.D.}$$

and the energy balance condition is indeed satisfied.

This proof is extremely relevant for the case when there are additional losses due to

nonlinear effects. These will lead to a change in the output power due to detuning from the optimum coupling condition, as is shown in Chapter 5.

APPENDIX G

Transient response of the OFRR

So far we have considered the steady-state response of the resonator. We can also arrive at expressions for the circulating and pump intensities by considering the transmission of the incident field component through the resonator loop by loop. The transmission coefficients (with reference to figure 5.1) are:

$$T_{13} = T_{24} = [(1 - k^2)(1 - 2\gamma_0)]^{1/2}$$

$$jT_{23} = jT_{14} = jk(1 - 2\gamma_0)^{1/2}$$

where the lumped coupler loss has been included in the modified transmission coefficients. T_L is the transmission coefficient around the loop as defined above. Then, considering the output field components after n circulations:

n = 0: $E_4 = E_1 T_{14}$

n = 1: $= E_1 T_{14} + E_1 T_{13} T_L T_{24}$

n = 2: $= E_1 T_{14} + E_1 T_{13} T_L T_{24} + E_1 T_{13} jT_{23} T_L T_{24}$ etc.

This is in fact a geometric progression, so that:

$$E_4 = E_1 jT_{14} + \frac{E_1 T_{13} T_{24} T_L \sum_{n=1}^{N} (T_L jT_{23})^{n-1}}{jT_{23}} \qquad \text{(G.1)}$$

At steady state, when $N \rightarrow \infty$, so that we can evaluate the series using

$$\sum_{n=1}^{\infty} a^n = \frac{a}{1 - a} \quad \text{for } |a| < 1$$

which yields:

$$E_4 = E_1 jT_{14} + \frac{E_1 T_{13} T_{24} T_L}{(1 - T_L jT_{23})} \qquad \text{(G.2)}$$

and which is in fact an identical expression to that derived using the coupled mode theory in Chapter 5.

The significance of the above expressions is as follows. Equation (G.1), in fact,

represents the complex, time dependent amplitude transmittance of the OFRR. The n-th term of this series represents the contribution to the light output which has circulated the ring n times. It can be seen that the magnitude of the n-th term is a decaying function of n (as $T_{23}T_L < 1$) that the light suffers on each roundtrip. Hence, it takes a finite number of circulations ($N \rightarrow \infty$) to reach steady state. We shall return to the dynamic characteristics of the OFRR when we consider the transient response of the Brillouin laser in Chapter 7.

The series for the circulating field is obtained in the similar manner.

n = 0: $E_3 = E_1 T_{13}$

n = 1: $= E_1 T_{13} + E_1 T_{13} T_L j T_{23}$

n = 2: $= E_1 T_{13} + E_1 T_{13} T_L j T_{23} + E_1 T_{13} T_L j T_{23} T_L T_{23}$

etc.

$$E_3 = E_1 T_{13} \sum_{n=0}^{N} (T_L j T_{23})^n \qquad \text{(G.3)}$$

and at steady state:

$$E_3 = \frac{E_1 T_{13}}{1 - T_L j T_{23}} \qquad \text{(G.4)}$$

which is again identical to eqn (5.5).

List of publications

The following is a list of publications arising from the work in this thesis at the time of submission, in chronological order, including conference presentations, letters, and papers:

1) **P. Bayvel** and I. P. Giles, 'Stimulated Brillouin scattering (SBS) in single-mode fibre optic resonators', presented at IEE colloquium on 'Nonlinear optical waveguides' held on 2 June 1988, IEE Digest No. 1988/88, paper 5

2) R. Kadiwar, **P. Bayvel**, and I. P. Giles, 'SBS in polarization maintaining all-fibre ring resonators', presented at SPIE conference 985 on 'Fibre Optics and Laser Sensors VI', 6 - 10 September, Boston, Massachusetts. Proc. SPIE **985**, 338 (1988)

3) **P. Bayvel**, J. Halley, R. Kadiwar, and I. P. Giles, 'Theoretical and experimental investigation of all-fibre single mode Brillouin lasers', presented at 14th European conference on optical communications, ECOC '88, 11 - 15 September 1988, Brighton. ECOC'88 conference proc. part 1, IEE Conference. Publ. **292**, pp 123-126

4) **P. Bayvel** and I. P. Giles, 'Operation of a semiconductor laser pumped, polarized, single mode all-fibre Brillouin laser', presented at the IEEE/OSA Meeting on "Nonlinear Guided Wave Phenomena - Physics and Applications", Houston, Texas, USA, 2 - 4 February 1989. 1989 Technical Digest Series, vol. 2, pp 57 - 60.

5) **P. Bayvel** and I. P. Giles, 'Linewidth narrowing in the semiconductor laser pumped single mode all-fibre Brillouin ring laser', Electronics Letters **25**, 260 (1989)

6) **P. Bayvel** and I. P. Giles, 'Evaluation of performance parameters of single mode all-fibre Brillouin ring lasers', Optics Letters **14**, 581 (1989)

7) **P. Bayvel**, 'Applications of SBS in optical fibre coherent systems', presented at the NATO Advanced Study Institute on 'Nonlinear Waves in Solid State Physics', Erice, Sicily, July 1989 [To be published in the NATO ASI Proceedings, 1990]

8) **P. Bayvel** and I. P. Giles, 'Frequency generation by four wave mixing in an all-fibre single mode ring resonator', Electronics Letters **25**, 1178 (1989)

9) **P. Bayvel**, P. Radmore, and I. P. Giles, 'All-fibre Brillouin amplifiers - in single mode fibres and fibre ring resonators', presented at IEE Colloquium on "Optical amplifiers for communications", held on 27 October 1989, IEE Digest No. 1989/119, paper 19

10) **P. Bayvel**, P. Radmore and I. P. Giles, 'Transient and steady-state characteristics of a Brillouin amplifier based on the all-fibre single mode ring resonator' - to be published in the special issue of Optical and Quantum Electronics on 'Optical Amplifiers', April 1990

11) **P. Bayvel** and I. P. Giles, 'Observation of Brillouin enhanced four wave mixing (BEFWM) in an all-fibre single mode ring resonator', to be published in Optics Communications, 1990

Other publications:

12) **P. Bayvel** and M. W. McCall, 'Continuous method for measuring the electro-optic coefficient in $Bi_{12}SiO_{20}$ - application to sensors', presented at the 3rd Eurosensors '87 conference on 'Sensors and their applications', 22 - 24 September 1987, Cambridge, UK, WA3, Conference Proc., pp 99-100

13) **P. Bayvel**, 'Investigation of the electro-optic properties of BSO and BGO - applications to sensors', International Journal of Optical Sensors **2**, 413 (1987)

14) **P. Bayvel**, M. W. McCall, and R. V. Wright, 'Continuous method for measuring the electro-optic coefficient in $Bi_{12}SiO_{20}$ and $Bi_{12}GeO_{20}$', Optics Letters **13**, 27 (1988)

15) **P. Bayvel**, 'Electro-optic coefficient in BSO-type crystals with optical activity - measurement and application to sensors', Sensors & Actuators **16**, 247 (1989)